IJEST

ISSN: 0973-6255
Vol. 16 No.1&2
January - December 2022

Indian Journal of Engineering, Science, and Technology

A Refereed Research Journal

Published by

BANNARI AMMAN INSTITUTE OF TECHNOLOGY

(Autonomous Institution Affiliated to Anna University, Chennai - Approved by AICTE - Accredited by NAAC with "A+" Grade)

Sathyamangalam - 638 401 Erode District Tamil Nadu India | Ph: 04295-226340 - 44 Fax: 04295-226666

E-mail: ijest@bitsathy.ac.in | www.bitsathy.ac.in

Stay Ahead

Indian Journal of Engineering, Science, and Technology

IJEST is a refereed research journal published half-yearly by Bannari Amman Institute of Technology. Responsibility for the contents rests upon the authors and not upon the IJEST. For copying or reprint permission, write to Copyright Department, IJEST, Bannari Amman Institute of Technology, Sathyamanagalam, Erode District - 638 401, Tamil Nadu, India.

Indian Journal of Engineering, Science, and Technology

ISSN: 0973-6255

Volume 16 Number 1&2 **January - December 2022**

CONTENTS

DESIGN AND FABRICATION OF DELTA 3D PRINTER USING A LEAD SCREW MECHANISM FOR PRINTING RECYCLABLE COMPONENTS

S.K. Dhinesh, P.Nagarajan, K.L.Senthil Kumar, M. Raghunath and P.A.Tharakeshvar
Department of Mechatronics,
Bannari Amman Institute of Technology, Sathyamangalam - 638401, Erode, Tamil Nadu
Email Id: dhineshsk@bitsathy.ac.in

Abstract

In recent times, the realm of additive manufacturing has witnessed a surge in interest, with a multitude of methods and techniques emerging. Among these, one particular style of 3D printing, known as the Delta structure, has garnered significant attention and intrigue. This paper delves into the intricacies of the Delta structure style, focusing on its unique capability to utilize recyclable filaments, thereby promoting sustainability and eco-friendliness in the field of 3D printing. The paper goes beyond a mere introduction and provides a comprehensive exploration of the advantages that the Delta structure holds over its counterpart, the Cartesian structure. By offering a detailed explanation, it sheds light on the specific features and characteristics that make the Delta structure an attractive choice for additive manufacturing enthusiasts. Moreover, the paper goes a step further by providing an in-depth description of the various components employed in the construction of a 3D printer utilizing the Delta structure. It meticulously examines the role and functionality of each component, emphasizing their significance in achieving optimal performance and precision. Furthermore, the paper delves into a crucial aspect of the Delta structure, namely the implementation of a screw rod mechanism as opposed to the more commonly used belt mechanism. By highlighting the advantages and benefits of incorporating a lead screw in the Delta structure, it offers valuable insights into enhancing the overall printing experience and output quality. In addition, the paper provides a comprehensive comparison between the Cartesian structure and the Screw rod Delta structure. By conducting a thorough analysis of both approaches, it elucidates the strengths and limitations of each, enabling readers to make informed decisions when selecting the most suitable 3D printing method for their specific requirements. In essence, this paper serves as a comprehensive resource for researchers, enthusiasts, and practitioners in the field of additive manufacturing. It goes beyond a surface-level exploration, delving into the intricate details and nuances of the Delta structure, while also shedding light on the broader context of 3D printing and its evolving landscape. By focusing on keywords such as 3D printer, Delta structure, Lead screw, and Additive manufacturing, this paper contributes to the growing body of knowledge in this dynamic and ever-evolving field.

1. INTRODUCTION

Additive manufacturing, also known as 3D printing, has experienced significant growth and development over the past three decades. While it has been commercially available since the early 1990s, its widespread adoption was hindered by high costs and maintenance challenges associated with early prototypes. The concept of 3D printing was first introduced in 1986 when the founders of the prominent 3D systems company filed a patent under the name "Apparatus used to produce three-dimensional objects by stereo-lithography," as documented in Google Patents. Since then, the global market for additive manufacturing has undergone remarkable evolution, as depicted in Figure 1, with a shift in focus from hobbyists to industrial applications. The applications of 3D printing have expanded to various industries, including MEMS, aerospace, automotive, and medical fields. This versatile technology has revolutionized manufacturing processes, enabling the production of complex components with enhanced precision and efficiency [1] [2] [3].

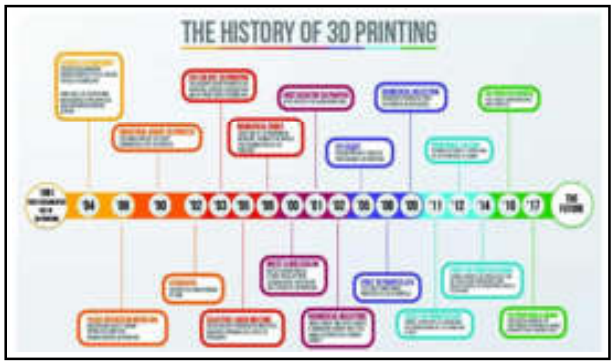

Fig 1. Evolution of 3D Printer

To understand the different types of 3D printers, it is essential to consider their classification based on structure, orientation, and printing technology. The most common type of 3D printer is the FDM printer, renowned for its accessibility and availability in various configurations and sizes. However, when examining the structure, 3D printers can be broadly classified into four major categories: Cartesian, Delta, Polar, and SCARA structures. The Cartesian structure, rooted in the Cartesian coordinate system used in mathematics, employs three axes (X, Y, and Z) to determine the position of the print head. This technology has gained widespread popularity due to its versatility and compatibility with different applications. On the other hand, the Delta structure, characterized by its fast-printing capabilities, utilizes fixed motors and extruders positioned on the top and sides, resulting in a lightweight print head that ensures high accuracy. The Polar structure, predominantly used for educational purposes, leverages cloud-based software for creating and managing 3D models. Lastly, the SCARA structure resembles the arm structure of a SCARA robot, providing increased mobility and simultaneous accuracy [4].This research paper primarily focuses on the Delta structure of 3D printers that utilize recyclable filaments. The paper aims to explore the working mechanism and components involved in the Delta structure printers. While traditional Delta printers commonly employ a belt system or guideway for vertical motion, this study introduces a novel approach using a thread screw rod. By implementing this method, the research seeks to achieve high accuracy coupled with fast motion, thus addressing a crucial aspect of 3D printing technology [5]. To validate the effectiveness of this approach, a comprehensive comparison between the Delta structure and the Cartesian structure 3D printers is conducted, considering various parameters. In conclusion, this research paper sheds light on the historical evolution and current state of additive manufacturing, specifically in the context of 3D printing. By focusing on the Delta structure with recyclable filaments, the study aims to contribute to the existing knowledge and understanding of 3D printing technology, offering insights into its working mechanisms, components, and comparative analysis.

The additive manufacturing market is expected to reach the $40 billion mark by 2026, as shown in Fig 2. The increased market size of additive manufacturing has led some specialists to consider that this technology will be the basis of the Fourth Industrial Revolution.

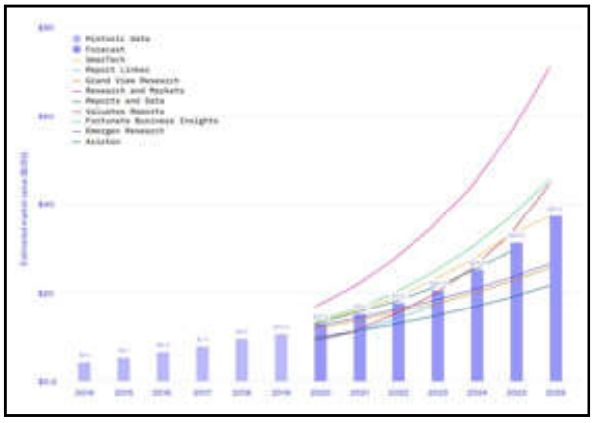

Fig 2. Forecast of 3D printer

1.1 Applications

Delta 3D printers have gained significant traction across industries due to their unique design and capabilities. Their high-speed and precise motion system, characterized by three vertical arms connected to a single moving platform, make them particularly suited for rapid prototyping and small-scale production tasks. In the automotive sector, Delta 3D printers are employed for crafting intricate prototypes of engine components, reducing development cycles. The aerospace industry benefits from their ability to manufacture lightweight yet robust parts for drones and satellites. Additionally, the food industry has embraced Delta 3D printers to create complex confections and custom-shaped edibles. Overall, the versatility of Delta 3D printers in producing intricate, structurally sound objects with speed positions them as valuable tools across industries, streamlining manufacturing processes and fostering innovation.

In recent years, the field of additive manufacturing has witnessed remarkable advancements in materials, software, and hardware, with profound implications for the Delta 3D printer structure and the broader additive manufacturing landscape. Material innovation, such as the development of high-performance polymers, composite materials, and even biodegradable options, has expanded the range of functional and durable objects that can be produced using Delta 3D printers. Moreover, advancements in software have enabled intricate design capabilities, facilitating the creation of complex geometries that fully utilize the Delta structure's inherent benefits in precision and speed. Hardware enhancements, such as more efficient effector mechanisms and improved motion control systems, have resulted in heightened printing accuracy and reduced maintenance requirements for Delta 3D printers. Looking ahead, the

potential for Delta 3D printers to fabricate large-scale structures, like architectural components, and to integrate multimaterial and multi-color capabilities could reshape industries such as construction and consumer goods. Furthermore, the sustainability aspect of Delta 3D printing, which often leads to reduced material waste compared to traditional manufacturing processes, aligns with the growing emphasis on eco-friendly practices. As these advancements continue to unfold, the Delta 3D printer structure stands poised to play a pivotal role in pushing the boundaries of additive manufacturing while addressing environmental concerns.

2. RESEARCH METHODOLOGY

The research paper delves into the fascinating evolution of 3D printers, exploring how the delta structure has emerged as a promising alternative to the traditional cartesian structure. Through an indepth analysis, it elucidates how the delta structure overcomes the limitations and challenges associated with the cartesian structure, revolutionizing the field of additive manufacturing. A significant aspect of the paper lies in providing a detailed explanation of the various components utilized in the delta structure. By elucidating the functionality and role of each component, the reader gains a comprehensive understanding of how these elements contribute to the overall performance and efficiency of the delta structure. Moreover, the paper sheds light on the economic considerations, particularly within the context of the African continent, where the availability and cost of replacement components pose challenges. To address this issue, the research explores the use of Ewaste from 2D printers and other reusable components, aiming to achieve cost-effective alternatives and promote local manufacturing of spare parts. In developing the locally made delta 3D printer, the research adopts the adoptive machine design technique, drawing inspiration and ideas from validated machines such as the Delta Pi 3D printer from Thing verse and the KLAKS 3D printer made in Ghana. Notably, the design incorporates the concept of square pipe linear rails, serving as both linear rails and support structures for the base and top plates. This creative integration demonstrates the innovation and resourcefulness involved in the development of the delta structure [6]. The paper's primary focus centre's on the advantages and implementation of the delta structure within additive manufacturing. It provides a comprehensive overview of the evolution of 3D printing, highlighting its transformation from a mere hobby to an efficient manufacturing method. Furthermore, the paper explores various 3D printing structures and styles before delving into the unique features and benefits of the delta structure. By emphasizing the design requirements and the materials used for different components, the research aims to provide guidelines for achieving smooth and optimal functioning of the delta structure [7].To support its findings, the research paper presents the design and fabrication of a low-cost delta 3D printer. The experimental testing of standard samples, along with graphical representations, enables the determination of optimal operational parameters for ensuring good quality and superior surface finish of printed parts. Through rigorous testing and comparison, the paper validates the efficacy of the proposed design and provides valuable insights into the performance of the delta structure [8]. In summary, this research paper offers a comprehensive exploration of the evolution and advantages of 3D printers, with a specific focus on the implementation and benefits of the delta structure in additive manufacturing. By delving into the various components, design considerations, and experimental results, the paper contributes to the growing body of knowledge in this field, paving the way for further advancements and applications of the delta structure in the realm of 3D printing

3. WORKING OF DELTA 3D PRINTER

The As the world becomes more digitalized and industrialized, 3D printers become inevitable in human life. So, there must be an exponential rise in the usage or need for the 3D printer. In today's world, the mainly used 3D printers are made up of cartesian type, which has the main drawback of the time consumption and rehabilitee. A delta-type 3D printer is a practical solution for this issue because the delta printer is known for its speed and print quality [9]. This can be achieved by the simultaneous working individual servo motor used in the printer and its design structure; there will not be any extra weight on the printer's head. Due to its ability to print complex structures and also, compared to other approaches, it enables adjustments without requiring additional tools or equipment. The Delta 3D printer has three similar towers or axes. Each tower is made up of a square tube and a carriage that runs up and down the column using a lead screw that is attached to the stepper motor; by using the rotation of the lead screw, the nut attached to the screw will move linearly up and down with the help of the axes as shown in Fig 3. The three coordinate axes are denoted A, B, and C.

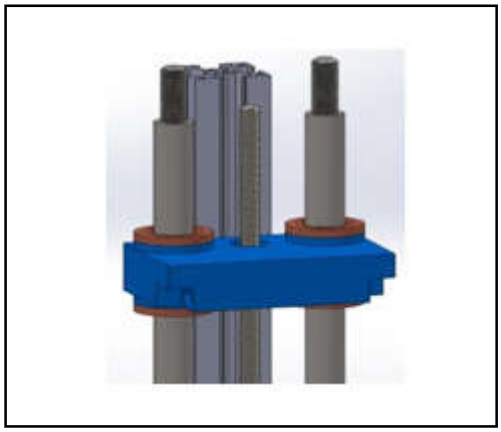

Fig.3 Lead screw attached with carriage

Each carriage has two parallel arms of the same length that connect to the effector platform. The parallel arms of the carriages connect to the effector platform to force the plane of the effector to be parallel to the plane of the bed. To ensure that the arms are parallel, the connection points on each carriage and the effector platform should be at the same distance apart. The coordinates X and Y are obtained from the synchronized movement of the three pairs of arms for the nozzle to reach a specific point [10]. The Z coordinate, on the other hand, is achieved when all carriages move up or down. By this mechanism, the printer head can move in all directions around the working volume of the printer, as shown in Figure 4.

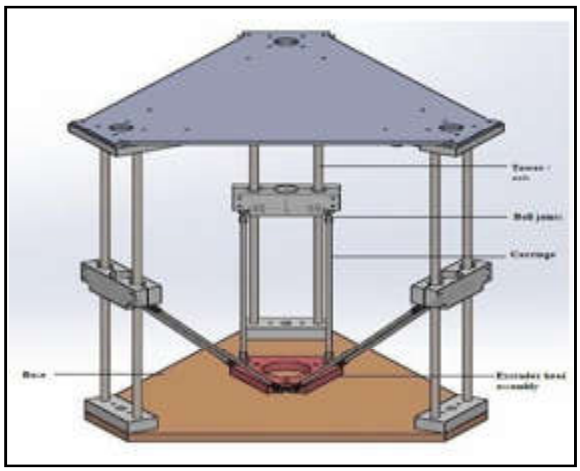

Fig 4. CAD model of 3D printer

The Bowden extruder motor assembly is the device that is used to feed the filament to the extruder head using the rotation force produced by the stepper motor fixed on that assembly. As a result, the filament flow can be controlled, as shown in Figure 5.

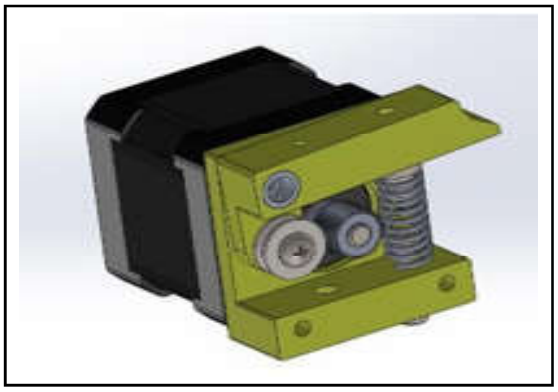

Fig.5 Filament feeder

4. LOGICAL ARCHITECTURE

The logical architecture of a delta 3D printer consists of several key components that work together to enable the printing process. The logical architecture contains of user interface, printer controller, delta robot mechanism, print head, print bed, filament feeding system, sensors and Power supply.

5. CALCULATION OF 3D PRINTER

The numerical simulations for the suggested Delta 3D printer are addressed in this section. The total mass to be handled by the stepper motor and the number of micro steps per millimeter were calculated.

5.1Mirostep Calculation

The method to determine the steps per millimeter of moving devices utilizing NEMA 17 motors might be written as.

$$\text{steps(mm)} = \frac{Mg\ X\ Microstepping}{Tip\ measured\ in\ millimeter\ per\ motor\ revolution(\gamma)} \quad (1)$$

$$\gamma = Belt\ pitch\ the\ X\ Teeth\ count\ of\ pulley \quad (2)$$

From Eq1, Eq2 1.8° or 0.9° for every step are possible with NEMA 17 stepper motors. The stepper motors used in this project have a step size of 1.8°. As a result, the following expression might be used to determine the proper

$$\text{steps/mm:} = \frac{360^0}{1.8^0}\ Steps\ per\ revolution \quad (3)$$

$$Microsteps\ of\ motor = \frac{200}{revolution} \quad (4)$$

$$Microstepping\ of\ Nema\ motor = 256\ micro\text{-}steps \quad (5)$$

$$\gamma = Belt\ pitch\ the\ X\ Teeth\ count\ of\ pulley \quad (6)$$

$$Hence,\ Steps\ per\ mm = \frac{200}{80}$$

$$= 640\ steps\ perrevolutions \quad (7)$$

From Eq 3,4,5,7 Consequently, 640 steps are needed by the motor for each millimetre

5.2 Load Carrying Calculation

The overall load of things that may be transported is influenced by the load of the carriage and the load of the bearing stack. The continuity equation is used to estimate the weight of the object to be moved.

$$W_0 = W_C + (W_B)\ W_E \quad (8)$$

From Eq8, Where WO is the weight of the object being moved, WC is the weight of the carriage, WB is the weight of the bearing stack, and WE are the weight of the extruder.

Given W_c = 39.10g, W_E = 39g and W_B = 3.15g

$$W_0 = 39.10 + (3X\ 3.15) + 39 \quad (9)$$

$$W_0 = 87.55g \quad (10)$$

$$W_0 = 0.08755kg \quad (11)$$

$$M_0 = W_0\ X\ \alpha \quad (12)$$

From Eq 11, Eq 12where MO is the object's Mass and an is the acceleration caused by gravity:

$$M_0 = 0.08755\ X\ 9.81\ ms^{-2} \quad (13)$$

$$M_0 = 0.8586\ N \quad (14)$$

The NEMA 17 stepper motor's minimum output force is 1.73 N, which is larger than the weight that has to be lifted x0.8586 N) From Eq(14), as well as other parts may readily slide along the square tube.

6. RESULTS AND DISCUSSION

The printing process begins with a power supply to the control board, which distributes it amongst the system components, as shown in Fig 6, and the print commands are also sent to the control board. The control board instructs the heating elements to melt the filament (printing material). With the help of the extruder motor assembly, a controlled amount of filament is deposited in a semiliquid form onto the build platform. This also controls the angle of each arm parallelogram to realize the shape of the 3D object.

All these mechanisms work together to aid the printer in the following x, y, and z coordinates to form the 3D object. The display helps the user see the progress made for an issued print and for menu selection. The cooling fans assist in keeping the control board cool and some parts of the extrusion mechanism. It also cools the printout as the printing is ongoing. A CAD model is essential for building a 3D object, so SolidWorks 3D modelling software was used to develop our proposed Delta 3D printer. Displays a 3D model of the proposed Delta printer with the various parts labelled.

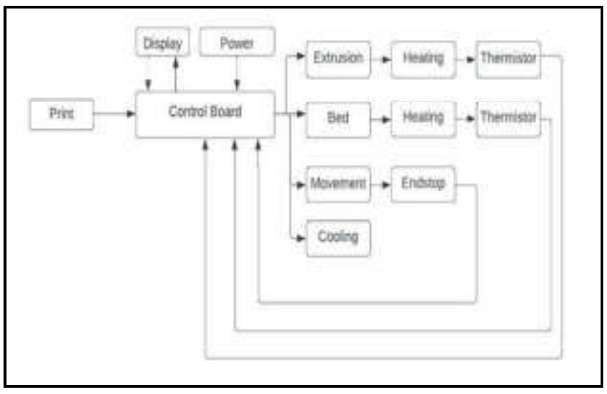

Fig.6 Working block diagram of 3D printer

The printer initiates the extruder's heating when a print command is initiated. As the printer heats the extruder by applying 12 V to the heating cartridge, it loads up the coordinates for the first layer of the print into its volatile memory. When the optimum extruder temperature is reached, 185 to 200°C for polylactic acid (PLA) and 220 to 240°C for acryl butadiene styrene (ABS), the printer homes the extruder nozzle. The home position corresponds to x = 0.00, y = 0.00, and z = MAX coordinates. Mechanical end stops are employed to energize stepper motors once the limit is attained. After homing the extruder nozzle, the printer moves the various motors to the corresponding coordinates while depositing the filament after the first layer; the printer prints the next layer using the coordinates available in its memory from the G code file. When the last layer is printed, the control board shuts off the extruder; 0 V is applied to the extruder. It then moves the extruder nozzle to the maximum z-axis position with the help of the end stops, and the printing process is terminated.

For printing ABS, a heated bed is used to prevent the warping of the printout. The heated bed has a spring spacer that allows for bed levelling and prevents heat transfer from the heated bed to the plywood base plate.

In this case, the heat bed is also heated during the start of the print to optimum temperature (90°C to 110°C) and shut off after printing the last layer. Fig 7s shows the flowchart of the printing algorithm.

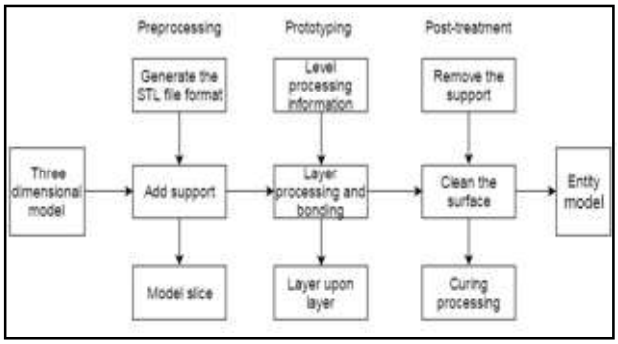

Fig.7 Flowchart for 3D Printing process

The fundamental benefit of a delta printer over a conventional cartesian-style printer is that it can print more quickly and precisely, which makes it ideal for research applications. In this research paper, the results of using a 3D delta printer would likely be discussed in the context of creating precise and complex structures, and also creating large-scale structures. As a result, while printing the complex object using this printer, gives more accurate geometries compared to the other printer mainly because of the screw rod is placed to actuate the vertical motion of the printer arm. This printer also has a printing volume of 90x150 mm this helps to print a larger 3D object with a printing speed of 150 mm/sec with a position accuracy of around 0.05 – 0.1mm.

As additive manufacturing continues to evolve, the Delta 3D printer structure holds significant promise for shaping future directions and applications within this dynamic landscape. The potential for Delta 3D printers to scale up in size and capabilities opens doors to innovative applications such as constructing entire buildings and fabricating large industrial components with unprecedented precision. This expansion could revolutionize industries like architecture, aerospace, and automotive manufacturing. Moreover, the inherent sustainability of Delta 3D printing, characterized by reduced material waste and energy consumption, aligns with the global imperative for eco-conscious practices. This sustainability aspect not only addresses environmental concerns but also contributes to a more efficient and resource-responsible production paradigm. As additive manufacturing, including Delta structures, gains traction worldwide, its impact on industries, economies, and society at large becomes increasingly pronounced. The shift towards localized and customized production could reshape supply chains, reduce shippingrelated carbon emissions, and spur economic growth by enabling small-scale, agile manufacturing enterprises. Thus, the Delta structure's potential to drive innovation, enhance sustainability, and reconfigure traditional industrial models underscores its pivotal role in the additive manufacturing revolution within the broader global context.

REFERENCES

[1] Chin, Seow and Dikshit, Vishwesh and Priyadarshini, Balasankar and Zhang, Yi, "Powder-Based 3D Printing for the Fabrication of Device with Micro and Mesoscale Features", Micromachines, Vol.11, 2020, pp. 658.

[2] Tan, Yu Jun and Tan, Xipeng and Yeong, Wai Yee and Tor, Shu, "Additive Manufacturing of patientcustomizable scaffolds for Tubular Tissues Using the Melt-Drawing Method", Materials, Vol. 9, 2016, pp. 893.

[3] B. a. N. S. H. a. Y. Y.-j. Ho, "A Review on 3D Printed Bio-Implant", International Journal of Precision Engineering and Manufacturing, Vol.16, 2015, pp.1035-1046.

[4] Morocho, Derlin and Sempurtgui, Anita and Celi, Ricardo and Loza, David and Alulema, Darwin and Proapo, Mariela, "Study, Design and Construction of a 3D Printer Implemented through a Delta Robot",

[5] Wang, Man and Sun, Zhenzhong, "Intelligent Fault Diagnosis of Delta 3D Printers Using Local Support Vectot Machine by a Cheap Attitude Multi-Sensor", pp.21-27.

[6] A. Simons, K.L.M. Avegnon, og C. Addy, "Design and Development of Delta 3D Printer using Salvaged e-materials", 2019.

[7] R.-S. Rozsos, Z. L. Buna, S. Bodi, "Design and Development of Linear Delta 3D printer", 2020, pp. 180195.

[8] M. J. Patel, K. Parmar, M. Patadia3, K. Patel, og S. Suthar, "Design and Development Delta 3D printer and its Experimentation," pp. 185-190, 2020.

[9] Anthony Simons, Kossi L. M. Avegnon, Cyrus Addy, "Design and Development of Delta 3D Printer".

[10] K. Gomathi, K.Arangamuthalvan, S. Deepigkashri, C.Dharnieshwaran, S.Dhivya and C.Praveen, "Design and Fabrication of low cost 3D printer", IOP Confernce Series: Material Science And Engineering, Vol. 1055, 2021, pp.012036.

INFLUENCE OF BRONZE SCRAP PARTICLES REINFORCEMENT ON MECHANICAL PROPERTIES OF AA 6063 MATRIX COMPOSITES

P.Sangaravadivel, D.Dinesh, A.D.Pradeep and A.Ramakrishnan
Department of Mechanical Engineering,
Bannari Amman Institute of Technology, Sathyamangalam - 638401, Erode District, Tamil Nadu
E-mail: sangaravadivelp@bitsathy.ac.in

Abstract

Composites are made to enhance the mechanical and other desired properties of the base material. In this present work, Phosphor Bronze (PBr) particles at 4% and 8% wt., collected as industrial residue and it is used as metallic reinforcements to develop an Aluminium (6063) Matrix Composite (AMC). Composites are prepared by using Stir Casting technique and Vickers Hardness, Impact and Micro Tensile tests are conducted to study its mechanical properties. The test specimens are prepared as per ASTM standards using Wire- Cut Electrical Discharge Machine (WEDM). The microstructure of the composites is examined by using optical microscope. Analysis of test results revealed that the hardness of the AMC increased initially at first and declines on further addition of reinforcement material. The tensile strength and impact strength are drastically reduced with phosphor bronze addition to AA6063.

Keywords: *Composites, Micro Tensile Test, Stir Casting, Wire EDM*

1. INTRODUCTION

In general, composites are made to enhance the mechanical and other desired properties of the base matrix material through addition of ceramics or oxides particle reinforcement in heterogeneous manner. This heterogeneity in composite is attributed to the difference in melting temperatures of the materials present in the composite. Properties of the created composites exhibit a significant difference when compared to that of the pure matrix material. AA6063 is an alloy of aluminum with magnesium and silicon as major constituent elements. The alloying element magnesium provides the alloy with increased strength, whereas silicon reduces the melting temperature of the metal. The recycling of machining scrap is practiced by involving them as reinforcement in the fabrication of metal matrix composites. Kenneth et al investigated the mechanical, wear and corrosion behavior of copper matrix composites reinforced with steel machining chips made through stir casting route. The steel chips obtained from milling of medium carbon steel are used to make the composites. After proper sieving process, an average steel chips size of 105µm is used for composite development. The results revealed that the porosity level decreases with the addition of steel machining chips compare to alumina. The improved hardness, tensile strength and wear are shown improved trend while adding steel chips into copper matrix. The increase in strength is reasoned to be on account of strong interfacial bonding between steel chips and copper matrix which supports the distribution and transfer of loads from matrix to reinforcement [1]. Rahman et al. studied the mechanical and wear behavior of aluminium 6061 composites reinforced with steel machining chips and found the hardness of the composite specimen increased with the increase of weight percentage of machining chips. The increase of high density reinforcement chips compare to aluminium matrix improves the hardness of composites. Due to addition of comparatively high brittle nature steel chips reinforcement reflected on improvement in tensile strength compared to unreinforced Al 6061 alloy. The wear indexes of the reinforced composite decreases imply high wear resistance compared to unreinforced base material [2]. Alaneme *et al.,* blended steel machining chips as reinforcement in Zn27Al alloy and made composites in stir casting technique. The analyses results of mechanical and wear characteristics exhibits improved hardness and wear resistance for 5 to 10 % addition of steel chips attributed to the inclusion of high hardness steel chips. The fracture toughness KIc shows an increased trend up to 5% addition of steel chips further an addition reduces the fracture toughness. It reveals the good interface bonding between matrix alloy and steel chips up to 5 % provides good structural integrity and addition of more than 5% cause uneven distribution and possibility

of agglomeration of reinforcement's results in decrease of wear and mechanical properties[3]. From the literature study, it is observed that the addition of high hardness machining chips / particles in the soft alloy may improve the mechanical and wear properties. In this work, an attempt has been made to fabricate the bronze machining scrap particles reinforced composites blended with AA 6063 matrix to investigate the results on mechanical properties[4].

2. MATERIALS AND FABRICATION

2.1 Matrix, Reinforcement & Stir Casting

By analyzing the demand of improving mechanical properties of AA 6063 in low cost, it is preferred to use residue of cylindrical grinding operation retrieved from industry i.e phosphor bronze (PBr) particles as reinforcement. Phosphor Bronze (PBr) is an alloy of copper with tin and phosphorus as its constituents. It is mainly noted for its mechanical properties of toughness and strength. It also possesses a low coefficient of friction and does not generate spark when contacted with other metals. Tin in phosphor bronze enhances the corrosion resistance of the alloy. It proved that the mixing of uniform sized reinforcement particles supports for the achievement of better properties in composites. In order to attain the uniform sized PBr machining particles, all the collected particles are undergone sieving process by the vibrating sieving machine shown in Figure 1.

Fig.1 Vibration Type Sieving Machine

The American standard sieves are 20 mm to 200 mm and they are designated based on the ASTM sieves E1 standards. The particles before and after sieving are shown in Figure 2.

A. Before Sieving B.After Sieving

Fig.2 Sieved Reinforcement Scrap Particles

In this study, Stir casting process as explained was employed to fabricate the aluminium matrix composite reinforced with phosphor bronze collected as scrap from industries. The stir casting process involves melting of the matrix metal at a temperature well below the melting temperature of metal. The reinforcement particles are then added to the molten metal and stirred for a standard time period using a mechanical stirrer. During the course of stirring, reinforcement material adheres to the base metal to form the metal matrix composite. The stir casting process involves melting of the matrix metal at a temperature well below the melting temperature of metal. The reinforcement particles are then added to the molten metal and stirred for a standard time period using a mechanical stirrer shown in Figure 3. There should be effective holding time of the metal matrix composites in the stir casting process. This effective holding time has a major advantage on the metal matrix composites such as distribute the particles in the liquid and create a perfect interface between the reinforcement and the matrix as shown in Figure 4. The composite specimens with 4% and 8% PBr scrap particles reinforcement are fabricated for testing the microstructure and mechanical properties.

Fig.3 Mechanical Stirrer

Fig.4 Stirring Process

2.2 Specimen Preparation

For our study, Wire-cut Electrical Discharge Machine (WEDM) is used for chipping out the specimen of required dimensions. Tungsten wire of diameter of 0.05–0.3 mm is used for cutting the specimen. A constant coolant supply ensures that the wire is not heated to a limit that it cuts-off. The coolant supply also lubricates the shearing process and does not allow damages to the work piece. The Wire EDM setup used for making the specimens is shown in Figure 5.

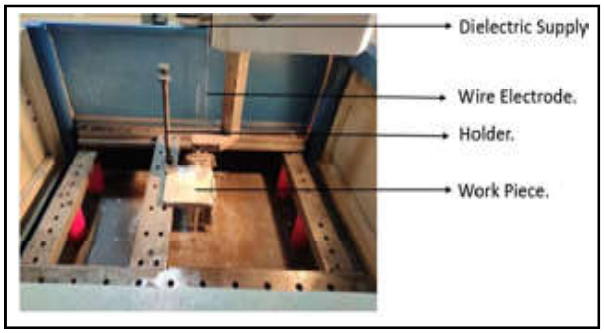

Fig.5 WEDM Setup

3. MICROSTRUCTURE ANALYSIS

The composite specimen of 1cm3 is taken to find the microstructure in optical microscope. The microstructure is analyzed to find the distribution of reinforcement particles in the composite. Manual polishing with course to fine grade emery polishing and subsequent double disk polishing is carried out with polisher. Etching is done with the Keller's Reagent which is a mixture of hydrochloric, nitric acid and hydrofluoric acid mixed along with distilled water under prescribed proportions to make ready for OM examination.

The images of Figure 6 & 7 shows the OM images of 4% wt. & 8% wt phosphor bronze reinforced AA6063 composites at 100 x magnification.

Fig.6 Image of 4% PBr Composite at 100x Magnification

Fig.7 Image of 4% PBr Composite at 100x Magnification

4. MECHANICAL PROPERTIES

4.1 Hardness Test

The Vickers hardness test was done on the prepared specimen by providing the indenter load of 5 kgf and the structural surface is viewed on the computerized hardness tester and readings are tabulated. The test results shown in Table 1 revealed an increase in the hardness property at 4% wt. and a decline in the same with 8% wt. addition of PBr Scrap particles reinforcement.

Table.1 Results of Vickers Hardness Test

Sl. No.	Specimens	Vickers Hardness (HV)
1	A1	89
2	AA 6063 with 4% PBr	132.5
3	AA 6063 with 8% PBr	93

Figure 8 clearly shows that an increase in hardness of the AA 6063 is possible with calculated addition of PBr as reinforcement, but decreases with further addition. This attributed that PBr 4% wt. itself fills all porosity. At 4% wt. on the addition of PBr the porosity in the AA 6063 gets filled up with the PBr particles and thus increases the hardness property. Thus, extra addition

above the 4% wt. PBr acts as a foreign particle invasion, thereby reducing its hardness property[5,6]. The indentation image generated though the Vickers hardness tester is appended as Figure 9. The distribution frequency graph for 4% wt. and 8% wt. of PBr in the composite is given in Figure 9 & Figure 10 respectively.

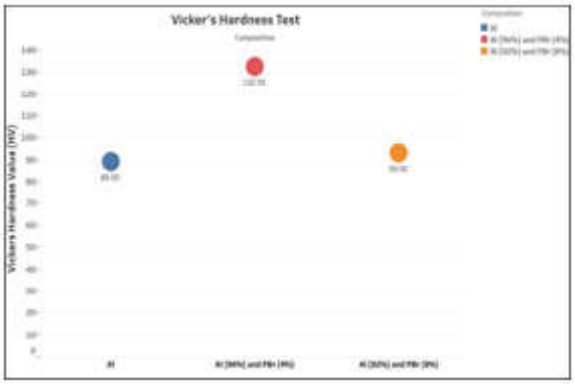

Fig.8 Graphical representation of vicker hardness test results

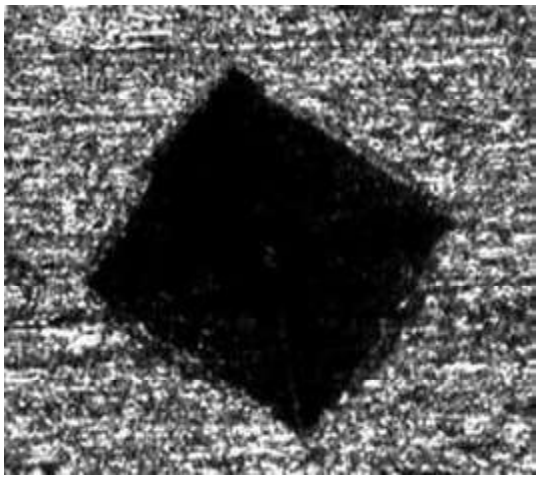

Fig.9 Image of Indentation generated in hardness test

4.2 Impact Test

Charpy impact test was performed to find the impact strength of the fabricated composite. The test results are tabulated in Table 2.

Table 2 Charpy Impact Test Results

Sl No.	Composition	Impact Value (J/mm^2)
1	Al	0.4
2	AA6063 with 4% PBr	0.0125
3	AA6063 with 8% PBr	0.025

A sharp decline in the impact strength of AA 6063 when PBr was added to it. Interestingly, the reduced impact strength at 4% wt. PBr had improved slightly on further addition of PBr i.e. at 8% wt. It is a clear indication from Figure 10, the impact strength of the prepared AMC has decreased when reinforced with PBr[7,8].

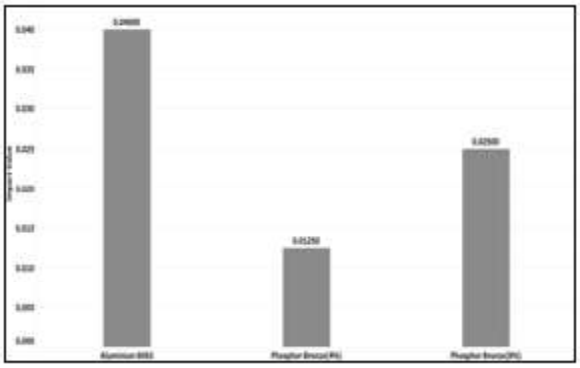

Fig.10 Graphical representation of charpy impact test results

4.3 Micro Tensile Test

The test results of Micro Tensile Test are shown in Table 3.

Table 3 Tensile Test Results in Elongation%

Sl. No.	Composition	Elongation (%)
1	Al	12
2	AA6063 with 4% PBr	5
3	AA6063 with 8% PBr	8.5

By observing the results, it was clear that there was a huge fall in the tensile property, measured by percentage elongation of material, with 4% wt. PBr addition to AA6063[9]. But there was a slight increase in the percentage elongation of 8% wt. PBr added AMC when compared with that of 4% wt. PBr added AA 6063 matrix[10]. Thus, the tensile properties as shown in Table No. 3 have drastically reduced on the addition of PBr to AA 6063, but the same improves with a further addition of PBr as depicted below in Figure 11.

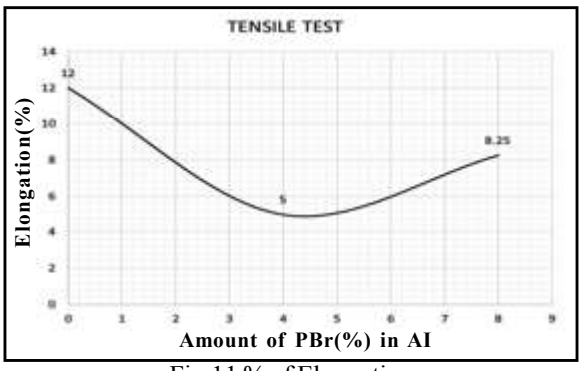

Fig.11 % of Elongation

4.3.1 Stress Strain Analysis

The stress- strain curve for 4% wt. and 8% wt. reinforced composites are given below in Figure 12.

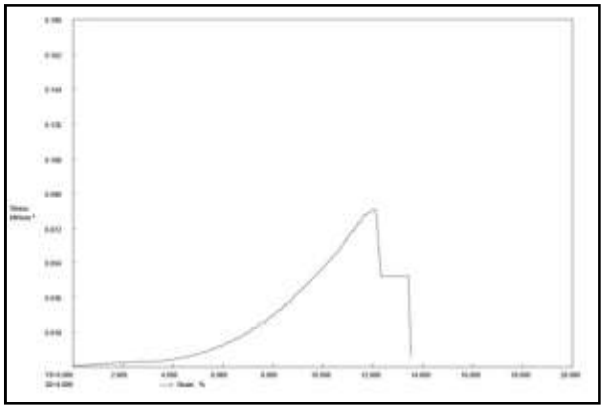

Fig.12 Stress-Strain Curve for 4% wt. PBr

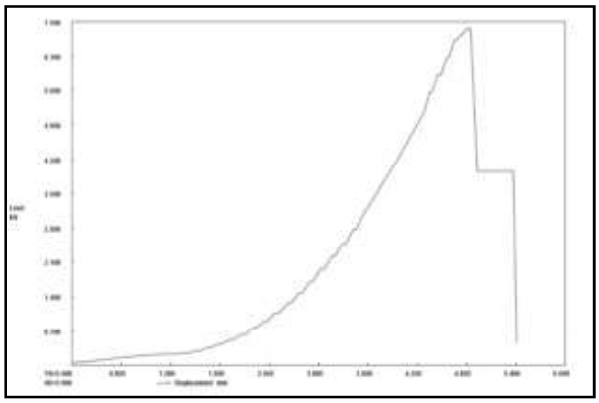

Fig.13 Stress-Strain Curve for 8 % wt. PBr

5. CONCLUSION

- The development and testing of Aluminium Matrix Composite with Phosphor Bronze as reinforcement material was done successfully in compliance with acclaimed standards.
- The results showed an enhancement in the hardness property of the AMC when calculated quantity of PBr is used as reinforcement.
- It is also found that the impact strength and tensile strength were decreased by the PBr reinforcement on AA 6063.
- Thus, calculated quantity of phosphor bronze can be used as reinforcement to improve the hardness of AA 6063.

REFERENCES

[1] K.K.Alaneme and B.U.Odoni, "Mechanical Properties, Wear and Corrosion Behavior of Copper Composites Reinforced with Steel Machining Chips", Engineering Science and Technology, an International Journal, 2016, Vol.19, pp.1593-1599.

[2] Md Sumair Ur Rahman and L.Jayahari, "Study of Mechanical Properties and Wear Behaviour of Aluminium 6061 Matrix Composites Reinforced with Steel Machining Chips", Materials Today: Proceedings , 2018, Vol.5, No.9, pp.20117-20123.

[3] K.K.Alaneme, K.O.Adeoye and S.R.Oke, "Mechanical and Wear Behaviour of Steel Chips Reinforced Zn27Al composites", Leonardo Electronic Journal of Practices and Technologies, 2016, Vol.29, pp.1-16.

[4] P. Iglesias, A.E.Jiménez, M.D. Bermúdz , B.C. Rao and S.Chandrasekar, "Steel Machining Chips as Reinforcements to Improve Sliding Wear Resistance of Metal Alloys : Study of a Model Zn-based Alloy System", Tribology International, 2013, vol 65, pp.215-227.

[5] A.Mohanvel, S.Suresh Kumar, T.Sathish, K.T. Anand, "Effect of ZrB2 Content on Mechanical and Microstructural Characterization of AA6063 Aluminum Matrix Composites", 2018, Vol.5, No.5, Part 2, pp. 13601-13605.

[6] Abhishek Kombaj, Sudir Kumar and Hari Singh, "Fabrication and Characterization of Al6063/SiC Composites", Proceedings of the Institution of Mechanical Engineers, Part B: Journal of Engineering Manufacture, 2013, Vol. 227, No.12, pp.234-239.

[7] V.Babu, B.P.Shanmugavel and K.A.Padmanabhan, "On the Microstructural Homogeneity and Mechanical Properties of Al 6063 Alloy Processed by the Cyclic Expansion Extrusion Process", Journal of Materials Engineering and Performance , Vol.29, 2020, pp.6870-6880.

[8] Shabana and R.V.Nikhil Santhosh, "Studying the Mechanical Properties of Aluminum 6063 Reinforced with Silicon Carbide and Mica", International Journal of Engineering and Advanced Technology, Vol.8, No.2S2, 2019, pp.153-156.

[9] I.Karthikeyan, V.Dhinakaran and V.Rajkumar, "Evaluation of Mechanical Properties of Aluminium 6063- Borosilicate Reinforced Metal Matrix Composite", AIP Conference Proceedings, Vol.2756, No.1, 2023, pp.24-32.

[10] Bassiouny Saleh, Bohai Ji, Reham Fa hi, Sensen Guo, Mahmoud H. Ahmed, Jinghua Jiang and Aibin Ma, "Utilization of Machining Chips Waste for Production of Functionally Gradient Magnesium Matrix Composites", Journal of Materials Processing Technology, Vol.308, 2022, pp.117702-117710.

MODELING AND ANALYSIS OF HEAT SINK OF A PROCESSOR (STEADY STATE THERMAL ANALYSIS)

K. Kamal Basha, N. Jayakumar, MKY. Paarthasarathy, V. Muralitharan and S.K.Vikneswaran
Department of Mechanical Engineering,
Bannari Amman Institute of Technology, Sathyamangalam-638 401, Erode District, Tamil Nadu
Email: kamalbasha@bitsathy.ac.in

Abstract

The use of electronic devices is increasing rapidly in various applications including aircraft, space vehicles, missiles, and ground stations. These devices generate a significant amount of heat during their operation, and if not properly managed, the heat can cause damage to the devices and reduce their lifespan. Heat sinks are commonly used to dissipate heat from electronic devices, and they play a crucial role in maintaining the temperature of the devices within the safe operating range. One of the most critical components in a computer that requires a heat sink is the processor (CPU) and GPU, which produce a substantial amount of heat during their operation. In addition to computers, heat sinks are used in other applications such as power electronics, telecommunication, and automotive elements. The design of an efficient heat sink depends on various factors such as fin geometry, base plate material, number of fins, and fin thickness, among others. Despite numerous efforts to develop a systematic method for determining an optimal layout for a heat sink, it remains a challenging task for designers. This research paper aims to analyze the thermal performance of a heat sink with rectangular fins having through holes for efficient cooling of electronic devices. The study will consider various geometric parameters to identify the optimal design of the heat sink. This paper will review the current literature on heat sinks, heat transfer, and thermal management techniques for electronic devices. The results of this study will provide valuable insights into the design of efficient heat sinks for electronic devices, particularly for processors in computers.

Keywords: *CPU, Electronic devices, GPU, Geometric parameters, Heat sink, Heat transfer, Optimal design, Processor, Thermal analysis, Thermal management.*

1. INTRODUCTION

Heat sinks are crucial components that disperse excess heat generated by electronic devices, including processors (CPU) and graphics processing units (GPU) in computers. Properly sized heat sinks maintain the semiconductor junction temperature at or below the maximum allowable temperature, ensuring optimal performance and longevity of electronic devices. The efficient dissipation of heat is achieved through a design and construction of a heat path from the device to the mounting surface and to the outside ambient. This paper will explore the thermal analysis of a heat sink in a processor, examining various geometric parameters that influence the optimal design[1].

1.1 Importance of Heat Sink in Electronic Devices

Electronic devices, including those used in strategic and military applications such as radars, communication sets, and amplifiers, generate a significant amount of heat. Inadequate thermal management can lead to reduced performance and even failure of the equipment. Thus, the design and implementation of a heat sink are critical to ensure efficient heat dissipation and the longevity of electronic devices[2].

1.2 Factors Affecting Heat Sink Design

Several geometric parameters influence the optimal design of a heat sink, including fin height, fin length, fin thickness, number of fins, base plate thickness, space between fins, fin shape or profile, and material[3]. A systematic approach to determining the optimal layout for a heat sink is challenging and requires consideration of all heat sources within an electronic circuit. To make FDM suitable for mass-production and more acceptable by industries, finding the optimal process parameters combination to improve the part quality and mechanical properties becomes of utmost importance.

1.3 Overview of Previous Research

Previous research has explored various aspects of heat sink design, including pin fin and slot parallel plate heat sinks with copper and carbon-carbon composite (CCC) base plate material, failure criteria, accelerated life testing, and modeling[4]. The ever-increasing miniaturization and functionality of microsystems packaging technologies present a challenge to thermal management techniques. Therefore, it is crucial to continuously improve and optimize heat sink design to ensure the efficient and safe operation of electronic devices[5].

1.4 Design Parameters

Design parameters must be taken into account when the system restrictions have been identified. The base plate thickness, the quantity, shape, and alignment of the fins, as well as the material of the heat sink, are all design considerations. Each of these characteristics has to be well-designed in order to get the lowest thermal resistance and pressure drop.

The following list of variables was taken into account when designing the heat sink:

- Material
- Number of fin
- Fin shapes

ANSYS is a software suite that provides engineering simulation solutions for a wide range of industries, including aerospace, automotive, energy, and biomedical. It offers a comprehensive set of simulation tools for structural, thermal, fluid dynamics, electromagnetic, and multiphysics analyses[6]. ANSYS is widely used in the engineering and manufacturing industries for product design, testing, and optimization. Its simulation capabilities enable engineers to make informed design decisions, reduce product development time and cost, and improve product performance and reliability.

1.4.1 Steady-State Thermal Analysis

Steady-state thermal analysis is used to calculate the effects of constant thermal loads on a system or component. In steady-state conditions, the temperature does not change with time, but remains constant over a period of time. It determines the temperature distribution, total heat flux, and directional heat fluxes of a heat sink with various fin geometries, such as rectangular fin and circular fin caused by thermal loads that do not vary over time. It is often performed before transient analysis to establish initial conditions[7,8].

1.4.2 Build Geometry

The flow of the coolant medium is greatly impacted by the arrangement of fins on a heat sink. Optimizing the configuration helps to reduce fluid flow resistance thus allowing more air to go through a heat sink. Its performance is also determined by the shape and design of its fins. Optimizing the shape and size of the fins helps to maximize the heat transfer density. Through modeling, the performance of different fin shapes and configurations can be evaluated[9]. To perform thermal analysis on a heat sink, a three-dimensional representation of the heat sink with rectangular, circular fins is modeled. The fins are assumed to have similar dimensions, thermal conductivity, material, and base temperature[10,11].

Mesh generation is the process of dividing a geometric domain into smaller subdomains called elements, which are connected at shared points called nodes or vertices. The resulting mesh can then be used for numerical simulations and analysis in various fields such as computational fluid dynamics, finite element analysis, and computer graphics[12,13] After constructing the geometry, ANSYS generates a mesh by breaking down the modeled system into finite pieces. This process ensures that the analysis accurately represents the physical behavior of the heat sink. Thermal analysis is essential for the design of efficient heat sinks[14,15]. The ANSYS Multiphysics software provides powerful tools for steady-state thermal analysis of heat sink designs with various fin geometries. By performing a steady-state thermal analysis, designers can determine the temperature distribution, total heat flux, and directional heat fluxes of the heat sink, providing a foundation for further optimization[16].

1.5 Factors for Designing Heat Sink

1.5.1 Major factors while designing a heat sink

- Thermal resistance
- Surface area
- Material
- Air flow
- Size and shape
- Compatibility
- Cost

- Thermal Resistance,Thermal resistance refers to the sum of resistances to heat flow between the die and the coolant fluid. These heat flow resistances include the resistance between the die and the component casing, the resistance between the casing and the heat sink (thermal interface resistance), and the resistance between the heat sink and the fluid in motion.
- Thermal resistance does not factor non-uniform heat distribution and it is unsuitable for modeling systems that are not in thermal equilibrium. Although the thermal resistance value is an approximation, it enables the modeling and analysis of the thermal characteristics of semiconductor devices and heat sinks.
- Surface Area Heat Sink, Surface Area has a significant impact on Heat Sink Thermal Performance in Forced Convection Applications. Increasing the surface area "exposed" to the air flowing in the area of the item being cooled is actually the fundamental function of a heat sink, which effectively removes heat using convection heat transfer.
- Material Heat sinks are designed using materials that have high thermal conductivity such aluminum alloys and copper. Copper offers excellent thermal conductivity, antimicrobial resistance, biofouling resistance, corrosion resistance, and heat absorption. Its properties make it an excellent material for heat sinks but it is more expensive and denser than aluminum.
- Heat sinks are typically made of etched silicon for small sizes, and metals such as aluminum and copper for larger sizes,because of their low price and good heat conductivity. Moreover, some heat sinks may combine multiple materials, such as copper with aluminum fins attached. Zinc may still be an excellent material for electronic cooling even if it has less thermal conductivity than copper and aluminum. When zinc is added to an alloy, porosity is removed during the casting process, giving it an advantage over copper and aluminium since they might not be completely free of pores after casting. Heat sinks are frequently made from materials with high thermal onductivity, as those in the table below (derived from the Heat and Mass Transport Data book Pg. No. 1), are commonly used for making heat sinks.
- Air Flow Because it is less dense and has a greater temperature, the air rises out of the heat sink. The heat sink will be cooled by the modest quantity of airflow created by this movement within the heat sink fins.
- Size and Shape Fin forms. There are numerous possible heat sink geometries. It is possible to have pin fins, straight fins, fluted fins, wavy fins, and fins with unconventional geometry. The most frequent ones are pin fins whose cross section might be circular, square, elliptical, hexagonal or any other acceptable shape.
- Compatibility Check under the Package Specs section for Sockets Supported. The part that establishes the mechanical and electrical connections between the processor and the motherboard is called a socket. Compare the Intel® CPU datasheet's TDP and socket information with the TDP and socket information of the CPU cooler.
- The cost of thermal conductive materials can vary widely depending on these factors like type of the material, Production process, Quality or purity. It's important to consider the specific requirements of the application and balance the cost of the material with its thermal performance and other properties to determine the most cost-effective solution. Diamond is the most thermally conductive material known, but it is also the most expensive. The cost of diamond varies depending on the quality and size, but it can range from thousands to tens of thousands of dollars per kilogram.

2. MATERIAL AND ITS PROPERTIES

Table 1 Material Table

INPUT				
Minimum TEMP	**Material**	**Thermal Conductivity in 25 DEG**	**Density g/CM3**	**Poisson Ratio**
90 deg	Aluminum Alloy 6063	210	2.69	0.3
	Copper Alloy 110	390.84	8.94	0.34

2.1 Design - Rectangular fin heat sink - Continuous Fins

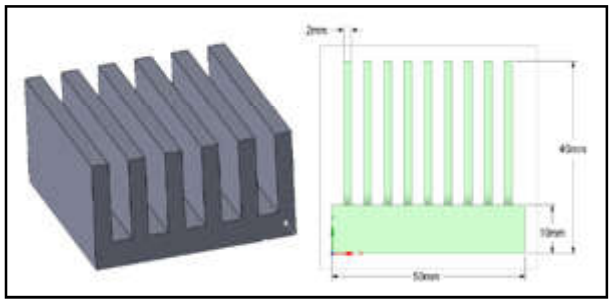

Fig.1 Design of rectangular fin

2.2 Design - Circular fin Heat sink - Discontinuous Fins

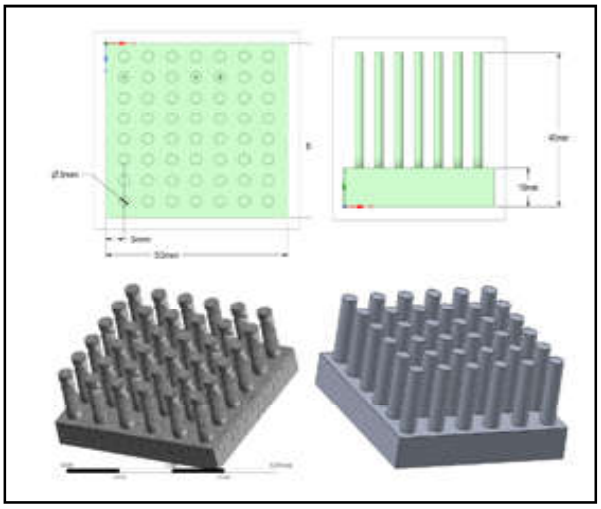

Fig.2 Design of Circular fins

2.3 Design-Rectangular Fin Heatsink-Discontinuous Fins

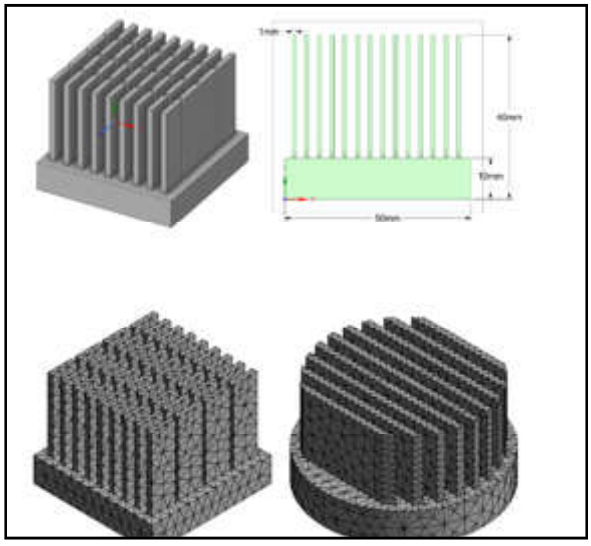

Fig.3 Meshing of Different fins

3. OBTAINED RESULT

Obtained results of Rectangular fins, Discontinuous rectangular fins, Circular fins, Circular base rectangular fins, Pins fins.

3.1 Rectangular fins

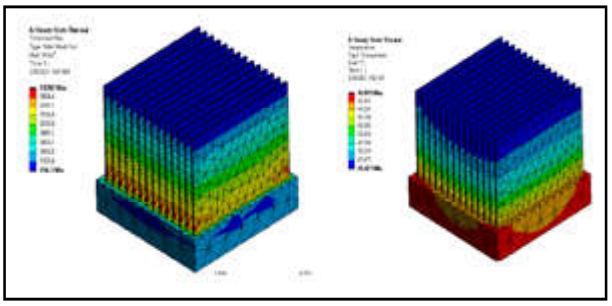

Fig.4 Temperature analysis of rectangular fins

3.2 Discontinuous Rectangular Fins

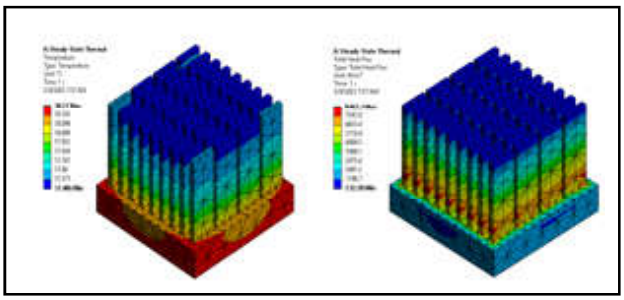

Fig.5 Temperature analysis of rectangular discontinuous fins

3.3 Circular base Pin Fins

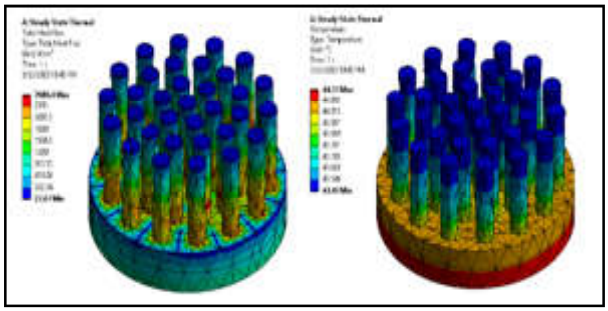

Fig.6 Temperature analysis of circular fins

3.4 Circular base Rectangular fins

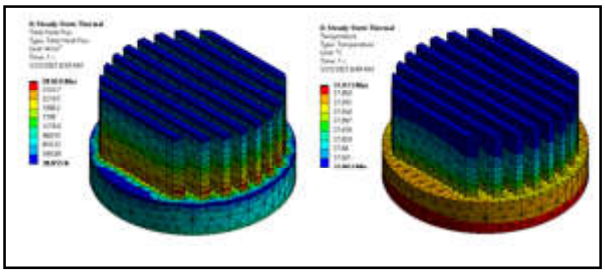

Fig.7 Temperature analysis of rectangular fins

Table 2 Obtained Temperature of Rectangular Fins

Rectangular fins				
Material Type	Avg Heat Flux (W/mk)	Temp max(c)	Temp min(c)	Temp avg(c)
Aluminum	4340.97	41.1464	40.3270	40.6538
Copper	4354.9	40.9093	40.4208	40.6161

Table 3 Temperature Analysis of Rectangular Discontinuous Fins

Discontinuous Rectangular Fins				
Material Type	Avg Heat Flux (W/mk)	Temp max(c)	Temp min(c)	Temp avg(c)
Aluminum	3597.14	38.2698	37.4861	37.8223
Copper	3604.47	38.0452	37.5786	37.7791

Table 4 Obtained Temperature of Circular Fins

Circular base Pin Fins				
Material Type	Avg Heat Flux (W/mk)	Temp max(c)	Temp min(c)	Temp avg(c)
Aluminum	1290.9	43.858	43.678	43.676
Copper	1292.2	43.815	43.708	43.670

Table 5 Obtained Temperature of Circular base Rectangular Fins

Circular base Rectangular Fins				
Material Type	Avg Heat Flux (W/mk)	Temp max(c)	Temp min(c)	Temp avg(c)
Aluminum	2227.6607	45.1012	44.7552	44.9156
Copper	2229.7190	45.0012	44.7955	44.8909

3.5 Pin fins

Table 6 Temperature Analysis of Pin Fins

Pin Fins				
Material Type	Avg Heat Flux (W/mk)	Temp max(c)	Temp min(c)	Temp avg(c)
Aluminum	2227.6607	45.1012	44.7552	44.9156
Copper	2229.7190	45.0012	44.7955	44.8909

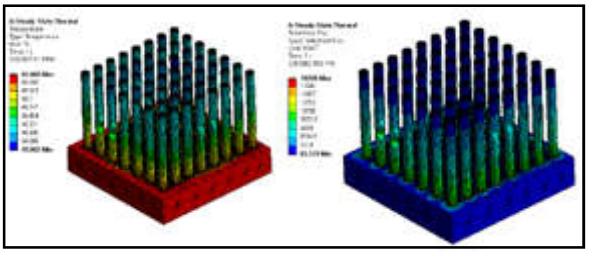

Fig.6 Temperature analysis of pin fins

4. RESULTS AND DISCUSSION

From the above analysis we can find out that aluminum Discontinuous rectangular heat fins gives us better result of Temperature(c)= 37.82238289 Then weight of aluminum Discontinuous rectangular heat fins lesser than copper Discontinuous rectangular heat finsTherefore, based on the results of this project, the use of discontinuous rectangular aluminum fins could be a cost-effective and efficient solution for enhancing heat transfer while minimizing weight and cost in various thermal applications.Interrupted rectangular fins offer several advantages over other fin geometries. That is because of the larger surface area for heat transfer compared to a continuous fin of the same dimensions. This increased surface area allows for more efficient heat dissipation, which can help to reduce the operating temperature of the system and improve its overall performance.

This chapter focuses on the study and presentation of various heat sink designs. The finite-volume approach is used in this program, which involves integrating the governing equations over a control volume to obtain the discretized equations. To begin with, the computational

domain is subdivided into a finite number of control volumes. The method is locally conservative as it is based on a local balance of fluxes in each control volume. In simpler terms, the approach used involves dividing the computational domain into smaller volumes and then applying mathematical equations to each of these volumes to obtain solutions for heat transfer. The method ensures that the total amount of heat entering a volume is equal to the total amount of heat leaving it, thereby ensuring that the method is locally conservative[17,18].

5. CONCLUSION

In this project, a comprehensive thermal analysis of different heat sink designs has been conducted using SolidWorks and ANSYS software. The aim of the study was to optimize the design of a heat sink to improve its thermal performance while considering its cost-effectiveness and aesthetic appeal. The results of the study showed that the interrupted rectangular fin design performed better than the rectangular fin, circular fin, and triangular fin designs in terms of total heat flux. This indicates that the interrupted rectangular fin design is more efficient in cooling electronic components. Furthermore, by altering the design of the aluminum heat sink, a higher heat transfer rate can be achieved, which is desirable for better thermal performance. The findings of the study also highlight the importance of aesthetics in designing heat sinks, as it is a critical factor in determining their competitiveness in the market. In addition to thermal performance, the production cost of the heat sink is also an important consideration, and the use of compact designs can help reduce material and production costs.

The study concludes that ANSYS software can be effectively used for the optimization of heat sink designs, which can ultimately result in the development of heat sinks with better thermal performance and reduced material usage. By considering all the factors, it is possible to create a heat sink design that is both cost-effective and aesthetically pleasing while also providing optimal thermal performance.

REFERENCE

[1] R.Dadsetani, G.A.Sheikhzade, M. Goodarzi, A. Zeeshan, R.Ellahi and M.R.Safaei, "Thermal and Mechanical Design of Tangential Hybrid Microchannel and High-Conductivity Inserts For Cooling Of Disk-Shaped Electronic Components", Journal of Thermal Analysis and Calorimetry. doi:10.1007/s10973-020-10232-w, 2020.

[2] K.Timbs, M.Khatamifar, E.Antunes and W.Lin, "Experimental Study on the Heat Dissipation Performance of Straight and Oblique Fin Heat Sinks Made Of Thermal Conductive Composite Polymers", Thermal Science and Engineering Progress, doi:10.1016/j.tsep.2021.100848, Vol.22, 2021, pp.100848.

[3] S.Meganathan, R. Arunkumar and A.Ponshanmugakumar, "Numerical Analysis of Passive Heat Sink for Different Shapes", Materials Today: Proceedings, doi:10.1016/j.matpr.2021.02.014, Vol.46, 2021, pp.3749-3755.

[4] B.Freegah, A. A.Hussain, A.H.Falih and H.Towsyfyan, "CFD Analysis of Heat Transfer Enhancement in Plate-Fin Heat Sinks with Fillet Profile: Investigation of New Designs", Thermal Science and Engineering Progress, doi:10.1016/j.tsep.2019.100458, 2019, pp.100458..

[5] H.E. Ahmed, B.H.Salman, A.S.Kherbeet and M.I.Ahmed, "Optimization of Thermal Design of Heat Sinks: A Review", International Journal of Heat and Mass Transfer, doi:10.1016/j.ijheatmasstransfer., Vol.118, 2018, pp.129-153.

[6] V.Naga Raju, P.Sivakumar, K.Lakshmi Narayana, A.Srujan, K.Mallikarjun and G Krishna, "Steady State Thermal Analysis of Heat Sink with Fins of Different Geometry", International Journal of Mechanical Engineering and Technology, Vol.8, No.5, 2017, pp.196-206.

[7] M. Chandra Sekhar Reddy, "Thermal Analysis of A Heat Sink For Electronics Cooling", International Journal of MechanicalEngineering and Technology, Vol.6, No.11, 2015, pp.145-153.

[8] R.Ali and M.T.I.Khan, "Heat Transfer Enhancement of a Plate-Fin Heat Sink Using Triangular Fins: A Numerical Investigation", International Journal of Engineering and Technology, doi:10.14419/ijet.v7i3.2.11338, Vol.7, No.3.2, 2018, pp.128-134.

[9] M.K. Raja, T.Iyappan and P.K. Nagarajan, "Heat Sink Optimization for CPU Cooling", AIP Conference Proceedings, 2016, 030090. doi:10.1063/1.5054505, 2018.

[10] Z.Yan, X. Ma, L.Sun and H. Zhang, "Numerical Analysis of the Heat Sink with Integrated Phase Change Material", Journal of Applied Fluid Mechanics, doi:10.29252/jafm.13.03.26547., Vol.13, No.3, 2020, pp.815-823.

[11] X.Bao, Y. Wang, and Y. Zhu, "Analysis of Heat Transfer Performance and Pressure Drop of a New-Type Heat Sink", Applied Thermal Engineering, doi:10.1016/j.applthermaleng., Vol.177, 2020, pp.115272.

[12] Y. Zhu, Y. Wang, and Y.Liu, "Thermal Performance Analysis of a Compact Heat Sink with Inner Micro-Channel Array", International Journal of Heat and Mass Transfer, doi:10.1016/j.ijheatmasstransfer., Vol.153, 2020, pp.119604.

[13] C.Chen, R. Wang, B. Yang, Y. Zhao and Y.Qian, "Thermal Analysis of Heat Sink in Three-Dimensional Printing Electronics Packaging". Journal of Mechanical Engineering, doi:10.3901/jme.2020.12.031., Vol.56, No.12, 2020, pp.31-39.

[14] Q.Wang, J.Li, L.Li, Y.Li and W.Li, "Experimental Study and Numerical Analysis of a Novel Cooling Module for Electric Vehicle Battery Thermal Management. Applied Thermal Engineering, Vol.186, 2021, pp.116432.

[15] S.Ravikumar., *et al* IOP Conf. Ser.: Mater. Sci. Eng., Vol.197, 2017, pp.012085.

[16] R. Singh, K.M. Pandey, and R.K. Pandey, "Numerical Simulation of Rectangular Pin Fin Heat Sink with Nanofluids", Materials Today: Proceedings, doi:10.1016/j.matpr.2017.12.305., Vol.5, No.2, 2018, pp.7422-7428.

[17] Ansys Mechanical APDL Verification Manual R2021.

[18] A Textbook on Strength of Materials, R K Bansal.

TIME AHEAD FOLK PROPHECY

K.T. Maheswari, R. Bharanikumar and M.S. Ajay Vishnu
Department of Electrical and Electronics Engineering,
Bannari Amman Institute of Technology, Sathyamangalam - 638401, Erode District, Tamil Nadu
Email:maheswarikt@bitsathy.ac.in, bharanikumar.rbk@gmail.com

Abstract

Today's populations are increasing which is unpredictable by a common individual. Also, it becomes harder for him to do construction of the correct volume needed for the upcoming year. This can be solved by providing a future population-finding model. Neighborhood and state legislatures rely upon little region populace figures to make significant choices concerning the advancement of nearby frameworks and administrations, including tutoring, transportation, medical services, energy, media communications, and water supply. Regardless of their significance, current techniques frequently produce profoundly incorrect figures, particularly at the little region scale. Ongoing years have seen promising improvements in time series gauging utilizing Artificial Intelligence across a great many social and financial factors. In the proposed work, Machine Learning helps us to solve many problems as we can solve future population predictions. The objective of this paper is to analyze the particular area for prediction and knowing the need for prediction. Then gather the best dataset for that specific area of a specific need to be predicted. With the help of a Machine Learning algorithm, the issue can be solved more precisely. Then a perfect Machine Learning model to be selected which will be more suitable for our gathered dataset. Power Bi is used for a more interactive dashboard for the user which gives a better understanding of the prediction output data. By proper implementation of the methodology, the user will be able to know his construction or business volume need to be inputted.

Keywords: *Administrations, Constructions, Frameworks, Machine Learning, Prediction, Population.*

1. INTRODUCTION

Little region populace gauges are broadly involved by government and business for some reasons. They illuminate choices about the development and allotment of subsidizing for streets, schools, matured care administrations, transport, and wellbeing administrations, among different purposes [1]. However little region populace conjectures will generally be definitely more inclined to mistake than gauges at bigger geologies. The more modest the populace, the bigger the mistake will in general be, especially for populaces of only a couple thousand individuals [2]. To some degree, this is on the grounds that information sets for little regions frequently have brief time frame series, less definite information, information quality issues, and loud examples [3].

In any case, it is additionally because of the restricted measure of exploration devoted to little region populace estimating contrasted with public level gauging. Lately one of the key regions for systemic advancements in time series estimating has happened in Machine Learning (ML). Not with standing, writing researching the turn of events and assessment of these techniques on little region populace datasets stays restricted [4].

Ongoing years have seen promising improvements in time series gauging utilizing AI across a great many social and financial factors. In any case, basically, no work has been embraced to research their likely application in demography, especially for little region populace gauging. In this paper, we depict the improvement of two Long-Transient Memory network models for work with little region populaces.

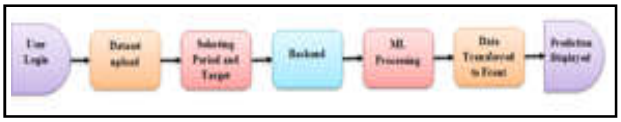

Fig.1 Block Diagram

We utilize the Keras Tuner to choose layer unit numbers, shift the window width of information, and apply a twofold preparation and approval system which supports work with brief time frame series and focuses

on later grouping values for estimates. These strategies are adaptable and can be applied to different informational collections. Review little region populace figures for Australia were made for the periods 2006-16 and 2011-16. Model execution was considered in contrast to genuine information and two benchmark strategies. The profound learning techniques delivered estimated mistakes similar to the benchmark techniques, particularly working on the 2006-based conjectures, yet not 2011-based figures created by one of the benchmark techniques.

Now a days we couldn't predict the future population for our Business. Road and building constructions to be constructed in required measures. Amount of croup cultivation to be known. To increase the country's economy structure [5]. Prof Stein Emil Vollset, DrPH has discussed the possible examples of future populace levels is basic to anticipating and making arrangements for changing age designs, asset and medical services needs, and ecological and monetary scenes. Future richness designs are a vital contribution for assessing future populace size, however they are encircled by extensive vulnerability and contrasting assessment and determining procedures, prompting huge contrasts in worldwide populace projections. Changing populace size and mature design can have significant financial, social and international effects in numerous nations.

Tom Wilson, Irina Grossman, Monica Alexander, Phil Rees & Jeromey Temple has discussed little region populace estimates are generally involved by government and business for different preparation, examination and strategy purposes and frequently impact significant speculation choices. In any case, the tool stash of little region populace guaging strategies and procedures is unassuming contrasted with the apparatuses for public and huge subnational provincial estimating. In this paper, we survey the present status of populace expectation in little regions and recommend regions for additional exploration. The article gives an outline of the writing on populace estimating techniques in little regions distributed in the period 2001-2020.

The primary objective of this paper is to improve the overall efficiency of population forecasting by building long-term structures, creating user friendly Propect model, to create accurate Machine Learning Model, to build back-end server using Flask and to build Good looking UI using Angular

2. METHODOLOGY BLOCK DIAGRAM

The proposed Block diagram shown in Fig.1 gives the flow of Data from User to ML model and back to frontend for result display [6-8].

2.1 Login Page

User has to login to the web app with credentials of sign up with his e-mal id. This login page is created with Angular CLI. In login page when user try to login it verifies the credentials with existing data. It is connected to Mongo DB via Flask – Backend Server. After verification then it directs to Data input page. In case of new user data entered in signup tab will be sent to backend server. Now this user is added into database and he can access the web-app anytime needed.

2.2 User Input

After user login in this page user has to upload his dataset for a specific area. Then he has to click on upload button. At that time the data set will be upload into database. Then he has to select period of time e.g., daily, weekly, monthly, quarterly, yearly. After selecting period, he has to select target means how many long data to be predicted. Finally summit button is clicked so that prediction process will be initiated in backend.

2.3 REST API Call

To send GET requests with query URL strings and parameters and process HTTP responses from REST API servers in your Angular 12 application using Httplient to retrieve and consume JSON data how to perform error handling for HTTP errors using RxJS throwError() and catchError() operators how retrying failed HTTP requests on bad network connections and canceling outstanding requests using RxJS retry() and takeUntil() operators [9].

2.4 Flask Server

Flask is a web application written in Python. It is developed by Armin Ronacher, who leads an international group of Python enthusiasts called Pocco. Flask is based on the Werkzeug WSGI toolkit and the Jinja2 template. Both are Pocco projects.

2.5 Machine Learning

Prophet is a procedure for forecasting time series data based on an additive model where non-linear trends account for annual, weekly and daily seasonality plus holiday effects. It works best with time series that have strong seasonal effects and several seasons of historical data. Prophet is robust to missing data and shifts in trend and usually handles outliers well [10].

2.6 Data Displayed

After all pre-processing, data training and prediction data is then transferred to frontend and displayed in chart format for better understanding. For chart ChartJS library is used for better understanding.

2.7 Power Bi

Power BI is an interactive data visualization software product developed by Microsoft with a primary focus on business intelligence. It is part of the Microsoft Power Platform. Power BI is a collection of software services, applications, and connectors that work together to transform disparate data sources into coherent, visually immersive, and interactive insights. Data can be entered by reading directly from a database, web page, or structured files such as tables, CSV, XML, and JSON.

3. PROPHET MODEL

3.1 Population Data

Population data were obtained for the longest available time series on a consistent set geographical boundaries for statistical area level 2 (SA2) areas, the smallest official spatial the unit for which estimated population figures (ERPs) have been published (ABS, 2017). The data consists of annual ERP totals for the period 1991 to 2016 (ABS, 2017) based on 2011 geographical boundaries. The 2016 median SA2 population in Australia was 9,681 with 95% lying between 2,559 and 29,279. SA2 areas with population less than 100 in any of the years assembly period were excluded from model training. These populations were merged into a "residual" area that was excluded from training but included in the forecasts so that forecasts can be limited to a national forecast. National population forecasts were required as data inputs or constraints for small area forecasts. We used the main series forecasts produced by the ABS that were closest to 2006 and 2011 leap year forecasts (ABS 2008, 2013a).

3.2 Data Pre-processing

Pre-processing refers to the transformations applied to our data before feeding it to the algorithm. Data pre-processing is a technique that is used to convert raw data into a clean data set. In other words, whenever data is collected from various sources, it is collected in a raw format that is not feasible for analysis [11-12].

3.3 The Need for Data Pre-processing

To get better results from the model used in machine learning projects, the data format must be correct. Some specified machine learning models need information in a specified format, for example the Random Forest algorithm does not support nulls, so to run the random forest algorithm, nulls must be managed from the original raw data set.

Another aspect is that the dataset should be formatted to run more than one machine learning and deep learning algorithm on a single dataset and select the best one.

3.4 Time Series Forecasting

Time series forecasting is the process of analyzing time series data using statistics and modeling to make predictions and inform strategic decision making. This is not always an accurate forecast, and the probability of forecasts can vary widely – especially when dealing with commonly fluctuating variables in time series data as well as factors beyond our control. Predictive insight into which outcomes are more likely – or less likely – than other potential outcomes. It is often the case that the more complex the data we have, the more accurate the forecasts can be. While forecast and "forecast" generally mean the same thing, there is a significant difference.

In some industries, forecasting may refer to data at a specific future point in time, while prediction refers to future data in general. Series forecasting is often used in conjunction with time series analysis. Time series analysis involves developing models to gain insight into the data and understand underlying causes. Analytics can provide the "why" behind the results you see. Forecasting then represents the next step in what to do with that knowledge and predictable extrapolations of what may happen in the future.

3.5 When Time Series Forecasting Should be Used

Of course, there are limitations when dealing with the unpredictable and the unknown. Time series forecasting is not infallible and is not appropriate or useful for all situations. Because there really isn't an explicit set of rules for when you should or shouldn't use forecasting, it's up to analysts and data teams to know the limitations of the analysis and what their models can support. Not every model will fit every data set or answer every question. Data teams should use time series forecasting when they understand a business question and have the appropriate data and forecasting capabilities to answer that question. A good forecaster works with clean, time-stamped data and can identify real trends and patterns in historical data. Analysts can distinguish between random fluctuations or outliers and can separate real insights from seasonal variations. Time series analysis shows how the data changes over time, and a good forecast can determine the direction in which the data is changing [13-14].

3.6 New in Prophet

When the forecasting model is not running as planned, we want to be able to tune the parameters of the method with respect to the specific problem. Tuning these methods requires a thorough understanding of how the underlying time series models work. The first input parameters for automated ARIMA are, for example, maximum orders of differentiation, auto-regressive components and moving average components. The typical analyst will not know how to modify these commands to avoid the behaviour, and that is the type of expertise that is difficult to acquire and expand.

The Prophet package provides intuitive parameters that are easy to tune. Even someone who lacks expertise in forecasting models can use it to generate meaningful forecasts for various problems in a business scenario.

3.7 Prophet Forecasting Model

We use a decomposable time series model with three main model components: trend, seasonality, and holidays. They are combined in the Equation (1):

$$y(t)=g(t)+s(t)+h(t)=\varepsilon_t \quad (1)$$

Where **g(t):** piecewise linear or logistic growth curve for modeling non-periodic changes in time series

s(t): periodic changes (e.g. weekly/annual seasonality)
h(t): effects of holidays (provided by the user) with irregular timetables
ε_t: the error term takes into account all unusual changes that the model did not handle

Using time as a regressor, Prophet attempts to fit several linear and non-linear functions of time as components. Modeling seasonality as an additive component is the same approach as exponential smoothing in the Holt-Winters technique.

3.8 Trend

A trend is modelled by fitting a piecewise linear curve over the trend or non-periodic part of the time series. A linear fit exercise ensures that it is least affected by spikes/missing data.

3.9 Nourishing Growth

An important question to ask here is – Do we expect the target to rise/fall throughout the forecast interval? More often there are cases with non-linear growth with running maximum capacity. Let us see an example below. Fig.2 shows the nourishing growth.

Let's say we're trying to predict the number of app downloads in a region for the next 12 months. The maximum number of downloads is always limited by the total number of smartphone users in the region. However, the number of smartphone users will increase over time. With the domain knowledge at his disposal, the analyst can define the variable capacity C(t) for the time series forecasts he is trying to make.

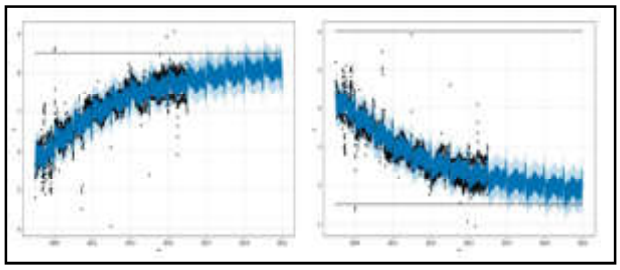

Fig.2 Nourishing growth

3.10 Points of Change

Another question to answer is whether my time series is encountering any major changing phenomena, e.g. a new product launch, an unforeseen calamity, etc. At such points, the growth rate may change. These change points are selected automatically. However, the user can also

enter change points manually if needed. In the graph below, the dotted lines represent the change points for that time series.

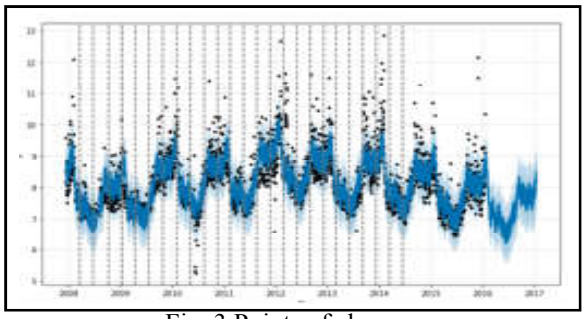

Fig. 3 Points of change

As the number of change points allowed increases, customization becomes more flexible. Basically, there are 2 problems that an analyst can face when working with the trend component , Overgrazing and Under-equipped. A parameter called changepoint prior scale can be used to adjust the flexibility of the trend and solve the above 2 problems. A higher value will fit a more flexible curve to the time series.

3.11 Seasonality

To adjust for and predict the effects of seasonality, Prophet relies on Fourier series to provide a flexible model. Seasonal effects s(t) are approximated by the following function (2):

$$s(t) = \sum_{n=1}^{N} \left(a_n \cos\left(\frac{2\pi nt}{P}\right) + b_n \sin\left(\frac{2\pi nt}{P}\right) \right) \quad (2)$$

Where P is the period (365.25 for yearly dates and 7 for weekly dates). The parameters [a1, b1, ….., aN, bN] need to be estimated for a given N to model seasonality.

The Fourier order N, which defines whether high frequency changes are allowed to be modelled, is an important parameter to set here. For a time-series, if the user believes that the high-frequency components are just noise and should not be considered for modelling, they could set the N od values to a lower value. If not, N can be tuned to a higher value and set using the prediction accuracy.

3.12 Holidays and Events

Holidays and events cause predictable shocks to the time series. For example, Diwali in India is held on a different day every year and a large part of the population buys a lot of new things during this period.Prophet allows the analyst to provide a custom list of past and future events. The window around these days is considered separately and other parameters are adjusted to model the effect of holidays and events.

4. RESULTS AND DISCUSSION

4.1 Frontend Design

In the Figure4 and Figure5 shows the User login and signup page in which user can enter into the prediction web app. If the user is new, he needs to create an account in signup page. When he enters his details, those data will be sent to backend and stored in Mongo dB database server. After all these processes he will be redirect to data entry page.

Fig.4 Login Page

Fig.5 Signup Page

The Figure 6 shows the data entry page where the user needs to upload the population dataset to the server. After the data entry completed prediction process will takes place in backend server.

Fig.6 User Data Entry Page

4.2 Output Chart

The Figure 7 shows the final output of prediction from our ML model used, Which is displayed in Line chart for better understanding.

Fig.7 Result Output Page

4.3 Power BI

The Figure 8, Figure 9 and Figure 10 shows the Power Bi dashboard of our predicted and preprocessed unpredicted dataset. Power Bi is a powerful tool for making dashboard like this it hakes the data more interactive and gives us better understanding of data than before.

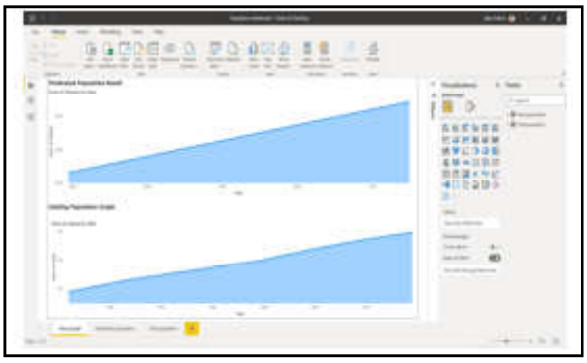

Fig.8 Powerbi Dashboard 1

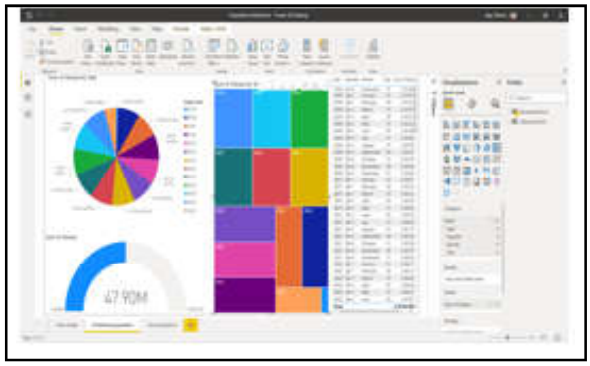

Fig.9 Powerbi Dashboard 2

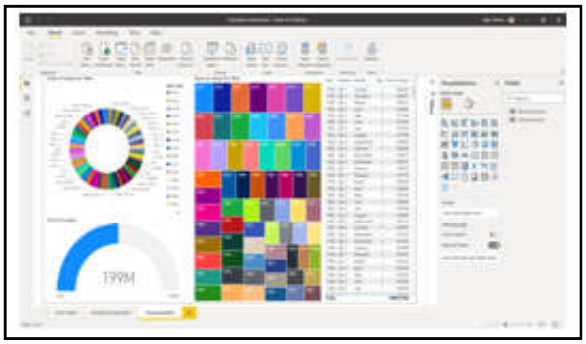

Fig.10 Powerbi Dashboard 3

5. CONCLUSION

Prophet's ease of use has made it a very good base model where your time series are easily split into simple time components. However, if your signal is noisy, fine-tuning the model's performance can be problematic. If your time series follow certain business cycles, you can achieve very decent performance quickly, without intensive feature engineering. However, the trend component is not always well estimated, which can cause significant performance drifts. Because of this, this model may require close monitoring and frequent human intervention. Hence the population forecasting is done successfully and displayed to user. And our objectives are all completed. Prophet is definitely a good choice for making quick and accurate predictions. It has intuitive parameters that can be tuned by someone who has good domain knowledge but lacks technical skills in predictive models. Readers can also try and fit Prophet directly to hourly data and discuss in the comments if they are able to get a better result.

REFERENCES

[1] Prof.Stein Emil Vollset,DrPH., "Fertility, Mortality, Migration and Population Scenarios for 195 Countries and Territories from 2017 to 2100: A Forecasting Analysis for the Global Burden of Disease Study",

[2] Adrian E.Raftery, Hana Sevcikova, "Probabilistic Population Forecasting: Short to Very Long-term",Oct,2017.

[3] Tom Wilson, Irina Grossman, Monica Alexander, Phil Rees & Jeromey, "Temple-Methods for Small Area Population Forecasts: State-of-the-Art and Research Needs", 2022, pp.865-898.

[4] Monica Alexander, Emilio Zagheni and Magali Barbieri, "A Flexible Bayesian Model for Estimating Subnational Mortality", 2017, Vol.54, No.6, pp.2025-2041.

[5] Leontine Alkema and Jin Rou New, "Global Estimation of Child Mortality Using a Bayesian B-spline Bias-Reduction Model, DOI: 10.1214/14-AOAS768., Ann. Appl. Stat., Vol.8, No.4, December 2014, pp.2122-2149.

[6] Renato M. Assunēćo, Carl P. Schmertmann, Joseph E. Potter and Suzana M. Cavenaghi, "Empirical Bayes Estimation of Demographic Schedules For Small Areas", Demography, Vol.42, No.3, 2005, pp.537-558.

[7] Jamal Fattah,Latifa Ezzine,Zineb Aman,Haj El Moussami and Abdeslam Lachhab, "Forecasting of Demand Using ARIMA Model", October 2018 International Journal of Engineering Business Management Vol.10, No.2, DOI:184797901880867.

[8] Haiyan Song and Gang Li, "Tourism Demand Modeling and Forecasting- A Review of Recent Research. January 2008 International Journal of Hospitality Management, Vol.22, No.4, pp.435-451.

[9] M.J. Baker and S.Hart, "The Marketing Book", Seventh Edition. April 2016, DOI:10.4324/9781315890005.

[10] Tereza Sustrova, "An Artificial Neural Network Model for the Wholesale Company Order's Cycle Management. June 2016 International Journal of Engineering Business Management, Vol.8, No.21, DOI:10.5772/63727, LicenseCC BY 4.0.

[11] Gulden Kaya Uyanik, Sakarya University, Nese Guler, "A Study on Multiple Linear Regression Analysis", December 2013 Procedia - Social and Behavioral Sciences, DOI: 10.1016/j.sbspro.2013.12.027., Vol.106, pp.234-240.

[12] Marcelo de Maio Nascimento, Elvio R Gouveia, Bruna R. Gouveia and Adilson Marques, "Exploring Mediation Effects of Gait Speed, Body Balance, and Falls in the Relationship Between Physical Activity and Health-Related Quality of Life in Vulnerable Older Adults", October 2022 International Journal of Environmental Research and Public Health, DOI:10.3390/ijerph192114135, Vol.19, No.21.

[13] Doaa Mohamed Tahoon, Noura Anwar Abdel-Fatah and Yasmine Sabry, "Social vulnerability of historic Districts: A Composite Measuring Scale to Statistically Predict Human-made Hazards", October 2022 Ain Shams Engineering Journal, DOI:10.1016/j.asej.2022.102002.

[14] Takele Atnafu, Giziew Almaz and Birhanu Melesse Gelaw, "Determinants of Soybean (Glycine max.) Market Supply in Northwestern Ethiopia", 1-DOI:10.1080/23322039.2022.2142313, November 2022 Cogent Economics & Finance, Vol.10, No.1.

OBSTACLE AVOIDANCE USING RPLIDAR S2

D. Selvamuthukumaran[1], R. Santhoosh[2] and P. Sakthivel[3]
[1]Department of Mechanical Engineering
[2,3]Department of Electrical and Electronics Engineering
Bannari Amman Institute of Technology, Sathyamangalam - 638 401, Erode Distrcit, Tamil Nadu
E-mail:selvamuthukumaran@bitsathy.ac.in

Abstract

This paper presents autonomous navigation i.e.., Obstacle avoidance of a robot using the SLAM algorithm. Collision avoidance is a critical requirement for any autonomous robot, and the core sensor of the robot is a two-dimensional lidar, which collects depth information from the environment the simulation is important for testing the software components, robot behaviour, and control algorithms in different surrounding environments. The proposed work uses the Robot Operating system as a framework and RP LIDAR S2 as its core sensor. The robot's created algorithm is simulated in the gazebo and Rviz is used for data visualization. A mapping package is used for mapping by utilizing laser and odometry data from the sensors. The created algorithm is based on Turtlebot which provides open- source software to perform navigation. The results of this experiment show that the robot can avoid objects in its path or stop if they are unavoidable. Following the experiment results, a discussion of problems and solutions is presented.

1. INTRODUCTION

Collision avoidance is a critical requirement for any autonomous robot, and simulation environments like Gazebo provide a safe and efficient way to test and develop such systems. The RPLIDAR S2 is a 2D laser scanner that is widely used for obstacle detection and avoidance in robotic applications[1]. In this paper, we will discuss the implementation of collision avoidance using RPLIDAR S2 in a mobile robot simulation environment created in Gazebo. The simulation environment provides a realistic and customizable environment for testing and evaluating collision avoidance algorithms[1]. We will discuss setting up the simulation environment, including creating a robot model and configuring the RPLIDAR S2 sensor. We will then describe the collision avoidance algorithm used in the simulation, which calculates the safe distance between the robot and obstacles in its path using data from the RPLIDAR S2. If the distance is too close, the robot is instructed to change its direction and avoid the obstacle. We will also discuss the advantages and limitations of using a simulation environment like Gazebo for collision avoidance testing. Advantages include the ability to test in a safe and repeatable environment, while limitations include the lack of real-world variability and the need for accurate modelling. Overall, collision avoidance using RPLIDAR S2 in a Gazebo simulation environment is an effective way to test and develop collision avoidance algorithms for autonomous robots. The simulation provides a realistic and customizable environment for testing and evaluating algorithms, allowing for faster and safer development of collision avoidance systems.

1.1 Applications

- Autonomous Vehicles: The most obvious application of collision avoidance using RP LiDAR S2 is in autonomous vehicles. Self-driving cars, trucks, and drones can use the sensor to detect obstacles in their path and avoid collisions[2].
- Robotics: Robots in manufacturing plants, warehouses, and other industries can use collision avoidance to navigate around obstacles and avoid collisions.
- Agriculture: Autonomous tractors and drones can use RP LiDAR S2 to navigate through crop fields, avoid obstacles, and detect crops for precision agriculture.
- Security and Surveillance: Security robots can use the sensor to navigate through buildings and detect intruders while avoiding obstacles.
- Mapping and Surveying: RP LiDAR S2 can be used in mapping and surveying applications to create 2D and 3D maps of buildings, roads, and other structures.
- EnvironmentalMonitoring: Autonomous drones equipped with RP LiDAR S2 can be used for environmental monitoring, such as monitoring forest fires, tracking wildlife, and assessing the health of ecosystems.

- Medical Robotics: RP LiDAR S2 can be used in medical robotics for navigation and collision avoidance in surgeries and other medical procedures.
- In conclusion, collision avoidance using RP LiDAR S2 has a diverse range of applications across various industries, making it an essential tool for ensuring safety in autonomous vehicles, robotics, and other applications.

2. METHODOLOGY

To implement collision avoidance using the RP LiDAR S2, ROS, SLAM, and Gazebo, we first need to connect the sensor to a computer and install the ROS package for the LiDAR sensor. The LiDAR sensor provides 2D point cloud data that contains the coordinates of the obstacles detected by the sensor. The ROS package can process this data and generate a 2D map of the environment.We can use SLAM to build a map of the environment while simultaneously keeping track of the vehicle's position within the map. Once we have the map, we can use the ROS Navigation Stack to plan a collision-free path for the vehicle. The Navigation Stack uses algorithms like A* or Dijkstra's algorithm to generate the collision-free path.The Navigation Stack also includes a local planner that can adjust the vehicle's trajectory to avoid obstacles in real-time. The local planner can use the LiDAR sensor data to detect any obstacles that come in the path of the vehicle and generate a new trajectory for the vehicle to avoid the obstacles.

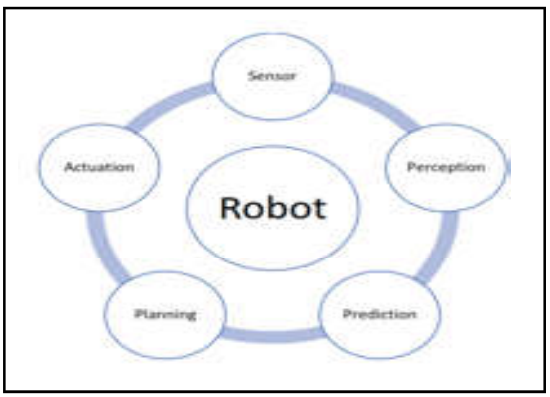

Fig.1 Robot working

3. SIMULATION OF COLLISION AVOIDANCE PROGRAM

Collision avoidance programming with RPLIDAR S2, SLAM (Simultaneous Localization and Mapping), ROS (Robot Operating System), and Gazebo can be a good way to develop and test collision avoidance algorithms in simulated environments. The RPLIDAR S2 is used as a sensor in this approach to collect data about the surrounding environment, and the data is processed using the SLAM algorithm to create a map of the environment. The ROS framework is used to integrate the RPLIDAR S2, SLAM, and collision avoidance algorithms, allowing for real-time sensor data processing and path generation for the robot. Gazebo, a physics-based 3D simulation environment that can mimic real-world scenarios, is used to create the simulated environment. Gazebo simulates the RPLIDAR S2 sensor, providing realistic sensor data to the ROS control system. The collision avoidance algorithm detects obstacles and calculates a safe path for the robot to navigate using the SLAM-generated map. Using this method, developers can test and validate the collision avoidance algorithm's performance in a simulated environment before deploying it in the real world. This can help reduce collision risk and improve the overall safety and reliability of robotic systems.

3.1 Logical Architecture

The sensors used for autonomous robots using LIDAR include LIDAR sensors, IMUs, and other sensors for measuring environmental factors. The perception module uses the sensor data to create a map of the environment around the robot, detect objects, and estimate their positions and velocities. The perception module uses algorithms such as simultaneous localization and mapping (SLAM) to build the map and detect objects. The planning and control module takes the data from the perception module and generates a path for the robot to follow. The path generated is based on the destination of the robot and the obstacles detected in the environment. The control module is responsible for implementing the path generated by the planning module by sending commands to the robot's actuators. The actuators are the mechanical components that move the robot. The actuators used for autonomous robots include motors, servos, and hydraulic and pneumatic systems. The communication module is responsible for establishing communication between the different modules of the robot. This module enables the robot to send and receive data and commands from the central control system. The central control system is responsible for coordinating the different modules of the robot. It receives the data from the sensors and the commands from the planning and control module and sends commands to the robot's actuators.

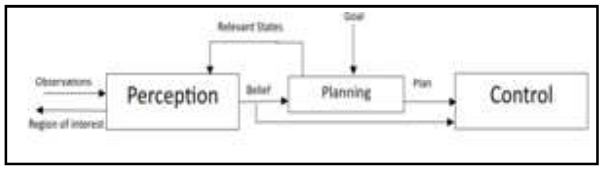

Fig.2 Logical Architecture

4. WORKING

The RP LIDAR S2 is the main sensor collects data by emitting laser beams in different directions and measuring the time taken for the beams to reflect back to the sensor[4]. The data collected by the sensor provides information about the distance, angle, and reflectivity of objects in the robot's environment. The sensor data is used to build a 2D map of the robot's environment, which includes information about the location and orientation of objects. The robot also uses this information to determine its own location and orientation in the environment, a process known as localization. The robot uses the 2D map and localization information to plan a path towards its destination. The path planning algorithm takes into account the robot's constraints, such as its size and speed, and avoids obstacles and other hazards. The robot's actuators, such as motors, are used to control its movement along the planned path. The robot continually updates its location and adjusts its path based on changes in its environment. The LIDAR sensor is also used to detect obstacles and other objects in the robot's environment. The robot can use this information to avoid collisions or modify its path to reach its destination. The robot can communicate with a central control system or other robots in the network to share information or coordinate actions.

4.1 Slam Algorithm

Autonomous robots can traverse both indoors and outdoors without clashing with obstacles. An approach for producing, updating, and estimating maps is simultaneous localization and mapping. The location of the robot. Some of the techniques used to solve it include the particle filter, Extended Kalman filter, Rapid SLAM, Covariance intersection, and Graph based SLAM. The SLAM method combines mapping, sensing, kinematic modelling, multiple objects, multiple cameras, moving objects, loop closure, exploration, and complexity. A range measuring device for viewing the surroundings is the essential component of SLAM. Many factors impact the range measurement equipment. The robot determines its position by using landmarks and measurement equipment and sensors. The robot extracts the input and detects the surroundings when a landmark is identified. SLAM algorithms include Core SLAM, Gmapping, Karto SLAM, Lago SLAM, and Hector SLAM. Gmapping, a particle filter-based

SLAM technique, is employed in this study. If there are some noisy and incomplete observations, the particle filter's purpose is to determine the posterior distributions of a Markov process's states[9].Initially, the particles are uniformly distributed across the environment. Each particle is assigned a weight that represents the likelihood of the corresponding pose hypothesis being correct. When the robot moves, the particles are propagated forward according to the motion model, which describes how the robot's pose changes over time. The motion model considers the control inputs, such as velocity or odometry readings, and adds noise to account for uncertainties in the motion[10].Approximations and updates are used by the particle filter. The distribution samples are supplied in the form of particles, and each particle is assigned a weight that quantifies the likelihood of particles being sampled. Gmapping is a Rao-Blackwellized particle filter that generates grid maps from laser data. This package includes a ROS wrapper for Open Slam's Gmapping. The gmapping package offers laser-based SLAM as a ROS node called slam gmapping. Using slam gmapping, you can generate a 2-D occupancy grid map using laser and posture data gathered by a mobile robot. Self-driving automobiles, underwater reef monitoring, mine exploration, and unmanned aircraft all employ the SLAM algorithm. SLAM techniques are implemented using ROS, an open-source operating system.

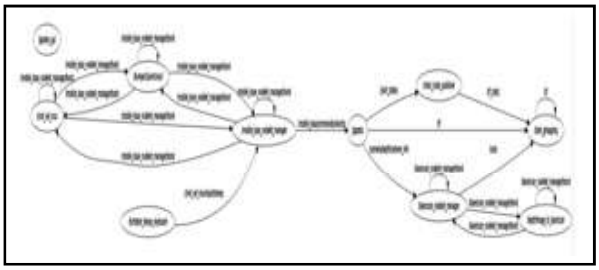

Fig.3 ROS SLAM RQT graph

4.2 Slam Implementation

4.2.1 Gmapping

The map is created by first creating the environment and importing turtlebot into Gazebo. A Kinect sensor is mounted inside the frame of the robot model, which has two wheels. The gmapping package is used to implement the mapping process in this project. To use gmapping,

the robot model must have odometry data and a horizontally mounted, fixed laser range-finder. The Kinect uses infrared sensors to capture a depth image of the environment and acts as a range finder device. As a color image format, it requires 16 bits per pixel infrared data with a resolution of 640 x 480.The depth image proc package in ROS is used to convert this depth image into a 3D point cloud. This 3D point cloud data is then converted to a 2D laser scan using the point cloud to laser scan package. A map is created in rviz by providing all of the required parameters to the packages in gmapping. Initially, the robot is moved in the simulated environment by sending velocity commands via keyboard using the teleop key package in ROS. The gmapping package includes a /map topic that the map server package can use to save the generated map. The map is now ready for use in autonomous navigation.

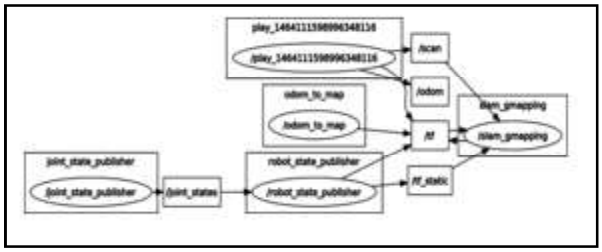

Fig.4 ROS Gmapping Node

4.2.2 Localization

Localization calculates the robot's position and pose in relation to itssurroundings. Laser data, odometry data, and an environment map are required to localize the robot. AMCL (Adaptive Monte Carlo Localization) is used by the turlebot to determine its location. It employs a probabilistic localization approach for two-dimensional robots. A particle filter is used in AMCL to track the robot's pose against the known map of the environment. KLD (Kullback-Leiblerdivergence) sampling is used to reduce computational requirements by automatically adapting for sample size.

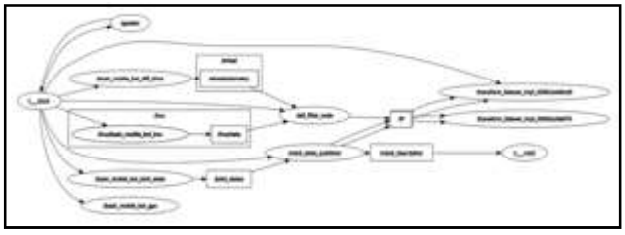

Fig.5 ROS SLAM Localization Node

4.2.3 Autonomous Navigation

Once the mapping and localization are completed, autonomous navigation canbegin. AMCL is implemented using ROS navigation stack packages. The ROS AMCL package includes a node for performing localization on a static map. This node receives TF data, 2D laser scan data from the robot, and the previously generated static map. The AMCL node publishes the robot's pose as well as its estimated position on the map. Two cost maps contain information about the obstacles in the simulated world. Global cost map is used for long-term path planning; it plots a long-term path over the map. The local cost map is used to avoid obstacles and plan local paths. The Rviz displays both the global and local cost maps. The robot can now move on its own. In Rviz, the 2D nav goal is used to assign a destination goal to the robot on the map as well as its orientation. The robot plans the path to the desired destination and sends velocity commands to the robot controller.

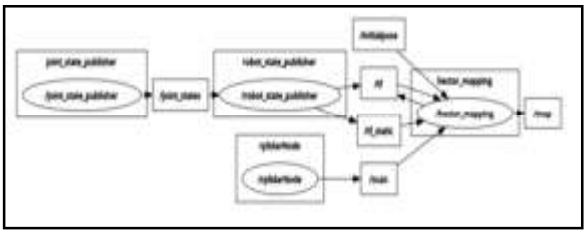

Fig.6 ROS SLAM Navigation Node

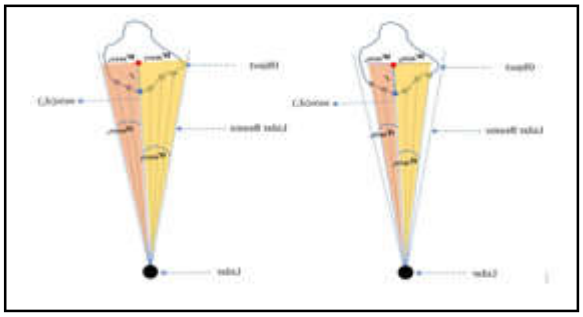

Fig.7 Calculating the minimum (at the left) and maximum (at the right) diameter of the object for a certain segment

4.2.4 Data Acquisition and Pre-Processing

The Lidar being employed measures 360 distance points. In the polar coordinatesystem, each raw laser point is represented as {(di, θi); 0 = i = 359}, where *di* is the distance measured from the observer robot's center to the object and θi is the measurement's relative angle[8]. In a first step, the collected Lidar data are recorded as a vector (*di, θi*), and then the stored data is verified to convert the infinity scan values, which indicate

that there is no obstruction in the way of the ray, to the maximum range value that the Lidar could measure (dmax).Similarly, any item positioned at (dmax) from the observer robot will be disregarded. In practice, there will be no infinity numbers; instead, Lidar will offer the maximum range value for objects outside its operational range. Also, at this level, some form of filtering can be used to reduce noise from the Lidar data. Nevertheless, because we did not add any noise to the simulated Lidar data, we did not use any filtering in this study.

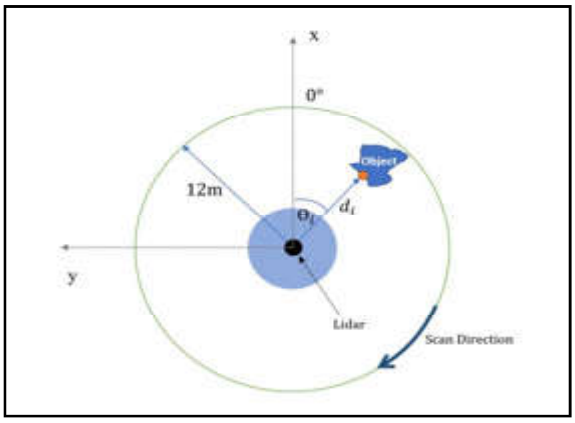

Fig.8 PLIDAR S2 scanning system. The maximum value of di (dmax) is 12m for RPLidar A1 Lidar.

4.2.4 Segmentation

Segmentation is the process of converting raw laser dots into primordial groupings of segments (usable data) that can be a robot, a person, or anythingelse. As a result, segments may be defined as a group of range measurements (points) in the plane that are near to each other and most likely belong to the same item. Point-Distance-Based Segmentation Techniques (PDBS) and KF-Based Segmentation Methods (KFBS) are the two types of segmentation methods. The first is associated with methods that use the Euclidean distance between ∂ nts as a breakpoint criterion condition, while the latter is associated with Kalman Filter approaches. The PDBS technique is used in our method. So, after reading the raw laser data and storing the values as a vector in the previous step, we attempt to detect the various possible objects in the environment by using derivative of data I which can be calculated by finding the difference between each distance point (*di*) and the one before it (*di-1*), then comparing the result with a specific threshold value (*dth*) that allows us to ignore small changes in scan data as follows:

i={di=di=1if\di-di-1\>dth, 0 otherwise}; 1=i=359

As an outcome, for each individual item in the picture, we will have a falling slope in derivative (i<-dth<0) that represents going from a large to a smallvalue in data, and a rising slop (0 <dth< i) that represents moving from a small to a large value in data. Hence, by merging each falling and rising edge from derivatives, we may obtain a likely segment representing an item in the environment. The illustration depicts a depiction of Lidar scan data for two separate items. (Cuboid and cylinder) and the ray number variations between each scan point and the preceding one.

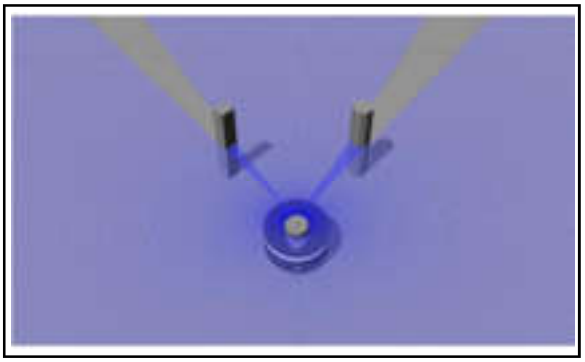

Fig.9 Simulation of a robot with two different objects (cuboid at the left and cylinder at the right) in Gazebo simulator

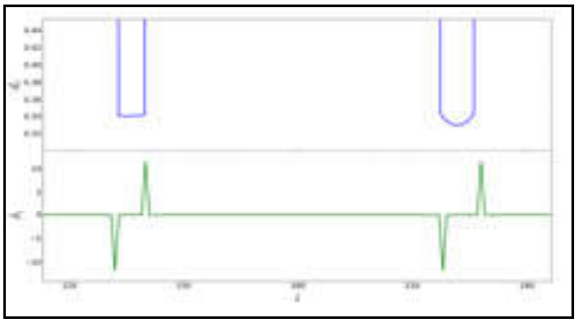

Fig.10 Representation of Lidar scan data (blue part) and the differences between each scan point andthe previous one according to the ray number (green part)

5. RESULTS AND DISCUSSION

By incorporating RPLIDAR S2 into a robotic platform, it can provide high resolution 2D point cloud data of the surrounding environment, which SLAMalgorithms can use to create an environment map[12]. The robot then uses this map to navigate and avoid obstacles in real time. The collision avoidance system can function by combining sensors such as RPLIDAR S2 with other sensors such as cameras, ultrasonic sensors, and IMUs. This data can be used by the robot to detect obstacles, calculate their distance and location, and navigate around them to avoid collisions. Overall, the combination of RPLIDAR S2, ROS, and

SLAM can provide an efficient and dependable solution for collision avoidance in a wide range of robotic applications, including drones, autonomous vehicles, andindustrial automation.

6. CONCLUSION

In this paper, we used ROS to analyze and successfully execute an autonomous collision avoidance system. The system's software and hardware are described in the preceding section. Turtle bot was used to experiment with and implement autonomous navigation in a simulated environment created with the help of Gazebo. For navigation, SLAM and route planning algorithms are applied. As shown in the preceding section, the map was successfully generated by robot and reached its destination without colliding. Through additional softwaredevelopment and analysis, the current work can achieve greater precision in navigation. The entire hardware implementation and calibration for increased precision are still in the works.

REFERENCES

[1] Amanda Dattalo, "Introduction", Ros.wiki.org.

[2] A. Cherubini, F. Spindler and F. Chaumette, "Autonomous Visual Navigation and Laser-based Moving Obstacle Avoidance", IEEE Transactions on Intelligent Transportation Systems, Vol.15, No.5, 2014, pp.2101-2110.

[3] G. Grisetti, C. Stachniss and W. Burgard, "Improved Techniques for Grid Mapping With Rao-Blackwellized Particle Filters", IEEE transactions on Robotics, Vol.23, No.1, 2007, pp.34-46.

[4] H. Malla, P. Purushothaman, S.V. Rajan and V. Balasubramanian, "Object Level Mapping of an Indoor Environment using RFID", 2014 November, In 2014 Ubiquitous Positioning Indoor Navigation and Location Based Service (UPINLBS), IEEE, pp. 203-212.

[5] H.I.M.A. Omara and K.S.M. Sahari, "Indoor Mapping using Kinect and ROS", In 2015 International Symposium on Agents, Multi-Agent Systems and Robotics (ISAMSR), IEEE, 2015, August, pp.110-116.

[6] D.M. Turnage, "Simulation Results for Localization and Mapping Algorithms", In 2016 Winter Simulation Conference (WSC), IEEE, 2016, December, pp.3040-3051.

[7] "Obstacle Avoidance with RPLIDAR A2 using ROS", by YohanJoo, This Article Provides A Detailed Explanation of How to Use The RPLIDAR A2 Sensor with the Robot Operating System (ROS) to Perform Obstacle Avoidance.

[8] "Real-Time Obstacle Avoidance with RPLIDAR S2 and Raspberry Pi" by Yuan Gao, This Article Describes How to Use the RPLIDAR S2 Sensor with a Raspberry Pi to Perform Real-time Obstacle Avoidance.

[9] "Obstacle Avoidance Using RPLIDAR and Arduino" by YegorSenin, This Tutorial Shows How to Use An Arduino board and the RPLIDAR Sensor to Perform Obstacle Avoidance.

[10] "RPLIDAR A2M8 and Obstacle Avoidance" by Jon Dahl, This Video Tutorial Demonstrates How to Use the RPLIDAR A2M8 Sensor with A Small Robot to Avoid Obstacles In Real-Time.

[11] "Obstacle Avoidance using ROS and RPLIDAR A1M8" by Keng Yap, This Tutorial Shows How to Use ROS and the RPLIDAR A1M8 Sensor to Perform Obstacle Avoidance.

[12] S. Zaman, W.Slany and G. Steinbauer, "ROS-based Mapping, Localization and Autonomous Navigation Using a Pioneer 3DX Robot and Their Relevant Issues. In 2011 Saudi International Electronics, Communications and Photonics Conference (SIECPC), IEEE, 2011, April. pp.1-5.

A MODIFIED DUAL INPUT BOOST DC-DC CONVERTER FOR SOLAR FED ELECTRIC VEHICLE SYSTEM

G.Nithya and J.Senthil Kumar
Department of Electrical and Electronics Engineering,
Bannari Amman Institute of Technology, Sathyamangalam - 638 401, Erode District, Tamil Nadu
E-mail: nithyag@bitsathy.ac.in,senthilkumarj@bitsathy.ac.in

Abstract

In India, the electric vehicle is becoming a more appealing option for avoiding the use of fossil fuels. Solar PV charges the battery of a commercial electric vehicle, and the battery drives the vehicle at the same time. Due to the nature of a classic buck-boost bidirectional DC-DC converter, solar PV output is underused when the battery capacity (SOC) achieves its optimum.To address the mentioned constraint, this paper presents a unique dual input boost (DIB) DC-DC converter for electric vehicles energized by photovoltaics. The recommended converter effectively uses solar PV power by operating in six different modes.It also offers the benefit of a wide range of speed control and decreases the number of conduction devices in each mode, lowering switching and conduction losses and improving efficiency.

Keywords: *Battery state of charge, DC-DC converter, DIB converter, E-vehicle*

1.INTRODUCTION

Electric vehicles, solar-powered EVs, an[d plug-in electric vehicles are becoming increasingly popular in recent years, and the industry is rapidly expanding. Nowadays, dc-dc converters are extensively employed in switchedmode power supply. These converters are typically used to step down or increase an unregulated input dc voltage. DC to DC converters come in a variety of topologies, including buck, boost, buck-boost, Cuk, Luo, SEPIC, and Zeta. The buck and boost converters are the simplest converter topologies out of all of these. From these two fundamental converters, several converters are derived. Each topology converter has its own operating theory, benefits, and drawbacks. Buck and boost converters are used by renewable energy sources to reduce or increase the unregulated output of intermittent energy sources.

In comparison to a one-way source system, the hybrid power source system has a high efficiency to give high quality. The solar panel's output power is influenced by irradiance, and because of its intermittency, it becomes a source of variable dc output. This inconsistent output voltage is not ideal for applications that rely on the battery supply. As a result, a controller is required to keep the output voltage constant. The battery should last longer if the converter is constantly putting pressure on it to charge it. The power dissipation in switching the MOSFET switch will be reduced by using negative voltage and negative current switching. In many real-time applications, the load necessitates a constant supply from the source. Two sources are connected as a circuit to make the device completely reliable.

The buck-boost converter topology provides superior solutions for DC-DC double input converter systems. On the storage side of a device with a storage function, the ability to transfer power in both directions is the most important aspect. The load can also be delivered simultaneously and independently by the input source. To offer a backup power supply from the battery, a bidirectional switch must be used to charge and discharge the battery between demand and generated power. The suggested converter is a buck-boost converter, which uses a buck converter to step down the voltage when the input voltage is high[1]. The boost converter ramps up the voltage from the solar panel because the voltage from the PV panel is an uncontrolled DC source. When the demand for voltage is great, the DC motor is driven by both battery backup and solar panel power. The "super boost" mode is the name for this operating mode. That is the aspect of the programme that is being proposed[2]. A DC to DC converter is any sort of energy converter that absorbs energy from one or more sources and distributes it to at least one or more charges utilising an inducer as a mechanism for storing and releasing energy. A "buck-boost" converter is a DC to DC

converter that can offer a set output voltage that is not limited by the voltage(s) of the input.The power path of a DC to DC converter is the section where energy flows from the source(s) to the charge dual-input converter's operational mode is to control the power path switches while concurrently drawing energy from two input sources. The concept and circuitry that govern the converters switch to achieve a consistent output voltage are known as the converter control scheme.

Typically, a DC-to-DC converter is utilised to meet these requirements, with the caveat that power and/or potency are not required for these less sophisticated topologies[3]. Due to the complexity of DC-to-DC converter design, using such topologies to render dual-input converters is tough. Currently, the most frequent technique employed by dual-input DC-to-DC converters is to use sophisticated analogue control loops to position and synchronise multiple converters. A fee is typically used to describe when a dual-input power supply has two inputs or power sources and when output.

The current is given to the load on demand, and the output normally contains a controlled voltage set by the power source. The inputs are usually installed voltages that may or may not be equivalent to the output voltage; the power source determines the current drawn from these inputs. The current or power obtained from the inputs is derived from each source either simultaneously or alternately during a dual-input power supply[4]. The current system will be fed by renewable energy sources such as solar cells and wind turbines. As a result, the device's input voltage would be variable and erratic. The output voltage will change as a result of this. Because the output is relevant to grid applications, it must be consistent. For the induction of a constant output voltage Vo, a feedback system is required. To keep the output voltage constant, a closed-loop PI controller is used.

The output voltage is measured and compared with the reference value whichis predefined in the controller, error value is produced. This error value is used as PI controller data to produce the necessary PWM signal to the switches used in the converter.If there are any fluctuations in the output voltage,but the controller will alter the pulse that should be given to the switch, thus keeping the voltage output constant. A buck-boost and a boost converter are included. It enlists the services of four diodes and four power switches. By adjusting the duty ratios of the switches, monitoring the maximum power of the PV source, setting the FC power, regulating the battery power, and calibrating the output voltage, hybrid photovoltaic/fuelcell/battery applications can be fitted.

As a summary of the literature done so far, some of the problems identified are described below:

- To operate the six operating modes in the traditional setup, three distinct converters are required[5]. Due to the presence of a common buck-boost cell in the proposed DIB converter, a single-stage converter may perform an equivalent procedure.This decreases the number of conductive devices and the number of components in each operating model compared to the existing configuration.

- In the current method, it can only be done in buck mode, so the input power cannot be supplied simultaneously to the load and the battery,but in our proposed solution, the input source will provide the energy to be loaded and the other source can be charged/discharged separately.

- In the present setup, the solar photovoltaic cell charges the battery utilizing a separate charging system, while the batteries power the vehicle by a bidirectional converter. In addition, it has the right to charge a source from outside. To solve this limitation, the traditional concept allows the proprietor to recharge the batteries from various sources such as the grid and others. This provides backup power and supports the utility when electric vehicles are connected to the utility grid at public car parks. This also allows voltage and frequency control by the utility grid and mitigates peak demand.

The Dual input super-boost converter drives the vehicle in high-speed operation on a battery and solar photovoltaic source. The working mode is called super-boost mode which is one of the proposed converter's related characteristics. They are described as follows:

- The first objective is to effectively utilize solar PV power.
- The second objective is to reduce the number of conduction devices.
- The third objective is to ensure the wide selection of speed control.
- The fourth objective is to check whether the proposed converter can charge the battery without any separate converter.

2. BLOCK DIAGRAM OF THE SYSTEM

Solar energy, regenerative breakdown, on-board generator, and external power can all be used to access the battery in an electric car. In most of those systems, the machine is powered by just one input power source at a time, such as a cell phone, which is powered by either the battery or an external charger, but never both. When there are many input sources, reduce loading at each one at the same time, especially if one of them is at risk of browning out owing to overloading.

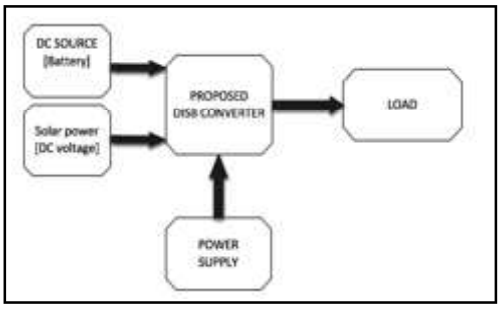

Fig.1 Block Diagram of DIB Converter

In such an application, a dual-input DC-to-DC converter can be used to monitor the amount of power drawn from each source in order to either decrease burden on sensitive power sources or maximise output. Multiple unidirectional boost converters are integrated on each side of the converter to accept completely diverse low-level dc inputs[10]. The output capacitors V_{01} and V_{02}, as well as the two output dc-link voltages. Boost converters that take in dc voltage from a variety of sources. To achieve the required constant output voltage, each boost converter is tightly regulated in the intended topology.

3. CIRCUIT DIAGRAM OF THE PROPOSED SYSTEM

To solve the complexity and ambiguity of the existing approach MIDC, Figure 2 shows a basic circuit diagram for commercial EVs. It captures a double boost, non-isolated input converter. It consists of three IGBT switches, Inductor L, a battery source for indicating solar power and a load capacitor C. For the combination of solar PV and battery, an isolated and non-insulated DC to DC converter was recorded[6][7]. The battery power, on the other hand, must be stored and realised using a DC-DC converter. Unlike the conversion depicted in Figure 2, battery charging can be scaled without the use of external converters. Several researchers have developed converter architectures to incorporate diverse power topologies such as FC, battery, and solar PV as hybrid battery charging systems utilising separate charging controllers and driving the car, based on the aforementioned commercial EV premise.

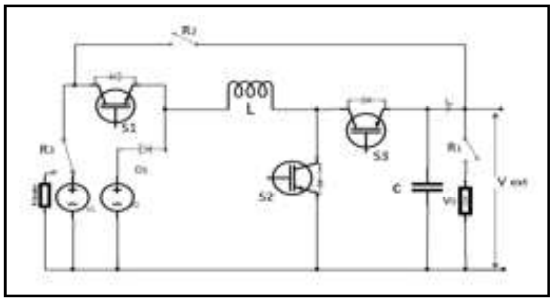

Fig.2 Proposed DSIB converter configuration

However, when the battery charging state (SOC) reaches its maximum value (i.e.SOC>80%), the charging controller enters standby mode, and solar power is used to operate the vehicle. To solve this constraint, this study offers a new double input super-boost (DIB) DC-converter to DC. These electric vehicles' owners can provide battery-powered fuel flexibility, safety, and smooth operation[8]. It provides power backup, which helps to support the network until electric vehicles are publicly connected to energy grid parking places. This allows the utility system to cope with stress while also reducing peak demand. Bidirectional DC-DC converters (BDC) are utilised for two-way power interchange and are generally employed in both buck and boost modes for increased dynamic response and efficient conveyance.

4. METHODOLOGY OF THE PROPOSED DSIB CONFIGURATION

To conduct the six modes in the proposed arrangement, three independent converters are required. However, because a similar buck-boost cell exists, the proposed DIB converter requires a single-stage converter to execute analogous tasks[7]. It decreases the number of conductive devices and the number of components in each mode of operation.This has an efficiency of higher dynamic performance with a large range of speed control. This defines the working wave form and its study of voltage gain.

4.1 Operating Principle and Analysis

- The proposed Dual input super converter works in 6 distinct modes

- Solar driven vehicle mode if (SOC>80 percent)
- Day time parking mode
- Regenerative braking

The DIB converter works for solar mode when the battery charging capacity is > 80%. The solar-photovoltaic facility is fed to the engine and thus S2 controls thespeed of the vehicle. The motor is driven from the V_2 battery source. This mode isdescribed as a battery-operated vehicle when solar irradiation is unavailable. The DIB converter works for solar mode when the SOC of the battery is >80%. The solar-photovoltaic facility is fed to the engine and thus S_2 controls the speed ofthe vehicle. The motor is driven from the V_2 battery source. When solar irradiation is unavailable, this mode is classified as a battery-powered vehicle. An external source of power is used to charge the battery (Vext) Parking mode is the service mode in the dark. When the SOC falls below 80% in regenerative braking mode, the inertial power available in the vehicle is extracted and fed into the battery, otherwise it is dissipated as heat via the braking resistor (R brake)[9]. The dual input super-boost converter uses both battery and solar electricity to power the vehicle during high-speed operation; this operating mode is known as super-boost mode, and it is one of the converter's distinctive features. Figure 4.1 shows a waveform of the DIB converter operating in Super Boost mode and it clearly shows the gating signal for the waveforms S_1,S_2,andVL,and IL.Vi at t_0 to t_1, s_1 is on and thus the current starting inductor rises from iL_0 to iL_1 due toV_1source. Instantly t_1, S_1 is switched off and, thanks to the sourceV_2, the inductor current rises from iL_1 to ILP during t_1 to t_2.Upon instant t_2, S_2 is turned OFF and the inductor then discharges[13].

The DIB converter operates in solar mode when the battery charging capacity is >80 percent. The solar-photovoltaic power is fed to the engine and thus S_2 controls the speed of the vehicle.The motor is powered by a V_2 battery source. This mode is defined as a battery-driven vehicular mode when solar irradiation cannot be accessed. The DIB converter is driven in two modes along with the SOC of the battery[12].

The voltage that occurs in the inductor is $(v_2–v_0)$ throughout t_2 to T_s. According tothe inductor's voltage and the time balance theory, the inductor voltage approximate value is zero for each stage[11].The expression is written as

$$v_1d_1+v_2(d_2-d_1)+(v_2-v_0)(1-d_2)=0 \qquad 910$$

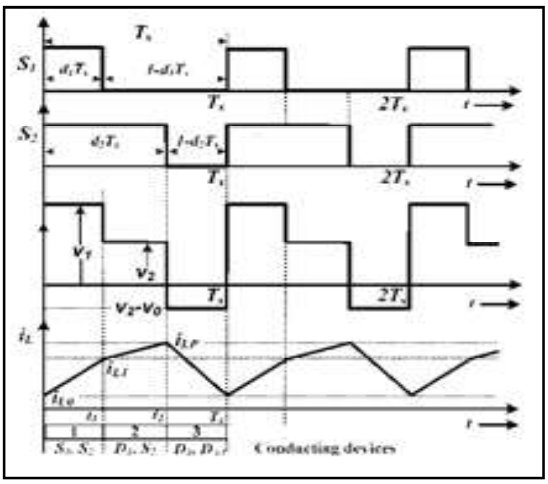

Fig.3 Operating wave form of the proposed converter

where d_1 is S_1's duty ratio and d_2 is the S_2's duty ratio. After simplify(1), the output voltage of the Dual input super-boost converter in super-boost operation

$$V_0=v_1d_1+v_2(1-d_1)\backslash(1-d_2). \qquad (2)$$

The maximum output voltage is sometimes obtained for super-boost mode atd1=0.6 and d2=0.8 and written at Vmax= 3V1 + 2V2 Unified output voltage (vp.u) is sometimes written for further study as

$$Vp.U=V0, \qquad (3)$$

$$Vmax=k+d_1(1-k)(3+2k)\backslash(1-d_2) \qquad (4)$$

The source ratio (V_2/V_1) is where k is voltage Specific characteristic of output voltage with duty ratio ($d_1$and d_2)for k=0.5.

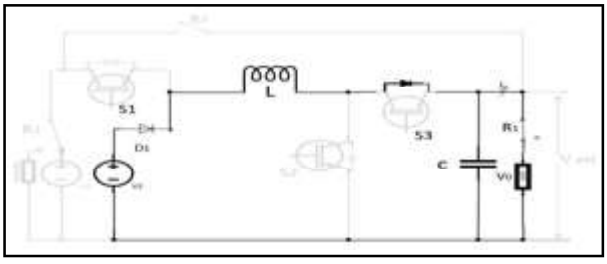

Fig.4.1(a)Charging state of the solar-powered mode

Figure.4.1(a) and (b) shows the analogous solar-powered vehicle circuit in charging and discharging mode. As S_2 switches on, the inductor stores the energy through source V_2. The inducer releases its energy through DA_3 to the charge. The above mentioned is that the battery supplies the facility to the charge during the absence of solar irradiation. The counterpart mode is identical to the operation mode. In comparison, S_1 is constantly turned ON.

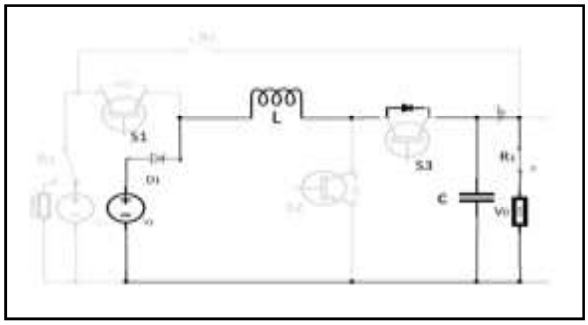

Fig.4.1 (b)Discharging state of solar-powered mode

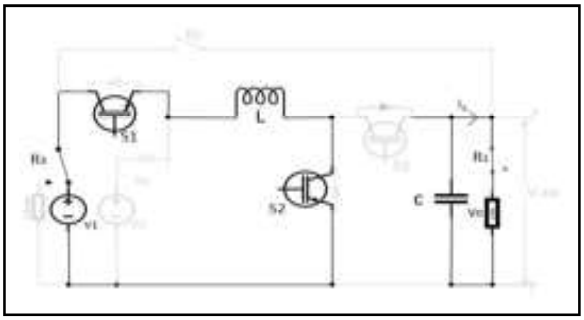

Fig.4.2(a) Super boost mode (S_1,S_2 ON)

The facility was managed in Super Boost mode by modifying d_1 and d_2.Because large power selection is also managed by these two control parameters of $D_1$and D_2 in super-boost mode.

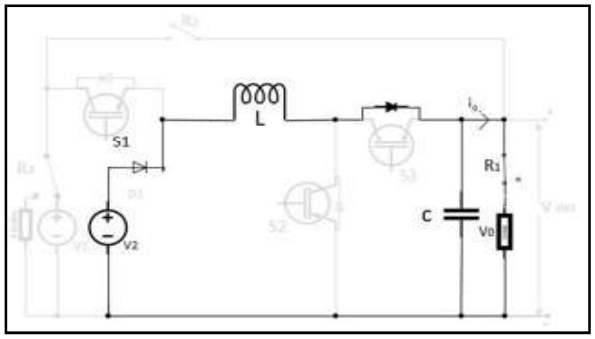

Fig.4.2(b) Super boost mode (D_1,S_2 ON)

The energy produced is supplied to the resistor before it reaches zeros rpm.The suggested duel input super-boost converter works in super-boost mode, thereby simply dissolving the circuit of this particular model illustrated in 4.2 (a), (b) and (c) for high-speed realization.

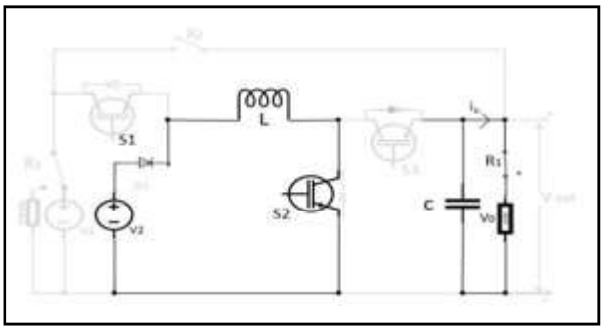

Fig.4.2 (c)Super boost mode(D_1,D_{A3} ON

4.2 Operating Modes

Table 1 Modes of Operation for Proposed DSIB Converter

Operating Modes	Switches	Active Device Diodes	Relays
Solar-powered	S_2	D_1,D_3	R_1
Battery-powered	S_1,S_2	D_3	R_1,R_3
Parking mode in daytime<80%	S_2	D_1,D_3	R_2,R_3
Parking mode in daytime > 80%	S_2	D_1,D_3	None
Parking mode in nighttime	S_3	D_1,D_2	R_3
RegenerativeBraking	S_3	D_1,D_2	R_1,R_3
Superboost	S_1,S_2	D_1,D_3	R_1,R_3

5. RESULTS AND DISCUSSION

Figure.5.1 shows the MATLAB Simulation of the proposed dual input super converter operating in super-boost mode. The output of the super boost mode of the converter is only taken into account for the optimal usage of the obtained solar power.The simulation results of input current and voltage, the PWM pulse given to the MOSFET switches, and the output voltage are shown. The duty ratio of the MOSFET is 0.8.

Figure 5.3 shows the input voltage and the battery input source which are considered as dual inputs. The external supply will be needed when there is intermittent solar energy.Figure 5.2 gives the PWM signals given the switching device.with duty ratio 0.8.

Figure 5.4 shows the battery state of charge at the initial level.When we make use the intermittent solar power the battery state of charge will increase which in turn increase the overall usage of obtained solar power. When state of charge reaches > 80 % the converter will work on battery powered mode.

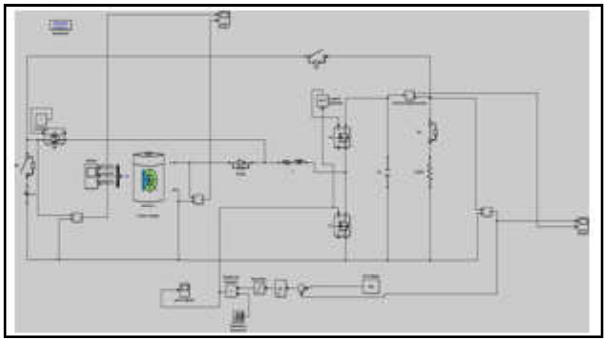

Fig. 5.1 MATLAB simulation ofthe proposed converter

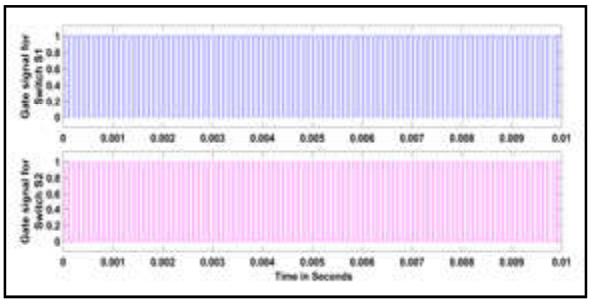

Fig.5.2 PWM signal given to the MOSFET

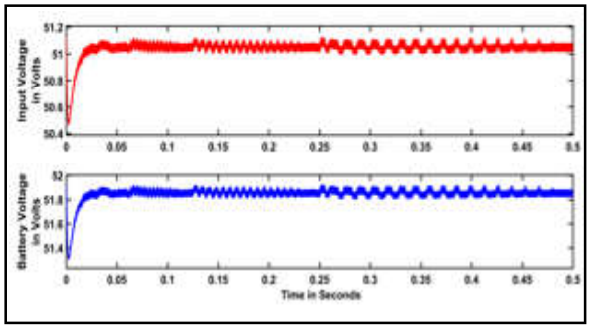

Fig.5.3 Input voltage and Battery Voltage

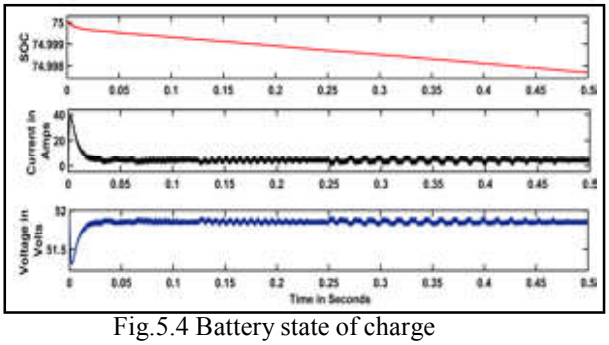

Fig.5.4 Battery state of charge

The experimental configuration consists of 12V MOSFET modules with a rated power of two kW. The inductor is charged in two states while the proposed DIB converter works in super-boost mode.In state1the inducer current increases thanks to source V_2, and it increases further due to source V_1 The inductor present inboth off-state S_1 and off-state S_2 decays. The output voltage for the DIB converter is essentially ripple-free.

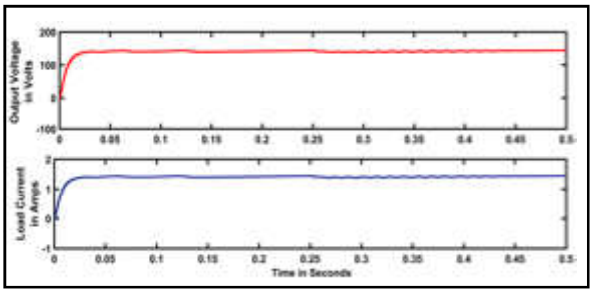

Fig.5.5 Output voltage and current of the converter in Superboost mode

Vehicle mode simulation operated during battery operation,and experimental findings are shown and in off-state S_2 the source V_1 provides the loading facility with S_1 and iL, and the inducer current is charged according to the service cycle. Also, the DIB Converter provides ripple-free output voltage. It's also seen from simulation results, with stronger correlation and performance-free notches.Furthermore, the proposed system is ripple-free in both modes, taken from the source by preserving the higher life there.

6. CONCLUSION

DIB DC-DC Converter topology was suggested for use with solar-powered EVs. It conferred the extensive operating wave and completely different mode of operation. The performance characteristics are defined as unified output voltage forthe planned DIB converter. Small-signal modeling was designed to improve the proposed transfer efficiency of the DIB device converter, a small signal modeling the averaging technique was created for the state region. The simulation tests are conferred to validate the function and performance of the intended DIB converter and are checked by experimental research. Each simulation and growing test validates that the proposed DIB converter is better suited for EV use.This paper proposes a dual input DC-DC system that can eliminate separate characteristic V-I sources.The suggested converter study was performed in detail below the buck-boosting and behaviour boosting. Study and simulation find the system's dynamic and steady-state answer satisfactory.The proposed DSIB converter, or energy spare, simultaneously varied from the same characteristic V-I supply.The proposed DSIB converter has a lightweight architecture and fewer half numbers, which improves total system performance and thus enhances the unit's usefulness for applications such as power generation, clean energy integration, hybridcars, aerospace,etc.

REFERENCES

[1] S.Athikkal, G.Guru Kumar and K. Sundaramoorthy, "Performance analysis of novel bridge-type dual input DC-DC converters", IEEE. Access.,Vol.5, 2017, pp.15340–15353.

[2] N. Beniwal, I. Hussain and B. Singh, "Control and Operation of a Solar PV-battery-grid-tied system in fixed and Variable Power Mode", IET Gener.Transm.Distrib., Vol.12, No.11, 2018, pp.2633-2641.

[3] Chen, Y. and Wu, L. (2017), "The Strategy of Electric Vehicle Fast-charging on Correcting Lope Iteratively", IEEE 2nd Advanced Information Technology, Electronic and Automation Control Conf. (IAEAC), Hongqing, pp.166-170.

[4] I.Federico, E.Jose and F. Luis, "Master–slave DC Drop Control for Parallel in Auxiliary DC/DC Converter Sin Electric Bus Applications", IET Power Electron., Vol.10, No.10, 2017, pp.1156-1164.

[5] K. Fahem, D.E. Chariag and L. Sbita, "On-board Bidirectional Battery Chargers Topologies for Plug-In Hybrid Electric Vehicles", 2017 Int.Conf. on Green Energy Conversion Systems (GECS), Hammamet, 2017, pp.1-6.

[6] N. Kim and B. Parkhideh, "PV-battery Series Inverter Architecture: A Solar Inverter for Seamless Battery Integration with Partial-Power DC-DC Optimizer", IEEE Trans.Energy Converters., Vol.34, Vol.1, 2018, pp.478-485.

[7] S. Li, K.M. Smedley and D.R. Caldas, "Hybrid Bidirectional DC-DC Converter with Low Component Counts", IEEE Trans.Ind.Appl., Vol.54, No.2, 2018, pp.1573-1582.

[8] F. Naseri, E. Farjah and T. Ghanbari, "An Efficient Regenerative Braking System Based On Battery/ Supercapacitor for Electric, Hybrid, and Plug- In Hybrid Electric Vehicles with BLDC Motor", IEEE Trans.Veh.Technol., Vol.66, No.5, 2017, pp.3724-3738.

[9] R. Sabzehgar, Y.M. Roshan and P. Fajri, "Modelling and Sliding-Mode Control of a Single-Phase Single-Stage Converter with Application to Plug-In Electric Vehicles", IET Power Electron., Vol.12, No.3, 2019, pp.620-626.

[10] A. Sivaprasad,G.GuruKumar and S. Kumaravel, "A Novel Bridge type DC-DC Converter for Hybrid Energy Source Integration", IEEE 1st Int. Conf.on Power Electronics, Intelligent Control and Energy Systems (ICPEICES), Delhi, 2016, pp.1-6.

[11] N. Vosoughi, M.Sabahi and E. Babaei, "Performance and Design Analysis of An Improved Non-isolated Multiple Input buck DC-DC Converter", IET Power Electron.,Vol.10, No.9, 2017, pp.1034-1045.

[12] F.Yang, H.Ge and J. Yang, "Dual-input Grid-connected Photovoltaic Inverter with Two Integrated DC-DC Converters and Reduced Conversion Stages", IEEE Trans.Energy Converters., Vol.34, No.1, 2018, pp.292-301.

[13] L.W.Zhou, B.X.Zhu and Q.M.Luo, "High Step-up Converter with Capacity of Multiple Input", IET Power Electron., Vol.5, No.5, 2017, pp.524-531.

DESIGN AND FABRICATION OF AUTOMATIC STARCH FEEDING ATTACHMENT IN POWERLOOMS

S.Velmurugan, N.Jayakumar, A.Tajdeen and A.Ramakrishnan
Department of Mechanical Engineering,
Bannari Amman Institute of Technology, Sathyamangalam - 638 401, Erode District, Tamil Nadu
E-mail: velmurugans@bitsathy.ac.in

Abstract

Nowadays availability of labours is a major problem in small scale industries, especially in powerlooms. In powerlooms starch feeding is done manually. In conventional powerlooms starch is fed to the threads in order to increase the texture and as well as the strength of the thread. But the starch feeding is not in uniform manner as it is done manually. Hence to make a uniform flow of the starch to thread, the automatic starch feeding attachment is a necessary one. Automatic starch feeding attachment has the advantage of providing uniform flow of starch to the thread and reducing the man-power. It does not require a separate power source; it utilizes the power wasted during the rolling process. The attachment involves a rotary cam which converts rotary motion into reciprocating motion and this is utilized for the to and fro motion of the slider. Starch is allowed to flow continuously through tubes which will get deposited evenly over the surface due to reciprocating movement.

Keywords: *Automated Mechanism, Cam and Follower, Powerlooms, Starch Feeding, Uniform flow*

1. INTRODUCTION

Power-looms are used to weave threads into sheets or clothes. This process involves a series of steps such as thread winding, rolling and weaving. The individual threads are winded parallel into a roll from which it is again rolled into a beam. During this stage an additional process called starch feeding is done in order to increase its strength and texture. It is a tedious process involving additional labour and time. It has certain disadvantages such as non- uniform flow and thread crossing. When the starch flow exceeds the required amount, sticking of threads occurs and if the flow is less, the desired strength is not obtained. Both of these cases are serious problems in weaving process. Conventionally, the starch feeding is done manually. A cloth is placed over the roller and the starch is poured over it directly at the required amount by a person. During the starch feeding process the starch fed to the threads is not in a uniform manner and it requires additional time in the thread warping process.

To reduce the additional time in the thread rolling process an automatic starch feeding attachment is a necessary one in the conventional power-looms. Automatic starch feeding attachment consists of following components: Cam and follower arrangement, base frame, supporting material, solid bearing, Hopper, Cloth holder, Pulley, Shaft, Pulley support, Nut and Bolt, Slider and its Case, Flow tubes and spring. Automatic starch feeding attachment does not require extra power source, it utilises the power in the conventional rolling process by connecting the pulley at end of the automatic starch feeding attachment to the main pulley of the Thread roller. Thus the attachment makes a uniform flow of the starch to the thread thereby increasing the texture as well as the strength of the thread without additional labour or external power source.

2. LITERATURE REVIEW

The research work revealed the socio – economic problems of powerloom industry [1-4] studied the powerloom industry. The main conclusions of the study are; the powerloom industry in Malegaon has seen many ups and downs in its development and it is one of the important industries. Personnel problems and labour welfare industry had explained about personnel management in the cotton textile industry [5& 6].

Erdman, A.G his research work he explained the problems and prospects of textile industry with special reference on the productivity of large and small scale textile industries. He attempted to throw light on the

factor productivity of the textile industry [7]. Wang deals the water washing device used in weaving in patent CN207313901U 20180504 consist of water washing assembly to increase the surface quality of the fabric but it affects the texture of fabric and also the complete model shows the complex working principle. Complex structure of this machine may be a problem during troubleshooting and huge moving parts in is assembly may consume more power [9].

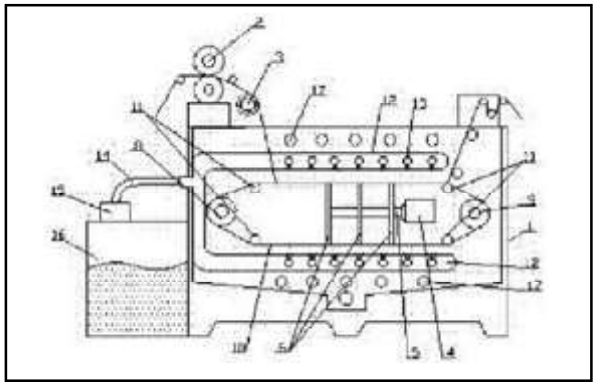

Fig.1 Design of water washing device used in weaving

3. PROBLEM STATEMENT & METHODOLOGY

3.1 Problem Statement

The starch feeding is done only by human labors. To reduce manual efforts a machine is to be proposed to supply starch automatically after weaving process.

3.2 Methodology

Starch feeding is done by continuous flow of fluid from tank to the clothes by potential energy of the stored starch. Starch is supplied all over the clothes by using Cam and follower mechanism, lever mechanism and reciprocating mechanism.

3.3 Advantages of Starch Feeding Attachment

- Increase the texture and as well as the strength of the thread.
- Consumption of time is very low when compared to manual work.
- Skilled worker is not required.
- Productivity is high.
- No need of electricity for feeding the starch.

3.4 Limitations of Starch Feeding Attachment

- Clothes passing through this system should be in constant speed in order to facilitate proper starch feeding.
- Starch level is maintained or else supply may not be proper.

4. DESIGN

Travel of the cam and lever assembly play a vital role in starch feeding. The optimum cam design and dimensions can be varied to increase the feeding width of the system. It can be done with the help of Displacement curve.

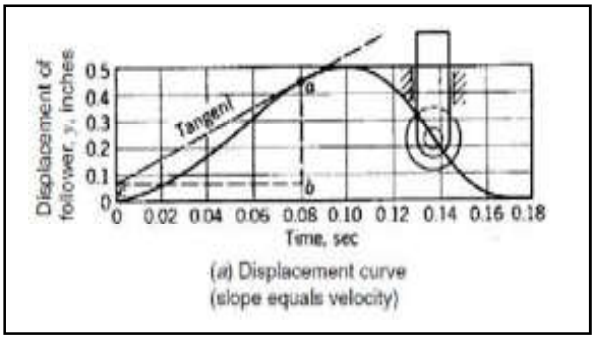

Fig. 2 Displacement curve

Table 1 Classification of Curves

Sl.No	Curve Type	Applications
1	Simple Polynomial Curves	Constant acceleration and constant jerk
2	Trigonometric Curves	Simple harmonic motion, cosine acceleration, and cycloidal acceleration
3	Constant Velocity Curve	Straight-line displacement at a constant slope and displacement is uniform
4	Constant Acceleration Curve	Constant positive and negative acceleration and smallest maximum accelerations for all points curves

Constant Velocity or uniform displacement curve is the simplest of all. It has a straight-line displacement at a constant slope giving the smallest length for a given rise of all the curves. When the straight-line curve is developed for a radial cam, it becomes the Archimedes spiral.

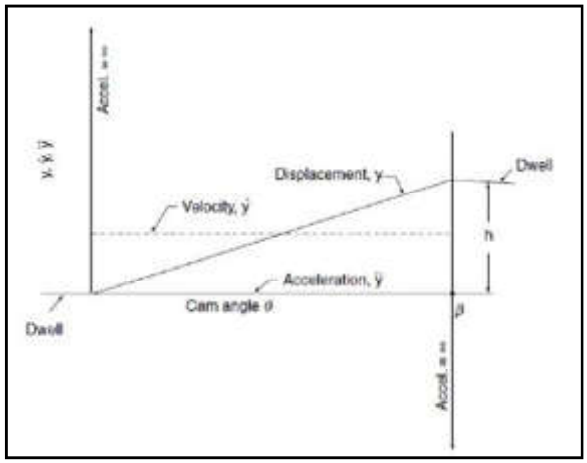

Fig. 3 Constant velocity curve of end cam

5. INVOLVED MECHANISMS

5.1 Cam and Follower Mechanism

The Cam and follower mechanism is used to convert rotary motion into linear motion. The Cam attached at one end of the shaft is rotated by means of a belt drive pulley attached along the other end of the shaft. The roller of the follower makes a linear motion along the Cam profile providing the necessary transformation of motion. Roller follower is preferred because of its low friction operation.

5.2 Lever Mechanism

The lever mechanism is used in order to increase the length of traverse of follower end. The follower is supported with a pivot which enables the lever action thereby increasing its traverse length up to three times its normal value. The end of the follower is made adjustable so as to attain various lengths of reciprocation. Spring is used at the smaller end to provide the necessary movement of the lever mechanism.

5.3 Reciprocating Mechanism

The reciprocating mechanism is used to provide uniform deposition of starch over the warp roll. The end of the follower has a slot in which the slider is attached by means of a link. The arc of the follower is transformed into straight line movement of the slider with the help of the slot in the follower end. The slider enclosed in the case moves to and fro and the flow tubes attached to it follows the same path. The movement of roller over the cam provides forward motion while the retraction of spring provides the reverse motion of the slider.

6. MODELING AND DESCRIPTION OF COMPONENTS

The individual components of the Automatic Starch Feeding Attachment in Powerlooms are modeled using solidworks 2016 software.

6.1 3D Modeling

The main components of the Automatic Starch Feeding Attachment are modeled separately and assembled (Figure 4).

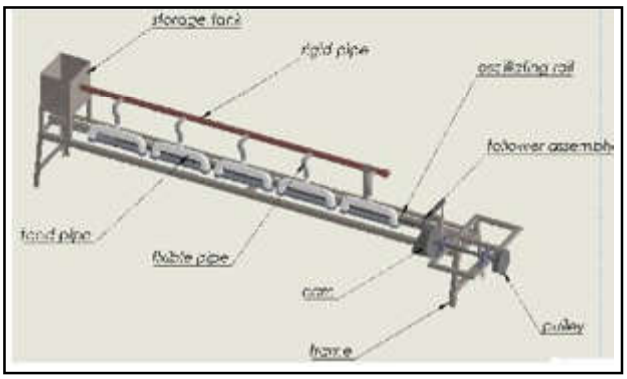

Fig. 4 3D model of the project

6.2 Components Description

6.2.1 Frame

The frame is the most important part of the machine. The entire weight is transmitted to the ground through this frame. Frame is the main part where other parts are assembled together. It provides the support for the oscillating assembly and Cam assembly. The following Figure 5 shows the Orthographic views of the frame with base plate. Frame base is constructed by "L" frame and the secondary member is made of square tubes. All the sub – assemblies are rest over the main frame.

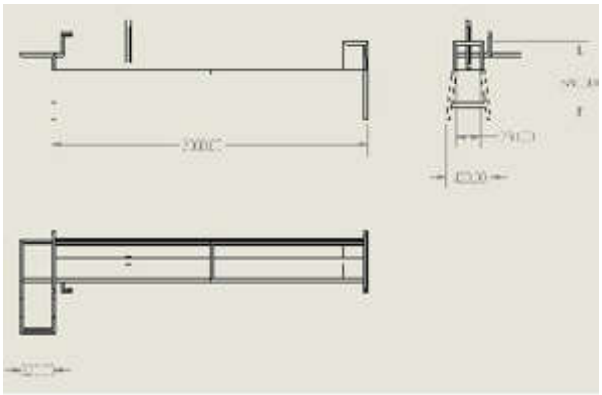

Fig. 5 Orthographic views of Frame (Scale 1:20 & All dimensions are in mm)

6.2.2 Motor

The motor is the power unit used in this project. It is high torque motor; it will make the system to oscillate the system. This engine has 10 rpm and 20 Nmm torque. The motor is fixed in the frame by using fasteners. Speed of the motor can be varied according to the type of fabric.

6.2.3 Cam

The following Figure 6 shows the end cam which is made up of mild steel. The Cam and follower makes system to oscillate by using motor. Cam is designed according to the application required. Cam has the travel of 120 cm, its base diameter is 200mm. It is machined using CNC VMC.

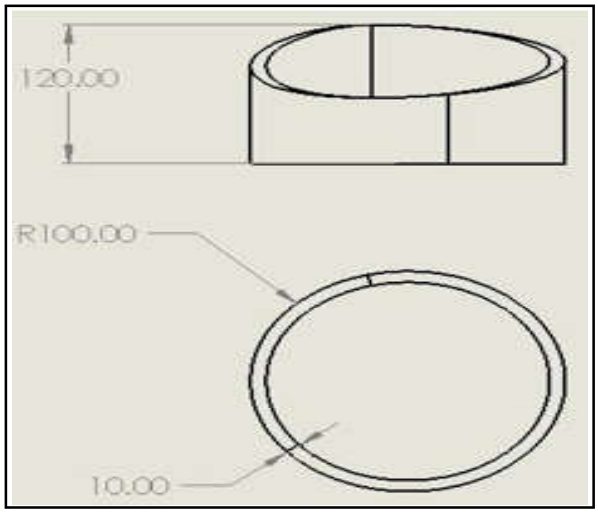

Fig. 6 Orthographic views of Cam (All dimensions are in mm)

6.2.4 Pipes and Hose

The pipe is fixed at the bottom of the tank using pipe joint and adhesives. It is supported at another end by supporting frame. Rigid pipe is placed in inclined position in order to make the constant discharge all over the system. Flexible Hose is used to make elastic joint between rigid pipe and the distribution pipe. Diameter of the pipe is the main factor because this will decides the discharge of the starch.

7. MANUFACTURING PROCESSES

7.1 Components for Fabrication

First step of fabrication is to get all the main components required for the project. The components needed for the project are

7.1.1. Frame Metals

The frame metals are made up of mild steel. It the main component which carries the other components of the machine. The frame is joined together using arc welding process and grinded using hand grinding machine to avoid sharp corners. The bearings are fixed to frame using fasteners by the process of drilling using M8 drill. Motor and Cam are assembled to the main frame through fasteners. This overall setup is mounted in a frame which have wheel in it, so it is to move in the field.

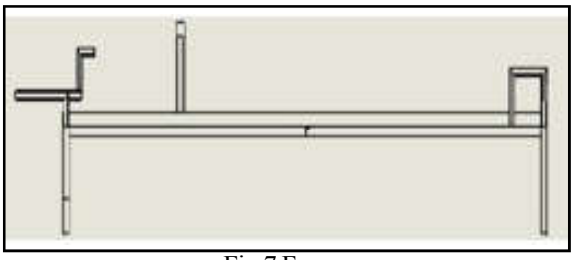

Fig.7 Frame

7.1.2 Motor

Motor is the source of rotating energy of the cam. It is a high torque low speed motor. This motor works on 10 rpm, speed of the motor can also be controlled. It is the frame by fasteners.

Fig. 8 Motor

7.1.3 Cam

The cam is made up of mild steel material. The thickness of the cam is 10mm and the cam is made with an constant velocity profile, CVP ensures the smooth movement of cam. It consists of shaft and cam with shaft and pulley is attached to the frame by the help of bearings. The following Figure 9 shows the end cam of the project.

Fig. 9 End Cam

7.1.4 Tank

The following Figure 10 shows the tank which is made up of GI sheet metal of 1mm thickness. It has capacity of 15; height of the tank is main factor to ensure the specific discharge. Tank used in the system is made by sheet metal bending process and it is attached to the frame by welding process.

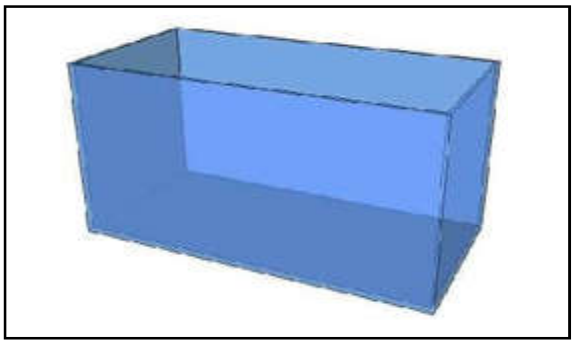

Fig. 10 Tank

7.1.5 Pipes and Hoses

The rigid pipe is fixed at the bottom of the tank using pipe joints and adhesives. These pipes and hoses are made up of PVC and nylon has a diameter of 25.4 mm. flexible pipe feed the starch to the oscillating assembly. Distribution pipe at the end of flexible pipe is attached to the oscillator by fasteners

Fig. 11 Pipes and Hoses

7.2 Assembled Model

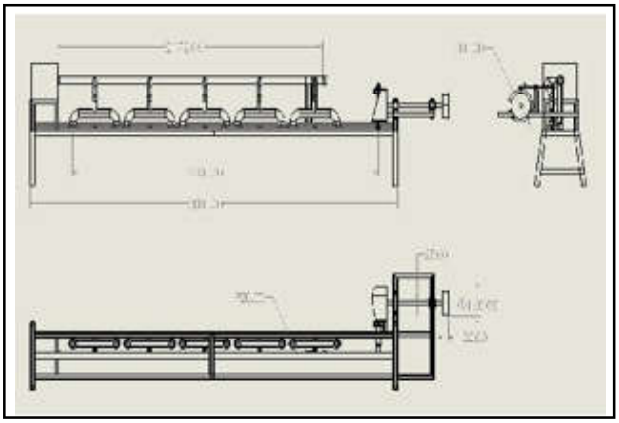

Fig. 12 Assembled model (All dimensions are in mm)

8. WORKING PRINCIPLE

The working principle of this machine is based on the working of oscillating cam and follower. In this machine starch is feed by potential difference between the inlet passage and outlet. Feeding is based on the height, dimension and the oscillation frequency of the system. Starch is feed in wave like pattern to cover the entire fabric length.

When system is started motor will rotate the cam thereby follower is oscillated and the oscillation is transferred to the oscillator by lever assembly. Rigid pipe is placed in inclined position in order to make the constant discharge all over the system. Distribution pipe is connected to the rigid pipe by flexible hose. The flexible hose is the elastic medium. The oscillator will reciprocates inside the oscillating rail.

Pipe holder is used to hold the distributing pipe with the oscillator. Starch from the tank is supplied to the fabric by using specially designed feeding pipe line. Starch is supplied for from stationary system to the oscillating system by means of flexible hose. Fluid flow is due to the gravitational force, fluid is supplied in the wave like pattern, which the tank at specified height and the diameter of the pipe provides specific discharge, this discharge and wave pattern of flow makes the system to completely cover the fabric and better properties.

This oscillating system have own power train in it, so it is easy to move anywhere, it only requires power supply for operation. The system can be redesigned for various fabric width by varying the size and geometry of cam and oscillating rail.

9. CONCLUSION

The importance of the textile industry in the economy is very high. Since there is no mechanism availability for starch feeding in powerlooms and reduction of additional labor requirement, the use of this automated starch feeding attachment is implemented. The uniform flow of starch is also able to obtained through this mechanism. The flow can be regulated easily using the valves attached at the end of flow tubes. The power usually wasted during the rolling process is utilized for the attachment so no additional power source is required. Since there is no additional power source, the energy is conserved and it does not leave any residues during operation. It has the same impact on environment as the

conventional starch feeding process. The attachment is made in such a way that it can fit easily with warping machines of varying sizes and varying pulley positions.

10. OUTCOME OF THIS PROJECT

- Uniform flow of the starch to thread
- Maintaining of uniform thickness of thread
- Avoiding of additional labour requirements
- Simple feeding mechanism
- Reduced time of process

11. FUTURE SCOPE

The following ideas are yet to be used for the future development of this project.

- This project will be developed by varying the flow rate of starch, so that it can be used for any kind of fabric.
- As a further development adaptive changeover of feeding width according to the fabric dimension.

REFERENCES

[1] Kunal Singha, Subhankar Maity, Pintu Pandit and Md.Ibrahim H. Mondal, "Introduction to Protective Textiles", In The Textile Institute Book Series, "Protective Textiles from Natural Resources", Woodhead Publishing, 2022, pp.3-38.

[2] Srivani Thadepalli and Shreyasi Roy, "Implications of Sustainability on Textile Fibres and Wet Processing, Barriers in Implementation" Journal of Sustainable Approaches in Textiles and Fashion, Online access, 2022, pp. 133-156.

[3] Seema Sekhri, Textbook of Fabric Science, 4th Edition: Fundamentals to Finishing.

[4] Schutz, R.A. "Theoretical and Practical Aspects of Sizing today and Tomorrow", Third International Sizing Symposium, 1977, pp. 12-16.

[5] Harry Nisbet, "Theory of Sizing", Emmott.&Company Ltd.

[6] Textile Manufacturer Year Book, Manchester: Emmot and Company, Ltd. 1924.

[7] A.G. Erdman, G.N. Sandor and Sridar Kota, Mechanism Design, Prentice Hall, 2001.

[8] Wang Rong, "Water Washing Device Used in Weaving", patent CN207313901U, 2018.

[9] Harold A. Rothbart, Cam Design Handbook.

A STUDY ON INFLUENCING FACTORS TO RETAIN AN EMPLOYEE IN THE IT INDUSTRY

K. Gokul and M. Freddy Chris
Department of School of Management Studies
Bannari Amman Institute of Technology, Sathyamangalam - 638 401, Erode District, Tamil Nadu

Abstract

Employees are one of the greatest assets of any organizations. An organization starts its journey towards certain destination by reaching that they may achieve their pre-set goals and objectives. Various resources (i.e., financial, raw materials, human) were contributed on the successful completion of the organization's journey. Among that Human Resource is the most valuable asset as it incurs lot of time, money, energy of others to transform the resources into output than other resources. An organization cannot utilize the skill of an employee immediately after the recruitment. They have to restructure the possessed skill into required structure which assist them to attain the output. To restructure an individual skill, an organization must spend some money and time. In return, company expects from those individual to stay back for long time and effective performance. Though an organization wish to retain an employee, worker consider various factors to retain in same organization. Employees are looking for the job which gives a Quality of Life. So only after considering certain factors workers decide about stay back in the same organization. For this study questionnaire had prepared and circulated among IT employees and 200 responses were collected. Some factors like Pay and Recognition, Employee Engagement, Team Support and Work Life Balance are treated as an independent variable which influenced an individual to retain. Among these factors "pay and recognition" as the most influencing factor of employee retention having β coefficient of 0.343, and "Team support" appearing to be the least important with β co-efficient of 0.161. Apart from IT Industry other industries like Banking, Textile, etc., have to be studied to identify the most influencing factor to retain an employee.

1. INTRODUCTION

An organization is a place where various people called employees are run towards the objective or goal set by the management. The goal may be financial based or non-financial based, management expects an employee to contribute to achieving the success. Employees are a great asset to an organization who is the predominant factor to bring back the investment as a return. Added to this, an employee also reasons to achieve other targets fixed by the management. Such an employee has a different capability and skill set which might be built with the help of company support. Companies are spending a lot of money to recruit and develop the skill of an employee. More than that company spends a lot of money to retain the employee with them for a long time.

Why companies are spending a lot of money to retain an employee? Is it difficult to recruit a new one? Though human resource is available in surplus, why companies are like to retain an employee?

The above questions are sensible but factually retaining an employee is a great asset for an organization. In the perspective of cost, both recruiting and retaining may be equal but recruiting a new employee consumes much time and cost. More than that the company should provide induction training to the new employee. This program initiates connectivity between a new employee and the management. Even though, selection of an employee is purely based on requirement some skill gaps might occur by default. Those gaps are filled by providing adequate training and development which also incurs some costs. As it is the introduction of new technology, companies are supposed to facilitate employees by providing the required training, which also incurs some cost. Anyhow the company has to spend some amount of money to provide these basic training which made an employee prepare himself to understand about an organization goal and its objectives.

The company starts to expect an employee to run towards the goal after his understanding of an organization's goal. It might take three to six months from

the joining date, depending upon the nature of the business and the management practice. The company also focuses on getting back the investment made on the employee to equip. So, it is evident that it took some time and money to prepare an employee. But some employees left the organization before meeting out the need of an organization which incurs a loss to the company. Apart from that, it is a very difficult and time-consuming process to recruit a new employee and provide training to them.

So, instead of going to a new one, companies are preferred to stay back with existing employees. In simple, we can say employee retention is making an employee stay with an organization. It involves satisfying an employee by motivating them and made them to embedded with an organization for a long time.

2. LITERATURE REVIEW

Organization Culture, Development opportunities, training and development, Autonomy are the factors that determine employee retention. These factors are less explored than supervision and leadership[1].

Employees are dissatisfied with recognition and performance appraisal provided by an organization. This study also found that the workload given by the management and the salary paid by the management is not related. They suggested paying the right salary and reducing the workload to an employee[2].

Best HRM practices play an vital role in employee retainment in today‘s competitive global market. This study implies that the best HRM activities increases organization productivity along with retaining an employee in same organization for a long time[3].

Employee participation and employee retention was discovered. Delegative participation, consultative participation, and indirect participation are four types of employee engagement that have a positive impact on employee retention[4].

The relationship between explicit corporate social initiatives taken by the organization and employee retention. Further econometric analysis based on a rigid matching approach, along with additional analyses based on survey data, suggests that the retention effect can be attributed to treatment at least in part, and is not solely a result of sorting certain kinds of employees into the social initiative[5].

The longer an employee is rewarded or compensated, the longer they retain employees, and there is a relationship between compensation and job satisfaction[6].

The impact of employer branding on existing employee retention. The study creates a conceptual framework of employer branding’s antecedents and outcomes. The study emphasizes the significance of the employer branding construct and its potential to address the looming issue of employee attrition[7].

The effect of a positive and supportive work environment on employee retention. Data were collected from 211 employees from 67 organizations. They found that employee retention is aided by a positive work environment, according to research. The association between a supportive work environment and employee retention is partially mediated by organizational involvement[8].

The relationship between training and development and employee retention. They found that the relationship between training and development and employee retention, Russell’s model of core affects is required. Furthermore, they recommend that studies on employee retention cover a broader spectrum of work attitudes with high pleasant forms of effect[9].

The influence of transformational leadership on employee retention in small and medium-sized businesses (SMEs), as well as the mediating and moderating roles of organizational citizenship behaviour (OCB) and communication. Data was acquired from 505 employees of SMEs using convenience sampling. The study’s findings show that transformational leadership and OCB have a positive and significant association[10].

The impact of work-life balance on job satisfaction and retention was explored. Work volition was also examined as a modulator of work-life balance and job satisfaction. The findings show that every work volition has a substantial influence as a moderator. Job satisfaction had a modest mediation effect on the association between work-life balance and retention, according to the study[11].

The employee satisfaction with work-life balance is revealed to be a mediator between perceived workload and intention to leave the occupation. They received 2134 respondents and concluded that increased workload

causes employee discontent, which leads to increased employee attrition[12].

Melinde Coetzee, Elleen Stoltz (2015)'s found that concerns, goals, and plans for employees' careers, and how these correlate to retention measures, are vital for retaining them. Some employees were able to achieve their life objectives, financial goals, and career goals with the help of the organization. Those employees were satisfied, indicating a favourable association between employee retention and satisfaction.

3. OBJECTIVES OF THE STUDY

- To identify the most influencing factors to retain employees in IT industry
- To explore the importance of retaining employee instead of hiring new one
- To compute measures taken by the IT Organizations to retain their employees

4. RESEARCH QUESTION

- What are the main factors which influence the employee retention?
- Why it is important to retain the employee instead of hiring new one?
- What are the measures to be taken to retain an employee?

4.1 Factors that Influence Employee to Retain in an Organization

Employees are stay back in an organization for long period due to various reasons which influenced them. Among that we consider four factors that influencing them to retain in an organization. Those factors are Pay and Recognition, Employee Engagement, Team Support and Work-Life Balance.

Employers who are savvy understand that attracting and retaining outstanding workers requires offering a competitive salary and benefits package. Wages, salaries, bonuses, and commission plans all fall under the category of compensation. Employers shouldn't overlook the benefits component of employee compensation and benefits because these add value to employment contracts by addressing the needs of the majority of workers.

Paying workers fairly demonstrates that you regard them as both employees and people. People feel better about reporting to work when they are valued. People are more motivated to come to work and perform a good job, and overall company morale rises. Employees are also more driven to produce better results when they are aware of bonuses or commissions. Plans for commissions and bonuses become the center of success. Giving commendable feedback based on accomplishments or performance is what recognition entails. This can occasionally take the form of an honor, bonus, promotion, or raise. Sometimes appreciation is expressed more casually, such as through a verbal thank-you or a handwritten note. All of these techniques may be effective, particularly if they are carried out quickly and sincerely. They're also motivating and exciting - everyone wants their good work to be applauded. Contrarily, appreciation entails recognizing a person's inherent worth. Their accomplishments are not the main point. It's their worth as a colleague and a human being.

Employees who are truly committed to their jobs and the companies they represent always operate in the best interests of those organisations. What impact does that then have? enormous benefits for both overall corporate performance and employee satisfaction.

"Organizations that engage their workforce the best grows their earnings-per-share more than four times faster than their rivals. Business units in the top quartile of engagement have significantly better customer engagement, higher productivity, better retention, fewer accidents, and 21% higher profitability than those in the worst quartile. Better health results are also reported by engaged workers. - Gallup, Jim Harter, "Employee Engagement on the Rise," August 2018.

The division of labor was an important part of the industrial revolution and the foundation of modern civilization. Additionally, that is yet another way to refer to teamwork. Teamwork among employees enables your workforce to develop specialized skills so that the best person for each task can complete it better and faster. In a nutshell, teams make work more efficient. Divide difficult tasks into simpler ones and work together to complete them faster. That may result in increased profitability, decreased expenses, improved productivity, and a number of other advantages. Recently, Aviva's study has caused some controversy. It demonstrated that, in the wake of the pandemic, people's priorities have shifted from salary to work-life balance. "More workers

said they were attracted to their current role for the work-life balance (41%) than the salary," according to Aviva. The rankings have changed since 2019, prior to the pandemic.

Work is an important part of our lives. We earn enough to keep the lights on, feed the family, and fill the emergency fund. Everyone is aware of the looming crisis in the cost of living and the rising cost of energy, both of which are on their minds. This does not diminish the significance of earning a living, but it does make it more difficult to strike a work-life balance!

4.2 Is it Better To Keep Employees than To Hire New Ones?

It's common for HR professionals to handle hiring, firing, and replacing employees. But if an organization wants to succeed, it's always a good idea to fire an old employee who has worked there for a long time. Many people in the business world aren't aware that employee turnover can have a significant negative impact on profits and cost a lot of money. Unless absolutely necessary, hiring a new employee to take the place of an existing one is always more expensive. It will cost each organization in both monetary and non-monetary terms. High turnover has negative effects like:

- Cost of hiring a new person (advertising, interviewing, screening, hiring)
- Cost of on-boarding a new person (training, management time)
- Lost productivity (a new person may take 1-2 months or more than that to reach the productivity of an existing person)
- Lost engagement (other employees who see high turnover disengage and lose productivity)
- Customer service and errors (new employees take longer and are often less adept at solving problems).
- Cultural impact (whenever someone leaves others take time to ask "why?").

An organization will be successful only by the employees working for it. So, Employee retention is key for the success of every organization. Responsibility for employee retention is not limited to HR persons, first-line supervisor plays a vital role in employee retention. One of the main reasons employees quit is the relationship with their first-line supervisor. The fact is many supervisors and managers are unaware how their actions and decisions affect employee turnover. A critical aspect of an effective retention strategy is manager training.

Another reason for leaving the job is career & skills development. In a study more than 40 percent of the respondents said they would consider leaving their present employer for another job with the same benefits if that job provided better pay and development in their career and looking greater challenges.

5. RESEARCH METHODOLOGY

The convenience sampling method is utilized in this study. Questionnaires have been created to investigate the factors that influence employee retention. Questionnaires were distributed to working persons in IT area via known sources such as friends, relatives, and coworkers. and the responses were collected through online. A total of 200 completed responses were received. These 200 responses have been taken as the sample for the research to identify the most influencing factors of employee retention.

6. RELIABILITY OF THE RESEARCH INSTRUMENT

Following the completion of the data collection, the researcher conducted a reliability test. Table 1 shows that the final Cronbach's Alpha values are greater than 0.7, indicating that the variables listed in the above table like Pay and Recognition, Employee Engagement, Team Support, and Work-life Balance are utilized to measure the construct are reliable.

Table 1 Final Reliability and Validity for Research Instrument

Construct	Cronbach's Alpha
Pay and Recognition	0.736
Employee Engagement	0.844
Team Support	0.710
Work-life Balance	0.737

7. DATA ANALYSIS & RESULTS

7.1 Confirmation of Factors of Employee Retention in an IT Industry

In order to confirm the influencing factors of employee retention scale, 9-item scale was used then.

Factor analyzed using the Principal Component method with Varimax rotation on the perceptions for the employees is performed for establishing the strength of the factor analysis solution as it is essential to establish the reliability and validity of the obtained reduction.

Table 2 Results of Factor Extraction for Work from Home

S. No.	Factor Name & Items	Factor loadings	Eigen Value	Variance in %	Communalities (h^2)
	Pay and Recognition				
1	I am getting right salary for my job which helps me to satisfy my needs	0.918			0.508
2	I am getting maximum benefits from my company	0.869			0.732
3	My company creates an opportunity to learning and development	0.784	**7.072**	**44.200**	0.825
4	My company provides me the great career opportunity	0.765			0.755
5	My company provides rewards for good performance	0.743			0.624
6	I satisfied with recognition given by my company	0.675			0.874
	Employee Engagement				
7	I have an opportunity to develop my leadership quality	0.867			0.871
8	I can able to take my own decision in my job	0.826			0.784
9	Company engaged me in various ways like clear communication about responsibilities, recreation activities, etc.	0.789	**2.354**	**14.715**	0.779
10	I am getting official acknowledgement whenever I am doing good	0.771			0.845
11	I am comfortable with my organization culture	0.640			0.739
12	My work is challenge and creates new experience every day	0.524			0.790
	Team Support				
13	I have very comfortable team in my company	0.911	**1.474**	**9.212**	0.714
14	I can able to maintain friendly relation with my colleagues after work time	0.874			0.770
	Work-life balance				
15	I can able to maintain good work-life balance	0.871	**1.416**	**8.853**	0.850
16	I am allowed to work in flexible time	0.813			0.858

Further, in order to assess the appropriateness of the data for factor analysis, the communalities (h^2) from table 3 is evaluated and it ranges from 0.508 to 0.874 that shows a relatively high level. It meant that factor analysis extracted a good amount of variance in the statements. The Eigen values range from 1.416 to 7.072 which are more than one show that the data sets are appropriate.

From the table 3, it was found that four factor solutions explain 51.380% cumulative variance, which is higher than 50%. Pay and recognition explains maximum variance 44.200% followed by employee engagement explains 14.715% and Team support explain 9.212% variance, and work-life balance explains 8.853% variance respectively.

It means that factor analysis has extracted a good amount of variance in the items. All items were found highly loaded under four factors, which indicate employees are highly satisfied with these statements.

7.2 Extent of Impact of the Factors to Retain an Employee in an IT Industry

The multiple regression model is carried out to measure the work life balance. The following hypotheses have been testing in this analysis

H1: Pay and Recognition has significant effect on employee retention

H2: Employee engagement has significant effect on employee retention

H3: Team Support has significant effect on employee retention

H4: Work-life balance has significant effect on employee retention

In this analysis, the opinion of the respondents on employee retention has been taken as dependent variable and the extracted score from factor analysis on each factor have been taken as independent variables. This model would help to determine the influencing factors to retain an employee.

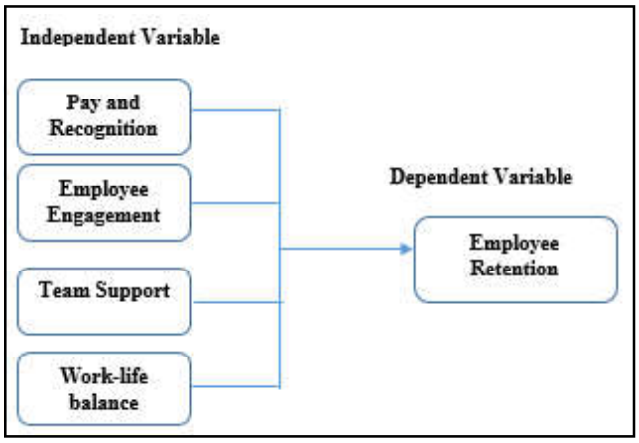

From Table 3, the coefficient of determination value is 0.762 which shows that 76.2 percentages of variations were expressed by all the factors of employee retention considered in the model for predicting overall Impact.

Table 3 Coefficient of Determination (R2), and Adjusted (R2)

R	Coefficient of Determination (R^2)	Adjusted R Square	Std. Error of the Estimate
.880	.0.762	0.760	0.656

From the table 4, the significance of F value is 0.000 which indicates that the model is statistically significant model at 0.05 level of significance.

In table 5, the significance values are less than 0.05 for all constructs. So, the hypotheses formulated for the study were accepted at 95% confidence level. All the factors have positive impact on employee retention.

7.3 Multiple Regressions Model For Study an Influencing Factor to Retain an Employee

ER=6.452+0.214PR+0.187EE+0.133TS+0.468WLB

ER represents Employee Retention
PR represents Pay and Recognition
EE represents employee engagement
TS represents Team Support
WLB represents Work-life Balance

The beta (β) coefficients provide the relative importance. The dimension with the largest coefficient represents the most important determinant of employee retention. The next largest coefficient represents the second most influential determinant and so forth. In other words, the higher the beta co-efficient, more the contribution of factors influencing employee retention.

The results indicate that the "pay and recognition" as the most influencing factor of employee retention having в coefficient of 0.343, and "Team support" appearing to be the least important with в co-efficient of 0.161.

7.4 Strategies that Can Be Implemented To Retain an Employee in an IT Industry

7.4.1 Invest In Employees' Careers

94% of employees, according to LinkedIn, said they would remain with their firm longer if it supported their professional advancement. Employees in the modern market are aware that in order to advance and stay competitive, they must maintain their skills current.

Table 4 ANOVA

	Value of Sum of Squares	Degrees of freedom	Mean Square	F	Sig.
Regression	110.042	16	6.878	9.382	.000
Residual	128.286	75	0.733		
Total	238.328	191			

Table 5 Standardized and Unstandardized Regression Coefficients for Factors to Retain an Employee

	Unstandardized Coefficients		Standardized Coefficients	t	Sig.	Result
	B	Std. Error	Beta			
(constant)	3.431	0.453	6.452	7.568	0.00	
Pay and Recognition	0.343	0.021	0.214	9.332	.000	H1 Accepted
Employee Engagement	0.211	0.031	0.187	8.478	.004	H2 Accepted
Team Support	0.161	0.041	0.133	5.561	.003	H3 Accepted
Work-life Balance	0.265	0.051	0.468	6.543	.001	H4 Accepted

Employers can take advantage of their staff members' drive for growth by offering mechanisms like mentorship programmes and funding further education for their personnel. Organizations can retrain and upskill their staff members with the use of online professional education courses like those Emeritus India provides, expanding their talent pool and elevating employee happiness.

7.4.2 Recognize Employee Contributions

Everyone enjoys feeling appreciated, and this is especially true at work. Although many firms lack formal recognition programmes, according to a Society for Human Resource Management (SHRM) poll, 68% of HR professionals felt that recognition was crucial for employee retention.

Companies should encourage managers to acknowledge the contributions of their immediate reports. They can even go a step farther and recognize employees that go above and beyond on a divisional or corporate level. That understanding is particularly crucial during the pandemic, when many employees have been required to handle challenging situations despite constantly shifting circumstances.

7.4.3 Prioritize Work-Life Balance

Work-life balance is a real concept. However, if employees simply have more work than they can feasibly complete or if the company culture expects them to check their email well beyond business hours, remote work and flexible scheduling policies will be of little assistance.

To ensure that workers don't have more work than they can handle and to promote open channels of communication concerning workloads, managers should periodically check in with staff members. Additionally, businesses can ease the pressure by reducing the number of pointless meetings and administrative tasks that take up time without providing much in the way of added value. In the end, businesses should compare the expense of hiring more employees to the cost of higher turnover in the event that workloads become intolerable.

7.4.4 Support Employee Wellbeing

It is understandable that over half of workers worldwide report feeling burned out given the ongoing pandemic and the political and economic unpredictability. The most effective strategies for preventing burnout include ensuring that employees have reasonable workloads, open lines of communication with management, and a supportive workplace environment. However, employers can also think about taking additional steps to support their employees' physical and mental health.

Employees may benefit from benefits like wellness reimbursements for massages or gym memberships, insurance coverage for counselling and other mental health services, or even access to online platforms for meditation or wellness.

8. DISCUSSIONS AND CONCLUSION

The study proves that the factors considered by the researchers have significant influence on employee retention. Employees feel that if they get proper recognition and satisfied pay, employees decided to stay back with the company for a long time. Other factors like employee engagement, team support and work-life balance also have considerable influence on retaining an employee in an organization. Further research is needed to understand the other factors influencing employee retention, also other sectors like banking, education, hospital, etc., have to study.

REFERENCES

[1] Abeysekera Ruwan, "Impact of Human Resource Management Practices on Marketing Executives Turnover of Leasing Companies in Sri Lanka", Contemporary Management Research, Vol.3, No.3, 2007.

[2] A. Abraham, "Job Satisfaction and Teaching Effectiveness: A Study On College Teachers", The Mobile Professor, Washingtom, D.C., American Council on Education, 1994.

[3] J. Abrams, S. Castermans, H. Cools, M. Michielsen, B. Moeyaert, N. Van Meeuwen and L.Van Nooten (2008)

[4] Learning and Talent Management: Factors which Influence the Retention of (talented) Employees, Unpublished Research Report", Faculty of Psychology and Educational Sciences, University of Leuven, Leuven.

[5] Alkhawaja and Arwa, "Leadership Style and Employee Turnover A Mythical Relationship or Reality? M.A., in Leadership Studies. Capstone project papers, Vol.16, 2017

[6] N.J.Allen and J.P. Meyer, "The Measurement and Antecedents of Affective, Continuance and Normative Commitment to the Organization", Journal of Occupational Psychology, Vol.63, No.1, 1990, pp.1-8.

[7] B.R. Ananthan and L.N. Sudheendra Rao, "Dynamics of Retention: Practices and Strategies, SCMS Journal of Indian Management, October-December, 2011, pp.120-124.

[8] L.J. Bassi and M.E.Van Buren, "Sharpening the Leading Edge", Training and Development, Vol.53, No.1, 1999, pp.23-32.

[9] J. Beardwell and M. Wright, "Recruitment and Selection: Human Resource Management: A Contemporary Approach", Harlow, Pearson Education Limited, 2012, pp.189-229.

[10] D. Branch, "Employee Motivation, Recognition, Rewards and Retention: Kicking it up a Notch", CPA Practice Management Forum, Vol.7, No.11, pp.5-7.

[11] S. Budhiraja and M. Malhotra, "Leadership Style and Organizational Effectiveness in Indian IT and Banking Industry", Indian Journal of Industrial Relations, Vol.49, No.2, 2013, pp.270-285.

[12] R.L. Cardy and M.L. Lengnick-Hall, "Will they stay or will they go? Exploring a Customer-oriented Approach to Employee Retention", Journal of Busienss & Psychology, Vol.6, No.2, 2011, pp.213-217.

AN INSIGHT INTO THE NUMERICAL APPROACH TO MODEL AND SIMULATE THE PROTON EXCHANGE MEMBRANE FUEL CELL

T. Raja[1] and G. Kumaresan[2]
[1]Department of Automobile Engineering, [2]Department of Mechanical Engineering,
Bannari Amman Institute of Technology, Sathyamangalam - 638401, Erode District, Tamil Nadu
E-mail: raja.thiya@gmail.com, raja@bitsathy.ac.in

Abstract

The output performance of the Proton exchange membrane (PEM) fuel cell is directly related to electrochemical reactions in the catalytic layer and avoiding flooding on the cathode side. The bipolar plate structure and their design or channel pattern configuration greatly influence the reactant transport and homogeneous distribution, water management without flooding. Various research focused on the optimisation and performance improvement have been carried out in recent years. Numerical simulations were carried out using computational ыuid dynamics method to compare the performance of fuel cell with the experimental output. The application of numerical method in the fuel cell has paved way for gaining greater understanding of a process and in improvement of the performance. This article represents the governing equations and the boundary conditions that are being used in the numerical modelling and simulation of the proton exchange membrane fuel cell.

Keywords: *Proton exchange membrane fuel cell, PEMFC, Governing Equations, CFD simulation, Computational fluid dynamic (CFD)*

1. INTRODUCTION

Proton exchange membrane fuel cell (PEMFC) converts chemical energy in fuel and oxidant into electrical energy. The important components of PEMFC are bipolar plate, membrane electrolyte and catalyst electrode, the bipolar plate is one of the most important components in the improvement of efficiency and power density of fuel cells[1]. The output performance of the Proton exchange membrane (PEM) fuel cell is directly related to electrochemical reactions in the catalytic layer and avoiding flooding on the cathode side.[2]

The performance of the PEMFC can be improved by optimizing its operating parameters, such as gas flow rate, operating cell temperature, inlet pressure, humidity condition, and flow channel type. The most commonly used bipolar plate configurations such as serpentine, interdigitate and parallel typically considered in many open literatures[3].

The objective of this work is to give an insight into the governing equations that are used in the numerical simulations of the proton exchange membrane fuel cell[4]. Numerical simulations using computational űuid dynamics methods are used to simulate the models and validated by compared with the experimental results [5].

2. NUMERICAL MODELING

In general, a PEMFC consists of a membrane coated with catalyst layers, two gas diffusion layers (GDLs), and two bipolar plates. In order to study the influence of the design parameters on the performance of fuel cells using 3D modelling software such as Solid works, and the gird generation and the computation are done in CFD[6]. The equations of the species transport, Navier-Stokes, energy, mass conservation, electrical charges, and Butler–Volmer are involved in the three-dimensional PEMFC model. Before the exportation of the geometries to the ANSYS Fluent software, computational meshes were generated using ANSYS-Meshing[7].

A three-dimensional hexahedral mesh type is used for most of the studied configurations except some configurations and combinations that have an unstructured grid (both tetrahedral and hexahedral meshes)[8]. A test of mesh independency is performed to choose this number, avoid long computational time, and ensure model accuracy. The computational model is shown below in figure.1.

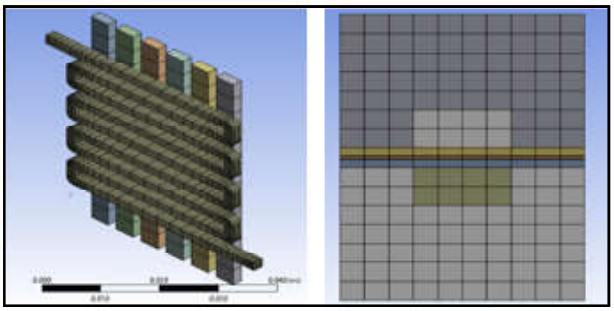

Fig. 1 Computational model and meshing

2.1 Model Assumptions

The following assumptions were applied in the developing the model calculation for the new bipolar plate design, based on the literature review from similar works[9].

- The Proton Exchange membrane fuel cell works in a steady state condition.
- The fuel cell is operated with a constant cell temperature, hence isothermal condition is assumed.
- The Butler-Volmer equation is employed to solve the electrochemical reaction in the catalyst layer.
- The gravitational effect on the reactant is not included.
- The reactant gas is considered as ideal gas and the working fluid as O2, N2 and water vapor (H2O) are incompressible fluid.
- Laminar flow is considered in the gas channel for small pressure gradient and low Reynolds number.
- The gas diffusion layer, catalytic layer and the membrane are isotropic and homogeneous porous media.
- The electrochemical reaction occurs on the surface of the catalyst layer.
- The membrane is permeable to water and impermeable to all gas species
- Multi-component diffusion is considered in this model.

3. GOVERNING EQUATIONS

The CFD models of the PEMFC are mainly composed of the fundamental transport equation and the electrochemical related equation[10]. The fundamental transport equation includes mass, momentum, energy conservation equation and species transport equation, and the electrochemical related equation is composed of electrochemical equation, current conservation equation, governing equation of activated polarization. The conservation equations for mass, momentum, species, charge, and energy are taken into consideration, with the PEM fuel cell model. The algorithm for simulation is shown in figure 2.

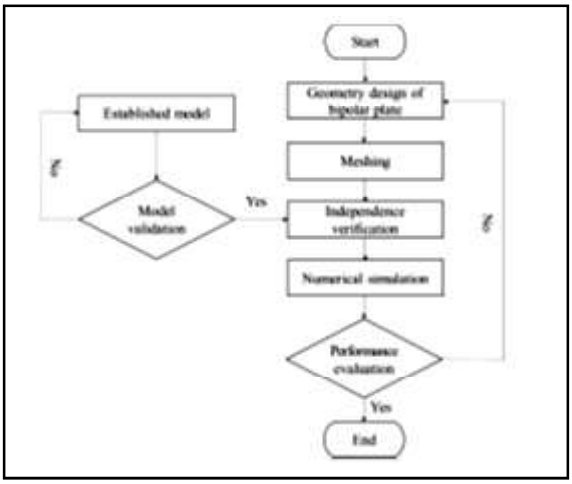

Fig.2 Algorithm for simulation of PEMFC

3.1 Mass Conservation Equations

The equation of mass conservation for the reactant gas in fuel cell channels and gas diffusion layer could be written as follows:

Continuity Equation [11]

$$\frac{\partial(\varepsilon\rho)}{\partial t} + \nabla.(\varepsilon\rho\bar{u}) = S_m$$

At Anode:

$$S_m == -\left(\frac{j_a}{2F}\right) M_{H_2} - \frac{2n_d j_a}{F} M_{H_2O}$$

At Cathode:

$$S_m = -\left(\frac{j_c}{4F}\right) M_{O_2} + \frac{(1+2n_d)j_c}{2F} M_{H_2O}$$

ε is the porosity
μ is the dynamic viscosity
ρ is the pressure
u is the velocity vector.

3.2 Momentum Conservation Equations

Momentum equations in the domain (Navier Stokes equations) are given by [12].

$$\frac{\partial(\varepsilon\rho\vec{u})}{\partial t} + \nabla.(\varepsilon\rho\vec{u}\vec{u}) = -\varepsilon\nabla\rho + \nabla.\left(\varepsilon\mu_{eff}\nabla\vec{u}\right) + S_u$$

Viscosity

$$S_u = -\left(\frac{\mu_{eff}}{K}\right)\varepsilon\bar{u} \quad , \quad S_u = -\frac{\mu_{eff}\varepsilon^2\bar{u}}{K}$$

Due to presence of porous media $S_{mom} = S_m \bar{u}$, Momentum source term due to the mass generation/ consumption in x, y, z directions on account of the electrochemical reactions.

3.3 Energy Conservation Equations

$$\frac{\partial(\varepsilon\rho C_p T)}{\partial t} + \nabla.\left(\varepsilon\rho\vec{u}C_p T\right) = \nabla.\left(k_{eff}\nabla T\right) + S_T$$

$$\nabla.\left(\rho\vec{u}C_p T\right) = \nabla.\left(k_{eff}\nabla T\right) + S_T \qquad [13]$$

$$\frac{\partial(\varepsilon\rho T)}{\partial t} + \nabla.\left(\varepsilon\rho\bar{u}T\right) = \nabla.\left(k_{eff}\nabla T\right) + S_T$$

C_p is the constant pressure specific heat T is the temperature

k_{eff} is the effective thermal conductivity of the mixture of gas and liquid water in the M and in the GC (V. Gurau, et al.,1998)

$$k_{eff} = \varepsilon k^f + (1-\varepsilon)k^s$$

where k^f is the thermal conductivity of fluid and k^s is the thermal conductivity of solid. Where, S_T is given by

$$S_T = I^2 R_{ohm} + h_{reaction} + \eta R_{a,c}$$

3.4 Species Transport Equation

Species transport equation is governed by the following: [14].

$$\frac{\partial(\varepsilon\rho\omega_i)}{\partial t} + \nabla.\left(\varepsilon\rho\bar{u}\omega_i\right) = \nabla.\left(\rho D_i^{eff}\nabla\omega_i\right) + S_i$$

ω_i –is the volume fraction of species

D_i^{eff} Denotes the effective species diffusion coefficient of i_{th} species in the mixture.

$$D_i^{eff} = \varepsilon^{1.5} D_i$$

D_i is a function of temperature and pressure (T, P)[15]

$$D_i^{eff} = \varepsilon^{1.5} D_i^0 \left(\frac{P_0}{P}\right)^{\gamma_p}\left(\frac{T_0}{T}\right)^{\gamma T}$$ (Sukkee U et al.,2000)

where D_i^0 is the mass diffusivity of species i at reference temperature and pressure (T_0, P_0). The reference values and the exponents (γ_p, γ_T). are defined in fuel cell model as: =101,324 Pa, =300 K, = 1 and = 1.5.

The source term in equation, can be introduced as follows: [16]

For anode side And for cathode side

$$S_{H_2} = -\left(\frac{j_a}{2F}\right)M_{H_2}$$

$$S_{O_2} = -\left(\frac{j_c}{4F}\right)M_{O_2}$$

$$S_{H_2O,react} = \left(\frac{j_c}{2F}\right)M_{H_2O}$$

j is the transfer current density

The overall consequence of the water transfer across the membrane is outlined by

$$S_{H_2O,flux} = -\frac{2\alpha_w j_c}{2F}M_{H_2O}$$

The total source term of water can be stated as

$$S_{H_2O} = S_{H_2O,flux} + S_{H_2O,react}$$

For the anode side For the cathode side

$$S_m = S_{H_2} + S_{H_2O} \qquad S_m = S_{O_2} + S_{H_2O}$$

3.5 Electrochemical Equation

The generated current, j, is represented by the famous Butler- Volmer equation in[17] anode and cathode, is also called the exchange current density(A/m3). The Butler Volmer equation, which is a default equation on the Ansys Fluent software[18], was used to calculate the transfer current inside the catalyst layer. The electrical current at the anode (Ja) and cathode (Jc) sides, was, therefore, calculated using the following equations [19].

$$j_a = j_{0,a}^{ref}\left(\frac{C_{H_2}}{C_{H_2ref}}\right)^{0.5}\left\{exp\left(\frac{\alpha_a F\eta_a}{RT}\right) - exp\left(-\frac{\alpha_c F\eta_a}{RT}\right)\right\}$$

$$R_a = \zeta_a j_{0,a}^{ref}\left(\frac{C_{H_2}}{C_{H_2ref}}\right)^{\gamma_a}\left(e^{\frac{\alpha_a F\eta_a}{RT}} - e^{-\frac{\alpha_c F\eta_a}{RT}}\right)$$

$$j_c = j_{0,c}^{ref}\left(\frac{C_{O_2}}{C_{O_2ref}}\right)^{1}\left\{exp\left(\frac{\alpha_a F\eta_c}{RT}\right) - exp\left(-\frac{\alpha_c F\eta_c}{RT}\right)\right\}$$

$$R_c = \zeta_c j_{0,c}^{ref}\left(\frac{C_{H_2}}{C_{H_2ref}}\right)^{\gamma_c}\left(e^{\frac{\alpha_a F\eta_c}{RT}} - e^{-\frac{\alpha_c F\eta_c}{RT}}\right)$$

$j_{0,a}^{ref}$ and $j_{0,c}^{ref}$ are the reference exchange current densities per active surface area. (A/m2)

ζ · is the active specific surface area

η_a and η_c Are the (surface overpotential) activation over potentials.

$C_{H2}$and C_{O2} the molar concentrations, local species concentration, reference value (Kmol/m3)

γ is the concentration dependence

α_a and α_c are the transfer coefficients at anode and cathode side.

F is the Faraday constant
R is the universal gas constant
T is the temperature

3.6 Current Conservation Equation (Electrochemical Model) Electrical Charges (Electrons and Protons) Conservation

The electronic charge conservation equation describes the proton transport inside the membrane-electrode assembly. Two transport equations regarding electron transportation through a solid material, and proton transportation through a membrane, were also coupled with the model. Electronic Charge: (20).

$$\nabla.(\sigma_e \nabla\varphi_e) + S_e = 0$$

Electron Through the solid material
Ionic Charge:

$\nabla.(\sigma_{ion} \nabla\varphi_{ion}) + S_{ion} = 0$ ion through the membrane

$$S_e = -j_{ai}\ ;\ S_{ion} = J_a \qquad S_e = j_{ci}\ ;\ S_{ion} = -J_c$$

The source terms indicate the volumetric exchange currents for the solid and membrane phases.
φ_e - Describs the electric potential in the solid phase (volts)
φ_{ion} - Describs the electric potential in the memberane phase (volts)
$\sigma_{e\,\&ion}$ - Electrical conductivity for the solid and membrane (1/ohm-m)

The transfer currents, or the source terms, are nonzero only inside the catalyst layers and are computed as:
For the potential equation in the solid phase,
R_{solid}=-R_{an}(<0)on the anode side and R_{solid}=+R_{cat}(>0) on the cathode side.For the potential equation in the membrane phase,R_{mem}-+R_{an}(>0) on the anode side and R_{mem}-R_{cat}(<0) on the cathode side.

3.7 Local Activation Losses

The driving force of the reaction is the activation overpotential on the surface (η), which is the difference between the potentials of the solid and membrane phases. The electric potential gain caused by the transportation from the anode jump to the cathode was evaluated by considering an open circuit scenario with the open-circuit voltage. V_{oc} on the cathode side;

The gain in the electrical potential from crossing from the anode to the cathode can be taken into account by subtracting the open-circuit voltage on the cathode.
$\eta_{an}=\phi_s-\phi_m$
$\eta_{cat}= \phi_s-\phi_m-V_{oc}$ [21] is the equilibrium potential according to the Nernst equations.

$$V_{oc} = 1.229 - 0.9 * 10^{-3}(T - 298.15) - \frac{RT}{nF} In \frac{C_{O_2}}{C_{O_2 ref}}$$

As long as the total electric current was generated at the cathode and anode, the current balance equation was valid.

$$\int R_{an} dV|_{anode} = \int R_{cat} dV|_{cathode}$$

The membrane conductivity σ_{ion} is a function of temperature is modelled by [22] and water content λ of the membrane which is defined as

$$\sigma_{ion} = \beta(0.5139\lambda - 0.326)^{\omega} e^{1268\left(\frac{1}{303} - \frac{1}{T}\right)}$$

Where $\beta = \omega = 1$ in the original correlation.

$$n_d = \frac{2.5}{55}\ \lambda$$

Membrane water content λ (Springer Tel et al.,1991) is the membrane water content which is expressed by the empirical correlation suggested [23].

$$\lambda = \begin{cases} 0.0043 + 17.18a - 39.85a^2 + 36a^3 & (a < 1) \\ 14 + 1.4(a-1) & (a < 1) \end{cases}$$

where ***a*** is the water activity, a is the water activity is defined as a sum of the ratio of partial pressure of water vapor to saturated water pressure and the double of water saturation, 2s

$$a = \frac{P_{wv}}{P_{Sat}} + 2s$$

Where s denotes the liquid water volume fraction. P_{wv} –is the water vapor pressure and computed based upon molar fraction of the vapor X_{H2O} and the local pressure.

$$P_{wv} = x_{H2O} P$$

The P_{Sat} is saturation pressure calculated in atm units using, [23].

$$P_{Sat} = 10^{-2.1794+0.02953T+9.1837*10^{-5}T^2+1.4454*10^{-7}T^3}$$

In addition, to determine the velocity uniformity, the uniformity index, γ, was calculated as presented in Eq. (15) based on the average velocity, u, and the area, A

$$\gamma = 1 - \int \frac{\sqrt{(\bar{u} - u)^2}}{2.A.\bar{u}} dA$$

Assuming that the material and operating parameters are preserved, therefore, the diffusion is equivalent, and the Sherwood number increases with the mass transfer. As a result, this quantity can be used as a reference to evaluate the best design considering the mass transfers .

$$S_h = \frac{h_m D_h}{D_{i,j}}$$

where D_h denotes the hydraulic diameter; $D_{i,j}$, the binary diffusion coefficient; and h_m, the mass transfer convection coefficient, which can be calculated based on the mass flow of reactants that have already reacted, m, and the generated electric current, A_{elect}.

$$h_m = \frac{\dot{m}}{A_{elect}(C_o - C_s)}$$

Finally, the fuel cell net power of the fuel cell, W_{net} is calculated using

$$W_{net} = W_{FC} - W_P$$
$$W_P = \Delta P \frac{\dot{m}}{\rho}$$
$$W_{FC} = I * V * A_{EL}$$

where W_{FC} denotes the fuel cell gross power; W_P, the pump power used to supply the reactant; m, the inlet reactant mass flow rate; ρ, the reactant density; and i%P, the pressure drops between the inlet and outlet of the channel.

3.8 Liquid Water Model

Liquid water transport in channel:[24]

$\frac{\partial(\varepsilon\rho_l s)}{\partial t} + \nabla.(\rho_l \vec{u} s) = r_w$ (Yan XH et al.,2019)

$$r_w = \begin{cases} (1-S)C_r \dfrac{P_{wv} - P_{sat}}{RT} M_{H_2O} & if(P_{wv} > P_{sat}) \\ SC_r \dfrac{P_{wv} - P_{sat}}{RT} M_{H_2O} & if(P_{wv} < P_{sat}) \end{cases}$$

$$\frac{\partial(\varepsilon\rho_l s)}{\partial t} + \nabla.\left(\rho_l \frac{kS^3}{\mu_l}\frac{dP_c}{dS}\nabla s\right) = r_w$$

s is the water saturation,
ε is the porosity
ρ_l is the density of liquid water
μ_l is the viscosity of liquid water
P_c is the capillary pressure

$$P_c = \begin{cases} \dfrac{\sigma\cos\theta_c}{\left(\frac{K}{\varepsilon}\right)^{0.5}}\left[\begin{matrix}1.417(1-s) - 2.12(1-s)^2 + \\ 1.263(1-s)^3\end{matrix}\right] & \theta_c < 90^0 \\ \dfrac{\sigma\cos\theta_c}{\left(\frac{K}{\varepsilon}\right)^{0.5}}(1.417s - 2.12s^2 + 1.263s^3) & \theta_c > 90^0 \end{cases}$$

Here, σ is the surface tension. θc is the contact angle.

4. BOUNDARY CONDITIONS

Bipolar plates, flow channel, anode and cathode diffusion layer, anode and cathode catalyst layer and proton exchange membrane are the computational domain of simulation. Suitable boundary conditions need to be specified for solving the model equations.

4.1 Inlet Boundary Conditions

Velocity of gases and mass fractions of species are fixed at the inlet. The mass flow inlet boundary is implemented for the channel inlet and the anode and cathode inlet mass flow rates are calculated by,

$$m_a = \frac{\rho_g^a I_{ref} \xi_a A}{2FC_{H_2}}$$

$$m_c = \frac{\rho_g^c I_{ref} \xi_c A}{2FC_{O_2}}$$

Here, m_a, m_c are the anode and cathode inlet mass flow rate, respectively. I_{ref} is the reference current density. ξ_a, ξ_c are the stoichiometry ratio of anode and cathode, respectively. A is the active area of fuel cell. F is the Faraday's constant. ρ - the density of the reaction gas. The molar concentrations of H_2 and O_2 are determined as:

$$C_{H_2} = \frac{\left(P_g^c - RH_a P^{sat}\right)}{RT_0}$$
$$C_{O_2} = \frac{\left(P_g^c - RH_C P^{sat}\right)}{RT_0}$$

where RH is the inlet relative humidity. R is the gas constant. Outlet boundary conditions: The pressure outlet boundary condition is applied at the channel outlet. Wall boundary conditions: According to the assumption of laminar flow in the PEMFC, no-slip boundary condition is used at the wall. [25]. For velocity, no slip boundary condition is adopted and for the mass fraction, the zero-flux boundary condition is adopted. Temperatures: The temperatures of the inlet gas and surrounding walls are set the same with the PEMFC operating temperature.

The temperature of the entire model is prescriptive and is defined as the operating temperature. Electric potentials: The electric potentials at the anode and cathode bipolar plate surfaces are defined as:

$$\begin{cases} \phi_e^{a,end} = V_{rev} - V_{cell} = \eta_{total} \\ \phi_e^{c,end} = 0 \end{cases}$$

where V_{rev}, V_{cell} and η_{total} are the fuel cell reversible voltage, output voltage and voltage loss, respectively. The reversible cell voltage , can be calculated as:

$$V_{oc} = 1.229 - 0.9 * 10^{-3}(T - 298.15) - \frac{RT}{nF} In \frac{C_{O_2}}{C_{O_2\,ref}}$$

The zero-flux boundary is set to the proton phase potential for all the outer boundaries, because no proton current leaves the PEMFC through any of the outer boundaries.

5. NUMERICAL PROCEDURE

The governing equations along with their appropriate boundary conditions, are discretized by the finite volume method [26)] The three-dimensional(3-D) multiphase model developed in the present study is implemented in a commercially used computational fluid dynamics (CFD) software package, ANSYS-22 FLUENT using the finite volume method based on the SIMPLE algorithm. The SIMPLE algorithm is applied in the solution method for the pressure-velocity coupling and for iterative calculation. [27]. The source terms and physical properties are implemented in a UDF user-defined function and the species and charge transport equations are solved through the software's user-defined scalars. The user-defined functions (UDFs) are used to solve the updated equations and physical parameters. The algebraic multigrid (AMG) method is used to accelerate the process of calculation and to improve the calculated convergence[28].

5.1 Model Validation

The PEMFC model is constructed in ANSYS Fluent. In order to verify the reliability of the numerical results, the simulation results of the are compared with the previous experimental data under the same working condition. The model validation is done with the experimental results as shown below in Figure 3.[29]

The CFD results are in acceptable agreement with the reference work indicating the model is reliable in this work. The experimental data agrees well with the simulated data and ensures the accuracy of the PEMFC model[30]. The model can be used for computational optimization.

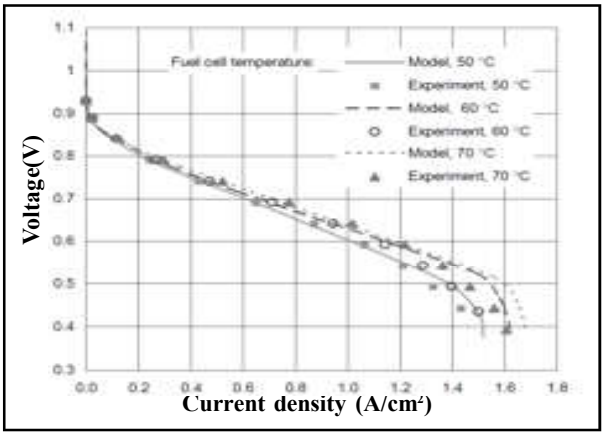

Fig.3 Comparison of the numerical results with the experimental data (Wang Lin et al)

6. CONCLUSION

The numerical modelling of the proton exchange membrane fuel cell mainly composed of the fundamental transport equation and the electrochemical related equation. The fundamental transport equation includes mass, momentum, energy conservation equation and species transport equation, and the electrochemical related equation is composed of electrochemical equation, current conservation equation, governing equation of activated polarization. The governing equations along with their appropriate boundary conditions, are discretized by the finite volume method. The model is implemented in a commercially used computational fluid dynamics (CFD) software package, ANSYS-22 FLUENT using the finite volume method based on the SIMPLE algorithm. The SIMPLE algorithm is applied in the solution method for the pressure-velocity coupling and for iterative calculation. The source terms and physical properties are implemented in a UDF user-defined function and the species and charge transport equations are solved through the software's user-defined scalars. The algebraic multigrid (AMG) method is used to accelerate the process of calculation and to improve the calculated convergence.

REFERENCES

[1] A. Arvay, J. French, J-C. Wang, X-H. Peng and AM. Kannan, "Nature Inspired Flow Field Designs for Proton Exchange Membrane Fuel Cell", e26. https:// doi.org/10.1016/j.ijhydene.2012.12.149, Int J Hydrogen Energy., 2013, Vol.38, No.9, pp.3717.

[2] RW. Barber and DR.Emerson, "Biomimetic Design of Artificial Micro-Vasculatures for Tissue Engineering", ATLA, 2010, Vol.38, No.(Suppl. 1), pp.67e79.

[3] RW. Barber and DR.Emerson, "Optimal Design of Microfluidic Networks Using Biologically Inspired Principles", Microfluid Nanofluidics, 2008, Vol.4, pp.179e91.

[4] F. Barbir, "PEM Fuel Cells: Theory and Practice", San Diego: Academic Press; 2005.

[5] JO. Bockris, AKN. Reddy and ME. Gamboa-Aldeco, "Modern Electrochemistry 2A. Fundamentals of Electrodics", 2nd ed. US: Springer; 2000.

[6] A. Chapman and I. Mellor, "Development of Biomimetic™ Flow Field Plates for PEM Fuel Cells", in The Eighth Grove Fuel Cell Symposium London; September 2003, pp.24e26.

[7] L. Fan, Z.Niu, G.Zhang and K. Jiao, "Optimization Design of the Cathode Flow Channel for Proton Exchange Membrane Fuel Cells", Energy Convers Manage, 2018, Vol.171, pp.1813-21.

[8] L. Fan, G.Zhang and K. Jiao, "Characteristics of PEMFC Operating At High Current Density with Low External Humidification", Energy Convers Manage, 2017, Vol.150, pp.763-74.

[9] YM. Ferng, Ay Su and SM.Lu, "Experiment and Simulation Investigations for Effects of Flow Channel Patterns On the PEMFC Performance", Int J Energy Res., 2008, Vol.32, pp.12-23.

[10] YM. Ferng and A.Su, "A Three-dimensional Full-cell CFD Model Used To Investigate the Effects of Different Flow Channel Designs on PEMFC Performance", International Journal of Hydrogen Energy, 2007, Vol.32, pp.4466-76.

[11] JH. Ferziger and M.Peric, "Computational Methods for Fluid Dynamics", Berlin: Springer-Verlag, 1999.

[12] Frano Barbir, "PEM Fuel Cells Theory and Practice, Sustainable World Series", Academic Press, 2005, pp.209-18.

[13] H. Heidary, MJ.Kermani, AK.Prasad, SG.Advani and B.Dabir, "Numerical Modelling of In-line and Staggered Blockages in Parallel Flow Field Channels of PEM Fuel Cells", https://doi.org/ 10.1016/ j. ijhydene.2016.10.076, Int J Hydrogen Energy, 2017, Vol.42, pp.2265-77.

[14] A.Iranzo, Mu noz M, F. Rosa and J. Pino, "Numerical Model for the Performance Prediction of a PEM Fuel Cell", Model results and experimental validation, https://doi.org/10.1016/ j.ijhydene.2010.04.129, Int J Hydrogen Energy, 2010, Vol.35, pp.11533-50.

[15] Jin Hyun Nam and M. Kaviany, "Effective Diffusivity and Water Saturation Distribution in Single-and Two-Layer PEMFC Diffusion Medium", Int J Heat Mass Tran., 2003, Vol.46, pp.4595-611.

[16] JP. Kloess, X.Wang, J.Liu, S.Shi and L. Guessous, "Investigation of Bio-inspired Flow Channel Designs For Bipolar Plates In Proton Exchange Membrane Fuel Cells", Journal of Power Sources, 2009, Vol.188, pp.132-40.

[17] AD. Le and B. Zhou, "A General Model of Proton Exchange Membrane Fuel Cell", J Power Sources, 2008, Vol.182, pp.197-222.

[18] X. Li and I.Sabir, "Review of Bipolar Plates in PEM Fuel Cells: Flow-field Designs", International Journal of Hydrogen Energy, 2005, Vol.30, pp.359-71.

[19] HC. Liu, WM.Yang, J.Tan, Y.An and LS.Cheng, "Numerical Analysis of Parallel Flow Fields Improved By Micro-Distributor in Proton Exchange Membrane Fuel Cells", Energy Convers Manage, 2018, Vol.176, pp.99-109.

[20] L. Wang, A. Husar, T. Zhou and H. Liu, "A Parametric Study of PEM Fuel Cell Performances", Int. J. Hydrogen Energy, https://doi.org/ 10.1016/ S0360-3199(02)00284-7, 2003, Vol.28, pp.1263-1272.

[21] RF. Mann, JC.Amphlett, BA.Peppley and CP. Thurgood, "Application of ButlereVolmer Equations in the Modelling of Activation Polarization for PEM Fuel Cells", J Power Sources, 2006, Vol.161, pp.775-81.

[22] AP. Manso, FF. Marzo, J. Barranco, X. Garikano and M. Mujika, "Influence of Geometric Parameters of the Flow Fields on the Performance of a PEM Fuel Cell A Review", Int J Hydrogen Energy, 2012, Vol.37, pp.15256-87.

[23] Manual ANSYS FLUENT Fuel Cell Module. Release 14.0. November; 2011, ANSYS Fluent Advanced Add-On Modules ANSYS, Inc Southpointe January 2016 2600 ANSYS Drive Canonsburg, PA 15317

[24] CD. Murray, "The Physiological Principle of Minimum Work", The Vascular System and the Cost of Blood Volume. Proc Natl Acad Sci USA, 1926, Vol.12, pp.207-214.
[25] CD. Murray, "A Relationship between Circumference and Weight in Trees and Its Bearing on Branching Angles", J Gen Physiol, 1927, Vol.10, pp.725-729.
[26] J. Nassau Christopher and K.Agarwal Ramesh, "Curvature Effects and Flow Uniformity Optimization of a Blood Microchannel", Mech Eng Mater Sci Indep Study, 2018, Vol.71.
[27] SV. Patankar, "Numerical Heat Transfer and Fluid Flow", New York: Hemisphere Publishing Corporation; 1980.
[28] SW. Perng and HW.Wu, "A Three-dimensional Numerical Investigation of Trapezoid Baffles Effect on Non-Isothermal Reactant Transport and Cell Net Power in a PEMFC", Appl Energy, 2015, Vol.143, pp.81-95.
[29] TE. Springer, "Polymer Electrolyte Fuel Cell Model", https://doi.org/10.1149/ 1.2085971, J Electrochem Soc, 1991, Vol.138, pp.2334-42.
[30] U.Sukkee, CY.Wang and KS.Chenb, "Computational Fluid Dynamics Modelling of Proton Exchange Membrane Fuel Cells", J Electrochem Soc., 2000, Vol.147, pp.4485-93.

DESIGN AND IMPLEMENTATION OF A CHAIN-OF-THINGS ARCHITECTURE FOR DIGITALLY MANAGING PRECISION AGRICULTURE

K. Raju[1], Steephan Amalraj[2], R. Lalitha[3] and Ramesh Kalyan[4]
[1]E.G.S. Pillay Engineering College (Autonomous), Nagapattinam - 611 002, Tamil Nadu
[2]Bannari Amman Institute of Technology, Sathyamangalam - 638 401, Erode District, Tamil Nadu
[3]Sathyabama Institute of Science & Technology, Chennai - 600 119, Tamil Nadu
[4]SNS College of Technology, Coimbatore - 641 035, Tamil Nadu
E-mail: profgkr@gmail.com, steephanamalrajj@bitsathy.ac.in,lalithakani1@gmail.com, g.rameshkalyan@gmail.com

Abstract

Integrating the potential benefits of Internet-of-Things with the decentralized logs of a blockchain network (i.e., called Chain-of-Things (CoT)) increases the effectiveness of various applications in smart farming (also known as precision agriculture). The demand to develop a secure platform capable of observing, authenticating, safeguarding, and studying agronomic information is important to focus on CoT networks. The CoT network provides a better way to replace conventional techniques to monitor, store, and share information in a more transparent, immutable, dependable, and decentralized way. In precision agriculture, CoT transforms the scenario to the internet of smart farms from only smart farms and provides more governance in the agricultural industry. The consequence of this integration provides more sovereignty and smartness in handling farming effectively. This study performs an inclusive survey on the significance of assimilating both IoT and blockchain networks (BCN) in creating applications of smart farming networks. Besides, we propose a novel CoT model with an efficient authentication protocol to digitally cope with different subdivisions in smart farming including crop yield analysis, monitoring the variable rate of fertility, diagnosis of diseases, weather prediction, animal grazing, and food supply. Active tracking and managing a CoT system in smart farming needs an efficient model for handling data flow and identifies the actions and communications among IoT maneuvers. This study exploits the Docker platform to implement nodes on the server as the containers and Hyperledger Fabric model to simulate the proposed model. The cryptocontract (smart contract) is created and deployed using the Hyperledger Composer. The effectiveness of the intended model is evaluated regrading execution time for device registration and sensor reading. Extensive empirical results reveal that the proposed CoT architecture provides an effective model for precision agriculture.

Keywords: *Power system, Security-constraint, Stability, Transient analysis*

1. INTRODUCTION

Reeling from the shocking impacts of macro and micro climatic changes and tremendous growth in patterns of utilization, the agronomic industry is undergoing a major crisis. At the same time, farming is one of the industries with the tiniest amalgamation of information and communication technologies [1]. However, recent research proves that the utilization of cutting-edge tools including deep learning, Internet of Things (IoT), big data, and BCN promise to fetch digitalization to the farming industry and address the issues regarding environmental monitoring, production sustainability, product traceability, equal pay for producers, reliance among supply chain stakeholders, and other issues [2]. By applying these advanced tools, it is become probable to collect, compute, and analyze smart big data about the status of the weather, crops, and soil together with additional services including food safety, livestock cropping, and crops and fruits supply chain.

The proliferation of smart sensors in IoT technology has transformed conventional farming into precision farming in an efficient way. By installing appropriate sensing elements in huge land tracts, farmers can gather a considerable amount of data about irrigation, temperature, crops, and soil acidity that could be integrated with previous data to deliver deep insights to farmers as well as agricultural officers and aid them to take the appropriate and timely verdicts [3]. But, most prevailing IoT frameworks follow highly centralized structural models, which are hampered by numerous

technical difficulties, like single-point failures and cyberattacks [4]. Of late, BCN has gained more reputation as a potential tool in the domain of smart farming owing to its intrinsic features including decentralization, transparency, immutability, autonomy, and accessibility. It performs the pivotal role of transforming the conventional approaches of recording, processing, and distributing farming data into a more dependable and secure way. The combination of IoT with BCN (i.e., called chain-of-things) is an additional significant support expected to reform the digital revolution of precision farming [5].

CoT enables us to transform to the internet of secured smart farms from only smart farms providing more governance in the supply chains management system. The consequences of this CoT networks result in increasing sovereignty and smartness in managing smart farming. The goal of the CoT platform in precision farming is to improve the quality of yield and endorse fair business and sustainable agronomic operations by meticulously exploiting cost-effective and low-power sensing elements (e.g., optical, mechanical, location, and airflow sensors). These sensors integrated with other technologies help in the procurement of real-time information about the crop, location, soil, etc. But, in a precision farming atmosphere, the utilization of IoT and internet technologies brings massive security threats to smart agriculture. Such threats can harmfully disturb financial prudence that relies profoundly on agronomy. Accordingly, economic loss, crop contagion, and excess waste have happened. Moreover, to realize sustainability in agronomy there is also an imperative condition on reliability, throughput, latency, robustness, privacy, and scalability, which must be explored. In this context, we develop a novel CoT architecture with an efficient authentication protocol to ensure the integrity of the gathered data in smart farming. This work targets to provide a real-world application to the farmer that delivers a complete, irreversible record and enables direct access to their gadget organized in various fields. Besides, it offers simultaneous monitoring as well as governance between the gadget and the end user through the IoT platform. The CoT network also provides adequate security and preserves privacy to the user data through BCN. The commercial model of the application is described by the cryptocontract which comprises conditions and rubrics. The intended method is implemented in a real-time IoT test bed which contains Raspberry Pi maneuvers and a system known as Hyperledger Fabric. Finally, a standard analysis is made to emphasize the importance of the CoT network using different evaluation measures. The empirical outcomes indicate the effectiveness of the proposed system.

The remaining sections of this article are structured as follows: Section 2 reviews the related works about IoT and BCN-based smart farming. In Section 3, we take an in-depth look at the integration of IoT and BCN in the proposed CoT model to identify network intrusion in the IIoT system. Then, the implementation details and the numerical results are presented in Sections 4 and 5. To end, conclusions are drawn in Section 6.

2. RELATED WORK

As far as we know, exploration of the collaboration between BCN and IoT is confined since BCN is reasonably appropriate for business and fiscal applications. This section explores the existing BCNs associated with sensors by studying several topical research works. Atlam et al. proposed an amalgamation of smart sensors with the BCN accentuate the reimbursements, issues, and upcoming trends of this integration [6]. Torky and Hassanein studied substantial solutions through which BCN can resolve several performance and security issues of IoT networks in smart farming [7]. Özyýlma and Yurdakul proposed an integrated BCN-based infrastructure with low-power resource-constrained IoT devices [8]. The authors employed smart things as BCN nodes and recommend a trigger-based message-sharing method for low-power sensors. They reviewed the utilization of cryptocontracts in smart things and define how cryptocontracts can enable and maintain smart communication among smart things.

Lin *et al.* proposed an autonomous, secured, open, and eco-friendly food safety system by integrating BCN and IoT tools, which deals with all stakeholders of precision farming, whilst there is no trust among them [9]. The authors used IoT sensors to substitute manual recording and authentication of data to the greatest extent, which can minimize human involvement in the network efficiently. In another research, the same authors developed an integral solution for long-range radio network servers to achieve a distributed, trusted, open, and tamper-proof model using BCN. An undeniable control is proposed to validate the transactional data that happened at a particular time in the system. Pranto et al. reconnoitered various features of integrating IoT devices with BCN in post-harvesting and pre-harvesting

processes of farming [10]. The authors developed a system that exploits BCN as the mainstay whereas IoT sensors procure data from the farms, and cryptocontracts control the communication among all the stakeholders. Xu et al. proposed a new model to use the processing capacity of IoT expedients to achieve the processing of gathered data through cryptocontracts [11]. The empirical outcomes show that this method can decrease the traffic on the IoT system and increase the performance of the transaction. In this study, a distributed model to preserve the privacy of the user on IoT maneuvers through the Ethereum platform is developed [12]. Also, a BCN is designed to communicate with the IoT devices and the end user. Hang et al. developed an integrated sensor-cloud technology for corporeal device management on CoT networks [13]. Also, this work deployed the CoT into a cloud structure to improve decentralization and data transparency. The intended model organize the corporeal means into the virtual resource pool and disclosures them as facilities. Fundamentally, BCN is employed as an interface between industrial resources and the cloud, ensuring data security and transparency in cloud technology.

Biswas and Muthukkumarasamy proposed a smart city application model to assimilate different IoT devices in a much more protected way [14]. The established model delivers different attributes, such as improved fault tolerance ability, extensibility, better dependability, and effective functions, which create a shared BCN where all devices could connect in a decentralized background. Dorri et al. proposed a simple structural design for IoT to reduce the communication and processing cost of conventional BCNs while preserving most of its privacy and security reimbursements [15]. A private irreversible record is developed to enhance the power dissipation property of IoT maneuvers. Furthermore, they exploit the disseminated reliance to minimize the computational time of block authentication.

The above-mentioned research works have some general technical problems that are very difficult to handle through classical IoT maneuvers in a resource-constrained system. However, the nonuse of innate virtual currency can eliminate the menace of cryptocurrency consideration, and can coarsely achieve the similar computational enactment related to other decentralized network. Besides, they organize the replica of the distributed ledger (DL) onto IoT maneuvers that perform as BCN peers. Thus, the transaction performance is seriously affected and it is difficult to satisfy the demand of an inclusive smart network with a large number of devices. For the necessity of the real-world implementation, the present work provides viable results that are scalable to huge systems with higher throughput and reduced delay. Furthermore, the applications that are well-matched with limited-resource environment of smart things are discussed as well.

3. COT – AN INTEGRATION OF IOT AND BCN TECHNOLOGIES

The convergence of BCN and IoT technologies signifies irreversible transformation towards Society 5.0 from Industry 4.0. Besides, this amalgamation is anticipated to significantly impact all aspects of the business and renovate the way we work within various industries. Hitherto, IoT system has been extensively espoused by various industries for achieving peer-to-peer interactions. While the present technologies make the notion of IoT possible, several issues lie ahead for helping the comprehensive real-time implementation of IoT solicitations. Recently, the BCN has gained widespread attention from scholars and industries for its transparency and security. The BCN has an inordinate capacity to be the architecture for connecting each device and for timestamping diverse information in Industry 4.0. Primarily due to its distributed characteristics in processing and managing data, the BCN can be an influential technology to resolve several IoT disputes, particularly security.

The inevitability of developing a protected and intelligent configuration leads to the integration of BCN with IoT devices in smart farming. With the help of BCN, conventional approaches used for accumulating and disseminating farming data are substituted with dependable, decentralized, and transparent data storage approaches. This integrated system helps us in managing the smart farming networks in a more protected and enhanced way. The concept of CoT, leveraging the nexus between IoT and BCN, is a significant contribution intended to reform the digital transformation of several platforms. This technology enables organizations to reinforce relationships among their core corporate partners, particularly with current consumers, and to entice new ones. Furthermore, it is used to resolve inherent issues such as identity, security, and interoperability problems related to connected things and to create well-organized pioneering applications in the healthcare supply network. CoT facilitates infrastructure for different communication and transactions environment

in smart farming. It enables several smart things to share farming data rapidly without mediation or authentication from financial entities and other trusted bodies.

4. PROPOSED COT PLATFORM FOR SMART FARMING

The study developed new CoT networks that can be employed as viable elucidations for key problems in IoT-based smart farming. Effective monitoring and managing a CoT system in smart farming needs an efficient model for handling data flow and identifies the actions and communications among IoT maneuvers. The intended CoT model should be flexible enough to facilitate the monitoring of different communication scenarios. The following subsections present the proposed model in detail.

4.1 Conceptual Model of Proposed CoT Platform

Figure 1 illustrates the conceptual model of the CoT framework for precision farming. This model contains the layer-based architecture by means of where each layer is isolated from the others to facilitate designers can substitute or include any new component without distressing the remaining sections of the network. The physical layer contains several related IoT maneuvers with the capabilities of data sharing, processing, and storage. The physical maneuvers can be categorized into two types including actuators and sensors. The sensors are employed to collect farming data (e.g., temperature, humidity, soil status, crop condition) and transmit this information to IoT servers for future analysis. The actuators are employed to achieve certain activities (e.g., trigger the alarm) based on instructions received from the clients. Local bridges assimilate physical maneuvers to the server using a networking system and function as the mediator for these expedients. Currently, embedded expedients such as Raspberry Pi can unswervingly access web services using REST-APIs (representational state transfer application programming interfaces).

In this study, we suggest two methods to enable communication with IoT maneuvers: (i) through the local bridges; and (ii) through direct communication networks. The main service delivered by this networking layer is the route control mechanism since IoT maneuvers do not have any inclusive internet protocol. This layer also comprises other units for delivering services, such as message broker, security management, and network management. The CoT service layer consists of a BCN, IoT server, and data storage. A service provider is acting as a server that can communicate with the BCN and the local bridges to deliver various facilities for clients (e.g., gathering information from the local bridge, distributing instructions to execute some actuator functions, probing information, or storing data through the BCN, etc.). The storage device that is present in the CoT service layer can record the profiles of the farmer as well as IoT devices and information gathered by sensing elements. It can either be software storage like a database or hardware storage such as a hard disk.

The CoT service layer establishes several services to exploit the key characteristics of BCN such as identity manager, smart contract, and device-to-device interaction. DL is an agreement of synchronized, shared, and replicated data that is distributed through the entire BCN in which all stakeholders with the system can have their identical replica of the DL. It also enables protected space to store the device structure and gathered information through IoT devices. Any modifications to the DL are revealed in all replicas within a minute, or for a few applications, a second. The DL can be classified into two types: permissionless and permissioned DL based on if only appropriate members or everyone can operate a node to authorize dealings. The data processing unit makes the BCN to be an effective network for incremental data storage.

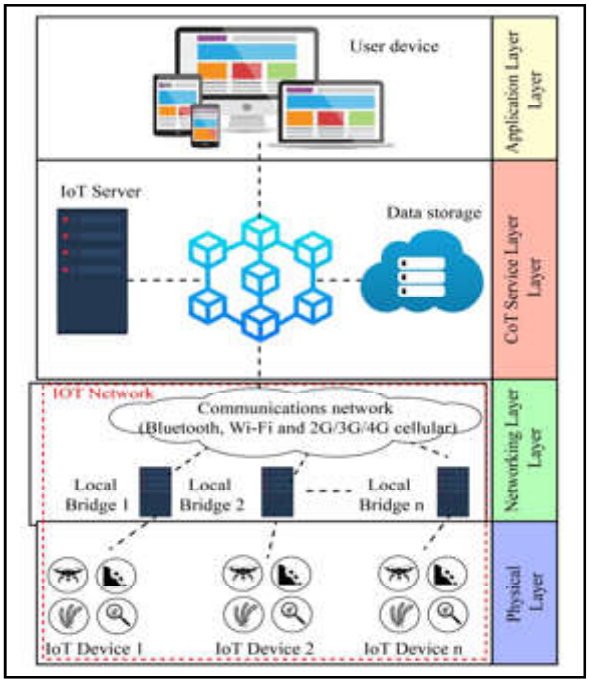

Fig.1 The conceptual model of CoT in smart farming

Numerous records of the transaction from different stakeholders are recorded in controlled systems of DLs, which make it a seamless resource for future study. Each stakeholder can gain approved access to a resource and gain this information. The cryptocontract is the type of code created by an outside agent to handle process and alterations in the DL. It is generally implemented and instantiated onto each node of the system. The event manager directs actions whenever a new block is incorporated into DL or activated every time the threshold value in the cryptocontract is satisfied. The interface reveals the facilities given by the BCN whereby the user can manage and access the system.

The application layer is the uppermost layer, where various APIs are used to get the information from smart things to processes and controllers. The user device can be any edge computing device including PCs, laptops, and smartphones by which clients can write or read data to the BCN. For instance, farmers can view the data from field monitoring analysis, crop yield analysis, diagnosis of diseases, etc. that are recorded in the BCN at a particular time. There are numerous networking protocols (e.g., WiFi, ZigBee, 3G/4G/5G cellular, and Bluetooth) used to implement IoT devices and applications.

4.2 Communication Model of the Proposed CoT Platform

The interaction among each element of the proposed CoT platform is described in Figure 2. The developed model includes not just a methodological structure but also a client service model that provides the DL and cryptocontract as facilities to the client. The user application module gives an in-built APIs to send transaction proposals (T_XP) to the BCN for retrieving facilities including farmer sign-up, device registration, and task creation services given by the BCN. Afore sending T_XP, the signing-up phase is mandatory to deliver a particular member with a credential, which comprises secret keys to sign the. A is a procedure to read or write data from the ledger of the BCN.

The farmer can send to register a new maneuver or create a new process via the IoT server. As a result, the server sends the application to the BCN to execute some processes and return gathered information or status variations from the device. As the identity of the farmer is genuine, the gadget related to the particular farmer can unswervingly send transactions (with farmer information) to the BCN. The gathering information or status is then added in the DL and related to the predefined value (i.e., threshold) set by the cryptocontract. If the value surpasses the predefined value, an alert will be engendered to the farmer.

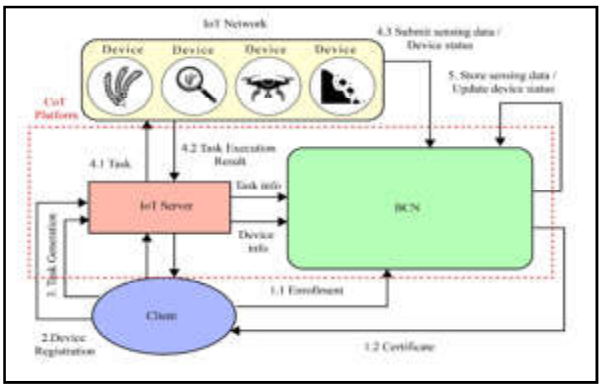

Fig.2 Communication among different elements in the CoT platform

The user application must have authorizations supplied by the identity manager to obtain the ratified approval for applying. The identity management service stores customer IDs and endorses users who need to register in the system. Transactions begin with client applications sending to nodes in the BCN. The interaction between the client application and the BCN occurs over the application software development kit. These nodes can either be subscribers or perpetrators. The subscribers generate and sign, respond to permitting, or negate endorsements. The perpetrators authenticate outcomes before writing the block to the DL. Each subscriber node accepts and performs the by calling on the cryptocontract in their virtual platform. It is noteworthy that in this phase, the implementation outcomes will not be stored in the DL. These subscribers just obtain the pair of Read and Written information (R-W pairs), which register what was read from the present condition when is created and what would be written once has been performed.

Every subscriber authenticates the R-W pairs and provides replies to the user for authorization. The user authenticates the ratifying signs to decide if a particular authorization strategy (the group of nodes that must approve the cryptocontract implementation outcomes) has been satisfied. Then the user client application posts the contracted and applies this together with R-W pairs to the agreement supervisor. The agreement ensures through the system, along with contracted, and R-W pairs are implemented; this data is assembled into a DL and distributed to all perpetrators. Every perpetrator

authenticates the by testing whether the R-W pairs counterpart to the present condition. Especially, the Read information still exists albeit the generated by the subscriber is equal to the present status. Once the perpetrator validates the, it is inscribed to the DL, and the status is appraised with the Write information from the R-W pair. Finally, the perpetrators asynchronously inform the user application about whether the generated thrived or not. Besides, the user application can record actions then only they can be acquainted with other perpetrators as soon as actions take place.

4.3 Cryptocontract in the CoT Platform

In the BCN environment, the cryptocontract performs as a secured and decentralized application that increases its reliance on the BCN and the basic agreement among the nodes. As they exist in the BCN, cryptocontracts have a distinctive identity through which the farmer can send a transaction to it. Based on the parameter that activates the threshold state, the cryptocontract then runs autonomously and inevitably in an approved way by each node in a BCN. Indeed, cryptocontracts are written in an application-specific or non-standard language (e.g., Solidity) to create agreement across all of the nodes. This is one of the major difficulties in the utilization of cryptocontract, as BCN designers must learn new coding software to write cryptocontracts, and this may fetch several issues on the programming side. Besides, the effectiveness of the transaction implementation is restricted because each transaction is performed consecutively by each node. To handle these problems, we exploit cryptocontracts onto a particular subdivision of nodes instead of to all nodes; therefore, the only requires to be approved by a group of nodes. This method also facilitates concurrent implementation to improve the efficiency and scope of the network. Moreover, we employ standard programming software including Java or Node.js to create the cryptocontract to enable designers to use their acquainted software.

The established cryptocontract includes several operations that enable us to communicate with the DL, which is an integration of the CoT network and state database. For instance, users can generate, apprise, and request device data from the DL by sending to the cryptocontract. It also offers a working mechanism to manage the submitted by the devices, including apprising status of actuators or gathering information from sensors. A block consists of a hash value of and the previous block to protect the data in the DL. Albeit the DL introduced by one node is tampered with, it cannot satisfy all the other nodes since the DL is disseminated all over the system. In a BCN system, genesis block is the primary one, which does not comprise any transactional data. Every other block comprises one transaction related to different resources (e.g., actuator, sensing element, etc.) in the DL status. The process executing on the cryptocontract accepts the transactional data and executes various updates and queries. The transaction is embedded in the block, and meanwhile, the DL status is appraised. Finally, the DL apprising result is transferred to the application as the reply.

4.4 Implementation Process

The user can send to the BCN in a network using their credentials. The following steps illustrate the procedure of registration and enrollment for the farmer.

- Registration: The farmer sends the registration request to the identity manager to obtain the identity through the client application. This request is processed by the identity manager, which generates and sends an enrollment secret to the farmer through the client app.
- Enrollment: The farmer sends the enrollment request to the identity manager through the client by sending the enroll ID and secret gained in the registration phase.
- Certificate generation: The identity manager sends the enrollment credential with a public key to the farmer through the client. Then, this is applied to request the transaction credential. Lastly, the is sent for ratifying the transactions.
- Network access: Once the enrollment is completed, the farmer is enabled to access and use network facilities.

5. PERFORMANCE EVALUATION

The developed model contains three development environments as a CoT network, an IoT device server, and the client application. This study exploits the Docker platform to implement nodes on the server as containers. Docker engine offers the Docker execution setting and Docker-compose enables the integrated development environment (IDE) to organize containers and images in the virtual machine. This study uses the Hyperledger Fabric software as a basis for creating applications or providing results with an integrated configuration. It is an open-source DL platform and permits elements (e.g.,

agreement and membership facilities), to be plug-and-play. Its flexible and adaptable structure meets the requirements of different industrial applications. It provides an inimitable method of agreement that provides better enactment while conserving user privacy.

This study creates four forms of nodes including client, candidate ratification, sorting, and application node. NodeJS64 v 8.12 is used to create the nodes and connects those nodes to the network to make interactions. This study creates 100 client nodes, 10 candidate ratification, one organizing, and 100 application nodes. User application is autonomous and can send proposals simultaneously. In the CoT network, all candidate ratification nodes require to approve the proposals. The composer-playground delivers an API to develop and execute the cryptocontract that comprises available resources and associated transactional data. More precisely, it creates a setting that swiftly simulates and tests a BCN. Couch DB is employed to store the current status of DL. The client tool of composer helps administrators and developers implement and process cryptocontracts effectively. The REST server generates appropriate APIs to expose the BCN logic to mobile or internet applications. The software tools stack used for realizing the CoT model in the Docker engine is given in Table 1.

Table 1 Technology Stack Used to Model CoT Network

Component	Specification
Processor	Intel i5-8500 with 3.00GHz and 12 GB RAM
Operating system (OS)	Ubuntu Linux 18.04.1 (Long-Term Support)
IDE	Docker-compose v 1.13.0
Runtime environment	Docker engine v 18.06.1-ce
Node	NodeJS64 v 8.12
Software development kit	Hyperledger fabric v1.2
Database	Apache Couch DB
User interface	Hyperledger composer-playground, composer REST server
Coding language	Node.js

The technology pile and development tools used for realizing the IoT device server are listed in Table 2. Android Things API is implemented on the Raspberry Pi to create the application using Java. The interaction between the IoT server and the device server and exploits the CoAP (constrained application protocol). We employ HTTP to enable interaction between the BCN and the device server, we employ HTTP. Physical sources (e.g., humidity sensor, temperature sensor, and water level sensor), are organized into CoAP as a fragment of the server. All the resources are allocated with an inimitable uniform resource identifier to be recognized by the server.

Table 2 Development Environment of IoT Device Server

Component	Specification
Hardware	Raspberry Pi3 Model B
OS	Android Things v0.8
Server	CoAP Server
Memory	1 GB
Back end tools	Californium CoAP, HTTP URL connection
IDE	Android Studio 3.1.4
IoT devices	Humidity, temperature, and water level
Coding language	Java

Table 3 lists the tools used to realize the BCN application. This application development environment is alienated into frontend and backend, which are realized by WebStorm and Eclipse Photon, correspondingly. Several tools including JavaScript, HTML, and Cascading style sheets (CSS) are employed as frontend tools. This study exploits two more prevalent non-proprietary frontend tools, Bootstrap, and jQuery, for developing applications. The Californium CoAP server is employed as the backend to configure the server that interprets the interaction between IoT devices and web applications. Notify.js is an additional jQuery plugin to create personalized reports for the user. We develop an user application using REST server to enable farmers/traders can create germane interfaces to send through POST or GET commands of HTTP requests.

Table 3 Technology Stack Used to Model the BCN Web App

Component	Specification
Server	Apache Tomcat
OS	Windows 10 Pro
IDE	WebStorm (2018.2.3), Eclipse Photon (4.8.0)
Browser	Firefox, Chrome
Back end tools	Notify.js, jQuery, Bootstrap, Californium CoAP,
Front end tools	HTML, Java, JavaScript, CSS

6. RESULTS AND DISCUSSION

6.1 Experimental Results and Discussion

This section provides tangible experimental outcomes to evaluate the effectiveness of the intended CoT model. Different trials are conducted by means of various

evaluation measures. The service execution time comprised the time for a to be directed and the time for an acknowledgment to be acquired by the client application. In this experiment, we use the Postman application (i.e., a tool to divide RESTful APIs). The Postman delivers lightweight APIs to modify scripts for modelling a substantial load on the system. Our first experiments analyze the performance of the proposed model in terms of time taken by the CoT model for device registration. The numerical results obtained from this experiment are listed in Table 4.

Table 4 Time Consumption for Registration

Execution Time (s)	Number IoT Devices		
	25 Devices	50 Devices	100 Devices
Maximum time	2.68	2.99	3.45
Minimum time	2.36	2.59	2.79
Average time	2.41	2.74	2.96

In this work, three device groups with 25, 50, and 100 devices data are simulated to evaluate the effectiveness of the intended model. This is realized through the modelling tool known as Hyperledger Caliper, which enables farmers or traders to develop the application of a particular BCN operation using some measures. This study evaluates the performance of the intended model by measuring the execution time device registration in terms of maximum, the average, and minimum time. The experiment related to a group with 25 devices, the maximum time is observed as 2.68s, the average time is 2.41s, and the minimum time is 2.36s. The experiment related to the group with 50 devices, the maximum time is observed as 2.99s, the average time is 2.74s, and the minimum time is 2.59s. For the 100-device group set, the maximum time is observed as 3.45s, the average time is 2.96s, and the minimum time is 2.79s. Figure 3 demonstrates the performance of different network scenarios with different number of devices in the group in terms of time consumption for device registration.

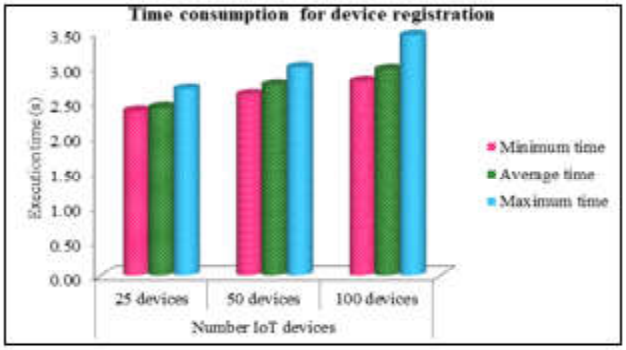

Fig.3 Time consumption for registration

In our second experiment, we assess the effectiveness of the anticipated model in terms of timing overhead for storing gathered data in the CoT. Each IoT maneuver includes an HTTP client that can accept the sensing data interface from the REST server. When the collected data is inserted in the BCN, the REST server obtained the implementation fallouts from the BCN and sent the reply to the maneuver. Figure 5 displays the performance of the proposed model in terms of time for sensing transactional data. In these experiments, the tests are carried out by a number of simultaneous users, and each test is repeated 10 times and we measured the average value to get reliable results.

Table 5 Time Consumption for Reading Sensing Data

Execution Time (s)	Number IoT Devices		
	25 Devices	50 Devices	100 Devices
Maximum time	2.78	3.05	3.34
Minimum time	1.98	1.69	2.04
Average time	2.49	2.68	2.77

The time consumption for reading data from the sensors by the intended CoT model to execute a transaction is noted in maximum, minimum, and average time. The experiment related to the group with 25 devices, the maximum time is observed as 2.78s, the average time is 2.49s, and the minimum time is 1.98s. The experiment related to the group with 50 devices, the maximum time is observed as 3.05s, the average time is 2.68s, and the minimum time is 1.69s. For the 100-device group set, the maximum time is observed as 3.34s, the average time is 2.77s, and the minimum time is 2.04s. Figure 4 displays the performance of different network scenarios with a different number of devices in the group in terms of time consumption for reading data from the sensors.

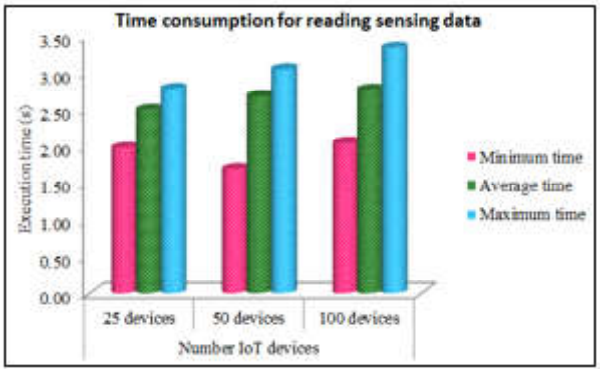

Fig.4 Time consumption for reading sensing data

From figures 4 is clear that the transaction execution time is amplified when the number of IoT devices increases. Nonetheless, the response graph was steady

and the entire transaction performance is evaluated if no network congestion occurred. Bitcoin consumes 10 minutes to mine a network; yet, its transaction normally demands different endorsements before it is confirmed. Accordingly, it can be anticipated that a transaction takes about an hour on average, which is intolerable to the common people. Ethereum transaction times are around 15 seconds but the average time would rise exponentially based on diverse network scenarios. The empirical fallouts from this work demonstrate that the proposed BCN platform outdoes most other prevalent BCN regarding transaction time. The limitation of this work is that the experiments are conducted on a bounded network.

7. CONCLUSION

With billions of smart maneuvers operating online, there are universal issues related to the scaling of IoT systems. These maneuvers are always heterogeneous and different. Hence, interoperability and identity need to be guaranteed in a protected way. The BCN delivers a new security infrastructure and mechanism to facilitate innumerable IoT maneuvers to have reliable interoperability for both commerce and data. This study proposes a novel CoT model with an efficient authentication protocol to digitally cope with different subdivisions in smart farming including crop yield analysis, monitoring the variable rate of fertility, diagnosis of diseases, weather prediction, animal grazing, and food supply. Active monitoring and managing a CoT system in smart farming needs an efficient model for handling data flow and identifies the actions and communications among IoT maneuvers.

The CoT model should be modular enough to facilitate the monitoring of different communication scenarios. This study exploits Docker platform to implement nodes and Hyperledger Fabric model to develop the CoT network. The cryptocontracts (cryptocontract) are created and deployed using the Hyperledger Composer. The effectiveness of the developed model is evaluated regarding execution time for device registration and sensor reading. Extensive empirical results reveal that the proposed CoT architecture provides an effective model for precision agriculture.

REFERENCES

[1] M. De Clercq, A. Vats and A. Biel, "Agriculture 4.0: The Future of Farming Technology", Technical Report, World Government Summit: Dubai, United Arab Emirates, 2018.

[2] G.A. Motta, B.Tekinerdogan and I.N.Athanasiadis, "Blockchain Applications in the Agri-Food Domain: The First Wave", Front. Blockchain, 2020, Vol.3, No.6.

[3] Vivek Sharma, Ashish Kumar Tripathi and Himanshu Mittal, "Technological Revolutions in Smart Farming: Current trends, Challenges & Future Directions", Computers and Electronics in Agriculture, 2022, Vol.201, pp.107217.

[4] L. Hang and DH.Kim, "Design and Implementation of an Integrated IoT Blockchain Platform for Sensing Data Integrity", Sensors (Basel), 14 May 2019, Vol.19, No.10, pp.2228.

[5] Mohamed Torky and Aboul Ella Hassanein, "Integrating Blockchain and the Internet of Things in Precision Agriculture: Analysis, Opportunities, and Challenges", Computers and Electronics in Agriculture, 2020, Vol.178, pp.105476.

[6] H.F. Atlam, A. Alenezi, M.O. Alassafi and G.B.Wills, "Blockchain with Internet of Things: Benefits, Challenges, and Future Directions", Int. J. Intell. Syst. Appl. 2018, Vol.10, pp.40-48.

[7] M. Torky and AE. Hassanein, "Integrating Blockchain and the Internet of Things in Precision Agriculture: Analysis, Opportunities, and Challenges", Computers and Electronics in Agriculture, 2020, Vol.178, pp.105476.

[8] K.R. Özyýlma and A.Yurdakul, "Integrating Low-Power Iot Devices to a Block chain-Based Infrastructure", In Proceeding of the Thirteenth ACM International Conference on Embedded Software 2017 (EMSOFT '17), Seoul, Korea, 15-20 October 2017.

[9] J. Lin, Z. Shen, A. Zhang and Y. Chai, "Blockchain and IoT based Food Traceability for Smart Agriculture", Proceedings of the 3rd International Conference on Crowd Science and Engineering (ICCSE 2018), Vol.3.

[10] TH. Pranto, AA. Noman, A. Mahmud and AB.Haque, "Blockchain and Smart Contract for Iot Enabled Smart Agriculture", PeerJ Comput Sci. Mar.2021, Vol.31, No.7, pp.407.

[11] Q. Xu, K.M.M. Aung, Y. Zhu and K.L.Yong, "A Blockchain-Based Storage System for Data Analytics in the Internet of Things", New Advances in the Internet of Things; Yager, R.R., Espada, J.P., Eds.; Springer: Cham, Switzerland, 2018; pp. 119–138.

[12] S.C. Cha, J.F. Chen, C. Su and K.H.Yeh, "A Blockchain Connected Gateway for Ble-Based Devices in the Internet of Things", IEEE Access, 2018, Vol.6, pp.24639-24649.

[13] L. Hang, W. Jin, H. Yoon, Y.G. Hong and D.H. Kim, "Design and Implementation of a Sensor-Cloud Platform for Physical Sensor Management on CoT Environments", Electronics, 2018, Vol.7, pp.140.

[14] K. Biswas and V. Muthukkumarasamy, "Securing Smart Cities Using Block chain Technology", In Proceedings of the IEEE 14th International Conference on Smart City, Sydney, Australia, 12-14 December 2016, pp.1392-1393.

[15] A. Dorri, S.S. Kanhere and R. Jurdak, "Towards an Optimized BlockChain for IoT", In Proceedings of the Second 1. International Conference on Internet-of-Things Design and Implementation (IoTDI), Pittsburgh, PA, USA, 2017, pp.18-21.

AUTONOMOUS MOBILE ROBOT BASED LOGISTIC ROBOT FOR INDUSTRIAL APPLICATION

M.C. Pravin, V. Vadivel Vivek and A. Sivaramakrishnan
Department of Mechatronics Engineering,
Bannari Amman Institute of Technology, Sathyamangalam - 638 401, Erode District, Tamil Nadu
E-mail: pravin@bitsathy.ac.in

Abstract

This study outlines the procedure and phases employed in the implementation of an autonomous mobile robot (AMR) for industrial logistics. Currently, AMRs play a vital role in logistics operations, and various models are available in the market. The focus of this work is the development of a user-friendly logistic robot with an accessible graphical user interface (GUI). AMRs are widely utilized in sectors such as automotive, large-scale industries, and even household appliances to transport goods from their source to designated areas. These AMRs are connected via a single Wi-Fi Module, which establishes a connection between the GUI, robot, and Wi-Fi Module. The GUI, serving as a General User Interface, enables users to create paths for the robot using a joystick as a means of navigation. Once the paths are recorded, the GUI allows the creation of multiple tasks. Eventually, the robot operates autonomously without human intervention. Upon completion of the operation, the robot returns to its original location at the charging station.

Keywords: *GUI, AMR, Wi-Fi, Robot, Logistics*

1. INTRODUCTION

Mobile robotics is currently one of the most rapidly growing fields of scientific research. Because of their capabilities, mobile robots can replace humans in a variety of fields. Surveillance, planetary exploration, patrolling, emergency rescue operations, reconnaissance, petrochemical applications, industrial automation, construction, entertainment, museum guides, personal services, intervention in extreme environments, transportation, medical care, and many other industrial and nonindustrial applications are among the many applications. The majority of these products are already on the market. Mobile robots can move autonomously (in an industrial plant, laboratory, planetary surface, etc.), that is, without the assistance of external human operators. A robot is autonomous when it can determine the actions to be taken to complete a task using a perception system. A cognition unit or a control system is also required to coordinate all of the robot's subsystems. The fundamentals of mobile robotics include locomotion, perception, cognition, and navigation.

As an AMR, this study is for specific use or application in mind. The term "AMR" refers to a highly developed type of programmed and automated system made to satisfy customer needs. Numerous innovative initiatives to develop superior AMR have been made in an effort to boost production.

The construction of the AMR includes NVIDIA JETSON TK1, and sensors. These complex manual processes are uniquely equipped with AMR. Therefore, it is ideal for improving human-machine interaction and lowering manual errors in the production process. As a result of the device's ability to mass create smaller components, more substantial final products are encouraged to be developed.

2. LITERATURE REVIEW

Hiep Do Quang et al discussed the simultaneous localization and mapping along with a path- planning method based on the navigation stack for the movement of unidirectional self-driving robots. The mobile robot must achieve both local obstacle avoidance and follow the global path during the moving process since the virtual environment contains both known static obstacles and unknown dynamic challenges [1].

Bavithran et al created an AI path-finding robot with multiple functions for this project. Our robot receives data from distance sensors, determines its path, and navigates using SLAM, an algorithm developed in a robot

operating system. For robot navigation and pathfinding, we used a robot operating system and the SLAM algorithm. op, PC, or via the web [2].

Rachael N. Darmanin *etal.,* proposed a feasible solution to the problem of autonomous exploration and mapping using a single mobile robot. Furthermore, the authors implement the proposed scheme within the Robot Operating System (ROS) and experimentally validate it with PowerBot, a real wheeled mobile robot outfitted with a 2D laser scanner [3].

Mark A. Post *et al.,* developed an Autonomous monitoring of agricultural farms and fields has recently become feasible due to ongoing advances in robotics technology, but many significant challenges remain. In this paper, we describe the current state of work to develop a fully autonomous [4].

Min Su Kim *et al.,* compared Robot Operating System (ROS) packages for mobile robot navigation on an embedded system. ROS includes a number of libraries and tools for developing complex robot software. We discuss the process of porting ROS to an open embedded platform that serves as the main controller for a mobile robot. In the case of driving the robot, ROS provides local path planners such as the base, elastic band, and timed elastic band [5].

M.S. Hendriyawan Achmad *et al.,* presentd a series of works in order to explore an unknown environment consisting of paths and obstacles using the Ackerman model of a wheeled mobile robot in this paper (car- like). ROS is used as a basic operation platform to handle everything from sensor interfacing to 2D/3D mapping and path planning [6].

Gigih Priyandoko *et al.,* developed a mobile robot assistance for the elderly, service mobile robots are playing a more critical role in today's society. The ability to follow an autonomous person is extremely important to the overall role of a service mobile robot in assisting humans. The goal of this paper is to create a robot that follows a person [7].

André Araujo *et al.,* described the complete integration of compact educational mobile robotic platforms based on an Arduino controller board into the Robot Operating System (ROS). To reduce development time, a driver interface in ROS was created to provide hardware abstraction and an intuitive operation mode, allowing researchers to focus primarily on their main research motivation, such as search and rescue [8].

G. Priyandoko *et al.,* discussed humans interacting with teleoperated unmanned mobile robot inspections in industrial plant areas, producing a 2D/3D map for further analysis. This experiment is divided into two parts: how humans and robots interact remotely using robust methods, and how the robot perceives its surroundings as a 2D/3D perspective map. ROS (robot operating system) was used as a tool in the research's development and implementation, resulting in a robust data communication method in the form of messages and topics [9].

Lino Marques *et al.,* discussed the collection of olfactive data and its application by a mobile robot to locate a specific odour source in a room with turbulent phenomena and multiple odour sources. Three navigation algorithms are evaluated in comparison to a simple gas sensor and an electronic nose. Their ability to locate an ethanol source in an obstacle-filled room is assessed. The first navigation strategy is based on chemotaxis in bacteria [10].

SidagamSankar *et al.,* presented a real-time remote-control system for human detection, tracking, security, and verification in such demanding environments. This type of system is useful for security monitoring, data collection, and experimentation. In the proposed system, a Microsoft Kinect RGB -D camera is used as a visual sensing device for the design of human detection and tracking [11].

M.A Molina et al how a ROS-based control system for a human leader and robot follower system is used with a Pioneer 3-DX robot. The approach for this work is to create a modular system to reach a human follower by utilizing PIONEER 3-DX and Carmine Prime Sense Sensors, which are supported by threads for each processing step via ROS packages [12].

Eko Rudiawan Jamzuri *et al.,* made a kid-size humanoid marathon robot software framework built on ROS is presented in this research. The identification of the marathon course was accomplished using colour filtering and contour selection methods. With a train accuracy of 99.92% and a validation accuracy of 99.87%, a two- stage ConvNet object detection method with a color-based region proposal was developed to recognize a marker [13].

Nils Rottmann et al., developed a Creating, Managing and keeping track of sophisticated autonomous and semi- autonomous robotic systems is difficult. Using Ubuntu Linux, the Robot Operating System (ROS) was created as a robotic middleware system that supports, among other things, hardware abstraction, message transmission between individual processes, and package management [14].

Ruijiao Li *et al.,* provided a multi-robot architecture for ambient supported living of the elderly and disabled that is based on the robot operating system (ROS). For various forms of human-robot interaction, a communication bridge is put forth, and ROS offers a framework for quick and reasonably priced system development [15].

2.1 Problem Identification

Mapping the Robot using codes is one of the complex processes and requires humans with skilled people. The accuracy of the programmed is also not perfect as required. So using this GUI for mapping quickly and creating the task makes it easy to complete the process with help of GUI and joystick.

2.2 Objective

Design and fabrication of the AMR based logistic Robot for Industrial Application. To minimize the timing consumption. Using GUI to control and monitoring the movement parts in the robot using ROS and Nvidia JetonTK1 for controlling the Logistic robot. The LiDAR is detecting the obstacles and intimate the same to the robot. Based, the task that programmed the robot avoid the obstacle and despite other path and move in that path with the help of LiDAR sensor.

2.3 Scope

The scope of the work is to carry load from one location to another location with the help of co nnected sensors and OS that are used in it. Using double LiDAR to convert this single direction movement Robot into bidirectional movement Robot.

2.4 Methodology

Below Figure 1 gives a glimpse on the end to end process carried out during the entire research work.

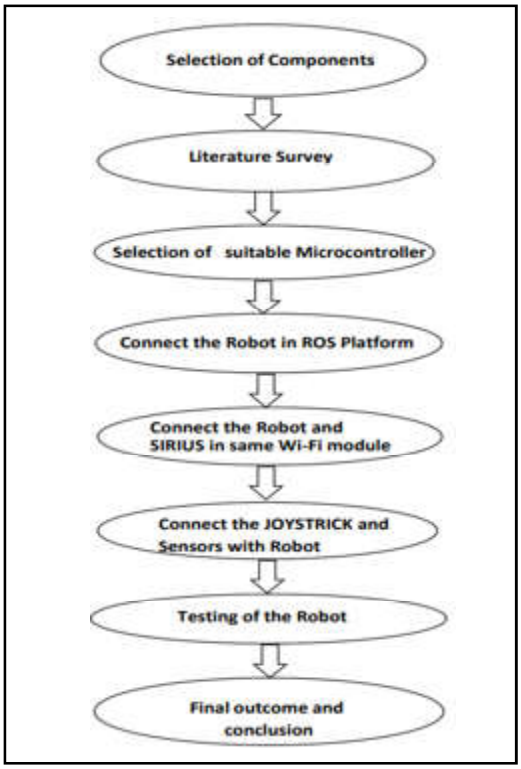

Fig. 1 Methodology

2.4.1 TeleOp

Teleop is the tab where the user can activate the robot to accept Joystick commands if any Manual operation of the robot is needed. Once activated, the robot quits all the current tasks and starts accepting manual commands from the joystick presented in the UI.

2.4.2 Mapping

Mapping is the tab where the initial mapping of the completely new Place is done. This can be easily done by activating the robot to start mapping the area and move along the path where you want to map.

Fig. 2 GUI Dashboard in TeleOp Mode

The UI also provides the user with the updated map simultaneously for easy mapping of the area. Once the map is saved, the user can then use the map to record the path in which they want the robot to move (Figure 2).

2.4.3 Record

The record page currently used to record the points in which the robot needs to move. Users can specify one or more points in which they want the robot to move. The robot then plans a shortest path between those points and reaches the destination.

3. COMPONENTS

3.1 Hardware Requirements

To make the logistic Robot is fully automated in its operations from starting point to end process. There are many lists of components required to complete the process. But here have only discussed a few main components which play a major role in this project. The list of components is:

1. Servo motor
2. NVIDIA JETSON TK1
3. LiDAR
4. Wi-Fi dongle
5. Joystick

3.2 Software Requirements

3.2.1 ROS

Robot operating system is an open source framework for building robotic systems that provides a wide range of software tools and libraries for developing, testing, and deploying robotics applications. ROS was created by Willow Garage, a robotics research lab, and is now maintained by the Open Robotics organization.ROS is designed to be modular and flexible, allowing developers to build complex robotic systems using a variety of hardware components and software modules. ROS's key features include: Communication: ROS includes a messaging system that allows different components of a robotic system to communicate with one another even if they are running on different computers or operating systems.Visualization: ROS includes tools for visualizing and debugging robotic systems, such as 2D and 3D. Libraries: ROS includes a large number of libraries for common robotics tasks such as sensor data processing, path planning, and control. Community: ROS has a large and active community of developers and users who contribute to the system's development and improvement. Overall, ROS is a powerful and adaptable framework for developing robotic systems, offering a variety of tools and libraries to make the development and deployment of robotics applications easier.

3.2.2 Linux for Tegra

Linux for Tegra (L4T) is a customised Linux distribution designed to run on NVIDIA Tegra SoC platforms, such as the NVIDIA Jetson family of embedded AI computing devices. L4T provides a complete software stack optimised for the hardware architecture of Tegra devices, including the Linux kernel, drivers, libraries, and development tools.

3.2.3 GUI

GUI stands for Graphical User Interface, which is a type of interface that allows users to interact with a computer using graphical elements such as windows, icons, buttons, and menus, rather than typing commands in a terminal or command-line interface. GUIs are commonly used in operating systems, applications, and websites to provide a user-friendly and intuitive way of performing tasks and accessing information.

4. EXPERIMENTAL PROCEDURE

This chapter would give an overview of the experimental procedures followed throughout the entire process. Each and every procedure tells us exactly how the process was exhibited, giving clear cut ideas and detailing every aspect of the procedure carried out. As this is a step by step procedure, nothing can't be skipped in- between and even the flow can't be altered. Each procedure requires a certain amount of time and all should be in accordance with the flow of happening. Below Figure 3 gives a glimpse of how the process flow happens in overall experimental procedure.

4.1 General User Interface

Create one GUI for controlling and monitoring the robot motion and battery health by using the GUI software. In this system all the hardware's and software's are connected in a single Wi-Fi module. The Wi-Fi module sends and receives data from the robot. All the data is fetched in the GUI.

In this system, using the joystick to plane the task to the system and recording the path of the robot also and

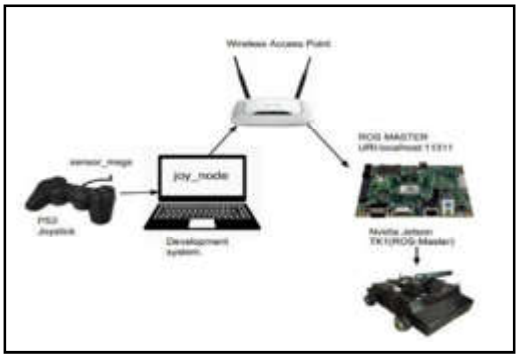

Fig.3 Schematic diagram of data flow

when the progress is completed the robot is returned to the origin point. Robot of charging station is origi n point implies that a charging station is a robot's starting point. This implies that the robot is designed to perform specific tasks or missions, which may include charging itself at the station. In any case, the charging station is an essential component of the robot's operation, providing it with the energy it requires to function properly. The phrase also implies that the robot may have a predetermined path or route to take, with the charging station serving as the starting and ending point of its journey.

Here, the GUI is named as the SIRIUS
Modes in GUI

- WEB Application
- Home (battery status, new task, notification, working time)
- TeleOp (Joystick status)
- Mapping (Robot visualization, TeleOp joystick movements)
- Record (Robot visualization, robot option (activation and deactivation)
- Visualgraph (Robot visualization, robot start and stop)
- Wi-Fi Connection

4.2 Web Application

A web application, also known as a web app, is a software application that runs on a web server and is accessed via a web browser over the internet or intranet. Web apps, unlike traditional desktop applications, do not require installation on a user's device and can be accessed from anywhere, at any time, and on any device with an internet connection.

Web applications provide interactive and dynamic functionality to users by utilizing various web technologies such as HTML, CSS, JavaScript, and server-side programming languages such as PHP, Python, Ruby, and Java. Online shopping websites, social media platforms, email clients, and cloudbased productivity tools are all examples of web applications.

4.3 Home

The introductory page of a website or web application is known as the home page, also known as the landing page or main page. It is the first page that a user sees when they visit a website and serves as a portal to other pages on the site. The home page is intended to give users an overview of the website's content and purpose, as well as to direct them to the information they seek. It usually has a site navigation menu, links to important pages or sections, and occasionally features like a search bar, news or events, or promotions.

A home page's design and content can differ depending on the website's goals and target audience, but its main purpose is to provide a clear and engaging introduction to the site and encourage visitors to explore further. In SIRIUS home page also same, here can able to monitoring the battery status and working time, assigning new task and storing the task. Checking the new notification from the Robots.

4.4 TeleOp (Joystick status)

The terms "TeleOp" and "Teleoperation" describe the use of a remote control, such as a joystick, to operate a machine or system from a distance. In a TeleOp system, the position of the joystick and any buttons or other controls that could be present are referred to as the device's status. The TeleOp system often uses this state to deliver command signals to the machine or system being controlled, such as a robot or unmanned vehicle. The operator can operate the machine or system in real-time by keeping an eye on the joystick's status, giving them more flexibility and adaptability in challenging conditions.

4.5 Mapping (Robot visualization, teleOp joystick movements)

In robotics, the process of visualizing or modelling the environment in which a robot is functioning is known as mapping. To create a 3D map of the area, this can be done using a variety of sensors and methods, such as Lidar, cameras, or sonar. The robot may utilize the map

to plan and carry out its movements, dodging obstacles and arriving at its objective.

Mapping may be used to describe the conversion of joystick commands into equivalent movements of a robot in the context of TeleOp joystick motions. The TeleOp system translates the operator's joystick commands into particular actions or motions that the robot will carry out. This mapping procedure may involve converting the analogue inputs from the joystick into distinct digital commands that the actuators or motors of the robot may carryout.

Another crucial component of mapping in robots is visualization. Even when the robot is functioning in a remote or dangerous region, operators may better comprehend and control the robot's activities by creating a visual depiction of its surroundings and movements. Maps in 2D or 3D, augmented reality displays, or vide o feeds from the robot's cameras or sensors can all be used as visualization aids.

4.6 Record (Robot visualization, robot option (activation and deactivation)

Recording in the context of visualization can also refer to the procedure of gathering and archiving visual information about the robot's surroundings and motions. In order to build a visual depiction of the robot's surroundings, this can use video feeds from the robot's cameras, data from the lidar point cloud, or information from other sensors. The utilization of this visual data for analysis, training, and other purposes is then possible.

Another application of robotics recording is to record the activation and deactivation of robot options or subsystems. Depending on the task, a robot may have multiple sensors or actuators that can be activated or deactivated. Recording these activations and deactivations can aid in tracking the robot's performance and identifying any problems.

4.7 Visual Graph (Robot visualization, robot start and stop)

Visual graphs could be used to display the robot's movements or actions over time, with markers indicating when the robot was started or stopped, in terms of robot start and stop. This could be helpful in analyzing the robot's performance, identifying problems or inefficiencies, and optimizing its operations.

4.8 WI-FI

Here, it is possible to determine whether Wi-Fi is active or not. Network status including all aspects of the wireless connection.

5. RESULTS

The AMR based logistic Robot works with the help of ROS and nVIDIA TK1. The SIRIUS have been designed and Robot in such a way that it is suitable for carrying the load. It is an easy process to move the heavy goods without human intervention. This allows less damage to the inventory products. The ROS and the nVIDIA TK1 were interfaced so that they can transfer data or signals between each other. The controller will also be interfaced with motors and sensors with the help of communication cables making the Robots. The mapping to the robot is controlled by a joystick. The joystick is used for navigating the Robot manually. By using the joystick both forward and backward. The system is perfectly able to perform the desired tasks. This system is more feasible compared to the existing system and travel time to retrieve an object is also minimized and the nVIDIA TK1is interfaced with the robot with the input of the controller of the robot. SIRIUS can also communicate with the help of Ethernet. The robot is programmed with the help of a python language and ROS to transport an object at the exact positions. The AMR based logistic system has also saved a lot of time and capital with the help of this the profit raised is also high.

6. CONCLUSION

A prototype is fabricated to create the AMR based logistic Robot. The project focuses on saving time for transporting the goods and producing more effective and accurate AMR for producing the maximum transportation rate of goods. It was achieved by using an SIRIUS and the AMR to achieve the logistics. Using the nVIDIA TK1and Servo motor to complete the progress. The process is controlled by an nVIDIA TK1and SIRIUS for regulating. The process is fully evaluated and further development is undergoing.

7. SCOPE FOR FUTURE WORK

In Future, it may be converted for heavy application. By inserting mechanical systems and planning to control with the same program and progress. Today, most of the

companies are focusing for automate the entire process same wide focused to automating the warehouse storage area to the working area. Slightly, using the AMR to perform this type task and reducing the manpower from the heavy load lifting process for considering the human ergonomics and for human and work safety too.

REFERENCES

[1] Hiep Do Quang,Tien Ngo Manh, Cuong Nguyen Manh, Dung Pham Tien and Manh Tran Van "An Approach to Design Navigation System for Omnidirectional Mobile Robot Based on ROS", in International Journal of Mechanical Engineering and Robotics Research, November 2020, Vol. 9, No. 11.

[2] S. Bavithran, S.Jeswin Paul and P.Kandha Raj, "Artificial Intelligence Based Mobile Robot", in International Journal for Research in Applied Science & Engineering Technology (IJRASET)ISSN: 2321-9653; IC Value: 45.98; SJ Impact Factor:7.429, May 2021, Vol.9, No.V.

[3] Rachael N. Darmanin and Marvin Bugeja, "Autonomous Exploration and Mapping using a Mobile Robot Running ROS", in ICINCO 2016-13th International Conference on Informatics in Control, Automation and Robotics.

[4] Mark A. Post, Alessandro Bianco and Xiu T. Yan, "Autonomous Navigation with ROS for a Mobile Robot in Agricultural Fields".

[5] Min Su Kim, Raimarius Delgado and Byoung Wook Choi, "Comparative Study of ROS on Embedded System for a Mobile Robot", in Journal of Automation, Mobile Robotics & Intelligent Systems, Vol.12, No.3, 25th October 2018.

[6] M.S. Hendriyawan Achmad, Nur Afzan Murtdza, Nor Anis Aneza Lokman, Mohd Razali Daud, Saifudin Razali and Dwi Pebrianti, "Exploration of Unknown Environment with Ackerman Mobile Robot Using Robot Operating System (ROS)", in ARPN Journal of Engineering and Applied Sciences, December 2015, Vol.10, No.23.

[7] Gigih Priyandoko,Choi Kah Wei, Muhammad Sobirin Hendriyawan Achmad, "Human Following on ROS Framework a Mobile Robot", in SINERGI, June 2018, Vol.22, No.2, pp.77-82.

[8] Andrй Araъjo, David Portugal, Micael S. Couceiro and Rui P. Rocha, "Integrating Arduino –based Educational Mobile Robots in ROS", in J Intell Robot Syst., DOI 10.1007/s10846-013-0007-4, 2015, Vol.77, pp.281-298.

[9] G. Priyandoko, T.Y. Ming and M.S.H. Achmad, "Mapping of Unknown Industrial Plant Using ROS-Based Navigation Mobile Robot", in IOP Conference Series: Materials Science and Engineering, 2017, Vol.257, pp.12088.

[10] Lino Marques, Urbano Nunes, Anэbal T. de Almeida, "Olfaction-based Mobile Robot Navigation", in Thin Solid Films, 2002, Vol.418, pp.51-58.

[11] Sidagam Sankar and Chi-Yi Tsai, "ROS-Based Human Detection and Tracking from a Wireless Controlled Mobile Robot Using Kinect", in Appl. Syst. Innov., 2019, Vol.2, No.5.

[12] M.A Molina, D.R Avendaco, L.E Solaque, N.F Velasco and C.A Pulido, "ROS-based Human Leader and Robot Follower Using a Pioneer 3- DX robot", UIS Ingenierias, Vol.15, No.2, pp.63-71.

[13] Eko Rudiawan Jamzuri,Hanjaya Mandala and rd Jacky Baltes, "ROS Based Software Framework for Kid -Size Humanoid Marathon Robot", in National Taiwan Normal University on October14, 2020

[14] Nils Rottmann,Nico Studt, Floris Ernst, Elmar Rueckert, "ROS-Mobile: An AndroidTM Application for the Robot Operating System".

[15] Ruijiao Li, Mohammadreza A. Oskoei, Huosheng Hu, "Towards ROS based Multi-Robot Architecture for Ambient Assisted Living", in 2013 IEEE International Conference on Systems, Man and Cybernetics.

INVESTIGATING DOUBLE ANTIOXIDATION MECHANISMS OF PHENOLIC ACIDS

G. Sivaranjani and K.Sadasivam
Department of Physics
Bannari Amman Institute of Technology, Sathyamangalam - 638 401, Erode Distrct, Tamil Nadu
Email: dftsada@gmail.com

Abstract

Quantum chemical calculation is carried out to evaluate the radical scavenging behavior of phenolic acids including caffeic acid (CA) and p-coumaric acid (pCA) with the aid of density functional theory (DFT). Theoretical computations are interpreted and investigated via M06-2X/6-311 G (d,p). Double thermodynamical mechanisms including d-HAT, d-SETPT and d-SPLET are performed to scrutinized the antioxidant capabilities at three different environments. Using above mentioned analysis the preferential antioxidant among the chosen compounds for neutralizing the free radicals.

Keywords: *Density functional theory (DFT), Double antioxidation mechanisms, d-HAT, d-SETPT, d-SPLET*

1. INTRODUCTION

Oxidative stress is produced by the rapid increase of free radicals due to exceeding level of antioxidant protection. Oxidative stress is associated with phenomenal diseases including diabetes, cancer, Parkinson's, Alzheimer disease and aging. Such ROS components are superoxide anion radical $O_2^{-\bullet}$, hydroxyl radical $HO^{\bullet}$, alkyl radical $R^{\bullet}$, peroxy radical $RO^{\bullet}$, nitric oxide radical $ROO^{\bullet}$ and lipin hydroperoxide radical LOOH) are commonly generated by harmful UV radiation and oxidative stress in human cells. Antioxidant helps to defend cells against reactive oxidative species (ROS) and quench the free radical [1].

Antioxidant is categorized into enzymatic antioxidant and non-enzymatic antioxidant. In enzymatic antioxidant, free radicals are either removed or break down by it and later alters the free radicals into a hydrogen peroxide (H2O2) whereas in non-enzymatic antioxidant, the antioxidant terminates the chain link of free radicals [2]. Furthermore, non-enzymatic antioxidant is split into a) synthetic antioxidant and b) natural antioxidant. The objective research is exploring the natural antioxidants in plant sources. DFT study is utilized to examine the structural-activity relationship as well as the chemical property of derivatives of cinnamic acid. The cinnamic acids includes caffeic acid (CA) and p-coumaric acid (pCA) are existing in coffee, vegetables and fruits demonstrate antioxidant, antidiabetics and antimicrobial capabilities [3]. All the two compounds are portrayed in Figures.1 and 2.

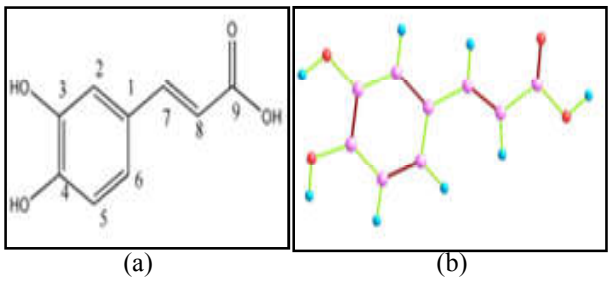

(a) (b)

Fig.1 (a) and (b) are atomic numbering and geometrical optimization structure of CA respectively

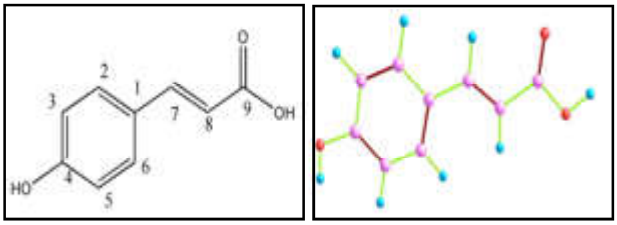

(a) (b)

Fig.2 (a) and (b) are the atomic numbering and optimized structure of pCA respectively

2. QUANTUM CHEMICAL TECHNIQUE

Quantum chemical method is performed via Gaussian 16W with the aid of M06-2X/6-311 G(d,p) higher level of theory. Solvent effects such as polar (water) and nonpolar (ethanol) phases are carried out using self-consistent reaction field polarizable continuum model (SCRF-PCM) at the same level of theory [4].

3. DOUBLE ANTIOXIDATION MECHANISMS

Double antioxidation mechanisms such as double hydrogen atom transfer (d-HAT), double sequential electron transfer proton transfer (d-SETPT) and double

sequential proton loss followed by electron transfer (d-SPLET) are employed to examine the antioxidant property of the chosen compounds.

3.1 Double Hydrogen Atom Transfer (d-HAT)

The d-HAT mechanism is carried out by transfer of successive hydrogen atoms. A H-atom is being transferred from the parent compound Anti(OH)x becomes Anti(OH)x-1O), in addition subsequent H-atom is being removed from Anti(OH)x-1O) becomes Anti(OH)x-2OO. The bond dissociation enthalpies (BDEs) of two step HAT mechanism is calculated by following relations (9) and (10).

$$BDE_1 = H_p - H_{r1} - H_h \quad (1)$$

$$BDE_2 = H_{r1} - H_{r2} - H_h \quad (2)$$

Where, Hp is the enthalpy of Anti(OH)x; H_{r1} is the enthalpy of the Anti(OH)x-1O·) from the H atom transfer; H_{r2} is the enthalpy of Anti(OH)$_{x-2}$OO; H_h is the enthalpy of the H atom [5].

3.2 Double Sequential Electron Transfer Followed By Proton Transfer (d-SETPT)

In first step of the d-SETPT mechanism, electron is transferred from Anti(OH)x that yields a $Anti(OH)_x^+$ in addition a proton is being removed generates Anti(OH)x-1O) in second step. In third and fourth steps, successive electron and proton are removed from Anti(OH)x-1O) and $Anti(OH)_{x-1}^+$ respectively. The ionization potentials (IP1 and IP2) and proton dissociation enthalpies (PDE1 and PDE-2) are employed to measure energy required to remove the successive electrons and protons ((11) - (14)).

$$AIP_1 = H_{e1} - H_p \quad (3)$$
$$AIP_2 = H_{C2} - H_{C1} \quad (4)$$
$$PDE_1 = H_{r1} + H_H + = H_{C1} \quad (5)$$
$$PDE_2 = H_{r2} + H_H + = H_{C2} \quad (6)$$

Where, H_{c1} and H_{c2} are the enthalpies of $Anti(OH)_x^+$ and $Anti(OH)_{x-1}^+$ respectively.

3.3 Double Sequential Proton Loss Electron Transfer (d-SPLET)

In d-SPLET mechanism, a proton and electron are detached in the beginning of two-steps yields Anti(OH)x-1O- as well as Anti(OH)x-1O). Afresh, deprotonation and deelectronation are manipulated in alternative steps generates Anti(OH)x-2O)O- and Anti(OH)x-2OO. Deprotonation and deelectronation of d-SPLET mechanism is calculated via proton affinities (PA1 and PA2) and electron transfer enthalpies (ETE1 and ETE2) by the following relations [6].

$$PA_1 = H_{ar1} + H_H - H_P \quad (7)$$
$$ETE_1 = H_{r1} + H_e - - H_{ar1} \quad (8)$$
$$PA_2 = H_{ar2} + H_H + - H_{r1} \quad (9)$$
$$ETE_2 = H_{r2} + H_e - - H_{ar2} \quad (10)$$

Where, H_{ar1} is the enthalpy of the Anti(OH)x and H_{ar2} is the enthalpy of the Anti(OH)x-1O•).

4. RESULTS AND DISCUSSION

4.1 Double Hydrogen Atom Transfer (d-HAT)

Analyzing the results from Table 1, in gas phase, it is found that lower magnitude of BDE1 is obtained at 3 OH and 4 OH of CA and pCA compounds respectively. Consequently, in solvent phases, BDE1 value is observed to be minimum at 4 OH site of both the compounds. It is summarized that 3 OH site of CA in gas phase is register lower BDE1 compared to their counter parts in both the solvent phases. Therefore, gas phase is favored for HAT mechanism [7].

The d-HAT mechanism is a transfer of second H – atom from the chosen compounds so as to suppress free radicals. The positions 4 – 3 OH (gas) and 3 – 4 OH (solvent) possess minimum BDE2, thus the sites require minimal energy to donate another H – atom (Table 2). It is concluded that 3 – 4 OH site of CA in nonpolar phase is suitable to donate second H – atom [8].

4.2 Double Sequential Electron Transfer Proton Transfer (d-SETPT)

In SETPT mechanism, minimal value of IP states specifies maximum capacity of losing an electron. It is noted from Table 3, the compound CA having higher ability to lose an in all three environments rather than pCA due to low IP1 [9]. Lower magnitude of PDE indicate higher capability for deprotonation. As illustrated in Table 3, 3 OH and 4 OH sites of CA and pCA possess least magnitudes of PDE1 respectively. Amid these two best sites, CA (3 OH) is suitable position for deprotonation in gas phase. In solvent phases, 4 OH of both compounds is capable of donating a proton and

conclude the compound CA is more facile for deprotonation. Summarizing that the compound CA can easily donate an electron and a proton in polar and nonpolar phases respectively [10, 11].

In d-SETPT mechanism, the ability of losing second electron can be computed via IP2. In CA, 3 OH radical (H – atom removed) assumed as a parent compound and is named as 3 OH parent compound and the same trend is followed for all configurations. Analyzing the data from Table 4, the compound CA obtains low IP2 in 3 OH parent compound compared to 4 OH of CA and pCA for all the phases. Least value of PDE2 indicates larger capacity of deprotonate a proton. It is found that 4 – 3 OH of CA and 4 OH – COOH of pCA having minimum PDE2 in both gas and solvent phases. Among these sites, CA (4 – 3 OH) is more preferential for donating second proton in gas phase.

Table 1 Bond Dissociation Enthalpy (BDE1) for the Compounds CA and pCA is Computed and Interpreted

Compounds	OH Sites	Gas phase	Polar phase	Nonpolar phase
		BDE1 (kcal/mol)	BDE1 (kcal/mol)	BDE1 (kcal/mol)
CA	3 OH	76.85	85.05	85.20
	4 OH	87.74	78.70	78.58
	COOH	111.4	112.12	112.10
pCA	4 OH	85.69	86.10	86.06
	COOH	111.35	112.33	122.78

Table 2 Second Order Bond Dissociation Enthalpy (BDE2) Values in kcal/mol of CA and pCA for Three Environments

Compounds	OH Sites	Gas phase	Polar phase	Nonpolar phase
		BDE2	BDE2	BDE2
CA	3-4 OH	108.14	97.94	97.04
	4-3 OH	97.25	103.39	103.66
	4OH-COOH	101.27	112.79	112.78
pCA	4OH-COOH	112.26	112.96	112.95

Table 3 The SETPT Mechanism is Performed and the Values are Interpreted in kcal/mol.

Compounds	AIP1			OH Sites	PDE1		
	Gas	Polar	Nonpolar		Gas	Polar	Nonpolar
CA	183.85	143.08	143.98	3 OH	206.77	255.73	254.98
				4 OH	217.66	249.38	248.36
				COOH	241.31	282.80	281.88
pCA	187.02	144.82	145.99	4 OH	212.43	255.04	253.83
				COOH	238.09	281.27	290.54

Table 4 Ionization Potential (AIP2) and Proton Dissociation Enthalpy (PDE2) of dSETPT, are Calculated and Tabulated for Three Different Phases

Compounds	AIP2			OH Sites	PDE2		
	Gas(kcal/mol)	Polar (kcal/mol)	Nonpolar (kcal/mol)		Gas (kcal/mol)	Polar (kcal/mol)	Nonpolar (kcal/mol)
CA (3OH)	417.19	411.73	412.21	3-4 OH	209.99	253.32	252.09
(4OH)	417.58	413.67	414.03	4-3 OH	209.60	251.38	250.27
				4OH-COOH	213.62	260.78	259.39
pCA (4OH)	420.31	420.92	420.85	4OH-COOH	216.66	259.36	258.21

4.3 Double Sequential Proton Loss Electron Transfer (d-SPLET)

In SPLET mechanism, loss of proton along with electron transfer identified the magnitudes of PA1 and ETE1 are computed and interpreted in Table 5. Both the compounds (CA and pCA) exhibiting smallest value of PA1 in 4 OH for all three media. Analyzing 4 OH sites of both compounds, it is observed that pCA and CA is suitable site for deprotonation in gas and solvent phases separately. Formulating the results for ETE1, the compounds CA of 3 OH and pCA of 4 OH positions

having higher ability of losing an electron in all three phases. Among two compounds, CA is the best compound for deelectronation [12, 13].

Subsequently, in d-SPLET mechanism, second proton and electron are released from their respective parent compounds of CA and pCA. Proton affinity PA2 for CA (gas) is smaller at 4 OH – COOH site than remaining sites as well as 4 OH – COOH of pCA compound is investigated from Table 6. Similarly, CA obtains lower magnitudes of PA2 at 3 – 4 OH (polar) and 4 – 3 OH (nonpolar) rather than pCA. The same protocol is followed for ETE2. The position 3 – 4 OH of CA is best radical scavenger in polar amid all three phases.

Table 5 First Level of SPLET Mechanism (PA1 and ETE1) for CA and pCA is Carried out by M06-2X/6-311 G(d,p)

Compounds	OH Sites	Gas		Polar		Nonpolar	
		PA1 (kcal/mol)	ETE1 (kcal/mol)	PA1 (kcal/mol)	ETE1 (kcal/mol)	PA1 (kcal/mol)	ETE1 (kcal/mol)
CA	3 OH	394.79	3.43	299.58	99.98	301.19	98.52
	4 OH	347.91	54.34	288.25	104.96	289.37	103.72
	COOH	349.04	76.87	292.80	133.83	294.61	131.99
pCA	4 OH	333.98	66.22	292.42	108.19	293.64	106.94
	COOH	349.02	76.84	292.95	133.89	294.69	142.60

Table 6 Proton Affinity (PA2) and Electron Transfer Enthalpy (ETE2) Values in kcal/mol is Compiled

Compounds	OH Sites	Gas		Polar		Nonpolar	
		PA2	ETE2	PA2	ETE2	PA2	ETE2
CA	3-4 OH	963.75	541.10	55.74	344.19	767.22	349.05
	4-3 OH	952.86	541.09	762.10	344.21	350.44	348.21
	4OH- COOH	932.17	516.39	776.88	349.57	364.82	353.47
pCA	4OH-COOH	964.21	537.44	793.95	366.48	799.86	372.40

5. CONCLUSION

The computational approach of DFT is employed to investigate the appropriate radical scavenger between the cinnamic acid derivatives. Double antioxidation mechanisms is performed with M06-2X and 6-311 G(d,p) for three media. Ability of transferring H – atom in more possible for CA at 3 OH (gas phase) and 3 – 4 OH (nonpolar phase) in HAT and d-HAT mechanisms respectively, compared to pCA.

CA is capable of losing an electron and proton is more easily in polar phase and gas phase (3 OH) in SETPT mechanism whereas 3 OH parent compound (polar) and 4-3 OH (gas) positions are suitable for removing successive electron and proton in d-SETPT mechanism. In SPLET mechanism, lower magnitudes of PA1 and ETE1 is observed at 4 OH in polar phase and 3 OH in gas phase for the compound CA. However, in PA2 and ETE2, both deprotonation and deelectronation are feasible at 3 - 4 OH in polar phase of CA.

REFERENCES

[1] S.B. Nimse and D.Pal, RSC Adv., Vol.5, 2015, pp.27986-28006.

[2] K.B. Pandey and S.I. Rizvi, Oxid. Med. Cell. Longev., Vol.2, 2009, pp.270-278.

[3] Nam Yi Kim, Nguyet Tran Trinh, Sang Gun Ahn and Soo A Kim, Int. J. Mol. Med., 2020, Vol.46, pp.449-457.

[4] Maciej Spiegel, J. Chem. Inf. Model., Vol.62, 2022, pp.2639-2658.

[5] D. Amić, V. Stepanić, B.Lučić, Z.Marković and J.M. Dimitrić Marković, J. Mol. Model., Vol.19, 2013, pp.2593-2603.

[6] Yan-Zhen Zheng, Zhong-Min Fu, Geng Deng, Rui Guo and Da-Fu Chen, Phytochem. Lett., Vol.180, 2020, pp. 112517.

[7] V. Deepha, R. Praveena and K.Sadasivam, J. Mol. Struct., Vol.1082, 2015, pp.131-142.

[8] Yan-Zhen Zheng, Yu Zhou, Qin Liang, Da-Fu Chen, Rui Guo, Cui-Ling Xiong, Xi-Jian Xu, Zhao-Nan Zhang and Zhi-Jian Huang, Dyes Pigm., Vol.141, 2017, pp.179-187.

[9] V.E. Atalay, I.S. Atish, K.F. Shahin, E.S. Kashikchi and M.Karahan, UNEC J. Eng. Appl. Sci., Vol.2, 2022, pp. 33-40.

[10] Y. Chen, H. Xiao, J.Zheng and G.Liang, PLoS One, Vol.10, 2015, pp.0121276.

[11] Jewel Hossen, Tarun Kumar Pal and Tariqul Hasan, Results Phys., Vol.4, 2022, pp.100515.[12] S.M. Dobrev and S.E. Angelova, Bulg. Chem. Commun., Vol.52, 2020, pp.48-53.

BRAIN TUMOR DETECTION USING DEEP LEARNING TECHNIQUE

T. Janani and P. Sobiyaa
Department of Information Technology
Bannari Amman Institute of Technology, Sathyamangalam - 638 401, Erode District, Tamil Nadu
E-mail: jananit@bitsathy.ac.in, sobiyaa@bitsathy.ac.in

Abstract

The International Association of Cancer Registries (IARC) states that 5-10 per 10,000 people have an instances of brain tumors are recorded each year in India, with over 80,000 individuals dying from them in 2021. An early and a proper treatment will be the remedy for stopping the spread of tumor cells in the brain. The advancement of technology in Medical field was comparatively increasing day by day for competing with the advanced technology we use Deep learning that uses interconnected nodes or neurons in a layered structure that resembles the human brain. Deep Learning models are able to detect more intricate features and able to process larger datasets more efficiently and accurately. Deep Learning can identify complex patterns in data that are too complex for traditional Machine Learning algorithms.

Transfer learning is a technique used in Deep learning where a model developed for one task is reused as the starting point for a model on a second task. This technique has been used to great success in deep learning applications. In this proposed method, transfer learning technique for brain tumor classification using ResNet50 with transfer learning was used. The proposed technique utilizes pre trained ResNet50 weights and fine-tunes them to classify brain tumors from MRI images. The standard dataset was used for the validation comprises of brain tumor MRI images which has 3064 T1- weighted images of three types of brain tumors: Glioma, Meningioma, and Pituitary. Then the weighted images are augmented and the dataset made into 24,512 images. The pre-trained networks VGG-16, GoogleNet are developed and performance metrics are compared with the proposed method. The results show that the proposed transfer learning technique with ResNet50 outperformed the other networks in terms of accuracy, F1 score, precision and recall. The real time dataset of 29 patients was used for testing the developed model which are obtained from Q-SCANS, Erode. By testing the T1-weighted images of real time dataset the developed model got an accuracy of 96 %. For the real time application, the model is designed as an GUI in python flask which is a micro web framework which will be available for the radiologists and doctors for assisting them in diagnosing the brain tumor.

1. INTRODUCTION

The most fatal diseases that exist today include brain tumors. The inner region of the human brain is encircled by a tumor, which is a collection of aberrant cells. It damages or compresses healthy tissues, which has an impact on the brain[1]. Additionally, it increases intracranial pressure, which has the potential to be lethal and speeds up the growth of tumor cells. It is therefore preferred since an early diagnosis or detection of brain tumors may increase patient survival. As a result, brain MRI classification has received a lot of attention in recent years[2].

Modern technology routinely uses Magnetic Resonance Imaging (MRI) to reveal important details about the form, size, location, and metabolism of brain Tumors, aiding in diagnosis. Many methods have been put out in the past for categorizing MRIs, from conventional methods to cutting-edge Deep Learning (DL) algorithms[3] like Convolutional Neural Networks (CNN)[4]. Data augmentation is an important technique used in computer vision and image analysis to increase the size and diversity of data sets. It is especially useful in the context of medical image analysis where limited data availability can be a challenge. In the context of brain tumor classification using Convolutional Neural Networks (CNNs), [5]data augmentation is used to artificially generate additional training examples from existing data, which can be used to further train and improve the performance of the network. Transfer learning is a technique in which a pre-trained model is used as the starting point for a new task. This technique can be used to reduce the time and cost of training a

model from scratch, as most of the parameters are already pre-trained. The transfer learning technique was used with the pre-trained model ResNet50.

2. METHODOLOGY

2.1 Magnetic Resonance Imaging and Brain Tumor

Magnetic resonance imaging (MRI) of the body uses radio waves, a computer, and a strong magnetic field to produce exact images of the interiors of the organs. To help explore, monitor, or dissect treatment for a substitute illness, the chest, midsection, and pelvis are used. The MRI procedure uses a strong magnetic field, radio waves, and a computer to produce exact images of inside body structures[6]. In MRI, radiation is not employed (X-rays). Detail-rich MR images, which are also utilized to identify disease, can be used by specialists to inspect the body. On a computer monitor, you can see the pictures. Additionally, they were copied to a CD, sent via email, or moved to a cloud server.

The magnet is surrounded all over table in 360 degrees. The typical MRI machine consists of a large, cylinder-shaped tube that is encircled by a circular magnet. On a table that glides into the magnet's center, the patient is lying down. The magnet no longer completely encloses the patients in some MRI machines, referred to as short-bore frames. Large diameter bores on some modern MRI scanners may be more comfortable for larger patients or those who are claustrophobic. The sides of the "open" MRI unit are open. They are especially helpful when examining larger patients or patients who have claustrophobia. Numerous test types can receive high-quality images from open MRI units.

2.2 Brain Tumor

An unnatural growth of cells in the brain or skull is known as a brain tumor. While tumor cells replicate uncontrollably, normal cells expand in a controlled manner as new cells replace old or damaged ones. Most malignancies from other parts of the body can travel to the brain, or tumors can form from the brain tissue itself which was classified into two categories primary & secondary.

2.2.1 Primary Brain Tumor

An abnormal growth that originates in the brain and typically does not spread to other body parts is referred to as a primary brain tumor. Both benign and malignant primary brain tumors are possible. A benign brain tumor rarely spreads, grows slowly, and has clear limits. Even though benign Tumors' cells are not cancerous, they can nonetheless be fatal if they are located near vital organs. A brain Tumor that is malignant grows rapidly, has distorted borders, and has spread to surrounding brain regions. Malignant brain Tumors are frequently referred to as brain cancer, but they do not meet the definition of cancer because they do not spread to other organs besides the brain and spine.

2.2.2 Secondary Brain Tumor

Secondary brain Tumors, and metastatic brain Tumors all refer to Tumors that start elsewhere in the body and spread to the brain. One or more Tumors may appear in the case of brain metastasis. The process of cells spreading to another area of the body is known as metastasis. Primary site alludes to the region of the primary malignancies. Cancers of the lung, breast, melanoma (skin), colon, and kidney frequently spread to the brain. The tumor is visible in the brain MRI in figure 1 When a cancer patient begins to experience neurological symptoms and a brain scan is ordered, a metastatic brain Tumor is typically identified.

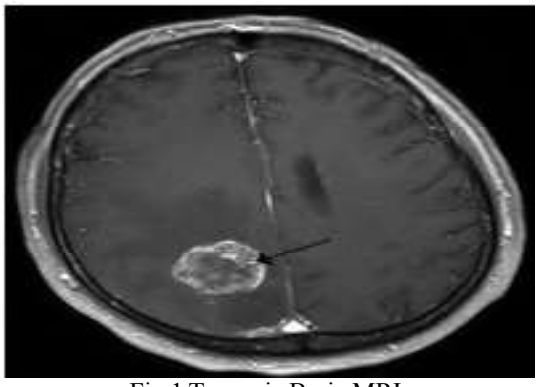

Fig.1 Tumor in Brain MRI

2.3 Convolutional Neural Network (CNN)

CNN (Convolutional Neural Network) is a type of neural network architecture used to process and classify images. CNNs are composed of multiple layers of neurons, each of which handles a specific task. The first layer of a CNN is a convolutional layer, which performs operations on the input data to detect features. This layer is followed by multiple pooling layers, which reduce the number of parameters and computation in the network by down-sampling the feature maps. The output of the pooling layers is then passed to fully connected layers,

which feed the data into a classification layer. CNNs are commonly used in computer vision applications, such as image recognition, object detection, and facial recognition.

Overall, CNNs are a powerful tool for extracting features from images and classifying them into different categories. CNNs are well-suited for applications that require high accuracy and predictive power. In addition, CNNs are relatively easy to implement and can be used for a variety of different applications. Overall, CNNs are a powerful tool for extracting features from images and classifying them into different categories. They are becoming increasingly popular for computer vision applications, and are also being used in natural language processing tasks. As the technology continues to evolve.

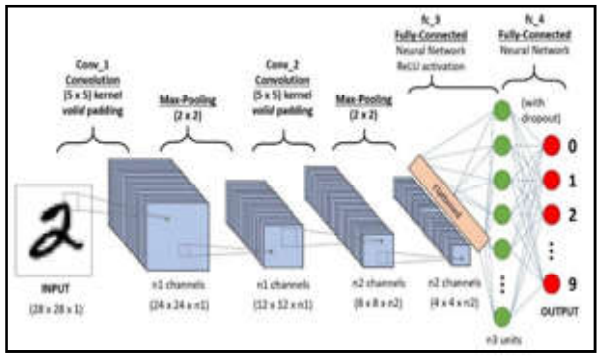

$$Y_i^{(l)} = \sum_{j=i|}^{n^{(l-1)}} K_{ij}^{(l)} * y_j^{(l-1)}$$

Fig. 2 CNN Architecture

CNN employs a linear mathematical operation called convolution. CNN has an input layer, output layer, and multiple hidden layers which are shown in the figure 2. The hidden layer consists of a convolution layer, pooling layer, activation function, normalization layer, and fully connected layer. In combination with a deep learning model called a convolutional neural network (CNN) to accurately classify brain tumors in a study published in the journal NeuroImage.

The architecture of GoogleNet is based on the Inception architecture which is referred in the same year. The Inception architecture is a modified version of the traditional convolutional neural network and uses a combination of 1x1, 3x3 and 5x5 convolutions to reduce the number of parameters in the network. The GoogleNet architecture also uses an auxiliary classifier to reduce the error rate. This classifier is connected to the network at different levels, and its purpose is to reduce the error rate by providing additional supervision to the network. The researchers used GoogleNet to identify the presence of brain tumors in MRI images. Overall, GoogleNet can accurately classify brain tumors in MRI images. This is an important step forward in the development of computer-aided diagnosis systems, as it can reduce the workload of radiologists and improve the accuracy of diagnosis.

2.4 AlexNet

Transfer learning using the AlexNet architecture was introduced by Krizhevsky et al. in 2012. It is a Deep Convolutional Neural Network (CNN) which is trained on a large amount of labeled data. The AlexNet structure consists of five convolutional layers and three fully-connected layers with a total of 62.3 million parameters. After training on the ImageNet dataset, AlexNet produces a powerful model that can be used to classify images in other domains. Transfer learning using AlexNet has been used to classify images in medical imaging, cell segmentation, facial expression recognition, etc. It has been used in neuro-imaging studies to classify brain tissues and for medical diagnosis such as the detection of tumors, retinal diseases, breast cancer, and brain tumors. The AlexNet architecture can also be used for transfer learning in computer vision tasks such as object detection and segmentation, scene recognition, and visual tracking. Transfer learning using AlexNet has become increasingly popular due to its performance and the ease of fine-tuning the network for new tasks. It can also be used to pre-train other types of neural networks such as recurrent neural networks. AlexNet has become a standard in many computer vision tasks and is a popular choice for transfer learning.

The model is initialized with the parameters of the pre-trained AlexNet network. Then, the new task-specific layers are added and the parameters are fine- tuned using the task-specific data. This allows the network to make predictions based on the new task while keeping the general capabilities of the pre-trained network. It is an efficient way to apply deep learning to new tasks, and can be used to quickly prototype or build production-ready models. Despite its success, there are still challenges to be addressed in transfer learning such as the sparsity of the training data, generalization, and scalability.

AlexNet is an eight-layer deep convolutional neural network, which was developed by Alex Krizhevsky, Ilya

Sutskever, and Geoffrey Hinton and published in their 2012 paper entitled "ImageNet Classification with Deep Convolutional Neural Networks". It is the first large-scale deep learning network to be applied to the task of object recognition. AlexNet consists of five convolutional layers andthree fully connected layers. It is explained that the first layer is a convolutional layer with 96 feature maps of 11x11 filter size and a stride of 4. The second layer is a convolutional layer with 256 feature maps of 5x5 filter size and a stride of 1. The third and fourth layers are convolutional layers with 384 and 384 feature maps respectively, both having a 3x3 filter size and a stride of 1. The fifth layer is a convolutional layer with 256 feature maps of 3x3 filter size and a stride of 1. The three fully connected layers are composed of 4096 neurons with a dropout value of 0.5. Finally, the output layer consists of 1000 neurons for the 1000 image classes in the ImageNet dataset. AlexNet also employs the use of ReLU neurons which

2.5 Data Augmentation

Data augmentation is an important technique used in computer vision and image analysis to increase the size and diversity of data sets. It is especially useful in the context of medical image analysis where limited data availability can be a challenge. In the context of brain tumor classification using Convolutional Neural Networks (CNNs), data augmentation is used to artificially generate additional training examples from existing data, which can be used to further train and improve the performance of the network. Data augmentation works by taking an existing image and manipulating it in various ways, such as skewing, scaling, and rotating, to produce realistic new versions of the image. This can be used to increase the data set size, as well as to add variability that can improve the accuracy of the model. Additionally, some types of augmentation can perform more complex manipulations of the data, such as changing the color and intensity of the image, or adding noise. This can be used to improve the ability of the model to generalize to unseen data. In terms of brain tumor classification, data augmentation can be used to artificially generate new tumors from existing ones, and add variability to the data set. This can help to ensure that the model does not overfit to the training data, and can improve its ability to classify new cases. Additionally, by adding noise to the data, it may be possible to make the classification more robust to image artifacts and improve its accuracy. Data augmentation can have a significant impact on the performance of a CNN for brain tumor classification. It can help to create more diverse and realistic data, which can improve the accuracy of the model, and allows the network to generalize better to unseen data. Additionally, by adding noise to the data, it can make the model more robust and less prone to image artifacts and other factors that can degrade accuracy. Finally, data augmentation can also be used to artificially create new training examples, which can help to further improve the performance of the model. The dataset has been augmented for processing of the data.

2.5.1 Features used for Data Augmentation

Rotation range is the range of degrees (0–180) within which images are rotated at random. To randomly convert images vertically or horizontally, there are two ranges to choose from: width shift and height shift. Shear range is used to apply shearing modifications at random. The zoom range allows for arbitrary in-image zooming. When there are no presumptions of horizontal asymmetry, horizontal flip is used to randomly flip half of the images (e.g., real-world pictures). The fill mode technique is used to fill in newly produced pixels, which may emerge following a rotation or a width/height change.

Here the table shows number of augmented samples in each set. Build of a custom dataset class that adds 8 various angles to each image: 0, 45, 90, 120, 180, 270, 300, and 330 degrees. Instead of caching all training samples in memory for augmentation, combing it with Pytorch's DataLoader class to provide real-time data loading, augmentation, and training.

Table 1 Split up for Augmented Samples Dataset

Number of augmented training samples	17152
Number of augmented validation samples	3680
Number of segmented testing samples	3680
Total	24512

2.6 Transfer Learning

Transfer learning is a powerful machine learning technique that leverages knowledge from previously trained models. It has been used to great success in many fields, including computer vision and natural language processing. In computer vision, transfer learning is used to take advantage of the knowledge contained in a pre-trained model, which can be used to classify images more accurately than training a model from scratch. In

the context of brain tumor classification, transfer learning can be used to improve the accuracy of a CNN- based classification system.

A pre-trained model can be used to extract features from the input images, which can then be used to train a classifier. By leveraging the knowledge contained in the pre-trained model, the classifier can be trained faster and more accurately than if it had to learn from scratch. There are several types of transfer learning that can be used for brain tumor classification. The most commonly used type is fine- tuning, which involves taking a pre-trained model and fine-tuning it using the input data. This can be used to improve the accuracy of a CNN-based classification system, as the pre-trained model can provide the network with a prior knowledge of the data. Another type of transfer learning is feature extraction, which involves extracting features from a pre-trained model and using them to train a classifier. In figure 5.4.1 the transfer learning process is introduced. This can be used to improve the accuracy of a CNN-based classification system, as the extracted features can provide the network with a prior knowledge of the data.

2.7 IMagenet

One of the most popular applications of transfer learning is using pre- trained models from ImageNet. ImageNet is a large database of images that was created for the purpose of object recognition. It contains millions of images with 1000 different classes of objects, and these images have been used to train deep convolutional neural networks (CNNs). These CNNs have been used to develop models that can detect and classify objects in images with high accuracy. Transfer learning involves taking these pre-trained models and using them as a starting point to develop models for other tasks. For example, a pre-trained model can be used to identify objects in a medical image, such as a brain MRI scan. By using a pre- trained model, the amount of data and computing power required to train a model is significantly reduced, resulting in a faster and more efficient model.

2.8 ResNet 50 with Transfer Learning

ResNet50 is a popular deep learning architecture that is a subset of the ResNet family of networks. ResNet50 is a 50-layer deep convolutional neural network developed by Microsoft Research that won the ImageNet Large-Scale Visual Recognition Challenge (ILSVRC) in 2015. ResNet50 is trained on the ImageNet dataset, which consists of millions of images belonging to 1000 different classes. The architecture of ResNet50 consists of 50 convolutional layers, each of which is followed by a batch normalization layer, a rectified linear unit (ReLU) activation layer, and a max pooling layer. In figure 5.6.1 the convolutional layers are divided into five stages, each of which contains 10 layers and is connected to the next stage via shortcut connections. These shortcuts provide a direct connection between two layers that are not adjacent in the network, thus allowing the network to learn more complex features. Additionally, ResNet50 makes use of ResNet blocks – groups of convolutional layers with an identity mapping – to reduce the network's depth and improve its accuracy. The model has achieved state-of-the-art results on numerous tasks and continues to be a popular choice for deep learning practitioners. ResNet has been used for various tasks such as image classification, object detection, and face recognition.

The main advantage of using ResNet50 for transfer learning is that the model has already been trained on a large and diverse dataset. This means that it can quickly adapt to any new task with minimal changes. It also has a relatively shallow architecture which makes it easier to fine-tune the weights. This makes it a good choice for transfer learning. In conclusion, transfer learning with ResNet50 is a very useful technique for quickly and easily achieving high performance on a newtask. The pre-trained model has already been trained on a large and diverse dataset, and the shallow architecture makes it easy to fine-tune the weights on a new dataset.

3. CONCLUSION

The Deep learning models are Data thirst algorithms which require a large number of data. Data augmentation is done for the standard dataset which made the 3064 images into 24,512 images. Transfer learning technique is used with ImageNet database with 1000 different class. Three models were developed in which, the VGG-16 with ImageNet database gives an accuracy of 98.5 %, recall is 98% and F1-score is 91.78% and GoogleNet with ImageNet database gives an accuracy of 95 %, recall is 97% and F1-score is 97.2% By comparing ResNet50 with transfer learning technique was used with ImageNet database gives an accuracy of 99.2 %, recall is 99 % and F1-score is 99% with the test loss 0. 0096.The problem of overfitting was resolved by introducing transfer learning. The real time datasets obtained from the Q-SCANS, Erode was used for testing

the ResNet50 Network with transfer learning which gives an accuracy of 96% which was comparatively higher than other networks.

REFERENCES

[1] S. Ahuja, B. K. Panigrahi and T. Gandhi, "Transfer Learning Based Brain Tumor Detection and Segmentation using Superpixel Technique," in IEEE Reviews on International Conference on Contemporary Computing and Applications (IC3A), 2020, pp. 244-249.

[2] J. Amin, *et al,* "A New Approach for Brain Tumor Segmentation and Classification Based On Score Level Fusion Using Transfer Learning", in Journal of Medical Systems, Vol.43, 2019.

[3] Alnemer, Alaa and Jawad Rasheed, "An Efficient Transfer Learning-based Model for Classification of Brain Tumor", in IEEE Reviews on International Symposium on Multidisciplinary Studies and Innovative Technologies (ISMSIT), 2021, pp.478-482.

[4] R. Chelghoum, A. Ikhlef, A.Hameurlaine and S.Jacquir, "Transfer Learning Using Convolutional Neural Network Architectures for Brain Tumor Classification From MRI Images", in Springer on IFIP International Conference on Artificial Intelligence Applications and Innovations, 2020, pp. 189-200.

[5] S. Deepak and P.M.Ameer, "Brain Tumor Classification Using Deep CNN Features via Transfer Learning", in Computers in Biology and Medicine, Vol .111, 2019, pp.103-345.

[6] S. Divya, L.P. Suresh and A.John, "A Deep Transfer Learning Framework for Multi Class Brain Tumor Classification Using MRI", in IEEE Reviews on International Conference on Advances in Computing, Communication Control and Networking (ICACCCN), 2020, pp.283-290.

TAMIL NUMERALS IDENTIFICATION IN PALM LEAF MANUSCRIPTS USING DEEP LEARNING

M. Pravin Savaridass[1], S. Sri Atchaya[2], J.Haritha[3] and S.Priyanka[4]

[1&3]Department of Electronics and Instrumentation Engineering, [2&4]Department of Biomedical Engineerinig
Bannari Amman Institute of Technology, Sathyamangalam - 638 401, Erode District, Tamil Nadu
E-mail: pravinsavaridass@bitsathy.ac.in,sriatchaya.bm20@bitsathy.ac.in,haritha@bitsathy.ac.in

Abstract

Palm leaves were one of the first writing materials, and humans have used them as writing surfaces. In order to share this information with the rest of the world and to stimulate further research into ancient literature, accessible access to historical manuscripts must be provided. In this study, a convolutional neural network (CNN)-based optical character recognition (OCR) system is utilised to accurately digitise and recognise Tamil palm leaf manuscript numbers. In ancient palm leaves, numbers and digits are written in Tamil numerals, which makes reading palm leaves challenging. Our approach thereby transforms Tamil numbers to standard numerals (Arabic letters). We are creating a technique based on deep learning to recognise the numbers. Our study utilises the convolution layer, pooling layer, activation layer, fully connected layer, and classifier of the convolutional neural network. The database of character sets was developed using scanned images of palm-leaf manuscripts. The database is divided into 12 unique classes, with around 700 records per class. Using the CNN model, a functional demonstration of the character recognition method for Tamil palm-leaf writing was created. It was determined that the CNN model had a higher rate of recognition. A high number of characteristics were gathered for each CNN layer, which significantly improved the prediction rate and accuracy.

Keywords: *Archaeology, Inscriptions, Image processing, Optical character recognition, Palm-leaf manuscripts, CNN*

1. INTRODUCTION

Palm leaf manuscripts are among the earliest types of writing in India, notably in the south.. In South and Southeast Asian nations like Nepal, Sri Lanka, Burma, Thailand, Indonesia, and Cambodia, it is also the main inspiration for writing and painting. Before the 10th century, there are no known palm- leaf manuscripts from India. The palm leaf was undoubtedly used far earlier than this, as evidenced by the fact that it is described as a writing implement in a number of literary works and that several sculptures and monuments depict it. Palm leaf manuscripts must be preserved because they include knowledge about past religious practices, astrology, astronomy, and medical practices from antiquity. The information in the inscriptions can be cross-referenced to provide insight into the world dynastic history. Information about the grandeur, way of life, economic situation, culture, and administrative practices used by several rulers and dynasties can be found in stone and palm leaf inscriptions found throughout the world. Rocks, pillars, slabs, stones, building walls, and temple bodies all have inscriptions. Additionally, it is present on seals, palm leaves, and copper plates. The epigraph refers to the study and the text of inscriptions is deciphered. This information is used by epigraphists to identify graphics, explain their significance, and categories applications according to historical periods and cultural contexts. Numerous methods are employed by different researchers to get around the difficult issues associated with deciphering numerals in stone and palm leaf inscriptions.

Digital images of palm leaf manuscripts are created mainly to preserve the information. To make the data on the images easily retrievable and processed, it is recommended to convert palm-leaf images into machine-readable languages. For this purpose, OCR (optical character recognition) is a possible choice. The resources and information recorded on palm leaf manuscripts are valuable. It is therefore required to build an automated system that can accept the images of inscriptions as input and produce text output. Figure 1 depicts the flow of the palm-leaf manuscript character identification system Image acquisition refers to the method of taking photos using cameras or other optical scanners. A technique called picture pre-processing is used to reduce image noise and change the pictures into a format that can be

processed. The technique of binarization involves transforming grayscale photos into binary. The presence of noise may reduce the character detecting system's effectiveness. The picture is first cropped to get rid of any unwanted parts, then it is skewed to make it seem better in the frame. The picture is skewered to the proper synchronization. An orientation angle is controlled by the skew detection function. The classifier is then used to identify the character and convert it into a current text. A trigram approach based on NLP is employed to infer the precise Unicode character. The relevant Unicode values are utilized in order for the algorithm matching pattern to correlate to numerals and matched numerals.

2. RELATED WORKS

R. Bremananth et al provided a method for identifying ancient Tamil numerals in rocks based on OCR. Morphological operations like segmentation and pre-processing are performed on the source picture [1]. The salt and pepper noise has been eliminated, the colour photographs have been improved, and they are now in grayscale. By utilizing the bounding boxes that are used to divide the dilated image, characteristics such as area attributes and corner points can be extracted numerical character recognition system

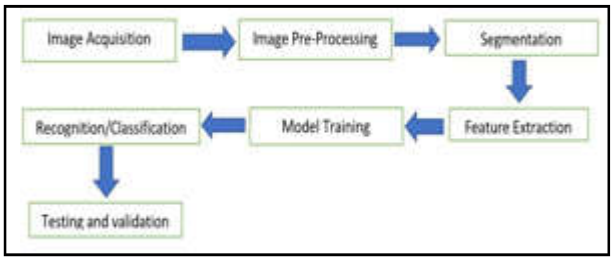

Fig.1 Block Diagram of Palm leaf manuscripts

KNN and ensemble learning are used to classify the numerals, and subsequently Unicode is used to match them. Pravin Savaridass M et al. developed a Tamil character identification algorithm and discussed the benefit of using the Self Organizing Map (SOM) model to record and analyse the invariant properties of the Tamil Scripts. [2]. The authors' proposed approach is different from a neural network in that it lacks a character-specific hidden layer. Input and output only require two layers. A Brahmi script recognition technique based on OCR is shown by Gautum et al. [3]. In this work, a geometrical technique is used for image retrieval. Optical scanners are used to scan images. The pre-processing stage also includes thinning, thresholding, and cropping. Numerals are then recovered from each line that is drawn between images during the segmentation process. The authors used a noise reduction technique in the pre-processing stage before attempting to completely eliminate the disturbance from the input image. The following morphological processes to be carried out are dilation and erosion techniques. The letters in the binary image are located using the linked component method. Each numbers was dissected into its component parts and matched to the relevant Tamil integers using correlation matching. G. Janani et al. developed an approach that is simple to learn and apply for identifying and analysing Tamil inscriptions. [4]. Words are classified into tags and word prediction. Manigandan et al. relying on the technology of OCR and NLP, recommended identifying Tamil numerals in inscription photographs from the ninth to the twelfth centuries. [5]. The writers split the images after collecting, editing, and processing them for the aforementioned work. Prior to segmentation, colour images were converted to binary and grayscale using a threshold value. SIFT (Scale Invariant Feature Transform) method was used to identify the characteristics images of every character, such as the quantity of lines, curves, loops, and points. Soumya et al. separated the lines and individual numerals from the inscription images using the closest neighbour method [6].The Fourier and wavelet transforms are used to extract aspects including structural, syntactical, statistical, and loop properties from the relevant data. Support vector machines (SVM), transudative SVM, and genetic algorithms are all used in the classification stage.

2.1 Image Pre-processing and Segmentation

Bandara et al. [7] developed a web-based recognition method in order to analyse and classify the inscription numbers in a database. The pre-processing phase includes border identification, segmentation, thinning, and binarization. Binarization is performed using Otsu's method, followed by thinning and feature extraction. The inscriptions were scanned using optical scanners by Gautum and Chai, who then cropped the photos. Techniques for thresholding and thinning were used at the pre-processing stage. When images have been divided into segments, numbers are collected from each line that has been recognised. Six geometric entities are required to derive the Circle, semi-circle, corner, intersection, bifurcation, and termination points are characteristics of the inscription[8]. Lakshmietal. wereabletoderivethreedistinctfeaturesfrom the character bitmap by scaling it [9,10]. After thinning, the character

image generates a single-pixel skeleton and segments, with intersectional features removed first.

The eight octagonal photos of the figure are then used to derive 16 shadow attributes.. In the final step, the histogram characteristics of the original scaled character image are extracted by detecting and segmenting contour points. For each segment, the histogram chain code characteristics are determined. Giridhar *et al.,*[8]. CNN's OCR capabilities for reading Tamil inscriptions were the focus of. The raw colour image is first converted to grayscale before convertingto binary image.Using the Otsu algorithm threshold, binarization is utilised toextract text from a noisy background. The binarized picture is then separated into letter blocks, each of which corresponds to a Tamil character.

2.2. Feature Extraction

The properties H-centre, V-centre, Height, Width, HP-Skewness, and Horizontal Projection are used to create numerals. Vertical projection, VP- Skewness, horizontal, right, and left diagonal stroke densities are used to extract features. Using optical character recognition, Kannada language numerals in epigraphs were identified (OCR) and fuzzy logic by Soumya et al. [6]. In order to extract statistical features, the authors used three different techniques. A one-dimensional statistical analyser was used to compute Mean, Standard deviation, and Variance. Kurtosis, entropy levels, and skewness were estimated using a histogram analyser, and the smoothness and coarseness of an image were determined using a GLCM analyser. Pictures with salt and pepper and Gaussian noise effects are sharpened, then a median filter is applied, followed by a morphological filter. Deleting minor items is a method. Another enlargement. The numerals in the image are then recovered using a process.

2.3 Classification Methods

For grouping the numerals in old inscriptions, Baheti M. J.*et al.* employed the K-means algorithm [11]. By using a Transform Feature Scale-Invariant (SIFT), Rajkumar *et al.,*[12] acknowledged old Tamil numerals, and a new strategy based on key point bags was developed. Subashini *et al.* [13] employed using a Support Vector Machine to classify data using the idea of decision planes that set choice constraints (SVM). The authors select the radial function kernel type for SVMs in this system to improve their performance. An extremely successful technique for forecasting the Tamil inscription centuries was multiclass SVM. Images were trained using neural networks, and they were matched to contemporary Tamil letters. According to Clanuwat *et al*. [14], there are parallels between early and modern Japanese character classifications. The experiment made use of two fully connected convolutional autoencoders. For training, mixed density networks (MDN) and data recurrent neural networks (RNN) are used Bhowmik, *et al*. [15] examine the classifier's performance using the elliptical technique and a variety of classifiers, such as Naive Bayes, Digging, Bagging, SVM, and MLP. With the objective of recognising Bangla words, the collected features were categorised using an ANN and the Histogram Oriented Gradient (HOG). The script achieved its highest recognition accuracy through a combination of wavelet feature extraction and GRNN classification[16,17]. For the purposes of image classification and detection, CNN is given a dataset of cropped images as input. Data augmentation and transfer learning are used to train CNN to categorise Indian numerlas base donKeras and Tens or Flow.

3. MATERIALS AND METHODS

3.1 Image Acquisition

The palm leaf manuscript must be identified and scanned at a resolution of at least 300 dpi using a high-quality scanner. Since the palm leaf is at least 250 years old and has a significant likelihood of leaf degradation, high-quality scanning is necessary to extract the data without losing any of it. In the pre- processing step, high quality scanned pictures were helpful in locating and eliminating noise in very ancient manuscripts.

3.2 Image pre-processing

Among the pre-processing steps are Binarization, gray scale correction. The binarization process uses adaptive thresholding, deep learning is utilized to extract features. Following that, a grayscale version of the scanned colour image is created.

3.2.1Noise Removal

For every AI-based recognition model, clean data is the final need to attain high accuracy. Noise reduction is the next significant step in pre-processing. Noise reduction is a crucial step in the proposed approach to provide cleaner data to the AI model. Different filtering methods, such as the median filter, Gaussian filter, and non-local means de-noising filter, are used to remove noise.

- **Median filter**
  The median filter is a filtering method for signal and image noise reduction. Since the median filter is well known for conserving edges during noise removal, it is extremely important in image processing applications. This form of noise reduction is widely applied as a pre-processing technique for palm leaf manuscript processing to enhance the outcomes. In the suggested research, median filtering was chosen since it occasionally preserves edges while removing noise.

- **Gaussian filter**
  A 2D convolution-based smoothing filter called the Gaussian filter is used to lower noise in visual data. The type of kernel used is the only distinction between the mean filter and the gaussian filter[18].

$$G(x) = \frac{1}{\sqrt{2\pi}\sigma} e^{\frac{-x^2}{2\sigma^2}} \quad (1)$$

Where σ stands for Standard deviation.
The 2D Gaussian function is given as

$$G(x,y) = \frac{1}{2\pi\sigma^2} e^{\frac{-x^2+y^2}{2\sigma^2}} \quad (2)$$

- **Non local mean denoising filter**
  Denoising images via nonlocal techniques is a technique is applicable in image processing. With non-local mean filters, the target pixel serves as the centre of attention while the means of neighbouring pixels are computed and given appropriate weights. After filtering, the image clarity is significantly improved while keeping its details. The Euclidean distance between picture patches with centres at p and q is given as d(B(p), B(q), and f is a decreasing function where c(p) is the discovered normalisation factor. Because the manuscripts for the proposed work are so ancient, it's possible that certain letters or numerals have degenerated. The non-local means de- noising function is therefore the best option

- **Image binarization**
  The filtered image is then converted into a binary image. The image can be binarized using a wide range of techniques, such as Otsu's binarization, adaptive thresholding, and the local minima and maxima method. The proposed technique uses adaptive thresholding to binarize the image, which generates a threshold value dynamically dependent on the location in the image. Several numerals must be segmented in palm leaf inscriptions to maintain continuity. Therefore, character segmentation requires the morphological processes. Several fundamental morphological processes, including dilatation, erosion, opening and closing, as well as the OCR method for character identification from images, are used for text extraction. After edge detection, morphological adjustments are made to the image by eroding principle.

- **Character segmentation**
  At the line, word, and character levels, Three independent classes of image segmentation that are possible. Because the proposed task involves handwritten script, where the words or lines cannot be separated, character level segmentation is advised. A character-based image is utilised at this stage of segmentation. Character level segmentation is used to try and break down an image into its individual numbers.

3.3 Model Training

3.3.1 Creation of Dataset

A dataset of isolated numerals will be built from all segmented and annotated patch images. It has 700-character samples and 12-character classes, with 500-character samples being used as a train set and selected depending on the character classes. As a test set, the remaining samples will be used. Each class has a varied amount of sample photographs. Some classes appear frequently in our palm leaf manuscript collection, whereas others are rarely utilized.

3.3.2 Creating CNN model

Features were extracted in this research using convolutional neural networks. All the image's pixel values are fed into the network's first layer as input data. In this study, the TensorFlow library is used. In this instance, a multilayer CNN is used for the feature extraction and classification process. The structure of the network is shown in Figure 3. Using a sliding window

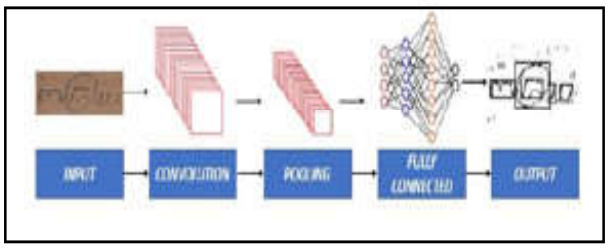

of 3x3 pixels and the 28x28 pixel input grayscale picture, the first convolutional layer (C1) is computed.

The convoluted output is followed by the ReLU function. ReLU functions do not saturate during convnet training, assisting in avoiding the vanishing gradient issue. To reduce the architecture's computational burden, a maxpooling operation may be utilised after each convolution operation, depending on the architectural design.

3.3 Testing and Validation

The samples are gathered, with 80% of them being utilised for training and the remaining 20% for testing. The model's precision is 82%.

4. RESULTS AND DISCUSSION

The project is done totally using Python. Image and character segmentation are done using open-source tools like OpenCV and PIL. Keras is used to implement converts, while TensorFlow is used as the backend. The training environment is the Google Co-lab GPU environment. Using the palm leaf manuscript's data that was previously trained in the CNN, a model is created for number recognition. The model is tested on a fresh palm leaf text that has undergone pre-processing and has many character data sets. The recognised numbers are then shown on top of each number in the manuscript output. The projected numbers on the palm leaf text are recognised and categorised using the CNN model. The CNN algorithm gives the computer instructions to learn from examples. In order to build and train the CNN model, produced data was used. For the palm leaf manuscript alone, a special data collection was created. Each number in the pre-processed image is segmented, and the dataset is formed by extracting numerical features from the segmented image. 100 input photos with various writing styles are used to train each recognized number. When the CNN model is given the newly pre- processed palm leaf manuscript image, the segmented numbers are detected with 82% accuracy.

Fig.4 Palm leaf manuscript image

Fig.5 Cropped input image

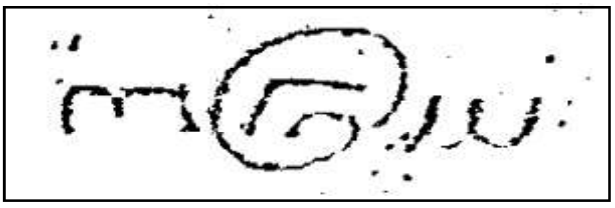

Fig.6 Pre-processed binary image

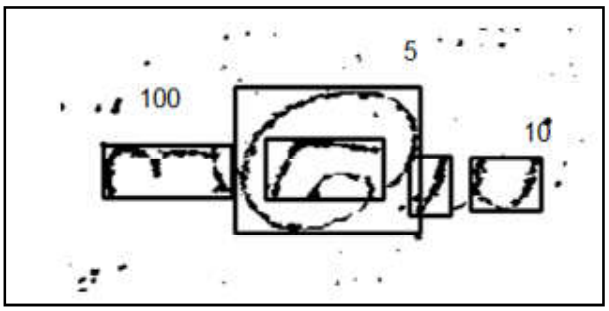

Fig.7 Character recognized Output image

5.CONCLUSION

To recover important historical data from those ancient times, the procedure of palm leaf manuscript picture decipherment is used. To begin with, image pre-processing techniques are used to get the numerical data set from the scanned Tamil palm leaf manuscript. The identification and understanding of palm leaf writings from many cultures has been the subject of several research. In the envisioned work, we use an OCR-based CNN model to identify and connect the ancient Tamil numbers found in these manuscripts with contemporary Tamil numbers.

According to the results, the created CNN is suitable for reading Tamil numbers from palm leaf manuscripts since it is more accurate.

REFERENCES

[1] R. Bremananth and A. Prakash, "Tamil Numerals Identification", In 2009, International Conference on Advances in Recent Technologies in Communication and Computing, IEEE, 2009, pp. 620-622.

[2] M. PravinSavaridass, J.Haritha, V.T. Balamurugan, K. S. Vairavel, N. Ikram, M. Janani and K. Indrajith, "CNN based Character Recognition and Classification in Tamil Palm Leaf Manuscripts", In 2022 International Conference on Communication, Computing and Internet of Things (IC3IoT), IEEE, 2022, pp.1-6.

[3] Gautam, Neha and Soo See Chai, "Optical Character Recognition for Brahmi Script using Geometric Method", Journal of Telecommunication, Electronic and Computer Engineering (JTEC), Vol.9, No.3-11, 2017, pp.131-136.

[4] G. Janani, V. Vishalini, and P. Mohan Kumar, "Recognition and Analysis of Tamil Inscriptions and Mapping Using Image Processing Techniques", In 2016 Second International Conference on Science Technology Engineering and Management (ICONSTEM), IEEE, 2016, pp. 181-184.

[5] T.V.V.D.V.N.B. Manigandan, V. Vidhya, V. Dhanalakshmi and B. Nirmala, "Tamil Character Recognition from Ancient Epigraphical Inscription using OCR and NLP", in 2017 International Conference on Energy, Communication, Data Analytics and Soft Computing (ICECDS), IEEE, 2017, pp.1008-1011.

[6] A.Soumya and G. Hemantha Kumar, "Recognition of Ancient Kannada Epigraphs using fuzzy-based Approach", in 2014 International Conference on Contemporary Computing and Informatics (IC3I), IEEE, 2014, pp.657-662.

[7] Bandara, Dammi, NalinWarnajith, Atsushi Minato and Satoru Ozawa, "Creation of Precise Alphabet Fonts of Early Brahmi Script from Photographic Data of Ancient Sri Lankan Inscriptions", Canadian Journal on Artificial Intelligence, Machine Learning and Pattern Recognition, Vol.3, No.3, 2012, pp.33-39.

[8] Giridhar, Lalitha, Aishwarya Dharani and Velmathi Guruviah, "A Novel Approach to OCR Using Image Recognition-Based Classification for Ancient Tamil Inscriptions in Temples", arXiv preprint arXiv:1907.04917, 2019.

[9] Lakshmi, C. Vasantha, Ritu Jain and C. Patvardhan, "Handwritten Devnagari Numerals Recognition with Higher Accuracy", in International Conference on Computational Intelligence and Multimedia Applications (ICCIMA 2007), IEEE, Vol.3, 2007, pp. 255-259.

[10] Bansal, Veena and M. K. Sinha, "A Complete OCR for Printed Hindi Text in Devanagari Script", in Proceedings of Sixth International Conference on Document Analysis and Recognition, IEEE Computer Society, 2001, pp. 0800-0800.

[11] M. J. Baheti, A.V. Mane, Shaikh Abdul Hannan and K.V. Kale, "Comparison of PCA and SVM for a west Indian Script- Gujarati", CiiT Journal of Digital Image Processing, Vol.3, No.11, 2011, pp.709-715.

[12] S. Rajakumar and V. Dr.SubbiahBharathi, "7th Century Ancient Tamil Character Recognition from Temple Wall Inscriptions", Indian Journal of Computer Science and Engineering (IJCSE), Vol.3, No.5, 2012.

[13] P. Subashini, M. Krishnaveni and N. Sridevi, "Period Prediction System for Tamil Epigraphical Scripts Based On Support Vector Machine", In International Conference on Information Systems for Indian Languages, Berlin, Heidelberg: Springer Berlin Heidelberg, 2011, pp. 23-30.

[14] Clanuwat, Tarin, Mikel Bober-Irizar, AsanobuKitamoto, Alex Lamb, Kazuaki Yamamoto and David Ha, "Deep Learning for Classical Japanese Literature", arXiv preprint arXiv:1812.01718 2018.

[15] Bhowmik, Showmik, Samir Malakar, Ram Sarkar and MitaNasipuri, "Handwritten Bangla Word Recognition using Elliptical Features", In 2014 International Conference on Computational Intelligence and Communication Networks, IEEE, 2014, pp. 257-261.

[16] http://tdil.mit.gov.in/GujaratiScriptDetailsApr02.pdf

[17] Dholakia, Jignesh, Archit Yajnik and Atul Negi. "Wavelet Feature Based Confusion Character Sets for Gujarati Script", in International Conference on Computational Intelligence and Multimedia Applications (ICCIMA 2007), IEEE, Vol.2, 2007, pp. 366-370.

[18] Pal, Umapada, Nabin Sharma, Tetsushi Wakabayashi and Fumitaka Kimura, "Handwritten Numeral Recognition of Six Popular Indian Scripts", in Ninth international conference on document analysis and recognition (ICDAR 2007), IEEE, 2007, Vol.2, pp. 749-753.

COMPARISON ON PERFORMANCE OF INJECTION MOULDING AND 3D PRINTED PARTS

N. Jayakumar, G. Senthilkumar, S.Velmurugan and K.Kamal Basha
Department of Mechanical Engineering,
Bannari Amman Institute of Technology, Sathyamangalam - 638 401, Erode District, Tamil Nadu
E-mail: er.jayakumar11@gmail.com

Abstract

The goal of this observation is to decide and evaluate the overall performance of PLA specimens produced via injection moulding and 3D printing through a range of mechanical trying-out procedures. This is to decide whether new cutting-side technology used in 3D printing is capable of replacing traditional production techniques such as injection moulding. Various destructive and non-destructive trying-out techniques are used according to British requirements which include the Charpy Impact check, tensile check, Compression test and Water Absorption check. Through using the same specimens and materials, analysis of results showed that Injection moulded additives achieved an advanced degree inside the departments of effect resistance, Ultimate tensile strength, Young's modulus, Compression test, water absorption and different properties.

Keywords: *PLA, 3D printing, Injection moulding, Ultimate tensile test*

1. INTRODUCTION

When designing components significantly recollect a lot of things on the way to in the long run form the overall performance and mechanical attributes of any given product. As generation is constantly being advanced and has been fine-tuned, there may be an array of producing techniques which could all produce equal searching merchandise with their character residences. For an engineer, it's miles of paramount significance in an effort to distinguish among those techniques and choose the proper course to permit for maximum overall performance for the proposed application. Many producers presently use traditional techniques which might be attempted and examined with an exceptional achievement rate, maximum notably, injection moulding. This technique has been proved to be perfect for prototyping purposes, giving producers a danger to expose customers a visible instance of the product. To benefit a deeper expertise of those techniques, and the way they impact the mechanical residences of the specimen, numerous mechanical assessments may be finished with inside the shape of unfavorable and non-unfavorable. The fundamental goal of this research is to supply equal specimens the usage of each method of producing and behavior a range mechanical assessment for you to finish which technique is superior. The proposed assessments encompass Charpy Impact take a look at, Tensile take a look at, Compression take a look at and Water Absorption. The principle at the back of that is that the usage of equal substances will preserve an detail of continuity on this aspect, even as being capable of pick out the important thing variations with inside the structural integrity of the component. In practice, those assessments will supply us critical data approximately the specimen, including effect resistance, Young's Modulus, final tensile strength, elastic load, elongation percent and others. Being capping a position to differentiate if a fabric is ductile or brittle is vital as it could form the manner the specimen behaves. By checking out the overall performance skills of those techniques can even permit a contrast to be made among the two. It may be thrilling to peer how each technique carries out and evaluate in opposition to every other.

2. LITERATURE REVIEW

The use of 3D printing technology is regarded as a highly adaptable technique that can produce a variety of customized final products. Utilizing bio-based materials can greatly reduce the environmental impact of the final 3D- printed products. The ratio of TPS:PLA:PBAT was set at 50:40:10 weight percent in this study's creation of a thermoplastic starch (TPS), poly (lactic acid), and poly (butylene adipate-co-terephthalate) composite specifically for FDM 3D

printing technology. In order to improve the blends' brittleness and produce better 3D printing filament, the chain extender ADR4468 (CE) was also introduced [1].

Injection molding and 3D printing are pivotal polymer processing technologies. Injection molding is ideal for mass production, while 3D printing excels in intricate geometries. Combining these technologies economically fabricates complex products. This study explores the potential of their integration, comparing bonding strength of PLA parts through overprinting and overmolding. A specialized injection mold allows rib injection onto a preform. Thermal properties are assessed through differential scanning calorimetry and thermogravimetric analysis. A rib pull-off test evaluates mechanical bonding strength in all manufacturing combinations. [2]

This study examines water absorption effects on PLA and PLA/Wood composites. Injection molding and 3D printing produced specimens for comparison. SEM morphology studies and tensile tests were conducted, along with HDT and crystallinity analyses. Water uptake increased notched impact strength in injection-molded specimens but not in 3D-printed ones. Both methods experienced reduced tensile properties and lower HDT values after water absorption tests. The study's significance lies in SEM morphology studies, water storage effects, and comparing production technologies. NFC compounds and composites were also investigated in relation to water storage. [3].

Fiber-reinforced 3D printing (3DP) is a new technology with potential for high-performance material fabrication. To assess its commercial viability, a comparative analysis with existing technologies is essential. This study developed ring-spinning travelers using fiber-reinforced 3DP, surpassing the capabilities of injection molding. The quality and performance of printed and molded travelers were compared. The results showed that fiber-reinforced 3DP offers flexibility in reinforcement patterns and materials, although printed travelers exhibited inferior surface characteristics and wear resistance. Recommendations were provided for traveler design and utilizing the technology's capabilities to enhance traveler performance. [4].

This study aimed to compare the performance of PLA-based materials produced through injection molding and 3D printing. Neat PLA, PLA/TPU blend, and GF-reinforced composites were examined. Mechanical properties (strength, modulus, toughness) were evaluated using tensile, flexural, and fracture toughness tests. Macro-level appearances, fracture surface morphology, and thermal behavior were also analyzed. The findings indicate that 3D printing is highly advantageous for shaping neat PLA and PLA/TPU blend, although there may be reductions in mechanical performance for PLA/GF and PLA/TPU/GF composites due to variations in GF reinforcement orientation. [5]

This study aims to compare the performance of ABS specimens produced via injection molding and 3D printing using various mechanical testing procedures. The objective is to determine whether 3D printing technology can replace traditional injection molding methods. Testing methods include Charpy Impact, Tensile, Flexural Bend, and Water Absorption tests, following British standards. The results, obtained from identical specimens and materials, indicate that injection molded components outperformed 3D printed components in terms of impact resistance, ultimate tensile strength, Young's modulus, flexural strength, water absorption, and other properties. It can be concluded that for applications requiring maximum performance in these attributes, injection molding remains the preferred method for manufacturing such components. [6]

Novel ways to tablet manufacturing are highly sought after as the pharmaceutical industry develops and more people turn to customized medications. The capacity to precisely control drug release is one of the primary factors leading to micro-scale batch production. This study provides evidence for the utilization of rapid tooling injection moulding (RTIM) in the production of tablets. Different structural elements were used in the fabrication of tablets to change the surface area while keeping the volume constant, resulting in different specific surface areas (SSA). [7]

This research aims to compare the quality of industrial and 3D printed mold specimens fabricated using injection molding and 3D printing. The objective is to explore the potential of new 3D printing technologies in replacing traditional injection molding processes. Both methods, 3D printing and injection molding, are utilized for producing plastic parts and components, each with its own advantages and disadvantages. 3D printing is an additive process that builds up layers of material, while injection molding fills a mold with molten material that solidifies. Although both techniques can be used for prototyping, there are significant differences between them. [8]

This study aimed to compare the physical and mechanical performance of PLA, ABS, and nylon 6 fabricated using fused deposition modeling (FDM) and injection molding. The viscosity of the samples was not affected by the different processing methods, and the density measurements showed less than a 4% difference. FDM samples exhibited approximately 108% higher water absorption compared to injection-molded samples. FDM had a minimal effect on the degree of crystallinity in ABS but increased the crystallinity of PLA and nylon 6. The tensile strength, Young's modulus, elongation at break, and impact strength of FDM samples were approximately 48%, 50%, 48%, and 78% lower, respectively, than those of injection-molded samples. These results provide valuable insights for manufacturing final products using FDM while considering the desired performance. [9]

3D printing offers new possibilities for manufacturing polymeric structures that are not achievable with injection molding. However, the manufacturing method can impact the mechanical properties of the components. This study compares the mechanical behavior of thermoplastic polyurethane specimens produced by two methods: SEAM technology (screw extrusion additive manufacturing) and conventional injection molding. Uniaxial tension tests are conducted on specimens from both methods, analyzing inelastic properties and tension until rupture. To minimize disturbances, the 3D-printed samples have a single strand per layer, and optical measurements are used for accurate cross-sectional area determination. The tests show that the inelastic material behavior is similar for both methods. However, 3D-printed specimens exhibit lower maximum stretch values at rupture and increased result variability due to surface structure differences. [10]

This paper compares polymer elements manufactured using injection molding and additive manufacturing techniques. Specifically, the analysis focuses on fused deposition modeling (FDM) and single screw injection molding, following thermoplastics processing standards. The study highlights the importance of the cross-section structure of FDM samples for fabricating high-strength components. Larger cross-section samples (4 x 10 mm2) with three perimeter layers and 50% infill exhibit lower mechanical strength compared to injection molded reference samples, reaching less than 60% of their strength. However, reducing the cross-section dimensions to 2 x 4 mm2 improves durability, achieving up to 110% of the tensile strength observed in injection molded samples. For large cross-section samples, strength increases with the number of contour layers, resulting in up to 97% of the tensile strength value for samples with 11 perimeter layers. Furthermore, reducing the thickness of deposited layers enhances the mechanical strength of the printed components. [11]

3. METHODOLOGY

Testing thermoplastics was recommended as part of the material selection approach. Once more, the chosen substance would need to be suitable for 3D printing and injection moulding. Although there are many various types of thermoplastics that may be employed, their accessibility is dependent on the particular resources that are available. Since polylactic acid (PLA) is readily available and regularly used in industry for certain applications, it was selected as the material in issue. The specimens adhered to the measures stated in each British ISO standard for the relevant test, were uniform in size and shape, and met other requirements. Producing each component using the selected methods came next.

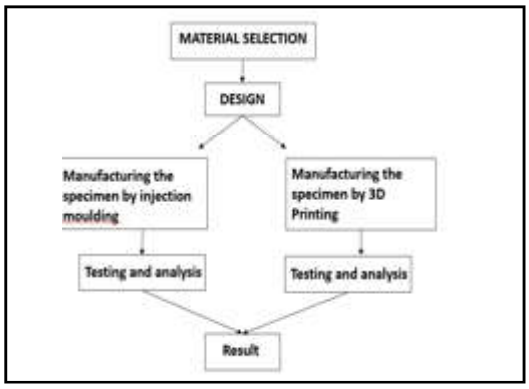

Fig. 1 Methodology

4. INJECTION MOULDING

As shown in the Figure 2 specimen's mould is already connected, and 7g of PLA pellets are added to the feed. The material should be dried for around two hours at 60 C, as advised by the manufacturer. With a temperature setting of 160°C, the feed screw revolved at a speed of 50 revolutions per minute. A charging tool was used to feed the pellets until they melted. Approximately 60 seconds of the feed and 2 minutes of mixing were spent together. The chemical was held in situ and flushed through the nozzle once it was ready. Since the nozzle could hold enough material to accomplish the injection, it was able to create two components without having to redo the entire operation.

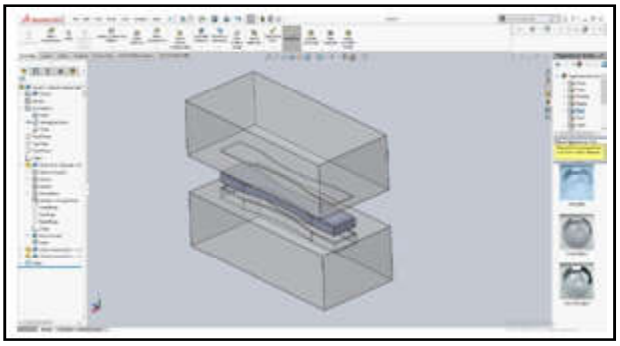

Fig.2 CAD model of Injection moulding

5. 3D PRINTING

Fusion 360 were used to construct the CAD models of the ASTM D638. The CAD model files were prepared and converted to STL format as shown in Figure 3. The object is then sent into a Creality ender machine, which uses a fused deposition model to create 3D printed components, after being subjected to slicing in the ultimate cura programme, where Gcode is created. Figure 4 shows the 3D printed part

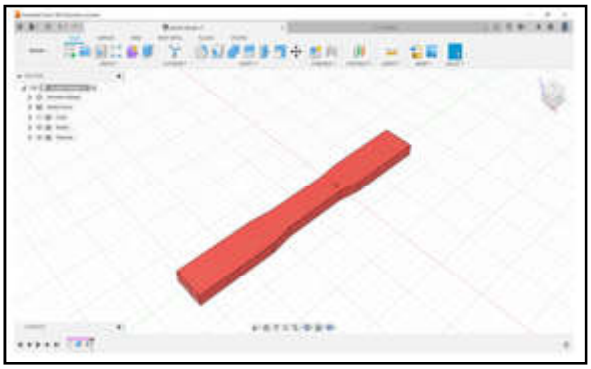

Fig. 3 CAD model of 3D printing sample

Table.1 3D Printing Process Parameters

Infill (%)	Nozzle Temperature (°C)	Bed Temperature (°C)
100	210	60

Fig. 4 3D printed part

6. CHARPY IMPACT TEST

As a result, it can conclude that the samples' outer layers are ductile and strong enough to totally destroy the pendulum. In contrast to the smooth surface of the injection moulded sample, the fracture of the totally ruptured sample was not "clean," and its fractured surface was highly rough. The centre of the substance, we can say, is quite porous, which is much less than injection moulding displays the sample's failure. The results of the non- notched samples exhibit a great deal of diversity when examined separately, particularly for the samples that were injection moulded.

7. COMPRESSION TEST

To assess the elastic and compressive fracture characteristics of brittle or low-ductility materials, compression testing is crucial. The modulus of elasticity, proportional limit, compressive yield point, compressive yield strength, and compressive strength may all be determined by compression experiments. These characteristics play a key role in figuring out if a material is suitable for a given application or would fail under a given set of pressures.

Table. 2 Compression Test for Injection Moulding

Sl.No.	Data	S1	S2	S3	S4
1	Peak point (KN)	216.34	218.43	220.52	222.61
2	Breaking point (N)	7.5	7.6	7.8	7.8
3	Yield Displacement (mm)	205.22	207.46	209.32	210.58
4	Displacement (mm)	8.2	8.5	8.7	8.8

Table.3 Compression Test for 3D printing

Sl.No.	Data	S1	S2	S3	S4
1	Peak point (KN)	215.98	216.43	218.52	219.61
2	Breaking point (N)	6.3	6.4	6.6	6.7
3	Yield Displacement (mm)	196.18	197.46	199.32	199.58
4	Displacement (mm)	5.4	5.5	5.7	5.8

8. TENSILE TEST

Analysis of samples from injection moulding also revealed stress whitening on the surface. "Necking" occurs in injection moulded samples when the material is put under the most stress. A significant amount of strain is focused in one area of the material during this type of tensile deformation, eventually lowering the cross-sectional area.

Table.4 Tensile Test for Injection moulding

Sl.No.	Data	S1	S2	S3	S4
1	Maximum Force (Fm), Kn	3.62	3.95	4.25	4.75
2	Disp. At Fm, mm	24.96	25.65	26.12	26.76
3	Max. Disp, mm	26.42	28.76	29.24	29.54
4	Tensile strength (Rm) N/mm	0.004	0.004	0.006	0.008
5	Elongation (%)	23.86	24.83	25.32	25.57
6	Reduction in area (Z)	93.97	95.15	95.65	96.17

Table.5 Tensile Test for 3D printing

Sl.No.	Data	S1	S2	S3	S4
1	Maximum Force (Fm), Kn	2.58	2.56	2.59	2.62
2	Disp. At Fm, mm	19.08	19.25	19.95	20.050
3	Max. Disp, mm	21.150 mm	21.925mm	22.455mm	23.124mm
4	Tensile strength (Rm) N/mm	0.002	0.002	0.002	0.002
5	Elongation (%)	16.66	16.93	17.47	17.964
6	Reduction in area (Z)	90.333	90.78	91.32	92.132

9. WATER ABSORPTION TEST

Three specimens of each type are adequate for this test, as indicated in ISO 62, 2008. The sample should first be weighed using a balance with a recording accuracy. To achieve uniformity and maintain a high level of precision, samples are individually submerged in water at 23°C (2°C). Both

3D printed samples and injection moulded samples go through this process. The samples are taken out of the water after 24 hours, quickly dried, and weighed on the same scale as before. Each sample's original and final masses are noted, and calculations are employed to calculate the percent change in mass for each sample. Both approaches produce less change overall and are therefore recommended in your application. The formula is: where m1 and m2 are the starting and final masses, respectively, after immersion. The data clearly show that the specimens created through 3D printing absorbed more water as shown in Fig. 6, leading to a bigger weight gain. In contrast, the mass of the injection moulding specimens barely changed as shown in Fig. 5, with specimen 3 exhibiting no changes at all. The experiment lasted for 24 hours; in reality, if it had gone on for longer, the outcomes might have been different. Analysis of the specimens revealed negligible changes in dimension, so this can be regarded as unimportant. Injection moulding is recommended for components since it is impractical for parts to gain mass and hence lose performance.

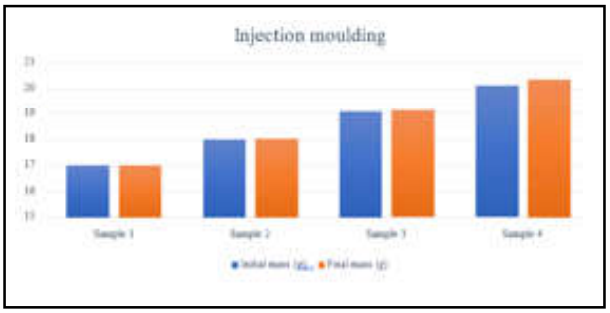

Fig. 5 Water absorption test results (Injection moulding)

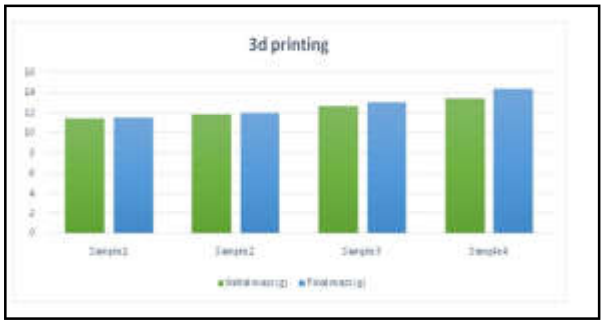

Fig. 6 Water absorption test results (3D printing)

10. SEM TEST

A crucial instrument in the examination of plastic failures since it can give specific details about the start and spread of cracks and look for particle and dust contamination as shown in Fig. 7 & 8. The portion of the model that looks at how latent variables and their measurements interact.

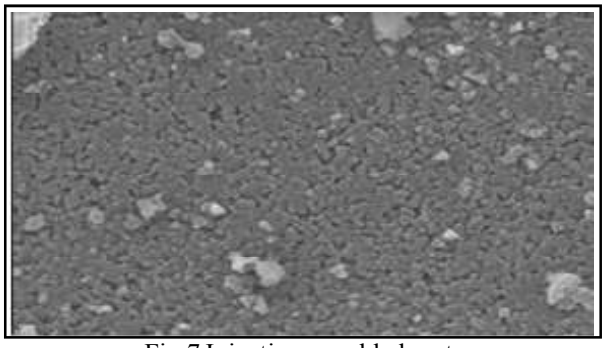

Fig.7 Injection moulded part

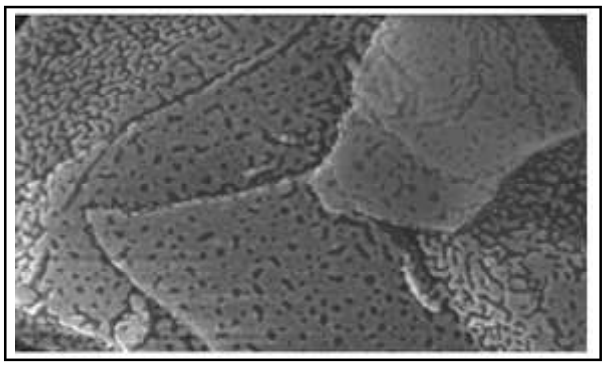

Fig.8 3D printed part

Now it has a clearer grasp of both processes, how they function, and what makes them unique from one another after finishing research on the fundamental distinctions between 3D printing and injection moulding. Due to this investigation, the drawbacks of 3D printing were discovered. This is done by carrying out a series of test procedures that describe the samples' qualities for use in diverse contexts. Charpy impact tests, tensile tests, 3-point bending tests, and water absorption tests were among the testing run. Important information was provided by each of them on characteristics including impact strength, maximum force, tensile strength, modulus, elongation, and tensile elongation. Since all tests were conducted on identically sized, identical-material samples, the mechanical properties of the samples were influenced by the production process, and the outcomes of each approach were quite trustworthy can be deduced to be true. Throughout the tests, the samples' tensile characteristics were noted. According to the given results for maximum force, tensile strength, and Young's modulus, injection moulding performs better than 3D printing in most instances. The key finding of this test is that injection moulding should be utilized for stressed sections. It's also important to note that the 3D printed samples exhibit less elongation, which is also desirable. More crucially, because the orientation of the build also influences the material's strength, 3D printing might not be achievable when several stresses are applied from various directions. Making a product that is weaker in one way than the other is not practicable. The Charpy impact test provided evidence supporting this finding, showing that the average impact strength of the notched and un-notched samples was much higher than that of the injection moulded ones. All of the results were dependable and consistent because they were quite near to the values listed in the data sheet for the technical literature. Once more, the production method of choice for items or components that absorb impact is injection moulding.

Table.6 Average Specimen Data

Sl. No	Parts	Injection Moulding	3D Printing
1	Tensile test, KN	4.134	2.587
2	Compression test, N	7.7	6.5
3	Impact test, J	45	19
4	Water absorption, g	0.0135	0.1453

11. CONCLUSION

According to the data, the deflection was similar for both techniques, but the injection-molded specimens could withstand almost twice as much force. From this, the material's modulus of elasticity was estimated, and injection moulding excelled in this area as well. Rapid prototyping is made possible by technological advancements, but 3D printing is not without flaws. With time, the difference between the two approaches may begin to close, particularly when attempting to preserve an isotropic rather than anisotropic structure. Nevertheless, for applications needing the best mechanical qualities, injection moulding remains the method of choice.

REFERENCES

[1] Dennis Mcguin, "Plastic Injection Molding vs 3D Printing–Which is Better", 2020.

[2] Boros, R., P. Kannan Rajamani and J. G. Kovõcs, "Combination of 3D Printing and Injection Molding: Overmolding and Overprinting", Express Polymer Letters, Vol.13, No.10, 2019, pp.889-97.

[3] Ecker, Josef Valentin *et al.*, "Mechanical Properties and Water Absorption Behaviour of PLA and PLA/ Wood Composites Prepared by 3D Printing and Injection Moulding", Rapid Prototyping Journal, Vol.25, No.4, 2019, pp.672-78.

[4] Kabir, S. M.Fijul, Kavita Mathur and Abdel Fattah M. Seyam, "Comparing Performance of 3D-Printed and Injection-Molded Fiber-Reinforced Composite Parts in Ring-Spinning Traveler Application", Technologies, Vol.9, No.4, 2021.

[5] Kaynak, Cevdet and S. Deniz Varsavas, "Performance Comparison of the 3D-Printed and Injection-Molded PLA and Its Elastomer Blend and Fiber Composites", Journal of Thermoplastic Composite Materials, Vol.32, No.4, 2019, pp. 501-20.

[6] A. Ganapathy, D. Chen, A.Elumalai, B.Albers, K.Tappa, U.Jammalamadaka, MJ.Hoegger, DH. Ballard, "Guide for starting or optimizing a 3D printing clinical service Methods", doi:10.1016/ j.ymeth.2022.08.003. Epub 2022 Aug 11. PMID: 35964862, Oct.2006, pp.41-52.

[7] Sohal and Gurdeep Singh, "Comparative Study and Analysis Of 3D Printed and Industry Printed Mould Cast", Vol.4, 2022, pp.1866-79.

[8] Lay and Makara *et al.,* "Comparison of Physical and Mechanical Properties of PLA, ABS and Nylon 6 Fabricated Using Fused Deposition Modeling and Injection Molding", Composites Part B: Engineering 176(July): 107341. https://doi.org/10.1016/ j.compositesb.107341, 2019.

[9] Oelsch and Erik *et al.* "Comparative Investigation on the Mechanical Behavior of Injection Molded and 3D-Printed Thermoplastic Polyurethane", Journal of Rubber Research, https://doi.org/ 10.1007/s42464-021-00092-w., Vol.24, No.2, 2021, pp.249-56.

[10] Podsiadiy, Bartiomiej, Andrzej Skalski, Wiktor Rozpiyrski, and Marcin Sioma, "Are We Able to Print Components as Strong as Injection Molded?- Comparing the Properties of 3d Printed and Injection Molded Components Made from Abs Thermoplastic", Applied Sciences (Switzerland), Vol.11, No.15, 2021.

AN IOT-BASED INFUSION PUMP

S. Albert Jerome, B. Bijoy, Nibin Sabu and Abin Nazer
Department of Biomedical Engineering,
Noorul Islam Center For Higher Education, Kumaracoil - 629 180, KanyaKumari District, Tamil Nadu

Abstract

A patient's circulatory system is controlled by an infusion pump to provide fluids and drugs in both large and tiny doses. Although rarely subcutaneous, arterial, and epidural infusions are employed, it is typically administered intravenously. An infusion pump's primary function is to help maintain IV patency. The Internet of Things (IoT) is utilized in this study to communicate data between the control and the infusion pump. This saves the doctor time, and the patient will be dynamically monitored.

1. INTRODUCTION

An Infusion Pump is used for delivering fluids as well as medicines in large and small amounts into a patient's circulatory system in controlled amount. It is generally used intravenously, although subcutaneous (under the skin), arterial and epidural (spinal cord) infusions are occasionally used. The major necessity of infusion pump is to assists in maintaining IV patency. In this paper, the physician can control the infusion pump from anyplace. For this Internet of Things (IoT) is used for transferring the data between the infusion pump and the control. This helps the physician to laborious time and the patient's monitoring will be dynamic.

2. LITERATURE SURVEY

This solved several problems, including software problems, alarm faults, battery problems, sparks, and shocks[1]. They and their team came up with a solution to address these issues. It can be lifted with one hand due to its weightlessness and the components of our project are durable, affordable, and easy to use.

Created a low-cost insulin infusion pump with the goal of helping Brazilians with type 1 diabetes[2]. The creation of the prototype is the outcome of industrial and academic collaboration in Brazil. We discuss the creation of such a prototype as well as the lessons discovered as a result of it.

Administered the chemical compounds for chemotherapy using infusion pumps[3]. Radiation that unintentionally enters the infusion pumps during therapy could harm the internal solid state integrated circuit chips. Such flaws could lead to improper dosing. The usage of infusion pumps during chemoradiotherapy persists despite manufacturer instructions that caution against using the devices in radiological settings. Device malfunction risk could be reduced with proper shielding of the gadgets while they are exposed to radiation.

Implemented smart pump–EMR interoperability to measurable, data-based improvements in IV medication safety and improved accuracy, timeliness, and efficiency of IV infusion documentation[4]. Revenue was increased due to improved charge capture for outpatient IV infusions. Non-lead composites for shielding. Micro particles of Bismuth (III) oxide (BO) were impregnated into two materials at various percent weights: Polydimethylsiloxane (PDMS) and Polyurethane Elastomer (PU). PDMS/BO samples attenuated X-rays of 52KVp at 4 mm thickness. PU/BO attenuated X-rays of 52KVp at 3 mm thickness.

Examined the issue with infusion pumps at the hospital for continuous drug monitoring to lower medical errors[5] . To increase precision, get rid of harmful pumps, and develop a staff-friendly pump formation. The medication mistakes were overcome, and the patients benefited greatly and were safer as a result.

Launched large-volume secondary infusion in the acute care situation, IV smart pumps are widely utilized for intermittent or one-time administration of pharmaceuticals such antibiotics, electrolyte replacements, and several oncology treatments[6]. The system and setup requirements must be fully understood in order to distribute secondary drugs consistently and accurately. Regrettably, it happens frequently for nurses to discover that a secondary drug has only been half administered while their programming called for a full

infusion. The technical prerequisites for using an IV smart pump to provide secondary drugs are covered in this article for all nurses.

Suggested a compact and economical integrated infusion pump system that isn't yet readily available in the Indian market at a low price. It delivers the right amount of insulin and keeps blood sugar levels within a certain range[7]. They came to the conclusion that ongoing monitoring was necessary, which may be seen as a disadvantage of the system.

Calculated the benefits of including a bedside central that manages all intravenous (IV) infusion pumps[8]. The execution time is not longer, usability is excellent, and medication error is decreased. Controlling and keeping an eye on the numerous infusion pumps is simple. The correctness of the result, however, has not been disclosed.

Run a time-series trial, compared error rates, and discovered that employing smart pumps can eliminate errors and time delays[9]. Serious drug incidents can also be found, as well. For enhancing and ensuring drug safety, it is necessary to understand technical and nursing behavioral variables. Before the use of smart pumps, they found significant mistakes.

About using intravenous infusions in neonatal and pediatric hospitals[10]. In the United Kingdom, traditional procedures are the only ones employed, so it is crucial to disclose the SCI, but standardizing also has little actual use. They came to the conclusion that study must be done to harmonize the SCI in order to increase acceptance.

Complete IV anesthesia in conjunction with the pumps[11]. The use of propofol for very prolonged periods in sick or young children is contraindicated due to the possibility of developing Propofol Infusion Syndrome. Complete ntravenous (IV) sedation and anesthesia are utilized in intensive care (PRIS). the introduction of pharmacokinetically-programmed pumps that may choose which infusion pump to use to maintain a specific concentration.

The significant risk factors that are present in intensive care units[12]. In order to prevent prescription errors, calculate drugs, and recognize and fix them, the smart infusion pump is employed. Especially for intensive care units, this smart pump technology establishes a minimum level of safety.

Mostly concentrated on pinpointing the regions that damage patients and prevent drug errors[13]. Keystroke error software is available, and infusion pump technology is used to prevent heparin-related mistakes as well as patient harm.

The potential use of intelligent intravenous infusion pumps to cut down on medicine administration mistakes[14]. Implementation, technical performance, usability, and user acceptance are among the three surveys that collect the data.

In Complete Intravenous Anesthesia, it was discussed the use of an automated drug delivery system with computer-assisted control to dispense propofol (TIVA)[15]. In order to simulate how the medicine degrades, a dilution chamber is employed. Monitored and evaluated is the concentration. They proved the viability and did so.

3.EXISTING SYSTEM

3.1 Power Supply System

An AC or DC supply can be used as the power source. Currently, rechargeable batteries predominate.

3.2 Detector Unit

Sensor unit consists of sensors such a thermopile array sensor, a liquid pressure sensor, a sound detection sensor, and a sensor for measuring liquid pressure.

3.3 Sound Detection Sensor

A sound sensor is a component that analyzes the intensity of sound waves to detect them and transforms them into electrical signals. The sound sensor includes an amplifier, peak detector, and capacitive microphone built-in.

3.4 Liquid Pressure Sensor

Pressure sensors for viscous liquids are transducers because they provide an electrical signal in proportion to the pressure they are measuring. This makes it possible for electronic equipment like microprocessors, programmable controllers, or computers to monitor pressure.

3.5 Air Bubble Detection Sensor

Two piezoelectric ultrasonic transducers, one serving as a transmitter and the other as a receiver, are typically used in non-invasive ultrasonic bubble sensors. Based on the significant acoustic impedance differential between the fluid or tubing wall and air, the principle of air detection in flowing fluid is based.

3.6 Temperature Sensor

Thermopile sensors are made to monitor temperature at a distance by spotting Infrared (IR) energy from an object. The amount of IR radiation released increases with temperature. Little thermocouples mounted on a silicon chip make up the thermopile sensing element, which absorbs the energy and generates an output signal.

3.7 Bolus

It enables you to schedule the delivery of a specified quantity of medicine or substance at a particular time.

4. METHODOLOGY

4.1 Proposed Methodology

This proposed system is used for controlling the infusion pump from any place. It consists of Node MCU (ESP-32), Liquid pressure sensor, Air Bubble Detection Sensor, Door Alarm, Peristaltic Pump, OLED, Occlusion Alarm. All the sensor details are sent to the NODE-MCU microcontroller after detecting fall. Based on the sensor output, the alarm will be triggered and the physician will be notified. In addition to this, immediate notification will be sent through wirelessly to the respective person to take further actions. As a result, all the patient parameters that are being tracked may be readily managed.

4.2 Advantages

- The proposed system is under the control of IoT, so that anyone can control it from anywhere.
- In the system advanced and secured program is used in which the spark from the circuit and most of the other errors will be removed.
- Occlusion alarm is used for quality alarm ringing.
- Peristaltic pump is used for obtaining the specific flow rate of the fluid.
- Thermopile sensor is used for detecting any other person's arrival.

4.3 Disadvantages

- The notification's arrival could be delayed
- Battery issues could result in significant damage.

4.4 Applications

- It is simple for everyone to maintain and control.
- Also included are the problems' fixes.

Fig.1 Block Diagram

5. COMPONENTS DESCRIPTION

5.1 Circuit Diagram

The circuit diagram consists of Node MCU ESP-32 in the middle, 12V battery, Power Regulator L298 on the right corner, Peristaltic pump in the top right corner of the Figure 2, temperature and humidity sensor in the bottom right corner for detecting external sources, Buzzer, OLED in the top left corner for viewing the values, Turbidity sensor for bubble detection in the left corner and Sound detection sensor with Mic for reporting noise in the left bottom corner.

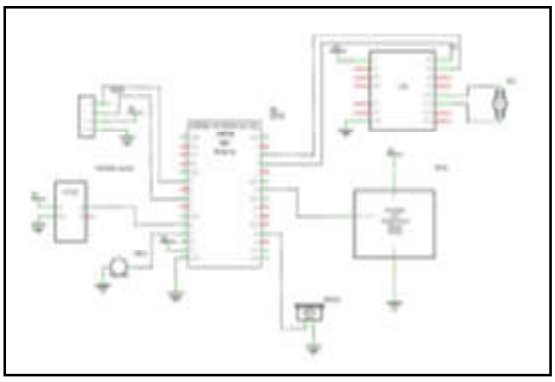

Fig.2 Circuit diagram

5.2 Micro Controller Unit (MCU)

A processing unit, memory modules, communication interfaces, and peripherals make up this intelligent semiconductor Integrated Circuit (IC). A wide variety of devices, such as washing machines, robotics, drones, radios, and game controllers, utilise MCUs, as shown in figure 3.

The development of Metal-Oxide-Semiconductor-Field-Effect-Transistor (MOSFET) technology is credited with giving rise to MCU. The MCU used to be a simple semiconductor IC with a CPU and memory module in its early stages. MCUs often use the Harvard architecture as their foundation.

Popular companies like Intel, Motorola, Microchip, and Atmel advanced the invention over the years. These firms mostly produce 8-bit MCUs with proprietary architecture. The ARM-based MCU is the exception, which uses the ARM architecture

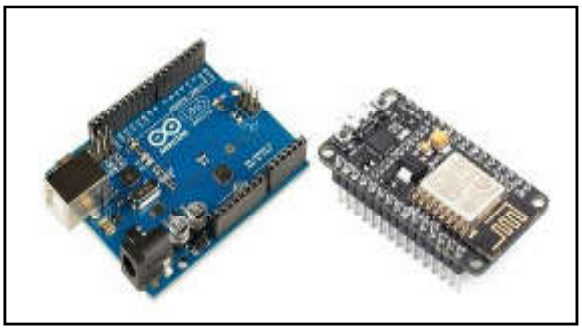

Fig.3 Microcontroller unit

5.3 Organic Light Emitting Diode (OLED)

It is a film formed of organic compounds that, in reaction to an electric current, emits light. Between two electrodes, one of which is transparent, is this layer. OLEDs are used to create digital displays for gadgets like televisions, computer monitors, and portable systems like smartphones, among other things. A layer of organic materials is typically sandwiched between two electrodes—the cathode and anode—and placed on a substrate to form the OLED, as shown in. Because of the pi electrons' subsequent delocalization as a result of conjugation over the molecules, organic molecules are conductive.

5.4 Sound Detection Sensor

Andrew S. Tanenbaum created the MIC-1 processor design as a straightforward yet comprehensive model

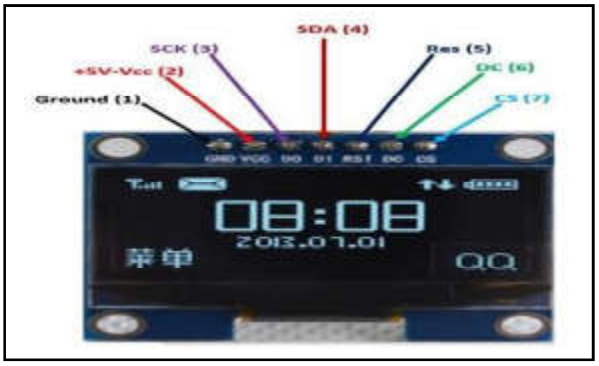

Fig.4 Organic Light Emitting Diode

for his instructional book Structured Computer Organization. A very basic control unit that executes microcode from a 512-word storage makes up the system. The Java Virtual Machine (JVM) interpreter source code may be obtained in the book. The Micro-Assembly Language (MAL) is designed to make developing a JVM interpreter simple.

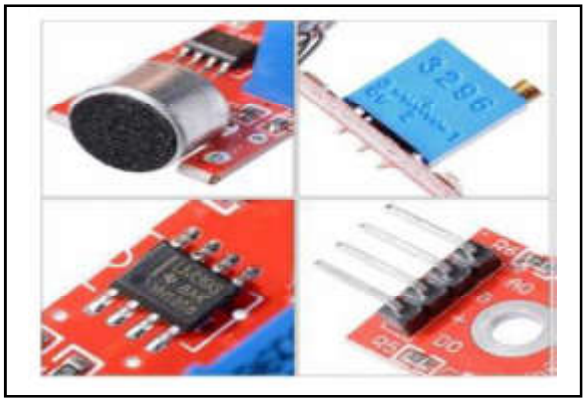

Fig.5 Sound Detection Sensor

5.5 Temperature and Humidity Sensor

A composite sensor, the DHT11 digital temperature and humidity sensor generates calibrated digital signals for both temperature and humidity. The technology of a dedicated digital modules collecting as well as the temperature and humidity sensor technology gives the device excellent dependability and superb long-term stability. The sensor comprises a resistive feel of wet component, a Negative Temperature component, and is connected to a high-performance 8-bit microcontroller.

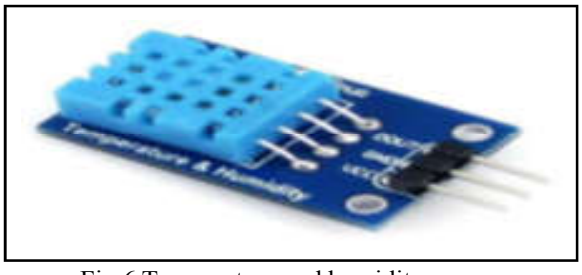

Fig.6 Temperature and humidity sensor

5.6 Peristaltic Pump

The term "peristaltic pump," sometimes known as a "roller pump," refers to a positive displacement pump that is used to pump a range of fluids. The fluid is housed in a flexible tube that is placed around the outside of the pump casing. Despite the development of linear peristaltic pumps, the majority of peristaltic pumps work in a circular motion. The flexible tube is compressed while the rotor rotates by several "wipers" or "rollers" that are attached to its outside circumference. When the compressed portion of the tube closes, the fluid must pass through the tube. Moreover, extra fluid is sucked into the tube when it returns to its original state after the rollers pass. Peristalsis is a process that occurs in many biological systems, including the gastrointestinal tract. The tube will often be compressed by two or more rollers, trapping a body of fluid in the space between them. The fluid is moved through the tube and out of the pump through the outlet. Peristaltic pumps can be indexed through partial revolutions to deliver lesser volumes of fluid or they can run continuously. Positive displacement pumps are capable of moving a range of fluids. This pump costs less to repair because it lacks valves, seals, and glands. Every peristaltic pump has a flexible hose or tube that creates an open flow path with a high resistance to abrasion and allows the movement of solids and viscous materials with ease.

The three-roller liquid peristaltic pump shown in Figure 7 uses this Kamoer 12V 540ml/min Silicon Tube brush motor. When pumping liquids when no direct contact with the liquid is necessary, the brand-new series of peristaltic pumps from Kamoer offers an easy option. Unlike other pumps, the KHM series pumps have a choice between a stepper motor and a 12 v DC brushed motor as their base motor. Instead of immediately impelling a silicone tube, these motors crush it, avoiding direct contact with the liquid in the process. A 12 V DC input is required for this pump, which has a maximum flow rate of 540 ml per minute.

Fig.7 Peristaltic pump

5.7 L298 Integrated Circuit

The 15-lead Milliwatt and PowerSO20 packages for the L298 are integrated monolithic circuits. It is a twin full-bridge driver with a high voltage and high current rating that can drive inductive loads including relays, solenoids, DC motors, and stepping motors and accept conventional TTL logic levels. A high-power motor driver module, the L298N Motor Driver Module can be used to operate both DC and stepper motors. A 78M05 5V regulator and an L298 motor driver IC make up this module. Up to 4 DC motors or 2 DC motors with directional and speed control can be controlled by the L298N Module..

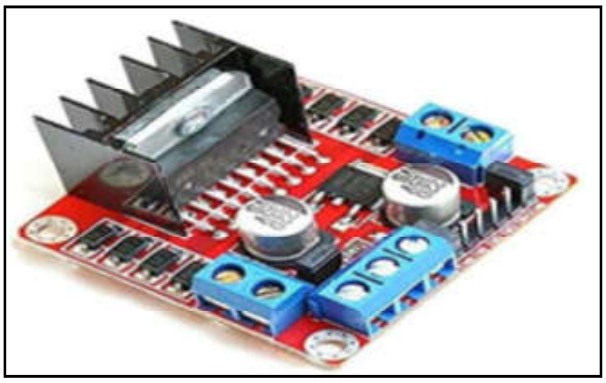

Fig.8 L298 Integrated circuit

5.8 Buzzer

As seen in Figure 9, an auditory signaling device like a buzzer or beeper could be electromechanical, piezoelectric, or mechanical. The signal is converted from audio to sound as its primary function. It is often powered by DC voltage and used in timers, alarm clocks, printers, computers, and other electronic devices. It can produce a variety of sounds, including alarm, music, bell, and siren, according on the varied designs.

Fig.9 Buzzer

5.8 Turbidity Sensor

The bubbles which are formed in the flow of IV are detected easily through this way in the sensor ,it works under the phenomena of turbidity in which it can be easily discovered and the result is shown in Binary forms (0,1). When the number is 0 then the flow is not interrupted when the value turns to 0 then the bubbles are detected. Turbidity is defined as the reduction of transparency of a liquid caused by the presence of undissolved suspended matter [1]. The origin of the particles found in seawater can be mineral (such as clay and silts) or organic (such as particulate organic matter or living organisms like plankton). Turbidity is not, however, a direct measure of suspended particles in water, but a measure of the scattering effect such particles have on light.

Fig.10 Turbidity Sensor

6. SOFTWARE REQUIREMENTS

Open-source prototyping platform Arduino is built on simple hardware and software. It is made up of a circuit board that can be programmed (known as a microcontroller) and ready-made software called the Arduino IDE that is used to develop and upload computer code to the actual board. The micro-features controller's are separated into a more usable container by Arduino's standard form factor. Arduino boards have the ability to read analog or digital input signals from a variety of sensors and convert them into an output, such as starting or stopping a motor, turning an LED on or off, connecting to the cloud, and many more operations. Via the Arduino IDE, you can use a series of instructions to direct the actions of your board's microcontroller (referred to as uploading software). Arduino does not require an additional piece of hardware (referred to as a programmer) in order to load fresh code onto the board, in contrast to earlier programmable circuit boards. Only a USB cable will do. Moreover, the Arduino IDE employs a condensed form of C++, which makes learning to program simpler. The functions of the micro-controller are finally broken down into a more approachable packaging by Arduino's standard physical factor. According to the different microcontrollers utilized, various types of Arduino boards are available. Although they are all programmed using the Arduino IDE, Arduino boards all share a similar trait. The distinctions are based on the quantity of inputs and outputs (the number of sensors, Lights, and buttons you may utilize on a single board), speed, operating voltage, form factor, etc. Some boards have no hardware programming interfaces because they are intended to be embedded, thus you would need to purchase them separately. A 3.7V battery can power some while a 5V power source is required for others.

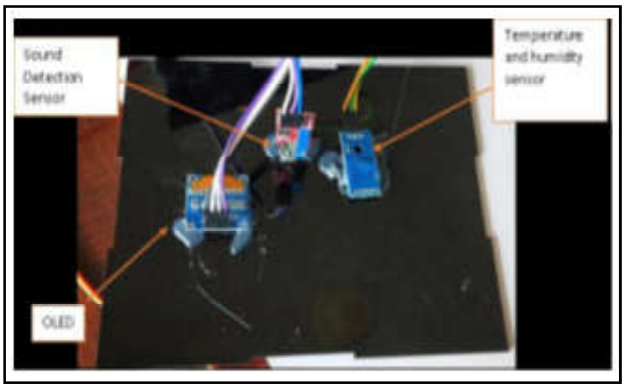

Fig.11 Front panel of the system

Fig.12 The hardware portion

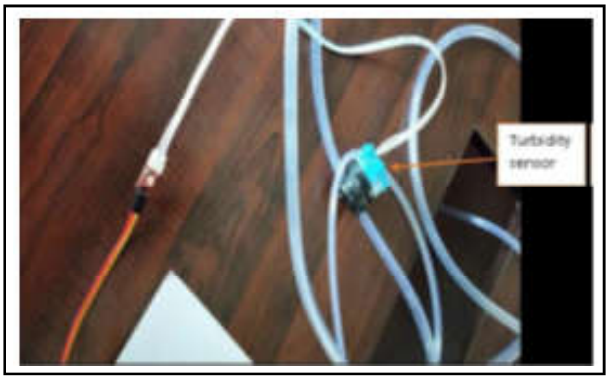

Fig.13 Turbidity Sensor or Bubble Detecting Sensor

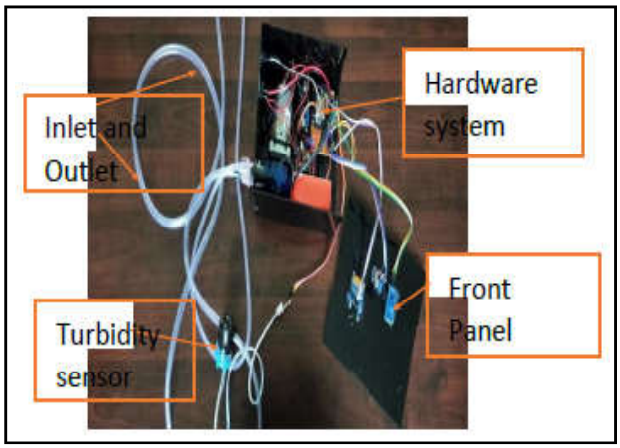

Fig.14 IoT based Infusion Pump

REFERENCES

[1] Sakthivel Sankaran, J. Deny and M.Pallikonda Rajasekaran, "Designed and Developed a Low Cost, Smart Infusion Pump to Deliver IV for Patients using LabVIEW Interface with Arduino", PMC Article, 10.12968/bjon.2004.17.10.29476, Vol.27, 2004, pp.54-67.

[2] Luiz Eduardo Galvao Martins, Hanniere de Faria, Lucas Vechete and Tatiana sousa Cunha, "Develop a Low-Cost Insulin Infusion Pump for the Treatment of Diabetes", PMC Article, 10.12968/bjon.2004.17.10.29476, Vol.21, 2004, pp.102-114.

[3] Isabella. L. Grassetti, Isabella. L. Curran, Anita. M. Petrilli and James O'Brien, "Discussed that Infusion Pumps Exposed To Radiation Must Be Protected From the X-Rays", International Journal of Engineering and Advanced Technology (IJEAT) , 10.35940/ijeat.A1137.1291S419, Vol.9, No.1S4, 2018.

[4] Jenifer Biltoft and Lonnie Finneman, "Discussed about Implementing a Smart Electronic Pump That Health Condition of the Patient around the Particular Region", AMJ Health-System Pharmaceutical, 10.2146/ajhp161058, Vol.75, pp.14, 2019.

[5] E. Moret, E. Muntane and P.Ricart Andreu, "Analyzed The Situation of Infusion Pumps at the Hospital for Continuous Monitoring Of Drug to Reduce the Medical Errors", AMJ Health-System Pharmaceutical, 10.2146/ajhp161058, Vol.7, 2016, pp.34.

[6] Karen. K. Giuliano, Daleen Penoyer, Rebecca. S. Mahuren and Melody Bennett, "Discussed that before the Introduction of the Infusion Pumps the Rate of Infusion were Calculated Manually", PMC Article, 10.1097/01.NAJ.0000767808.75464.c3, Vol.16, 2006, pp.56-64.

[7] M. Deepalakshmi and Dr.R.Jayaparvathy "Proposed Small Size and Cost-Efficient Integrated Infusion Pump System", AMJ Health-System Pharmaceutical, 10.2146/ajhp161058, Vol.22, 2015, pp.64.

[8] Frank Doesburg and Maarten. W. Nilsen, "Estimated the Advantages of Adding the Bedside Central that Controls all the IV Infusion Pumps", PMC Article, National Library of Medicine, 0.1371/journal.pone.0183104, Vol.18, 2020, pp.132-141.

[9] Jeffrey M. Rothschild, Noah syroid, "Performed a Time-Series Trial and Compared the Rate of Error and Found That, the Errors and the Time Delay Can Be Solved By Using Smart Pumps", PMC Article, 10.1097/01.ccm.0000155912.73313.cd, Vol.21, 2007, pp.160-179.

[10] Thorunn Oskarsdottir, David Harris and Adam Sutherland, "Discussed about the Usage of Intravenous Infusions Paediatric and Neonatal Units", AMJ Health-System Pharmaceutical, 10.2146/ajhp, Vol.14, 2021, pp.168-177.

[11] Brian J. Anderson, James D. Morse, Luis Ignacio Cortinez, "The Total Intravenous Anesthesia to Implement Along With the Pumps", Pediatric Anesthesia, Wiley Online Library, https://doi.org/10.1111/j.1460-9592.2009.03072.x, Vol.20, 2021, pp.223-232.

[12] Linda J Murdouch and Victoria. L. Cameron "Discussed About The Serious Risk Factors Being Faced In the Intensive Care Units", PMC Article, 10.12968/bjon.2006.17.10.29476, Vol.13, 2007, pp.141-156.

[13] Karen Wilson and Mark Sullivan, "Focused in Identifying the Areas That Causes Harmful To the Patients And Prevent the Medication Errors", PMC Article, 10.1093/ajhp/61.2.177, Vol.15, 2017, pp.112-122.

[14] Pascale Carayon and Ann scoofs Hundt "Discussed about Implementation of Smart Intravenous Infusion Pump to Reduce the Medication Administration Errors", PMC Article, 10.12968/bjon.2014.17.10.29476, Vol.34, 2014, pp.129-142.

[15] Mark H. Myers , Yaqin Li and Francine kivlehan, "Discussed about the Automatic Drug Delivery Method with a Computer-Aided Control for Propofol Delivery in Total Intravenous Anesthesia", PMC Article, 10.12968/bjon.2014.17.10.29476, Vol.19, 2014, pp. 67-81.

A REVIEW OF RADIOLOGICAL IMAGES WITH MACHINE LEARNING MODELS FOR THE DETECTION AND PREDICTION OF COVID-19

P. Nithin[1], V. Murugan[2] and G. Murugeshwari[3]
[1]Department of Articifical Intelligence and Machine Learning
Bannari Amman Insitute of Technology, Sathyamangalam - 638 401, Erode District, Tamil Nadu
[2]Department of Computer Science, Government Arts And Science College, Kadayanallur - 627 751, Tamil Nadu
[3]Department of Computer Science and Engineering, MS University, Tirunelveli - 627 012, Tamil Nadu
E-mail:ithinp@bitsathy.ac.in,smv,gmurugeswari@msuniv.ac.in

Abstract

In the field of science, the scope of advancement paves to diagnosing accurately. The lives and circumstances of people around the world are getting worse as COVID-19 instances rise daily. The purpose of this study is to detect disease and then use machine learning techniques to assess whether a person has a virus or another common condition. This article describes the diagnosing COVID 19 using efficient radiology images (CT scan) with help of multiple review articles. With COVID-19 anyone can be affected and become seriously ill or die at any age. Diagnosing it at early stage can be life saving more over it helps to treat the affected person effectively. Importance of review articles is rising to find out the best source available in the contemporary area of study. Supervised machine classification is an important tool used for extracting quantitative information. Unsupervised machine learning has the advantage of being able to make use of data that has not been labelled. The way in which people "learn" in their everyday lives is directly imitated by reinforcement machine learning. The goal of this comparison is to determine which model is the best successful in identifying and forecasting illness. According to the findings of the majority of investigations, researchers have concluded that supervised learning technique provides more accurate predictions of the outcomes. During supervised learning, this method of converting inputs into derived outputs is performed by using a set of factors and algorithms that are created from beginning. This will also assist us in applying experience to optimize performance requirements. Recent research indicates that categorization models are superior to other models in terms of accuracy.

Keywords: *COVID-19, radiological images, machine learning, CT scan, Detection and Prediction.*

1. INTRODUCTION

The continuous pandemic of the COVID-19 diseases caused by the Coronavirus has resulted in a crisis in health care all across the world in 2019-2020. In this pandemic condition, the most difficult problem is figuring out how to diagnose COVID-19 patients. COVID-19, also known as the coronavirus, is a virus that causes the infectious illness known as the acute respiratory syndrome COVID-19 (SARS-COV2)[1]. The first case of the coronavirus illness was discovered in Dec 2019 in Wuhan, China, and since then it has spread around the globe. The case of the patient suffering from pneumonia with an undetermined aetiology was reported for the first time to the WHO headquarters in China in Dec of 2019. By the end of Dec 2019, the illness has already infected every single country on the planet. The illness quickly spread across the area, and the number of reported cases increased. After then, the WHO announced that it is a pandemic. As of the 20th of November, there had been a total of 61308116 instances of the Coronavirus, 1437835 fatalities, and 42395359 individuals who had recovered. The number is continuing to increase all over the globe where there were[2].

Despite the fact that radiological screening is not indicated for diagnostic purposes as soon as the patient enters the clinic, it may be performed. The image from the chest X-ray is helpful for observing the effects of therapy as well as comorbidities in very unwell individuals. The diagnosis of coronavirus from a chest X-ray and its distinction from lung illness with indistinguishable opacification is a perplexing function that depends on the availability of specialist radiologists to perform[3].

Under the cell membrane is where all of the necessary components for the formation of a new virus come together. Therefore, the most recent viral production begins near the membrane of the cell. The various sections of each lung are referred to as lobes. In most cases, during normal breathing, air travels unimpeded down the trachea. The trachea is divided into three primary sections: the first is a big tube known as the bronchus, the second is a series of smaller tubes known as the bronchioles, and the last section is comprised of alveoli. The alveoli and air passages of the trachea are both flexible and polymorphic in nature. When you breathe in, each air sac expands like a little balloon; when you exhale, the sacs contract and lose their inflated state. On both sides, the alveoli are surrounded by capillaries, which are tiny blood veins that provide oxygen and nutrients to the cells that make up the lungs. Figure 1 depicts the concept of machine learning in its entirety.

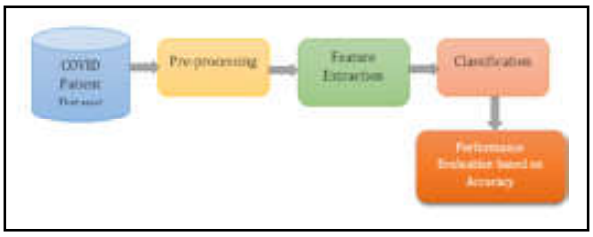

Fig. 1. The Process of Machine Learning

The proper identification of COVID-19 has the potential to lessen the strain placed on the medical and healthcare system. Some models of prediction integrate a number of factors in order to make an estimate. These factors may include computer tomography (CT) scanning, clinical symptoms, lab testing, and the combination of these factors. The data that was given by kaggle.com was used to train this model. As a result, this approach is applicable on a worldwide scale for the purpose of efficient screening and the prioritising of tests for the virus in the general population. It is possible to utilise the images obtained from CT scans and X-ray scans as an alternative way for detecting people who are impacted by Covid-19. We have investigated the usage of deep learning algorithms for COVID-19 identification using radiological images and presented our findings.

2. RELATED WORKS

For a very long time, algorithms for ML have been used in a variety of applications that need the identification of potentially harmful risk factors. Using ML modelling, the authors of this study show that it is feasible to forecast the number of persons who are influenced by a COVID-19 like a potential danger to human beings. The results of this analysis indicated that the risk factors connected to COVID-19 included exponentially smoothness (ES).

Screening for SARS-CoV-2 in an efficient manner not only makes a rapid and precise diagnosis of COVID-19 possible, but it also lessens the load placed upon healthcare systems. There have been attempts to develop prediction models that estimate the likelihood of infection by incorporating a variety of criteria . These are meant to aid medical staff worldwide in the procedure of triaging patients, which is especially crucial considering the available resources in the healthcare industry.

With the use of CT chests radiomic features, the objective is to build a two-step ML conceptual system that can diagnose and predict the existence of lungs in COVID-19 as well as non-COVID-19 bronchitis patients. This system would use CT chest radiomic characteristics. When complicated medical datasets are analysed using machine learning, health care professionals are presented with significant chances to design a COVID-19 diagnosis system that is both straightforward and very effective. This research article's objective is to derive risk variables from medical studies of early COVID-19 infected individuals using four different classical machine learning algorithms. The publication can be found here[4].

The condition is diagnosed with the use of an RT-PCR kit, which stands for real-time reverse transcriptase-polymerase chain reaction. Because there are not enough kits available, questionable individuals cannot be treated immediately, which results in the spread of illness [5]. In order to come up with an alternative, radiologists studied at the developments that have been made in radiological imaging, such as CT scans, which give detailed and high-quality photographs of the body.

In order to halt the progression of this pandemic and provide prompt care to those who have been afflicted, it is of the utmost importance to identify positive cases as soon as they are discovered. Because there are currently no accurate and automatic toolkits on the market, there has been an upsurge in the need for supplementary diagnostic tools [6]. Recent research that made use of radiology imaging methods has led researchers to the conclusion that photographs of this kind may convey important data about the COVID-19 virus.

An automatic DL-based classification model based on a CNN is presented in the research article [7]. For COVID-19, this model has a high detection rate. The training dataset includes 3,616 COVID-19 lung X-ray images as well as 10,192 normal chest X-ray images that were subsequently enhanced. Through using dataset, eleven different pre-existing CNN models were employed to establish the early assessment of COVID-19 symptoms. MobileNetV2 demonstrated a level of potential that qualified it to be considered for further development.

To examine the possibilities of ML approaches for diagnosing COVID-19 cases based on X-ray data, with the aim of assessing the usefulness of such techniques and putting them to use [8]. Due to the fast spread of the illness [9], one of the most significant difficulties that is now being faced all over the globe is the diagnosis. There have been over 1.6 million confirmed instances of COVID-19, which indicates that the illness is rapidly spreading across the globe to a growing number of nations. Recent figures suggest that the number of individuals who have been identified with COVID-19 is expanding at an exponential rate.

As a result, there is an immediate need for rapid identification with clear visibility of the infection, which is necessary in order to provide a means by which a patient who may be infected with COVID-19 may be spared. In light of recent developments in technology [10], the combination of DL classifiers and MRI scans yields more encouraging results that are comparable to those obtained from conventional RT-PCR testing, all while achieving a higher level of precision in the detection and prediction of COVID-19 cases.

The burden that is being put on healthcare systems may be alleviated if the early diagnosis of this kind of virus can be achieved [11]. X-rays of the chest have become an increasingly important part of the diagnostic process for lung disorders including pneumonia. This imaging method may be used to provide a diagnosis of COVID-19, which is due to the fact that it is a kind of influenza.

The researchers are making consistent attempts to find the potential remedies that may be used to bring this pandemic under control in their different regions [12], which is one of the techniques that is both widely used and very successful. Whereas RT-PCR has been the most reliable test for diagnosing COVID-19 illness, this is also the least time-consuming, needs specialised facilities, and has a reagent scarcity. Alternatively, the bulk of past research [13] has focused on chest CT pictures and x Rays images using deep-learning algorithms.

The goal of this work [14] is to build a CNN model called 'COVID-Screen-Net' for multi-class classification of chest X-ray pictures into 3 types: COVID-19, streptococcus illness, or normal. The timely detection and isolation of people who are infected is a critical component in reducing the rate at which the virus is spreading [15]. Due of the pandemic, supplies of the reverse transcription reaction technique, which is the conventional method for identifying COVID-19, are in low supply and require a significant amount of time.

In this research [16], This comparison research was done to guarantee that machine learning algorithms accurately predict and identify infected individuals. In this aspect, supervised learning algorithms are more effective than other algorithms. This study aims to show the accuracy of this prognosis in putting an end to the present pandemic. The diagnosis of illnesses makes substantial use of supervised ML in particular. Compared to previous methods, this machine learning approach yields dependable results. To properly predict and identify Coronavirus illness, the researchers trained and evaluated a large number of models, such as linear regression, naive Bayes classifier, SVM, decision tree, and ResNet50, among others.

Deep learning and transfer learning are the two types of learning approaches that are used in this study [17] to construct accurate, generic, and resilient models for identifying COVID-19. In order to take use of the full potential of the produced models, either CNN or transfer-learning models are used, or alternatively among the scientific community in the use of imaging biomarkers for the purpose of enhancing COVID-19 identification and treatment [18]. Exploratory techniques such as AI-based models might give a thorough understanding of the fundamental pathophysiological processes and assist explain the complicated biological systems.

3. DISCUSSION

The persistence of this research is to determine which methods of ML are the most reliable when it comes to diagnosing and predicting disease. The whole planet is now facing a precarious situation as a result of COVID-

19. During the course of the epidemic, further research has been conducted in order to correctly and promptly identifies persons who are infectious. This comparative table 1, which was derived from that research, demonstrates the significance of supervised learning when it comes to generating predictions based on clinical features, symptoms and chest X-rays. Some researchers have utilized a wide variety of classification models and algorithms, including such shallow single-layer perceptron neural networks, Bayes Net, multinomial Naive Bayes classifiers, logistic, Gaussian process regression, SVM, J48 and so on.

Table 1 Comparative Analysis of Algorithm

Study	Algorithm & Methods	Accuracy (%)
Mojjada et al., (2020)	LASSO, Exponential Smoothing	83
Zoabi et al., (2021)	Baseline Model, SHapley Additive exPlanations (SHAP)	95
Khaniabadi et al., (2022)	NB, SVM, Bagging, RF, KNN, Decision Tree and Ensemble Meta voting	93
Sun et al., (2020)	LR, SVM, PR, DNN	-
Kogilavani et al., (2022)	VGG16 DenseNet121 MobileNet NASNet Xception EfficientNet	VGG16 -97.68%, DenseNet121 - 97.53%, MobileNet - 96.38%, NASNet - 89.51%, Xception - 92.47%, EfficientNet - 80.19%,
Ozturk et al., (2020)	DarkCovidNet	87
Akter et al., (2021)	MobileNetV2	MobileNetV2 - 98 %
Bustos et al., (2022)	Hyper-parameter optimization	90
Alazab et al., (2020)	Deep CNN	94
Panwar et al., (2020)	deep transfer learning algorithm	95
Kumar et al., (2020)	XGBoost predictive classifiers	97
Gupta et al., (2020)	deep transfer learning algorithm	95
Ardaci et al., (2021)	nCOVnet	84
Dhaka et al., (2021)	silver bullet test	86
Luz et al., (2022)	Reverse transcription polymerase chain reaction method	89
Bhardwaj et al., (2021)	ML-based supervised algorithms	93
Qaid et al., (2021)	Novel machine-learning approach	82
Bouchareb et al., (2020)	explicit radiomics	-

Some researchers used CNN, RNN, and regression in their analyses. Others used a combination of the two. The results of all of the tests and studies have shown that the use of supervised learning methodologies alone is sufficient to provide results that are of a higher accuracy. The data shown in the table above might be valuable in the development of a dependable algorithm for determining whether or not individuals are infected with the Corona virus. It delivers outcomes that are greater in accuracy and more specific than those produced by regression and convolutional neural networks. In addition, the findings of this research might be used to the development of a whole new algorithm for properly diagnosing this life-threatening illness. It is possible that the study will be fruitful if we concentrate on developing an original categorization model.

4. CONCLUSION

This comparison research was carried out in order to confirm that ML models are successful in predicting and detecting infected persons. In this aspect, the efficiency of algorithms designed for supervised learning is superior to that of other algorithms. This study aims to illustrate how accurate this prognosis will be in bringing an end to the present pandemic so that we may finally put a stop to it. In the area of illness diagnosis, the use of ML has shown promising results, with enhanced specificity and accuracy. This conclusion may be drawn from the findings. In particular, the process of illness detection takes heavy use of supervised machine learning. The researchers accurately predicted and detected Coronavirus illness by training and testing the data set with a wide variety of models, such as ResNet50, naive Bayes classifier, linear regression and Decision tree and support vector machine, amongst others. These models were utilised to predict as well as identify the sickness properly. This research will be developed in order to develop a unique tool for early illness detection, namely COVID-19, based on supervised ML models.

REFERENCES

[1] R.K.Mojjada, A.Yadav, A.V.Prabhu and Y.Natarajan, "Machine Learning Models for Covid-19 Future Forecasting", Materials Today: Proceedings, 2020.

[2] Y. Zoabi, S. Deri-Rozov and N.Shomron, "Machine Learning-based Prediction of COVID-19 Diagnosis based on Symptoms", npj Digital Medicine, Vol.4, No.1, 2021, pp.1-5.

[3] P. M. Khaniabadi, Y. Bouchareb, H. Al-Dhuhli, I. Shiri, F. Al-Kindi, B.M.Khaniabadi and A. Rahmim, "Two-step machine learning to diagnose and predict involvement of lungs in COVID-19 and pneumonia using CT radiomics. Computers in Biology and Medicine, Vol.150, 2022, pp. 106165.

[4] N.N. Sun, Y.Yang, L.L. Tang, Y.N. Dai, H.N.Gao, H.Y. Pan, and B.Ju, "A Prediction Model Based On Machine Learning For Diagnosing the Early COVID-19 Patients. MedRxiv, 2020.

[5] S.V. Kogilavani, J. Prabhu, R. Sandhiya, M.S. Kumar, U. Subramaniam, A. Karthick and S.B.S. Imam, "COVID-19 Detection based on Lung CT Scan Using Deep Learning Techniques", Computational and Mathematical Methods in Medicine, 2022.

[6] T. Ozturk, M. Talo, E. A.Yildirim, U.B. Baloglu, O. Yildirim and U.R. Acharya, "Automated Detection of COVID-19 Cases using Deep Neural Networks with X-ray Images", Computers in Biology and Medicine, Vol.121, 2020, pp.103792.

[7] S. Akter, F.J.M. Shamrat, S.Chakraborty, A.Karim and S.Azam, "COVID-19 detection using deep learning algorithm on chest X-ray images. Biology, Vol.10, No.11, 2021, pp.1174.

[8] N.Bustos, M.Tello, G. Droppelmann, N. Garcна, F. Feijoo and V.Leiva, "Machine Learning Techniques as an Eыcient Alternative Diagnostic Tool for COVID-19 cases, 2022.

[9] M. Alazab, A. Awajan, A.Mesleh, A.Abraham,V.Jatana and S.Alhyari, "COVID-19 Prediction and Detection Using Deep Learning", International Journal of Computer Information Systems and Industrial Management Applications, 12th June), 2020, pp.168-181.

[10] H. Panwar, P.K.Gupta, M.K. Siddiqui, R.Morales-Menendez, P.Bhardwaj and V. Singh, "A Deep Learning and Grad-CAM based Color Visualization Approach for Fast Detection of COVID-19 cases Using Chest X-ray and CT-Scan Images", Chaos, Solitons & Fractals, Vol.140, 2020, pp.110190.

[11] R. Kumar, R. Arora, V. Bansal, V. J.Sahayasheela, H.Buckchash, J. Imran and B. Raman, "Accurate Prediction of COVID-19 using Chest X-ray Images through Deep Feature Learning Model with SMOTE and Machine Learning Classifiers", MedRxiv, 2020.

[12] H. Panwar, P.K.Gupta, M.K. Siddiqui, R.Morales-Menendez and V. Singh, "Application of Deep Learning for Fast Detection of COVID-19 in X-Rays using nCOVnet. Chaos, Solitons & Fractals, Vol.138, 2020, pp.109944.

[13] I. Arpaci, S. Huang, M. Al-Emran, M.N.Al-Kabi and M. Peng, "Predicting the COVID-19 Infection with Fourteen Clinical Features Using Machine Learning Classification Algorithms", Multimedia Tools and Applications, Vol.80, No.8, 2021, pp.11943-11957.

[14] V.S. Dhaka, G. Rani, M.G. Oza, T. Sharma and A.Misra, "A Deep Learning Model for Mass Screening of COVID 19", International Journal of Imaging Systems and Technology, Vol.31, No.2, 2021, pp.483-498.

[15] E. Luz, P. Silva, R. Silva, L.Silva, J.Guimarres, G. Miozzo and D. Menotti, "Towards an Effective and Efficient Deep Learning Model for COVID-19 Patterns Detection in X-ray Images", Research on Biomedical Engineering, Vol.38, No.1, 2022, pp.149-162.

[16] P.Bhardwaj and A.Kaur, "A Novel and Efficient Deep Learning Approach for COVID 19 Detection using X ray Imaging Modality", International Journal of Imaging Systems and Technology, Vol.31, No.4, 2021.

[17] T.S. Qaid, H. Mazaar, M.Y.H. Al-Shamri, M.S. Alqahtani, A.A. Raweh and W. Alakwaa, "Hybrid Deep-learning and Machine-learning Models for Predicting COVID-19", Computational Intelligence and Neuroscience, 2021.

[18] Y. Bouchareb, P.M.Khaniabadi, F.Al Kindi, H. Al Dhuhli, I. Shiri, H.Zaidi and A.Rahmim, "Artificial Intelligence-driven Assessment of radiological Images for COVID-19", Computers in Biology and Medicine, Vol.136, 2021, pp.104665.

A COMPREHENSIVE ANALYSIS OF THE RETURN ON EQUITY FOR SELECTED FMCG COMPANIES USING DUPONT FRAMEWORK

S.Nagarajan and S.Murugappan
Department of School of Management Studies (SMS)
Bannari Amman Institute of Technology, Sathyamangalam - 638 401, Erode District, Tamil Nadu

Abstract

Profitability alone does not determine a company's efficiency. There are also more ways to assess its effectiveness. The purpose of this study is to assess the firm's competency using one such measure, i.e the Return on Equity (ROE) of chosen FMCG companies that belongs to the top 5 in Market Capitalization. It is done by taking into account the numerous elements that influence the Return on Equity. The research is descriptive and is carried out with the assistance of secondary data gathered from reliable websites. The information gathered comes from the income statements and balance sheets of selected FMCG firms. The research makes use of the Five-factor DuPont Model, which includes Financial leverage, Asset Turnover Ratio, Tax Burden, Interest Burden, and Operating Profit Margin. These tools analyze the financial performance of chosen FMCG firms (Hindustan Unilever Limited, Nestle India Limited) over 10 years. The regression analysis is used to understand the relative influence of the five measures on the ROE of the chosen companies.

Keywords: *DuPont Model, FMCG, Return on Equity, Ratio's*

1. INTRODUCTION

Financial decisions and managerial decisions are crucial for every organization to run its business effectively[1]. Under this financial analysis plays a major role in analyzing the past performance of the company, evaluating the present scenario of the company, and forecasting the future performance of the company with the help of financial documents such as Income statements and Balance sheets. Both reveal the true and fair financial position of the company[2]. Other than these two statements the stakeholders have required to make further analysis of the company to make prompt decisions. This study has been particularly made for the top 5 FMCG companies by market capitalization in NSE by attempting the Dupont Framework by analyzing the financial statements[3]. The companies such as Hindustan Unilever Limited, Nestle India Limited, Dabur India Limited, Britannia Industries Limited, and Godrej Consumer Products Limited[4].

1.1 Objectives

- To analyze the ROE for selected FMCG companies using the DuPont framework.
- To establish the strength of ROE by developing the regression equation based on ROE factors
- To know whether the FMCG companies can generate positive ROE for shareholders based on secondary data collected.

1.2 Scope of the Study

- The study comprehends ROE disintegration with the help of DuPont Analysis to assess the financial performance of the selected FMCG companies.
- The study is done with the help of secondary financial data of selected FMCG companies for 10 years from 2012 to 2021.
- The selection of these 2 companies for the study is strictly based on the availability of required data for the past 10 years.
- Further, the selection of 2 companies for the study is strictly based on their highest market capitalization and financial data availability for the past decade.

2. REVIEW OF LITERATURE

Review of Literature refers to the study of journals, articles, or any other sources pertinent to a particular area of research. By conducting this review, we can get a depiction, summary, and also critical assessment concerning the research problem being explored. It provides a synopsis of the sources we have collected

while exploring a particular topic. It helps in ascertaining new ways to interpret former research. It also assists in pinpointing our research within the framework of prevailing research. It is an inscribed summary of major works and other sources on a designated topic, especially to DuPont analysis.

In their analysis, they looked at HDFC's financial performance in India. They gathered data from the firm for over ten years for their investigation[5]. They also looked at the relationship between several performance indicators that influence HDFC's financial success. The housing sector performed best in the economy, with more home loans due to lower interest rates, which may be the cause for the biggest asset turnover, according to this study. It also claims that HDFC's financial performance is pretty consistent and that nominal volatility in the ROE is replicated[6]. In addition, during the past ten years, the Net Profit Margin has shown qualified consistency. According to the study, this was attributable to the company's adoption of a cost strategy while interest rates were rising and a perceived distinctiveness approach when interest rates were falling.

With the aid of DuPont analysis, examined the financial soundness of the Nepal Electricity Authority in his study. The researcher looked at the NEA's yearly reports from 2012 to 2019 for this purpose[7]. In his investigation, the researcher used both descriptive and analytical methods. The findings show that despite being a unique purveyor in the country, the firm's financial performance in the first five years was dismal. However, during the next two years, it has improved[8]. The reason for the negative ROE in the first five years is that the NPM(Net Profit Margin), which is one of the essential important indicators of ROE, is negative. According to the study, the company has also been exposed to a significant level of financial risk in terms of equity multiplier[9]. However, both the NPM and the EM have improved in the last 2 years of research.

With the help of DuPont Analysis, examined the Insurance Sector in the South Asian Region in their study. The researchers looked at the insurance sectors of nations in the South Asian area, including India, Pakistan, Bangladesh, and Sri Lanka[10]. The primary goal of this research is to see if investors prefer high-profit firms or not. They employed two approaches to do this. The first is based on Net Income, which is an effective technique, while the second is based on DuPont analysis, which is an effort method[11]. When compared to the effort approach, the outcome demonstrates that the effect technique falls short. As a result, investors utilize the DuPont technique to rate companies proficiently. As a result, it recommends that investors should choose the effort technique over the impact way.

3. RESEARCH METHODOLOGY

3.1 Research Design

According to the findings of the Review of Literature, extensive research has already been undertaken in the chosen subject of study, in many sectors of the business, under a range of economic circumstances. However, the research gap shows that only a little research has been conducted in recent years in the FMCG industry in the Indian context. Furthermore, given the descriptive nature of the prior researchers' research works in similar DuPont model studies, it is decided to use a Descriptive Research methodology in the research work titled "A Comprehensive Analysis of the Return on Equity (ROE) for selected FMCG Companies Using DuPont Framework[12]."

Descriptive Research designates a population, situation, or phenomenon in an organized and precise fashion. It aims to answer what, when, where, and how questions only and not the why question. It is used when the researcher wants to detect features, frequencies, trends, and classifications[13]. It does not influence the variables, instead only discerns and measures it

In the business scenario, "Descriptive statistics give a useful overview of a variety of data kinds." For example, brokers and investors may utilize a historical(past) account of return behavior to make efficient investment decisions in the upcoming years by undertaking analytical and empirical investigations on their assets."

3.2 Data Type and Sources

Secondary financial data is used in this research project. Income statements and Balance sheets of selected FMCG companies from 2012 to 2021. Secondary data are data that was obtained by an earlier researcher and then used by another researcher in his study. This secondary dependability is determined by the extent and correctness of the initial study collected by the preceding researcher[14].

Secondary financial data for the current study was gathered from reputable websites such as Screener, Money Control, and the official company's websites. The research design, sample size, sampling techniques, and sample frame involved are not appropriate for this research method due to the secondary data employed.

3.3 Tools of Analysis

The primary tool used in the study includes the Five-Factor DuPont model of ROE extraction. Multiple Linear Regression analysis, and Correlation Analysis. All of these assessments are accomplished with the help of the Microsoft Excel application and SPSS Software.

DUPONT MODEL FORMULA

DuPont Analysis (3 Factor) ROE = Net Profit Margin * Asset Turnover * Financial Leverage
Net Profit Margin = Tax Burden * Interest Burden * Operating Profit Margin

Dupont Analysis (5 Factor) ROE = Tax Burden * Interest Burden * Operating Profit Margin * Asset Turnover * Financial Leverage
Dupont Analysis (5 Factor) ROE = (Net Income/ EBT) * (EBT/EBIT) * (EBIT/Sales) * (Sales/ Assets) * (Total Assets/Shareholders Equity)
ROE = Net Income / Equity
Net Profit Margin: It is a measure of profitability. It is obtained as a percentage of net profit concerning sales.
Net Profit Margin = Net Profit / Revenue * 100
Asset Turnover Ratio (ATO): It is used to describe the company's efficiency in using its assets to generate revenue. It is obtained by dividing the company's revenue by its assets.
Asset Turnover Ratio = Sales/Total Assets
Financial Leverage (FL): It refers to the usage of debt funds to finance the purchase of assets.
Financial Leverage (FL) = Total Assets/ Shareholders Equity
Tax Burden: Taxability is the ratio of profit owned after tax.
Tax Burden (TB) = Net income/EBT
Interest Burden (IB): It is the rate of profit earned after the payment of interest payments.
Interest Burden = EBT/EBIT
Operating Profit Margin (OPM): It refers to an operating income of the number of sales.
Operating Profit Margin = EBIT/Sales

2.3.1 Multiple Linear Regression Analysis of ROE

The Analysis of Multiple linear regression is accomplished to evaluate the power of the connection between the Independent Variables on the Dependent Variable. In our case, the Dependent Variable is ROE and the Independent Variables are the 5 factors of ROE viz. FL, ATO, OPM, TB, and IB[6]. The below equation represents multiple linear regression.

$Y = \beta_0 + \beta_1 X_1 + \beta_2 X_2 + \beta_3 X_3 \ldots + \beta_n X_n + \varepsilon$
Y = Dependent Variable (ROE)
$X_1, X_2, X_3 \ldots X_n$ = Independent Variables (5 Factors)
$\beta_1, \beta_2, \beta_3 \ldots \beta_n$ = Coefficients of Independent Variables
β_0 = Y-intercept (Constant) and
ε = Standard Error

Thus, having made the basic concepts and approaches for the study clear from the literature review and drawing a framework for the analysis from the research methodology, the researcher now proceeds into analysis followed by interpretation in the upcoming chapter.

4. DATA ANALYSIS AND INTERPRETATION

4.1 Multiple Linear Regression Analysis of ROE

Hypothesis testing

Null Hypothesis H0: All the IVs don't have a significant influence on ROE.
i.e., H0: $\beta 1 = \beta 2 = \beta 3 = \beta 4 = \beta 5 = 0$
Alternate Hypothesis H1: At least one IV have a significant influence on ROE.
i.e., H_1: At least one β_i #0

Interpretation

The above table clearly shows the ROE influence of Hindustan Unilever Limited by independent variables is concatenated. There is a negative correlation between ATOHUL on OPMHUL and TBHUL, a positive correlation between ATOHUL on FLHUL and IBHUL, a negative correlation between FLHUL on OPMHUL and IBHUL, a positive correlation between FLHUL on TBHUL, and a negative correlation between OPMHUL on TBHUL and IBHUL and between TBHUL on IBHUL. Both the positive and negative interaction between these Independent variables influences the Dependent variable (ROEHUL).

Table 3.1 HUL(Input)Data - Regression Analysis-2012-2021

YEAR	ROE HUL	FL HUL	ATO HUL	OPM HUL	TB HUL	IB HUL
2012	76%	310%	205%	15%	77%	100%
2013	134%	422%	223%	19%	76%	99%
2014	112%	389%	213%	18%	76%	99%
2015	108%	358%	222%	20%	69%	100%
2016	63%	225%	218%	19%	69%	100%
2017	66%	233%	211%	20%	69%	99%
2018	72%	245%	199%	21%	71%	100%
2019	77%	237%	211%	22%	70%	100%
2020	82%	245%	197%	23%	74%	99%
2021	17%	144%	68%	23%	75%	99%

Table 3.2 Correlation Analysis - Evaluation IVs – HUL

	ATO HUL	FL HUL	OPM HUL	TB HUL	IB HUL
ATO HUL	100%				
FL HUL	63%	100%			
OPM HUL	-47%	-57%	100%		
TB HUL	-28%	34%	-33%	100%	
IB HUL	33%	-7%	-26%	-45%	100%

Table 3.3 Regression Analysis - ROEHUL, FLHUL, ATOHULAND OPMHUL

Model Summary

Model	R	R Square	Adjusted R Square	Std. Error of the Estimate
1	.998a	0995	0993	2.76770

a.Predictors:Constant), OPMHUL,ATOHUL,FLHUL

Coefficients[a]

Model		Unstandardized Coefficients		Standardized Coefficients	t	Sig.
		B	Std. Error	Beta		
1	(Constant)	-128.712	12.570		-10.240	.000
	FLHUL	.339	.015	.912	22.449	.000
	ATOHUL	.216	.026	.310	8.214	.000
	OPMHUL	3.590	.466	.274	7.706	.000

a. Dependent Variable: ROEHUL

Coefficients[a]

Model		Unstandardized Coefficients		Standardized Coefficients	t	Sig.
		B	Std. Error	Beta		
1	(Constant)	-230.973	177.106		-1.304	.262
	FLHUL	.316	.014	.849	22.612	.000
	ATOHUL	.272	.027	.390	9.881	.001
	OPMHUL	4.025	.405	.307	9.934	.001
	TBHUL	.899	.338	.093	2.658	.057
	IBHUL	.240	1.624	.004	.148	.890

a. Dependent Variable: ROEHUL

Interpretation

After using backward elimination technique of regression analysis, the Adjusted R2 value is 0.993 which shows that there is a high positive Correlation between the Dependent variable (ROEHUL) and Independent Variable (5 factors). From the ANOVA table, again the F- Significance is 0.00 which is much less than the P-value which is 0.05, it shows that there is 99.99% confidence of the model is statistically significant.

The coefficient of FLHUL, ATOHUL, and OPMHUL is 0.339, 0.216, and 3.590. It explains that every unit increase in values of FLHUL, ATOHUL, and OPMHUL increases by 0.339, 0.216, and 3.590 respectively. As per the Hypothesis, we accept the Alternate Hypothesis(H1).

The final regression equation for ROE(HUL) can be written as:

ROEHUL=128.712+0.339(FLHUL)+0.216 (ATHUL) +3.590 (OPMHUL)+2.769

Table 3.4 NIL(Input) Data - Regression Analysis – 2012 – 2021

YEAR	ROE NIL	FL NIL	ATO NIL	OPM NIL	TB NIL	IB NIL
2012	59%	287%	161%	19%	69%	98%
2013	47%	267%	144%	19%	67%	98%
2014	42%	205%	169%	18%	67%	99%
2015	20%	216%	134%	10%	69%	100%
2016	30%	207%	134%	18%	65%	94%
2017	36%	215%	136%	19%	67%	95%
2018	44%	220%	140%	23%	66%	96%
2019	103%	374%	172%	23%	74%	95%
2020	103%	391%	169%	22%	74%	94%
2021	103%	394%	179%	21%	74%	93%

Table 3.5 Correlation Analysis - Evaluation IVs – NIL

	FLNIL	ATONIL	OPMNIL	TBNIL	IBNIL
FLNIL	100%				
ATONIL	78%	100%			
OPMNIL	53%	49%	100%		
TBNIL	94%	77%	32%	100%	
IBNIL	-54%	-27%	-66%	-40%	100%

Interpretation

The above table clearly shows the ROE influence of Nestle India Limited by independent variables is concatenated. There is a positive correlation between FL on ATO, OPM, and TB, a negative correlation between FL on IB, a positive correlation between ATO on OPM and TB, a negative correlation between ATO on IB, a positive correlation between OPM on TB, a negative correlation between OPM on IB, negative correlation between TB on IB. Both the positive and negative interaction between these Independent variables influences the Dependent variable (ROE).

Table 3.6 Regression Analysis - ROE and ROE Factors – NIL

Model Summary

Model	R	R Square	Adjusted R Square	Std. Error of the Estimate
1	1.000[a]	.999	.998	1.52715

a. Predictors: (Constant), IBNIL, ATONIL, OPMNIL, TBNIL, FLNIL

ANOVA[a]

Model		Sum of Squares	df	Mean Square	F	Sig.
1	Regression	9346.771	5	1869.354	801.551	.000[b]
	Residual	9.329	4	2.332		
	Total	9356.100	9			

a. Dependent Variable: ROENIL

b. Predictors: (Constant), IBNIL, ATONIL, OPMNIL, TBNIL, FLNIL

Coefficients[a]						
Model		Unstandardized Coefficients		Standardized Coefficients	t	Sig.
		B	Std. Error	Beta		
1	(Constant)	-189.503	47.854		-3.960	.017
	FLNIL	.169	.027	.415	6.203	.003
	ATONIL	.319	.054	.176	5.867	.004
	OPMNIL	2.071	.248	.242	8.349	.001
	TBNIL	2.569	.578	.281	4.440	.011
	IBNIL	-.677	.328	-.050	-2.064	.108
a. Dependent Variable: ROENIL						

Interpretation

From the model summary, the value of R is 1, which shows that there is a high positive correlation between the Dependent variable (ROENIL) and Independent Variable (5 factors). The value of R2 is 0.999. In multiple Linear Regression, the Adjusted R2 value is considered. The 99.8% shows the Variability in the Dependent Variable (ROENIL) by the Independent Variables (5 Factors). From the ANOVA table, the F- Significance Value is 0.00 which is much less than the P-value which is 0.05, it shows that there is 99.99% confidence of the model is statistically significant. From the above coefficient table, there is 1 Independent Variable that has a P-value of more than 0.05. As per Hypothesis, the Null Hypothesis(H0) is rejected, and the Alternate Hypothesis(H1) is Accepted because one variable in the independent 1 variable(IBNIL) is not equal to 0.05. By using the Backward elimination technique of regression, this model has to be Rerun after eliminating the insignificant variables (IBNIL). The model has to be Rerun only considering the Independent variables of FLNIL, ATONIL, OPMNIL, and TBNIL.

Table 3.7 Regression Analysis - ROENIL, TBNIL, OPMNIL, ATONIL, FLNIL

Model Summary				
Model	R	R Square	Adjusted R Square	Std. Error of the Estimate
1	.999a	.998	.996	1.96295
Predictors©Constant), TBNIL,OPMNIL,ATONIL,FLNIL				

ANOVA						
Model		Sum of Squares	Df	Mean Square	F	Sig.
1	Regression	9336.834	4	2334.209	605.791	.000b
	Residual	19.266	5	3.853		
	Total	9356.100	9			
Dependent Variable:ROENIL						
Predictors©Constant), TBNIL,OPMNIL,ATONIL,FLNIL						

Coefficients[a]						
Model		Unstandardized Coefficients		Standardized Coefficients	t	Sig.
		B	Std. Error	Beta		
1	(Constant)	-259.965	43.109		-6.030	.002
	FLNIL	.179	.034	.439	5.186	.004
	ATONIL	.272	.063	.150	4.285	.008
	OPMNIL	2.332	.274	.272	8.508	.000
	TBNIL	2.638	.742	.288	3.554	.016
a. Dependent Variable: ROENIL						

Interpretation

After using backward elimination technique of regression analysis, the Adjusted R2 value is 0.996 which shows that there is a high positive Correlation between the Dependent variable (ROE) and Independent Variable (5 factors). From the ANOVA table, again the F- Significance is 0.00 which is much less than the P-value which is 0.05, it shows that there is 99.99% confidence of the model is statistically significant. The coefficient of FLNIL, ATONIL, OPMNIL, and TBNIL is 0.179, 0.272, 2.334, and 2.638. It explains that every unit increase in values of FLNIL, ATONIL, and OPMNIL increases by 0.179, 0.272, 2.334, and 2.638 respectively. As per the Hypothesis, we accept the Alternate Hypothesis(H1).

The final regression equation for ROE(NIL) can be written as:

ROENIL = -259.965 + 0.179 (FLNIL) + 0.272 (ATONIL) + 2.332 (OPMNIL) + 2.638 (TBNIL) + 1.962

5. FINDINGS

5.1 Findings – Multiple Linear Regression Analysis – Nestle India Limited

- There is a high positive correlation between the dependent variable (ROE) and the Independent variable (5 factors). The adjusted R square value is 0.996.
- There are 2 Independent Variable (IB and TB) that has a P-value of more than 0.05.
- As per Hypothesis, the Alternate Hypothesis (H1) is accepted
- After Eliminating the insignificant variable, the model has rerun. The adjusted R2 is 0.993.
- Every unit increase in values of FLHUL, ATOHUL, and OPMHUL, ROEHUL increases by 0.339, 0.216, and 3.590 respectively
- Regression equation framed considering only the significant variables

ROEHUL = - 128.712 +0.339 (FL) +0.216 (ATO) +3.590 (OPM)+2.769

4.2 Findings – Multiple Linear Regression Analysis – Nestle India Limited

- There is a high positive correlation between the Dependent variable (ROENIL) and Independent Variable (5 factors). The adjusted R square is 0.998
- There is 1 Independent Variable (IBNIL) that has a P-value of more than 0.05.
- The alternate hypothesis(H1) is Accepted
- After Eliminating the insignificant variable, the model has rerun. The adjusted R2 is 0.996.
- Every unit increase in values of FLNIL, ATONIL, and OPMNIL, ROENIL increases by 0.179, 0.272, 2.334, and 2.638 respectively
- Regression equation framed considering only the significant variables

ROENIL = -259.965 + 0.179 (FLNIL) + 0.272 (ATONIL) +2.332 (OPMNIL) +2.638 (TBNIL) + 1.962

Interpretation

From the model summary, the value of R is 0.99, which shows that there is a high positive correlation between the Dependent variable (ROEHUL) and Independent Variable (5 factors). The value of R2 is 0.998. In multiple Linear Regression, the Adjusted R2 value is considered. The 99.6% shows the Variability in the Dependent Variable (ROEHUL) by the Independent Variables (5 Factors). From the ANOVA table, the F-Significance Value is 0.00 which is much less than the P-value which is 0.05, it shows that there is 99.99% confidence of the model is statistically significant. From the above coefficient table, there are 2 Independent Variable that has a P-value of more than 0.05 As per the Hypothesis, the Null Hypothesis(H0) is rejected, and the Alternate Hypothesis(H1) is Accepted. By using the Backward elimination technique of regression, this model has to be Rerun after eliminating the insignificant variables (IBHUL and TBHUL). The model has to be Rerun only considering the Independent variables of FLHUL, ATOHUL, and OPMHUL.

6. CONCLUSION

The FMCG sector is one of the Fourth largest sectors contributing to a GDP and it is a fast-growing sector. The industry's success is dependent on the firm's management making sound financial, investment, and operational decisions. Investors are always seeking new methods to spend their hard-earned money for it to develop alongside the firm for long-term rewards. ROE is one such measure that investors use to assess the company's success. As a result, by effectively utilizing internal factors such as optimal leverage utilization, efficient asset utilization, and operational efficiency, these firms in the FMCG sector can create a good value platform to improve ROE healthily, attracting loyal

investors who can mutually benefit each other. The DuPont model of ROE extraction backed by Comparative Analysis, and regression analyses of ROE of businesses in the FMCG sector, enabled me to achieve the research goals by detecting an overall declining trend in ROE over the last decade. It also enabled to provide significant recommendations to enterprises in the FMCG sector on how to enhance the ROE of their firms and thereby the industry as a whole.

REFERENCES

[1] Ramu, Srilakshmi and Satyanarayana, "Financial Performance Analysis of Hdfc Using Dupont Analysis", Inspira-Journal of Commerce, Economics & Computer Science (JCECS). Vol.05, No.02, 2019.

[2] Risal and Nischal, "Performance Scrutiny of Nepal Electricity Authority using DuPont Analysis", PYC Nepal Journal of Management, Vol.12, 2019, pp.79-85.

[3] Raza, Syed Ali and Jawaid, Syed, Tehseen and *et.al*, "A DuPont Analysis on Insurance Sector of South Asian Region", 2013.

[4] Padake and Vaishali, "Measurement of Efficiency of Top 12 Banks in India Using DuPont Analysis", The IUP journal of Bank Management. Vol.XIV, 2015, 59-68.

[5] Manjunatha and Praveen, "A Study of Indian Software And Networking Companies Using Extended Dupont Model", JNNCE Journal of Engineering & Management. Vol.2, No.1, 2018.

[6] Loukopoulos, George and Roupas and Theodoros, "Financial Analysis of the Greek Private Health Sector over the Last Decade (2002-2012), Retrieved from ProQuest Database, Vol.17, No.2, 2014, pp.3-19.

[7] Sachdev, Kartik, Jamaiyar and Arushi, "Use of Five Point Du Pont Model and Regression Tools to Study Information Technology Sector of India", Retrieved from ProQuest Database, Vol.3, No.2, 2015, pp.25-39.

[8] Kyriazopoulos, Georgios, Chrissochoidou Noula and *et. al.,* "Profitability of Cooperative Banks With Dupont Analysis", Evidence Of Greek Banking System, 2014.

[9] C.S. Sheela and K.Karthikeyan, "Financial Performance of Pharmaceutical Industry in India using DuPont Analysis", European Journal of Business and Management, Vol.4, No.14, 2012.

[10] Hao, Yue & Choi and Seung, "Operating Performance of Chinese Online Shopping Companies: An Analysis Using DuPont Components Sustainability", 10.3390/su11133602, Vol.11, 2019, pp.3602.

[11] Singh, Fulbag, Mogla and Monika, "Profitability Analysis of Acquiring Companies", Retrieved from ProQuest Database, Vol.16, No.5, 2010, pp.72-83.

[12] Mohammad Omar Faruk and Rokshana Alam, "A Comparative Financial Performance Analysis of Bangladeshi Private Commercial Banks", Retrieved from ProQuest Database, Vol.6, No.1, 2014, pp.129-146.

[13] Oriskoova, Denisa & Paksiova and Renata, "Dupont Analysis of Companies of The Slovak Republic Engineering Industry", 2020.

[14] Botika and Marianna, "The Use of DuPont Analysis in Abnormal Returns Evaluation: Empirical Study of Romanian Market", Procedia - Social and Behavioral Sciences, Vol.62, 2012, pp.1179-1183.

AUTOMATED STORAGE AND RETRIEVAL SYSTEM FOR AGRICULTURAL WAREHOUSE MANAGEMENT

M. Raghunath[1], P. Nagarajan[2], K.L. Senthil Kumar[3], S.K. Dhinesh[4]
P.A.Tharakeshvar[5], A. Prasanna[6] and A.Kavinkanth[7]
[1,2,3,4]Department of Mechatronics
[5,6,7]Department of Electronics and Communication Engineering,
Bannari Amman Institute of Technology, Sathyamangalam-638 401, Erode District, Tamil Nadu
Email Id: nagarajanp@bitsathy.ac.in

Abstract

The Automated Storage and Retrieval System (ASRS) is an extensively utilized solution in agricultural warehouses, facilitating streamlined operations and efficient inventory management. To further enhance the system's effectiveness, we propose the deployment of a sliding rack-based system in our research. This system offers significant advantages, particularly in reducing the travel time of robots involved in the retrieval and storage of agricultural products. By minimizing the time required for these tasks, the system enables more effective time management within the warehouse. The ASRS system itself automates the process of storing and retrieving objects, thereby minimizing manual labour and increasing operational efficiency. In order to implement the automation aspect of the sliding rack-based system, we are developing a prototype that incorporates a Programmable Logic Controller (PLC). The PLC serves as the central control unit, facilitating the coordination and synchronization of various components. To accurately determine the position of components during retrieval, we utilize a camera module, which provides visual feedback to the system. This information is crucial for the precise movement of the FANUC 6-axis robot, which is specifically selected for its capability to efficiently retrieve components. The integration of the robot with the PLC enables full automation of the entire process. This integration allows for seamless communication and coordination between the robot and the control system, ensuring precise and efficient component retrieval. As a result, the prototype system represents a significant step forward in improving the operational efficiency of agricultural warehouses. The potential impact of this prototype in the agricultural warehouse industry is substantial. By significantly reducing retrieval and storage times, the system optimizes inventory management and contributes to more efficient warehouse operations. Additionally, the reduction in manual labour required for these tasks leads to improved resource allocation and reduced labour costs. Ultimately, the implementation of this prototype system holds great promise for enhancing productivity, reducing operational expenses, and improving overall efficiency in agricultural warehouses.

Keywords: *Agricultural warehouse, ASRS, Automation, Storage, Retrieve,*

1. INTRODUCTION

Storing raw materials and finished products is a crucial aspect of organizational operations. Traditionally, agricultural warehouses have been established and maintained to fulfil this purpose. However, the existing manual maintenance systems often require large land areas, significant manpower, and substantial financial investment. To address these challenges, automation emerges as a viable solution. The Automated Storage and Retrieval System (ASRS) offers an automated approach to agricultural warehouse management. ASRS was first introduced in the 1950s and has since gained widespread adoption in distribution and production environments. An ASRS comprises racks mounted on sliders that slide out to store and retrieve products efficiently. The utilization of ASRS systems witnessed a significant increase between 1994 and 2004 in both production and distribution environments. Compared to nonautomated or manual systems, ASRS systems provide several advantages such as optimized utilization of floor space, enhanced reliability, reduced labor costs, and decreased error rates. However, they also have certain disadvantages, including a high initial investment and limited flexibility. This research paper focuses on

the construction of an Automated Storage and Retrieval System and presents a prototype model based on rack sliding. The proposed system eliminates the stationary nature of traditional setups and offers improved functionality. The prototype model has been developed and thoroughly analyzed to assess its performance and feasibility. By addressing the construction and analysis of this innovative ASRS system, this research aims to contribute to the field of automated agricultural warehouse management [1] [2] [3], Shown in Figure1.

Fig.1 ASRS in Agriculture Warehouse Management

1.1 Applications

The applications of Automated Storage and Retrieval Systems (ASRS) in agricultural warehouse management are pivotal for improving productivity and streamlining operations. ASRS technology offers numerous benefits for the agricultural industry. Firstly, it enables efficient inventory management by automating the storage and retrieval process of agricultural products [4] [5]. With ASRS, the system automatically stores and retrieves items, reducing the need for manual labor and minimizing errors. This leads to increased accuracy, improved order fulfillment, and enhanced customer satisfaction. Additionally, ASRS optimizes space utilization within agricultural warehouses. By utilizing vertical space effectively, the system maximizes storage capacity, allowing for the accommodation of a larger quantity of agricultural products in a limited area. This results in better organization, reduced clutter, and improved accessibility, ultimately enhancing overall warehouse efficiency. ASRS also facilitates faster order processing and reduced turnaround times. With automated retrieval and storage mechanisms, agricultural products can be quickly located and delivered to the desired locations within the warehouse. This expedites order fulfillment, reduces waiting times, and enhances supply chain efficiency. Moreover, ASRS systems offer real-time inventory tracking and management. By integrating with advanced technologies such as barcode scanning, RFID (Radio Frequency Identification), and warehouse management software, the system provides accurate and up-to-date inventory information. This enables better inventory control, reduces the risk of stockouts or overstocking, and supports effective demand planning and forecasting [6]. Overall, the applications of ASRS in agricultural warehouse management significantly contribute to increased operational efficiency, reduced costs, improved inventory control, and enhanced customer satisfaction. By embracing this technology, agricultural warehouses can achieve higher productivity levels and gain a competitive edge in the industry [7] [8].

1.2 Recent Advancements

Recent advancements in Automated Storage and Retrieval Systems (ASRS) have witnessed a remarkable fusion of robotics and automation in the agricultural sector. One of the key breakthroughs lies in the implementation of data-driven decision-making, where cutting-edge technologies like artificial intelligence and machine learning analyze various parameters such as crop maturity, weather conditions, and market demand to determine the optimal basis for both storing and retrieving agricultural produce. This dynamic approach allows ASRS to adapt in real-time, optimizing storage conditions, shelf life, and retrieval timing to minimize waste and maximize the quality of harvested crops. Furthermore, the incorporation of autonomous robotic vehicles, equipped with specialized end-effectors for delicate handling of fragile produce, ensures efficient movement within the storage facility, providing a seamless link between data-driven insights and practical execution. This convergence of modern technology not only enhances the overall efficiency of agricultural supply chains but also contributes significantly to sustainable farming practices by reducing post-harvest losses and resource consumption.

2. METHODOLOGY

The methodology of incorporating a camerabased Automated Storage and Retrieval System (ASRS) in a research paper requires a wellstructured approach to effectively implement and analyse its performance within the specific research context. Initially, the research paper should clearly define the objectives and research questions, such as investigating the impact of the camera based ASRS on warehouse efficiency or evaluating its accuracy in identifying and retrieving specific items.

Subsequently, the paper should outline the selection criteria used to choose the camera system, considering factors like resolution, image processing capabilities, and compatibility with the existing infrastructure. The methodology should then describe the installation process, including camera placement, calibration procedures, and integration with the ASRS control software. Additionally, it is crucial to address the data collection methods employed, such as capturing images of stored items, tracking their movement within the warehouse, and recording retrieval accuracy. This can be achieved through image analysis algorithms, object recognition techniques, or manual annotations. Furthermore, the research paper should discuss the data analysis techniques used to evaluate the camera based ASRS performance, such as assessing item recognition rates, retrieval speed, and error rates. Statistical methods, image processing algorithms, and comparative analyses may be applied to interpret the collected data. Overall, the methodology section of the research paper provides a systematic framework for implementing and analysing the camera-based ASRS, offering insights into its functionality and performance in the specific research setting [8] [9].

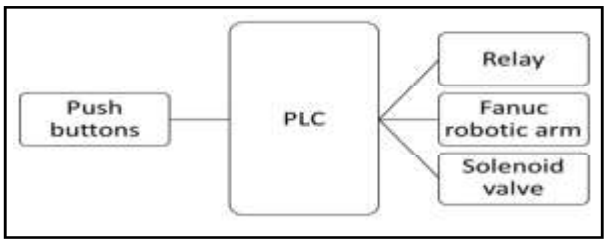

Fig.2 Proposed block diagram of automated storage and retrieval system.

2.1 Logical Architecture

In this proposed system, the basic fundamental building block diagram of a ASRS Systems is push buttons, PLC, relay, solenoid valve, Fanuc, double acting cylinder and the applications. As a result, the fundamental building block diagram below is a suggested model for our proposed work, and it depicts the relationships between the diagram's blocks. In our suggested work, the push buttons are connected to the PLC, and once the push button is pressed the input signal is given to the PLC. [10] [11]. The PLC then gives the output to the relay and the double acting cylinder is actuated to open the rack. Once the rack is open the Fanuc then picks the material and places it in the rack. Then the rack closes. The Figure 3 shows the flowchart of the working of our proposed system

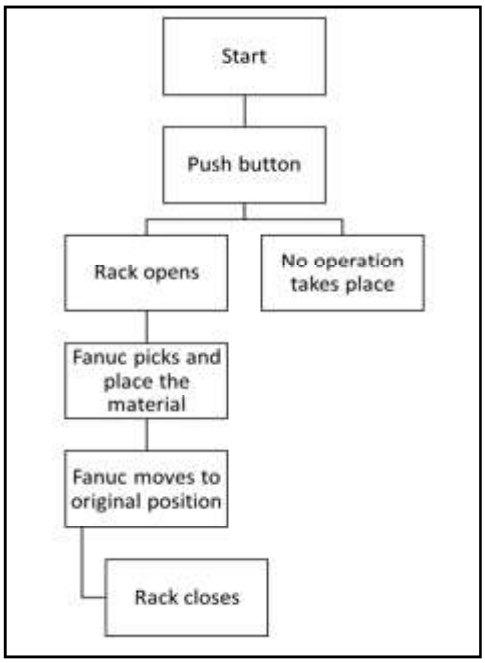

Fig.3 Flowchart of proposed model

2.2 Design and CAD Model of ASRS

The outer frame is made using Aluminum extrusions which acts as a main supporting body of the whole system . The Aluminum extrusion is also used inside the frame which is used to place the slider for mounting the racks. The system consists of 9 racks so 9 supporting aluminum extrusion is fixed inside the frame. For mounting the cylinder on both sides of the Aluminum Frame we use a 3D printed clamp. The 3D printed clamp was designed for the dimensions of the cylinder on both ends. The cylinder is mounted in a straight line to the racks. The end of the cylinder piston is connected to the back side of the racks. As there were 9 racks 9 separate double acting cylinders were used. The racks are mounted on the sliders which are mounted on the aluminum extrusion placed inside the Frame.

The rack was made using transparent acrylic sheets and it is made in the shape of a drawer. As the rack was mounted on the sliders they could open and close with the help of air cylinders. The solenoids are also mounted within the frame, they were mounted on an aluminum plate attached at the back of the system in perpendicular to each of the cylinders so that it is easy to connect the solenoids to cylinder ,here also totally 9 solenoids were used.

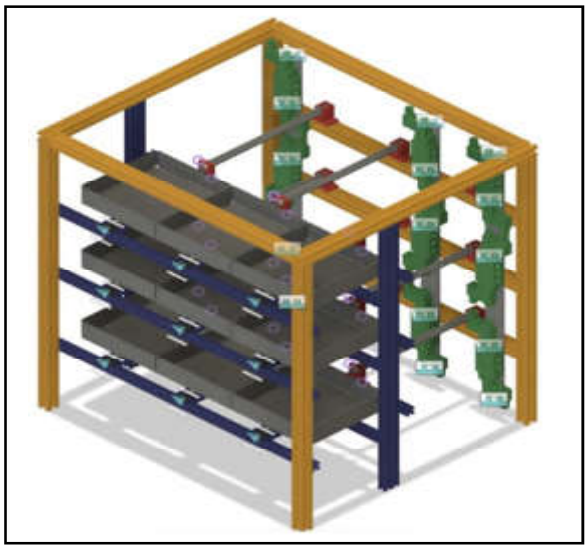

Fig.4 Isometric view of the ASRS Design

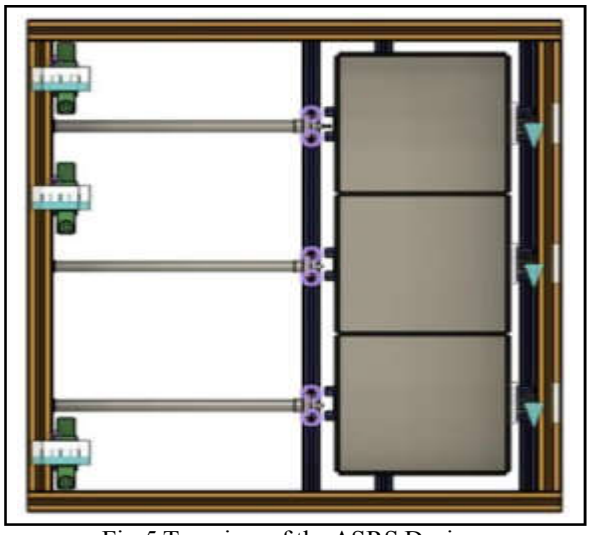

Fig.5 Top view of the ASRS Design

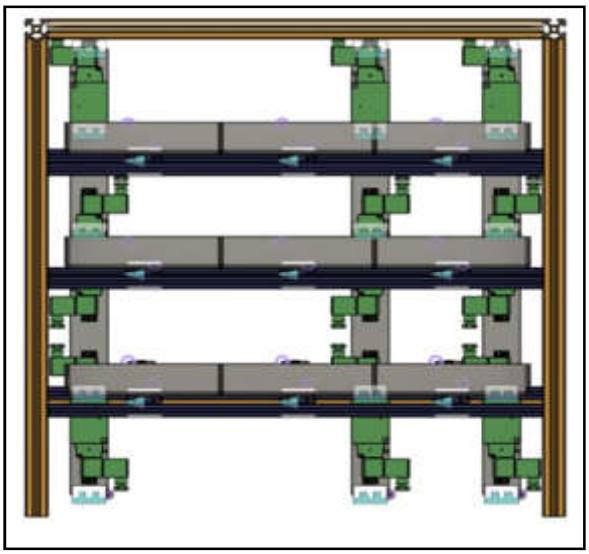

Fig.6 Front view of the ASRS Design

2.3 PLC Panel Circuit Design

MCB is used for the fuse control. Behind MCB SMPS is placed which is used to power the PLC.PLC acts as a centralized controller of the system. Relay is used to give 230v to the solenoid to change the position or switch the position between the solenoid to either forward or backward of the piston movement. PLC controls the relay for changing the position by giving 24V power supply to it. The output from the PLC controller is given to the input of Robot controller.

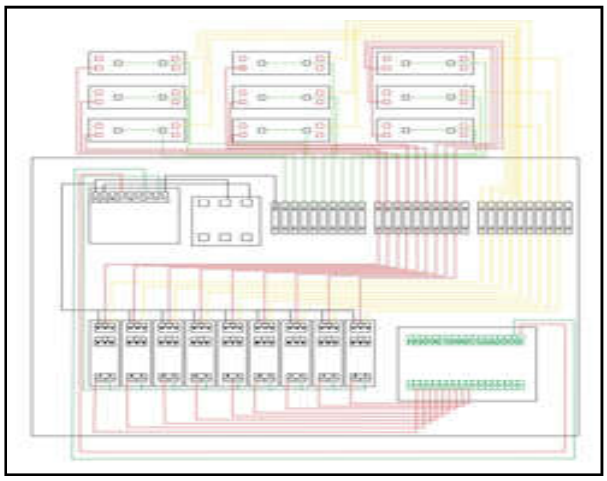

Fig.7 PLC Panel circuit design

2.4 Fabrication Frame Setup

The setup contains the solenoid valve and the pneumatic cylinders mounted on the frame. The acrylic sheets were made into a rack and it is mounted on the slider and connected with the cylinder. The pneumatic cylinder is used for movement of the racks and solenoid valve is used for controlling the direction of the Cylinder and to control the pressure exerted by the air supply. We are using a flow control valve. It ensures that the air flows uniformly throughout the entire system of cylinders.

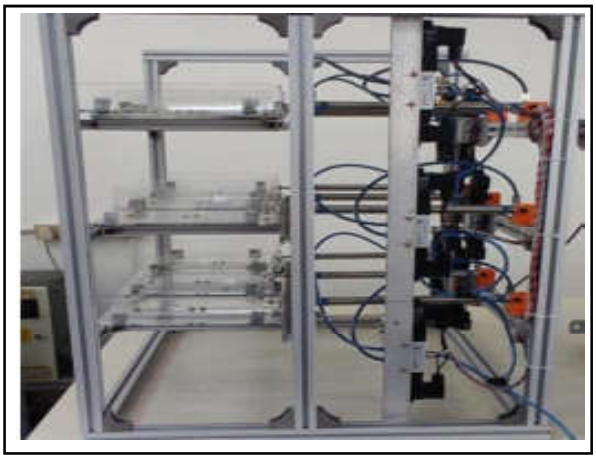

Fig.8 Frame Setup

2.5. Panel Setup

The SIMATIC S7-200 smart , push button, relay, MCB, SMPS. The push button gives the input to the PLC. The PLC gives the output to the relay which is connected to the output of the PLC. The relay gives the signal to the solenoid valve which actuates the cylinder. Then the arm picks and places the object. Then the rack closes.

Fig.9 Panel Setup

2.6 PLC Ladder Logic

PLC (Programmable Logic Controller) ladder logic plays a crucial role in the operation of Automated Storage and Retrieval Systems (ASRS). Here's a short note explaining the concept ASRS is a computercontrolled system used in warehousing and distribution centres to automatically store and retrieve items with high efficiency and accuracy. PLCs are widely employed as the control systems for ASRS due to their ability to handle complex automation tasks. Ladder logic is a programming language used in PLCs, particularly suited for designing and implementing control systems. It derives its name from its visual representation, resembling a ladder with rungs and rails. Each rung represents a logical condition or action to be executed. In the context of ASRS, ladder logic is utilized to manage and coordinate the various components of the system. It enables the control of conveyors, lifts, shuttles, robots, and other devices involved in the storage and retrieval processes. The PLC logic is shown in Figure 10,11,12,13.

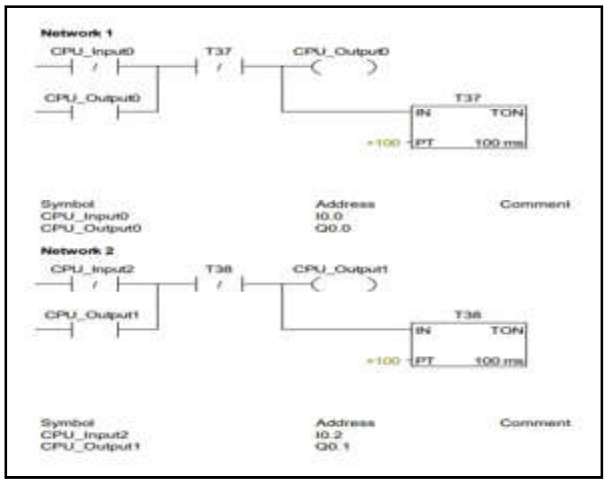

Fig.10 Ladder Logic

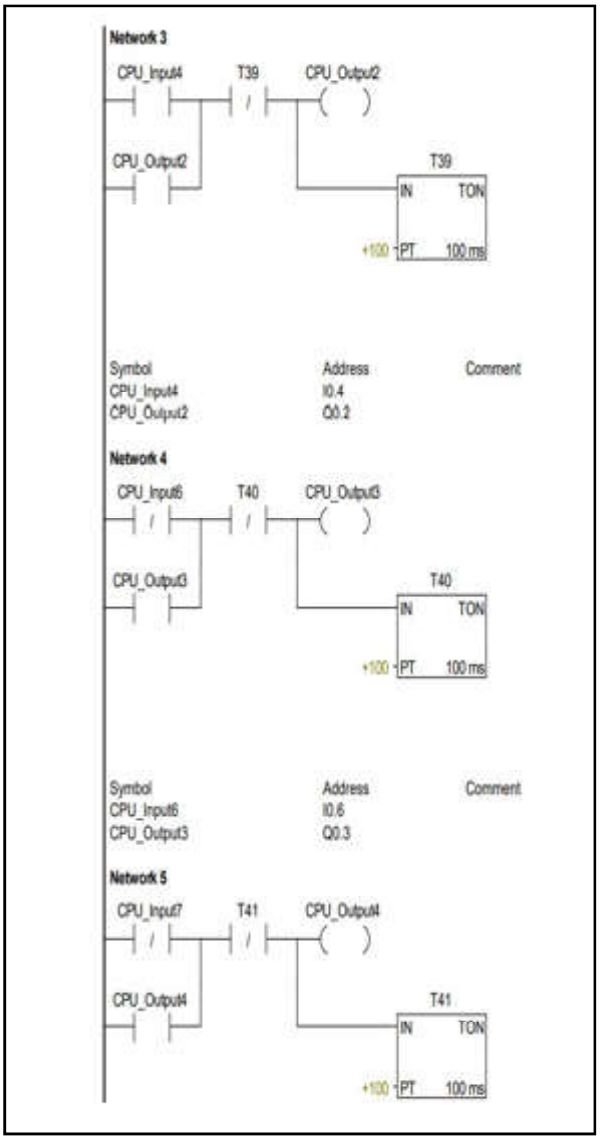

Fig.11 Ladder Logic

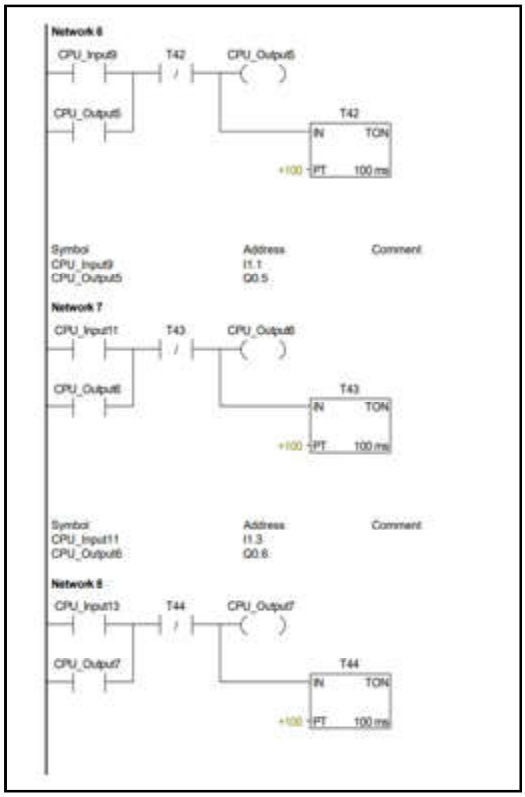

Fig.12 Ladder Logic

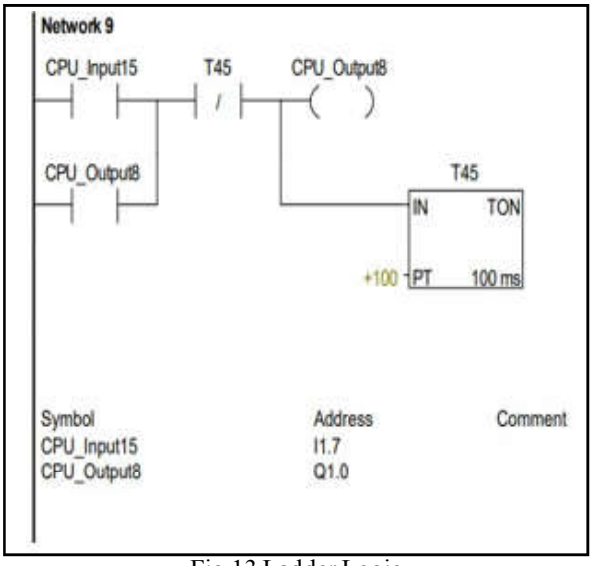

Fig.13 Ladder Logic

2.7 Software Architecture

Software architecture for an Automated Storage and Retrieval System (ASRS) employing a FANUC robot is a pivotal design framework that orchestrates the seamless integration of hardware and software components. At its core, it encompasses the division of functionalities into distinct layers, including a robust control layer that manages the FANUC robot's movements and interactions within the ASRS, an intelligent perception layer equipped with sensors and vision systems for real-time environment awareness, and a high-level management layer that coordinates task scheduling, system monitoring, and user interactions. This architecture leverages FANUC's advanced robotic capabilities, ensuring efficient material handling and precise positioning within the ASRS, ultimately optimizing warehouse operations and enhancing productivity while accommodating scalability and adaptability to meet evolving industry demands.

3. RESULTS AND DISCUSSION

The ASRS system works with the help of PLC and 6 Axis Fanuc robots. The racks have been designed and machined in such a way that it is suitable for agricultural warehouses. It is an easy process as only one rack moves and the other remains stable. This allows less damage to the inventory products. The robot and the PLC were interfaced so that they can transfer data or signals between each other. Individual push buttons for every rack have been used. If we click a button that rack opens and the robot after some time automatically picks the product or place depending on the need. Database is created and the details of products is stored so it can help for inventory maintenance. Further a camera can be added and this camera can be interfaced with the robot controller and the CNN(computational Neural Network) can be used for image processing of the camera module and it will help the robot to find the position of components in the racks for their retrieval. This method adds more feasibility to the system. The system is tested for feasibility approaches and computer vision is established for establishing the position of the objects or racks to pick or place based on the algorithms. various algorithms for vision systems have been tested and the best out of the algorithms of the system has been chosen.

Fig.14 The ASRS whole system

3. CONCLUSION

A prototype was fabricated to create the Automated agricultural warehouse Process in an Industry. The project focuses on the automation and effective movement of materials in the agricultural warehouse. It was achieved by using a Double Piston cylinder to move the racks in forward and backward position. A Fanuc Robotic Arm was deployed to position the production material in the rack and by the reverse process of the cylinder the rack closes. The process is controlled by a PLC Controller, in the company of push button, relays and solenoids. The process is fully evaluated and further development is undergoing.

REFERENCES

[1] Thirugnanasambandam, Ajay, Arulraj, Vinoth and Stephen, "Design Optimization and Development of an Automated Storage and Retrival System", IOP Conference Series, Material Science and Engineering, Vol. 912, 2020, pp. 032031.

[2] Lin, Lin&Shinn, Seong&Gen, Mitsuo&Hwang and Hark, "Network Model and Effective Evolutionary Approach for AGV Dispatching In Manufacturing System", Journal of Intelligent Manufacturing, Vol.17, 2006, pp.465-477.

[3] Blum, Christian &Roli and Andrea, "Metaheuristics in combinatorial optimization: Overview and conceptual comparison," ACM Computing Surveys(CSUR), Vol.35, 2003, pp.268-308.

[4] Huh, Jaeseok & Chae, Moon-jung & Park, Jonghun&Kim and Kwanho, "A Case-based Reasoning Approach to fast Optimization of Travel Routes For Large Scale AS/RSs," Journal of Intelligent Manufacturing, Vol.30, 2019, pp.17651778.

[5] Boysen, Nils and De Koster, Ren{\'e} and Weidinger, Felix, "Warehousing in the Ecommerce Era: As Survey," European Journal of Operational Research, Vol.277, 2019, pp.396-411.

[6] Lee, Carman KM & Lv, Yaqiong & Ng, KKH & Ho, William & Choy and King Lun, "Design and Application of internet of Things-Based Warehouse Management System of Smart Logistics", International journal of Production Research, vol. 56, pp. 2753-2768, 2018.

[7] Azadeh, Kaveh & Roy, Debjit & De Koster and Ren{\'e}, "Design Modelling, and Analysis of Vertical Robotic Storage Retrival Systems," Transportation Science, Vol.53, 2019, pp.1213-1234.

[8] Chen, Wanying & De Koster, Ren{\'e} & Gong and Yeming, "Analysis and Design of Rack Climbing Robotic Storage And Retrival Systems," Transportation Science, Vol.56, 2022, pp.1658-1676.

[9] Calzavara, Martina & Glock, Christoph H & Grosse, Eric H & Sgarbossa and Fabio, "An integrated storage assignment method for manual order picking warehouses considering cost, workload and posture", International Journal of Production Research, Vol.57, 2019, pp. 2392-2408.

[10] Proth, J-M & Sauer, Nathalie and Xie, Xiaolan, "Optimization of the number of transportation devices in a flexible manufacturing system using event graphs", IEEE Transactions on Industrial Electronics, Vol.44, 1997, pp.298-306.

[11] Yu, Yugang & De Koster and MBM, "Designing an optimal turnover-based storage rack for a 3D compact automated storage and retrieval system", International journal of production research, Taylor \& Francis, Vol.47, 2009, pp.1551-1571.

DESIGN AND FABRICATION OF AN AUTOMATED SOLAR PANEL CLEANING MACHINE

S. Sundar[1], S.K.Dhinesh[2], KL.Senthil Kumar[3], M.Raghunath[4], P.Nagarajan[5], A.Kavin Kanth[6] and P.A.Tharakeshvar[7]

[2,4,5]Department of Mechatronics Engineering,
[1]Department of Electrical and Electronics Engineering,
[3]Department of Mechanical Engineering,
[6,7]Department of Electronics and Communication Engineering,
Bannari Amman Institute of Technology, Sathyamangalam -638 401, Erode District, Tamil Nadu
E-mail:sundars@bitsathy.ac.in

Abstract

This paper discusses the significance of solar photovoltaic (PV) technology in meeting global energy demands. Solar PV technology is widely used due to its abundant availability in nature compared to other resources. It serves as the fundamental source for all other energy sources. The invention of solar panels has simplified the process of energy storage by converting solar energy from the sun into electrical energy, which can be utilized for various industrial and domestic purposes. However, since solar panels are typically exposed to the open environment, they tend to accumulate dust, dirt, bird excrement, and pollen grains on their surfaces. This accumulation significantly reduces the efficiency of the panels, necessitating regular cleaning to overcome this issue. Manual cleaning methods are commonly employed, but they pose several challenges, such as increased cleaning time and the need for manual labour. Moreover, the location of the solar panels further complicates the cleaning process. In addition to these challenges, manual cleaning is also affected by the intensity of sunlight reflected from the panel surface on sunny days. This can cause discomfort to manual workers and impede the cleaning process. To address these issues, an automated solar panel cleaning system is proposed in this project. The primary objective is to develop an automated system that can effectively clean solar panels, ensuring their efficiency is maintained while reducing the need for human intervention in the cleaning process.

Keywords: *Solar panel, Dust cleaning, Automatic cleaning, Efficiency, Solar energy*

1. INTRODUCTION

Solar PV is commonly employed in dusty environments like tropical regions. As the consumption of solar energy grows, it becomes more vital to overcoming the loss of efficiency. Normally, the peak efficiency of solar energy ranges from 11% to 17%; however, soiling such as dust reduces efficiency significantly [1][2]. Due to dust restrictions, this results in a loss of efficiency of 27 percent per year. To overcome this cleaning process is implemented. Usually, manual cleaning is done in most places, but it gets difficult when there is more panel to be cleaned. Manual cleaning has its drawbacks which are overcome by automatic cleaning systems [3]. In manual cleaning, the person cleaning the panel gets affected by the reflection of sun rays from the panel and it takes lots of time to clean all the panels. These limitations are improved by the automatic solar panel cleaning system. Automatic cleaning systems help in enhancing the time and save the amount invested in manual cleaning. This process can be both dry cleaning (which removes only the sand particles) and water cleaning (which removes the pollen grains and birds' excretion). They limit the water consumed in manual cleaning [4][5]. Since the benefit of using an automated cleaning system is more, most countries use this type of cleaning where manual cleaning is limited.

1.1 Applications

The application of an automated solar panel cleaning machine offers numerous benefits in the maintenance and efficiency of solar panel systems. Firstly, it eliminates the need for manual labour, reducing the time and effort required for cleaning. By automating the cleaning

process, it ensures consistent and thorough cleaning, which is crucial for maintaining optimal energy production. The machine can be programmed to clean at regular intervals, preventing the accumulation of dust, dirt, and other debris that can hamper the panel's performance. Additionally, an automated cleaning system reduces the risk of damage to the panels that can occur during manual cleaning [6][7]. By minimizing human interference, the machine improves safety and reduces the potential for accidents. Furthermore, the automation of the cleaning process allows for efficient cleaning even in challenging locations, such as rooftops or remote solar installations, where manual cleaning would be difficult or impractical. Overall, the application of an automated solar panel cleaning machine enhances the longevity and productivity of solar panel systems, contributing to the sustainability and reliability of renewable energy generation.

Fig.1 Solar Panel

2. METHODOLOGY

The proposed system works with a microcontroller (ESP32) which has inbuilt wi-fi and Bluetooth modules with operating voltage of 5 to 12 volts. The microcontroller sends a signal to the planetary motor of the cleaning system when it's time to clean a solar panel. A bump sensor (limit switch with roller) is attached to the end of the system to state the completion of the process and send feedback to the microcontroller. The power supply to the system is generated from the switched-mode power supply (24V,12V, and 5V). The cleaning mechanism contains microfibers, brushes, and wipers for cleaning the solar panel [8]. The water spraying system is also installed to spray the water all over the panel and to reduce the wastage of water. Two heavy-duty planetary motors are used for the mechanism for moving the system following the process and rotating the cleaning system.

The block diagram describes the electrical flow of the automated cleaning system. The components to be

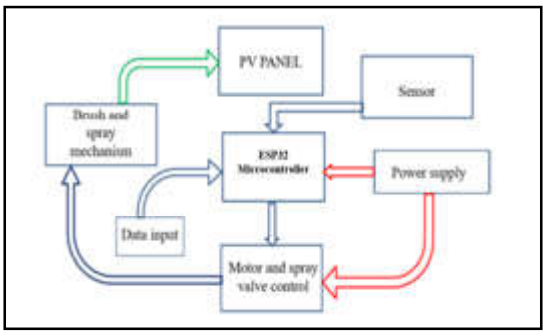

Fig.2 Methodology

used for the workflow are stated in the block diagram model for better understanding and readability. Here the microcontroller ESP32 is placed in the centre to indicate the importance of the component in the system. The connection from the microcontroller is given to the motor driver and then it is given to the motor [9]. The motor driver is used between the controller & the motor to control the speed and direction of the motor.

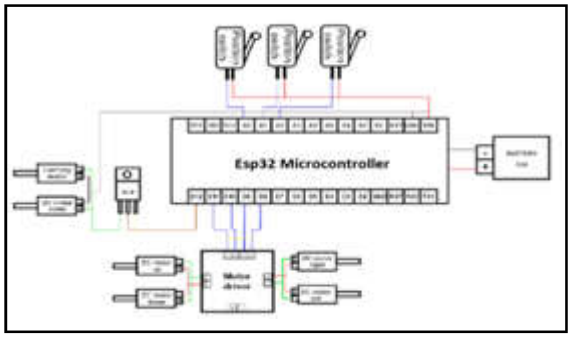

Fig.3 ESP 32 microcontroller

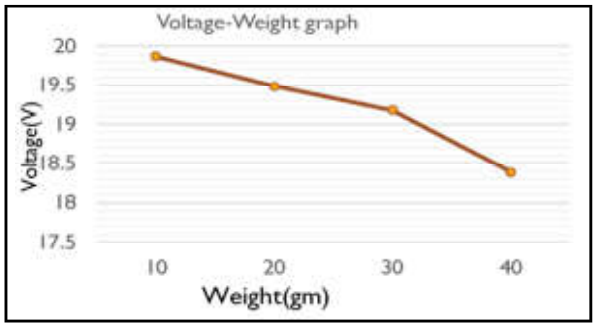

Fig.3.1 Voltage diff based on particle

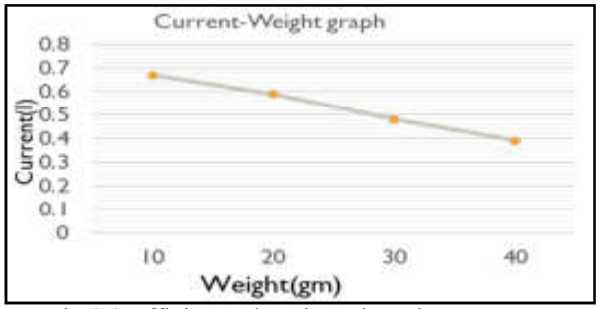

Fig.3.2 Efficiency dropdown based on current.

The above-mentioned graph Fig 3 shows the decrease in current and voltage with an increase in the dirt deposition layer. The graph was studied for sand particles present in the solar panel. In some regions, the sand content in the air may be higher, so around that region, the solar panel placed may have a maximum sand deposit on them [10]. This reduces the power produced by the solar panel. This may be a problem for a single day but when taken for a month or year they have significant losses.

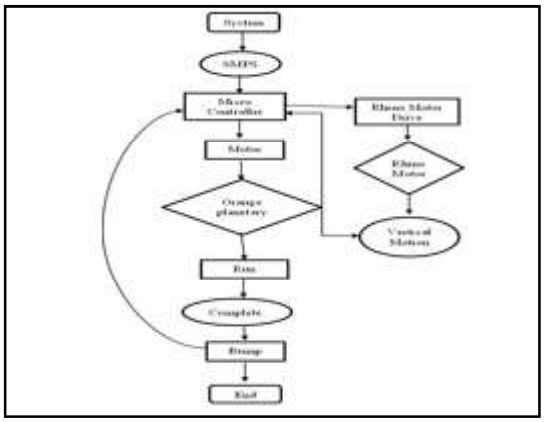

Fig.4 Flow Chart

3. DESIGN

Before making the prototype, we have done the designing part with the solid works software. Here we have completed the model with the preferred dimensions. The CAD model of the inner and outer frame is shown in figure 5 and 6.

Fig.5 Outer frame

The outer frame (figure 5) is made up of an aluminium 20 X 30 frame which has high strength and is not easily brittle. Its weight is about 20 Kg which is going to hold and move the 15 kg of the inner frame. This frame is going to place on an external frame that is fixed with the solar panel and clean the panel which is placed in series. Pulley is placed in this frame which going to handle the Y-direction motion of the system and the wheels attached between the outer frame and external frame is rotating with a motor is implemented for an X-direction motion. The inner frame (figure 6) is made from an aluminium 20 X 20 frame, which is durable and not easily fragile[11][12]. It weighs roughly 10 kilograms and will support and move the brushes and internal setup up and down, which weighs 15 kilograms. This frame will be mounted on an outer frame that is attached to the external and will clean the panels in sequence. This frame has a pulley that will manage the rolling motions of the microfiber brushes. Clearance between the frame and solar panel is calculated and placed accordingly

Fig.6 The inner frame attached to outer frame

Fig.7 Automated cleaning system mounted on solar panel

As shown in figure 7 automated cleaning system is mounted on the solar panel with an external frame attached to the panel. The inner frame is composed of an aluminium 30 X 30 frame, which is strong and not easily broken. It weighs around 10 kilograms for 5 meters and will support and help to move the entire setup, which weighs about 25 kilos, towards the X-direction. The motion towards the X-direction will be controlled by the rack and pinion system integrated with that frame. The distance between the frame and the solar panel is determined and then placed. Support to the frame

towards the ground is given with a distance of 5 meters each. Has per the design and the plan we have to make had set up of ten solar panels in a single series. In which the cleaning system cleans the panels at a stretch. These frames are not permanently attached to the system. The cleaning system is attached to it at the time of work. Meanwhile, this frame is attached to the solar panel permanently. Due to its material composition, it does not easily oxidize this was a key aspect to select this frame.

4. HARDWARE ARCHITECTURE

The ESP32 microcontroller (figure 8) is utilized as a system controller to monitor and control the process. To maintain the process in the loop, they monitor the conclusion of one step and notify the start of the next. They include Wi-Fi and Bluetooth components. They may be programmed in Python as well as Arduino. Its price is lower in comparison to other microcontrollers, but it is more sophisticated since it incorporates a single-core RISC V CPU. The internal structure includes antenna switches, power management modules, a low noise receiver amplifier, a power amplifier, filters, and an RF balun. The use of the ESP 32 microcontroller facilitates communication between the components. The module's programming is rather straightforward. Another major benefit of this module is that it can endure temperatures up to 140 degrees Celsius lower than -40 degrees Celsius when a solar panel is hit by approximately 120 degrees Celsius of the head.

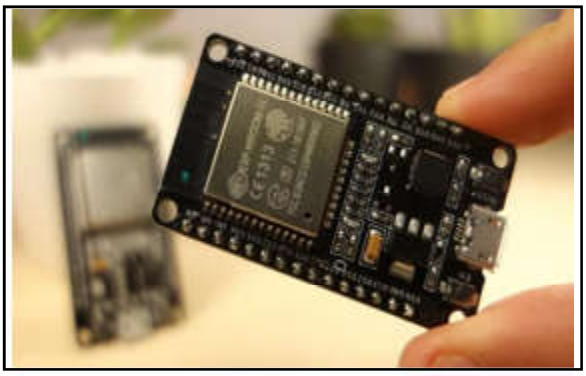

Fig.8 ESP 32 Controller

The ESP32 (figure 9) contains 39 digital pins in total, 34 of which can be utilized as GPIO and the other pins as input pins. They have 18 channels for 12-bit Analog to Digital converters and 2 channels for 8-bit Analog to Digital converters. They contain 16 distinct channels for PWM signal generation and 10 GPIO pins to facilitate capacitive touch functionalities. The ESP32 contains a multiplexing function that allows the programmer to set any GPIO pin for PWM or other serial communication via the software. The ESP32 supports three SPI interfaces, three UART interfaces, two I2C interfaces, two I2S interfaces, and the CAN protocol.

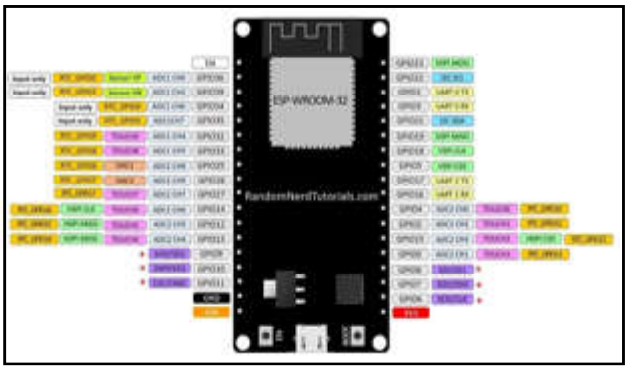

Fig.9 Pin Mode of ESP 32

The ESP32 has three UART (figure 10) interfaces for TTL communication. This would need three sets of Rx and Tx pins. Because all six pins are software adjustable, any GPIO pin may be designed to function as a UART. External Interrupt: Because the ESP32 supports multiplexing, any GPIO pin may be configured as an interrupt pin. These pins are utilized for SPI communication: GPIO23 (MOSI), GPIO19 (MISO), GPIO18 (CLK), and GPIO5 (CS). This is the first of two SPI sets supported by the ESP32. These pins are utilised for SPI communication: GPIO13 (MOSI), GPIO12 (MISO), GPIO14 (CLK), and GPIO15 (CS). This is the second set of SPI connectors that the ESP32 supports. GPIO21 (SDA) and GPIO22 (SCL) are used for IIC communication using the Wire library. The Enable (EN) pin serves as the ESP32's reset pin. By setting this pin to LOW, the microcontroller is reset.

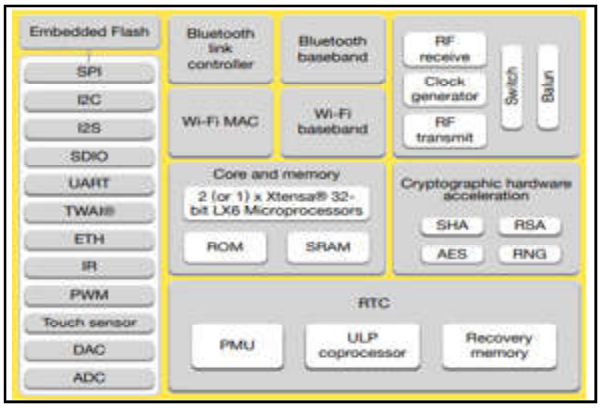

Fig.10 Features of ESP 32 - Link

The external frame of the body is designed using Aluminium Material, based on the purpose and need we have used two different sizes of aluminium frames which are 20*20 for the internal frame which holds the brushes and mover in the Y direction and 20*40 is used for the

outer frame which carries the eternal frame and moves in an X direction. The main reason for choosing the aluminium frame (figure 11) is its weight and its tensile strength. Using this kind of material is also cost-efficient and can withstand the head.

Fig.11 Aluminium Frame 20X40

Similar to the other power suppliers, SMPS (figure 12) transverse AC or DC to DC loads, regulate the power supply and distribute a stable voltage to all connected components. Due to its compact size and structure, it is easily adapted to any already designed model, it prevents a device from voltage fluctuation. Nowadays it is widely used in most electrical and electronic devices such as personal computers, and 3D printers. Two different types of SMPS are used: Mean Well LRS-35-12 and LRS-75-24. LRS-35-12: Mean Well LRS-35-12 is manufactured by a Taiwanese company. They weigh around 3kg. They have an output voltage of 12v and an output of 35-watt. Mean Well LRS-75-24: Mean Well LRS-35-12 is made in Taiwan. They are around 3kg in weight. They feature a 24v output voltage and a 75-watt output.

Fig.12 Switch-mode power supply

For this process, the Rhino ig52 motor is a planetary gear motor (figure 13) with high torque at low speed. High torque is required since the outer frame holds a weight of more than 50kg. They have an rpm of 210 with high efficiency. The Rhino 210 rpm IG52 motor produces 40kgcm of rated torque and 102 kg cm of stall torque. As a result, the motor may be utilised up to 102 kg cm, however, it should not be heated over 45°C. The Rhino IG52 motor's base motor is a high-quality industrial grade 100W 2810 rpm motor, which produces 210 rpm at the output shaft thanks to the strong all-metal planetary gearbox. The torque Volume Ratio is higher than any comparable motor in the category. When compared to other brands of gearbox motors, this one operates quietly. Due to the high-accuracy gearbox, there is very little no-load current. A minimum safety margin of 1.5 times the peak wattage rating is required. For positive coupling applications, a keyway slot and key are supplied on the shaft. The 12mm alloy steel shaft delivers a strong and long-lasting output.

Fig.13 Rhino ig52 planetary motor

This working module bump sensor (figure 14) is used to sense the end of one process and recommence the next process. The bump sensors (bump switch) are digital sensors, with a robot program to perform a variety of tasks. The bump sensor (bump switch) can detect and avoid obstacles. The bump sensor is combined with the limit switch and roller lever. Switch Limit Switches are utilized for Heavy obligation E.O.T. Cranes, Hoists to forestall the movement of raising movement on power and control circuits up to 500 V and 40 Amps. persistent current. The breaking point switch typically stays shut and removes the ability to stop the engine of the crane. As far as possible switch works when it arrives at a foreordained position when the switch is moved over a projecting part fixed on the support. As far as possible switch is fitted with four arrangements of contacts that remove two periods of the engine in one or the other bearing and is appropriate for a 500 V stockpile framework. The breaking point switch contacts are naturally reset when the switch gets back to zero situation because of spring activity. The base and cover have machined surfaces to safeguard against soil and residue.

Fig.14 Bump sensor

V slot wheels (figure 15) are highly used wheels with aluminium frames; it easily runs between the frames and we are also able to control their motion with the screws. These wheels are made up of rubbers it may also withstand heat is one of the main accepts to select. It needs low maintenance; no need for lubricants is also the main advantage. When weight is increased then the moment of the wheel is very smoother. Nowadays it highly uses 3D Printers.

Fig.15 V Slot Wheel

It fits exactly with the aluminium frame. It produces less wear and tear with the aluminium frame (figure 16). Its less weight is one of the reasons to use this. Its metallic body is free from rust and does not get easily oxidised with the environment. The life span of this is very high when we compare it to others. Its drilled slots are used to hold them with the frame so there is no need for some more drilling in the wheels.

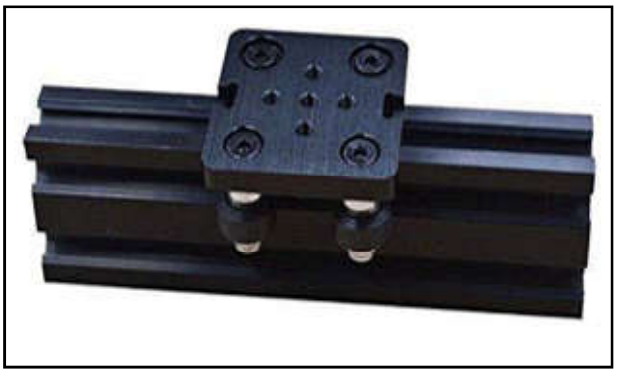

Fig.16 Wheel with aluminium frame

RMCS-1102 (figure 17) is Rhino Motion Controls better than ever DSP-based miniature venturing drive for 1.8deg Bipolar Stepper Motors. It is intended for smooth and calm activity without settling for less force and control at higher paces. It has impeded the engine yields, over-voltage, and under-voltage security. Accomplishes miniature venturing utilizing a coordinated PWM yield drive and high accuracy current criticism and this is totally quiet when the engine is halted or turning gradually. It for all intents and purposes dispenses with halted engine warming paying little mind to drive supply voltage utilizing a DSP-based PID current control circle. Its shut circle control gains are aligned on fire up in view of engine qualities and furthermore changed progressively while the engine is moving. This control calculation makes it equipped for accomplishing better force at higher rates in contrast with equivalent drives in its reach. The PULSE/STEP, DIRECTION inputs are optically disengaged. The two sources of info work with 2.5V, 3.3V or 5V rationale drive signals. The info drive current is 5mA at 2.5V so practically all rational families (74LS, 74HC, and so forth) can be utilized to drive these information sources. Each piece of information gives individual anode and cathode associations with the opt isolator taking into consideration numerous information drive interfaces.

Fig.17 Rhino motor drive

The outer wheel is made up of hard plastics and integrated with bearings for smooth motion in x direction. Moment speed is moderate because of the bearings where else it withstands the heat is the most important factor for this wheel. Its design is easy to attach to the motor and the frame. Its high tensile strength is mainly based on its design (figure 18). Due to its structure and size, it is easily attached to the aluminium frame and it can be easily fixed with the frame. Using ball bearings is also an important feature in the selection of the product.

While that bearing is made up of mild steel it was not easily rested. It is easily adaptable to the external atmosphere.

Fig.18 Outer Wheel

L298n (figure 19) is a motor module drive which simply controls the speed and direction of the DC motors. They have dual H-bridge drive which allows them to control two motors at the same time. They can drive the motor between 5v to 35v, with a peak current of up to 2A. The motor drive module can control up to two or four motors. It is ideal for robotic applications and well-suited for connection to a microcontroller requiring just a couple of control lines per motor. It can also be interfaced with simple manual switches, TTL logic gates, relays, etc. PWM- A DC motor's speed may be adjusted by adjusting its input voltage. PWM is a frequent way of doing this (Pulse Width Modulation). PWM is a technology that adjusts the average value of the input voltage by transmitting a series of ON-OFF pulses. H-Bridge- The spinning direction of a DC motor may be altered by altering the polarity of its input voltage. An H-Bridge is a typical method for accomplishing this. An H-Bridge circuit is made up of four switches, with the motor in the centre, making an H-shaped structure.

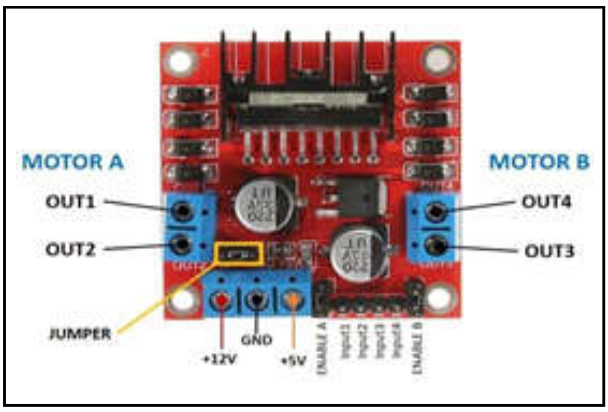

Fig.19 Pin diagram of Motor drive module

Mild steel rod (figure 20) is used to hold the wheel and connect to the motors those rods with a diameter of 12 mm, which has the ability to hold and move the hole setup and are also it made up of mild steel which is more available and rust-free and attached to frame with it is also possible. Microfiber is a synthetic fibre with a diameter of fewer than ten micrometres and a finer thread count than denier or decitex. This is less than the diameter of a silk strand (approximately one denier), which is around one-fifth the diameter of a human hair. Polyamides, Polyesters (e.g. Kevlar, Nomex, trogonidae, nylon) or a combination of polyamide polypropylene and polyester are the most common types of microfibers (figure 21). Microfiber mats, knits, and weaves are utilized in clothing, furnishings, industrial filters, and cleaning products. Softness, toughness, absorption, water repellence, electrostatics, and filtration capacities are all elements considered while determining the size, form and combinations of synthetic fibres. Microfibers were originally popularized in Sweden in the early 1990s, and they became a popular commodity in Europe during the next decade. In cleaning solutions, microfiber can be manufactured wholly of polyester or a combination of polyamide (nylon) and polyester. It can be woven with the latter being the preferred material for single-use or disposable cloths. Throughout the manufacturing process, the fibre is split to form multi-stranded fibres in high-quality fabrics for cleaning. When a cross part of the split microfiber fabric is magnified, an asterisk appears. The split fibres and small individual filament diameters make the cloth more effective than other materials for cleaning. The structure collects and traps dirt while also absorbing liquids. With the exception of certain microsuede mixes, where the surface is manually manipulated to provide a soft plush feel, microfiber leaves no lint. A split microfiber is best for cleaning water-soluble stains and waxes. Microfiber that is on to be split is essentially soft fabric. Threonyl exception is cloths used for facial cleansing and removing sunscreens, skin oils (sebum), and mosquito repellents from an optical surface such as cameras, phones, and eyeglasses, where higher-end proprietary woven, 100% clothes with 2m filaments will absorb these oils without smearing and also it doesn't. In this project, we use a microfiber brush to clean the surface of the solar panel.

Fig.20 MS Shaft Rod 12 mm

Fig.21 Microfiber brush

5. RESULTS AND DISCUSSION

We developed a compact and robust design for the automated solar panel cleaning machine. The frame provided stability and support for the entire system, while the mobile platform allowed the machine to move along the solar panel array. The fabrication process involved sourcing high-quality materials and components, such as durable metals for the frame, reliable motors for movement, and high-pressure water nozzles for effective cleaning. We utilized precision engineering techniques to ensure accurate assembly and alignment of the various components. The fabrication was completed within the specified budget and timeline. To evaluate the performance of the automated solar panel cleaning machine, we conducted a series of tests in real-world conditions. We measured the cleanliness of the panels before and after cleaning using a solar irradiance meter and compared the results. The results demonstrated that the automated cleaning machine effectively removed dirt, dust, and other contaminants from the solar panels. The post-cleaning measurements consistently showed an increase in solar irradiance, indicating improved energy output. The machine successfully reduced the need for manual cleaning, saving time and effort for solar panel maintenance.

6. CONCLUSION

In a bid to significantly enhance the operational efficiency of solar panels and surmount the challenges posed by their maintenance, a cutting-edge automatic solar panel cleaning system has been meticulously designed and developed. This innovative system effectively addresses the issue of undesired debris accumulation on the panel's surface. Employing a sophisticated mechatronics framework, the automated cleaning system executes its tasks with remarkable precision and reliability. It boasts the integration of dual motors, orchestrating seamless movement along both the x and y axes. Complemented by adept wipers and brushes, the system diligently removes dirt and particles, ensuring optimal solar panel functionality. The strategic inclusion of WIFI modules elevates the user experience, simplifying system control and management. In view of the substantial costs associated with manual cleaning procedures, this state-of-the-art automated solar panel cleaning solution emerges as a pragmatic and economically viable choice.

REFERENCES

[1] Amanda Dattalo, "Introduction", ros.wiki.org.

[2] A.Cherubini, F. Spindler and F. Chaumette, "Autonomous Visual Navigation and Laser-Based Moving Obstacle Avoidance", IEEE Transactions on Intelligent Transportation Systems, Vol.15, No.5, 2014, pp.2101-2110.

[3] G.Grisetti, C.Stachniss and W. Burgard, "Improved Techniques for Grid Mapping With Rao-Blackwellized Particle Filters", IEEE transactions on Robotics, Vol.23, No.1, 2007, pp.34-46.

[4] H. Malla, P.Purushothaman, S.V. Rajan and V.Balasubramanian, "Object Level Mapping of an Indoor Environment Using RFID", In 2014 Ubiquitous Positioning Indoor Navigation and Location Based Service (UPINLBS) IEEE, 2014 November, pp. 203-212.

[5] H.I.M.A. Omara and K.S.M.Sahari, "Indoor Mapping using Kinect and ROS", In 2015 International Symposium on Agents, Multi-Agent Systems and Robotics (ISAMSR), IEEE, 2015, August, pp.110-116.

[6] D.M.Turnage, "Simulation Results for Localization and Mapping Algorithms", In 2016 Winter Simulation Conference (WSC) IEEE, 2016, December, pp.3040-3051.

[7] "Obstacle Avoidance with RPLIDAR A2 using ROS", by YohanJoo: This Article Provides A Detailed Explanation Of How To use the RPLIDAR A2 Sensor with the Robot Operating System (ROS) to Perform Obstacle Avoidance.

[8] "Real-Time Obstacle Avoidance with RPLIDAR S2 and Raspberry Pi", by Yuan Gao: This Article Describes How to Use the RPLIDAR S2 Sensor with a Raspberry Pi to Perform Real-time Obstacle Avoidance.

[9] "Obstacle Avoidance Using RPLIDAR and Arduino", by YegorSenin: This Tutorial Shows How to Use An Arduino board and the RPLIDAR Sensor to Perform Obstacle Avoidance.

[10] "RPLIDAR A2M8 and Obstacle Avoidance", by Jon Dahl: This Video Tutorial Demonstrates How to Use The RPLIDAR A2M8 Sensor with A Small Robot to Avoid Obstacles In Real-Time.

[11] "Obstacle Avoidance using ROS and RPLIDAR A1M8", by Keng Yap: This Tutorial Shows How to Use ROS and the RPLIDAR A1M8 Sensor to Perform Obstacle Avoidance.

[12] S. Zaman, W. Slany and G.Steinbauer, "ROS-based Mapping, Localization and Autonomous Navigation Using a Pioneer 3DX Robot and Their Relevant Issues", In 2011 Saudi International Electronics, Communications and Photonics Conference (SIECPC), IEEE, 2011April, pp.1-5.

OPTIMIZED ENSEMBLE CLUSTERING TECHNIQUE TO DETECT THE FAKE NEWS IN SOCIAL MEDIA

M. Pandiyan[1]and S. Logeswari[2]
[1]Department of Information Science and Engineering
Bannari Amman Institute of Technology, Sathyamangalam - 638 401, Erode District, Tamil Nadu
[2]Department of Information Technology,
Karpagam College of Engineering, Coimbatore - 641 032, Tamil Nadu
E-mail:pandiyanm@bitsathy.ac.in, logeswaris@bitsathy.ac.in

Abstract

There is a rapid increase in the internet usage along with the advent of social media websites like Facebook, Twitter, Instagram led to huge information sharing across the world. But not all the information that is shared on social media platforms is reliable. Fake news costs a lot in terms of people's life and money. Categorizing the particular text as misinformation or disinformation is really a difficult and much needed task. In this paper, we propose a model which uses machine learning techniques like GLoVE word embeddings and advanced ensemble approach like stacking for automatic detection of the fake news articles. Based on different textual properties, we train the system and make the model to learn and evaluate their performance.

Keywords: *Ensemble approach, Fake news detection, GLoVE, Online fake news, Stacking.*

1. INTRODUCTION

There is a huge information sharing in social media websites witnessed flourishing of news channels. The news channels greatly gained from the universal usage of social media websites and so they can give streamlined news in real time to people. Initially the news channels dispersed the news only through the newspapers and magazines, but the impact of digital form of news like online news platforms, e-papers, blog posts and other digital media formats [1] made the accessibility much easier. This helps the people to get the latest news (both real and fake news) at very fast rate from any corner of the world. News referrals from Facebook accounted for almost 70% of network usage to news portals [2]. The social media websites play a vital role in spreading awareness among people. It allows the users to suggest their ideas and post their views on the various topics like politics, education, science and health etc. Not only in the positive means but also the social media websites are used for propagating negative ideas by certain entities commonly for their own economic benefits [3, 4] and in many cases for making opinions favorable for a sector, misinformation and disinformation. This trend of information manipulation is generally called as fake news. The information manipulation played a great role in every aspects of a life. Since the last decade, there is a steep increase in the spreading of fake news. It is evidenced from 2016 US elections where the data manipulation (fake news) played a major role. It played a role in deciding the outcome of the election. It was also found that many shooting incident happened in US due to fake news posted in social media sites. Such proliferation of fake articles in the internet and social media websites which broadcasts fake news has led to many issues in politics and also in boarder disputes, riot control, defense sector and sports inc[3]. Another great example of fake news proliferation is seen in case of spread of corona virus and the home remedies which are not accepted by health organizations. This caused misleading to the people. Following the demonetization of Indian currency in 2016, fake news like spying technology in the currency had been shared on various social media websites. And such area affected by fake news is the financial markets, where a rumor can have disastrous consequences and can bring the country's market to a halt. It is evidenced from many financial scams that occur across the world.

There are lot of real time examples where people have reacted preposterously to news which is later realized to be fake. As the ratio of fake news increases gradually every day, it automatically impacts the authenticity of the news. So it is important to take a decision to maintain the authenticity of the news posted in social media.

In this paper, various features of the news were analyzed including the depth, size, breadth and similarity of true and false articles. Mostly the previously done literature had used specific datasets especially political domain datasets. In our system, we use both supervised and unsupervised learning algorithm. This helps to detect the fake articles from any domain. We used GLoVe word embedding for feature extraction and machine learning advanced ensemble method. This advanced ensemble method such that stacking helps to reduce error rate. Also it enables the training phase of the model much efficient.

2. LITERATURE SURVEY

Various computational techniques are used to detect the reliability of the news content. This includes websites like "Politifact'', "Snopes" and "The Quint" etc. which check the reliability of the facts. Similarly there exist a huge number of databases created and maintained by researchers and domain experts to categorize the list of fake websites [5]. But the problem is the specification of domains in that websites, mainly politics excluding other domains like sports, science and technology. S.Vosoughi et al. [6] analyzed the spreading of fake news article in comparison with true news on the internet and social media platforms based on diffusion. Ahmed et al. [7] involved the extraction of textual features such as n-grams from text and to train different Machine leaning models. It included the study of the effect of n-grams size on total performance.

l used various value of n like n=1 (unigram), n=2 (bigram), etc. The models used here are K- Nearest Neighbor (KNN) which depends on the similarities between the words, Support Vector Machine (SVM) which is based on the hyper plane, Logistic Regression (LR) to determine the target value. But the drawback is that when the number of n in n-grams increased, then the overall accuracy decreased. Shu et al. [8] acquired better accuracies by the combination of the features such as linguistic with auxiliary information like user social activity on social media platforms and the trueness of the previous text shared by them. They used various data mining algorithms for features extraction. Primarily we focus on network analyses and linguistic approach.Wang et al. [9] analyzed various textual features and used metadata for training machine learning models. The neural network used Softmax activation function for the processing the input text and to estimate the fake article. The auto tuning of the hyper parameter is done using grid search.

The study by Riedel et al. [10] used stance detection system assigning four labels and term frequency for extracting linguistic properties. Four labels used are agree, disagree, discuss and unrelated. The classification is done by the technique called Multilayer Perceptron Classifier (MLP). Iftikhar Ahmad et al. [11] used different machine learning algorithm using ensemble methods like Bagging and Boosting along with the Voting Classifier. The Voting classifier has three learning models including Logistic Regression (LR), Naıve bayes and KNN models. The Bagging algorithm used 100 decision trees and Boosting is done using XGBoost and AdaBoost. Rishibha Sharma et al. [12] used machine learning algorithms like Global Vectors for Word Representation for word embedding and extracting the linguistic feature and LSTM neural network for the classification to detect the real and fake news articles. The system is based on the co-occurrence of the word and word frequencies.

3. PROPOSED SYSTEM

In our proposed system which is shown in Figure 1, we are aggregating the efficiency of fake news detection by introducing an advanced ensemble technique like stacking along with many linguistic feature sets extracted using GLoVe to detect the reliability and authenticity of the news. Also it classifies as true article or fake article. The novelty of our proposed system is the use of ensemble technique like stacking along with GLoVe. The dataset used in this research are available online and can be extracted from the internet. The steps involved in the proposed system are given below.

Step 1: Data Cleaning and Exploration Phase

- Filter the article's unwanted variables like author name, date, URL and category.
- Remove the article with no subject / article having less than 25 words.
- Remove the stop words like "is", "are", "that" etc. which creates noise to the input data.

Step 2: Extraction of Linguistic Features using GLoVe

- Represent the textual characteristics into numerical value (vector format).
- Obtain the relationship between the similar words and determine the co-occurrence of the words.

Step 3: Create the Model using Advanced Ensemble Techniques

- Split the entire data into training and testing and further split the train data into 10 stacks.
- Group the 10 stacks into 2 groups and use 2 different voting classifiers.
- Create the base models using voting classifier algorithms.
- The first voting classifier has 2 learning models :
  - i. Logistic Regression
  - ii. Random Forest
- The second voting classifier has 2 learning models :
  - i Linear SVM
  - ii K Nearest Neighbor
- From these 2 base models, predict the final Meta model.
- Train the model
- Detecting whether the news article is fake or not using testing data.

The below Figure 1 illustrates the proposed model.

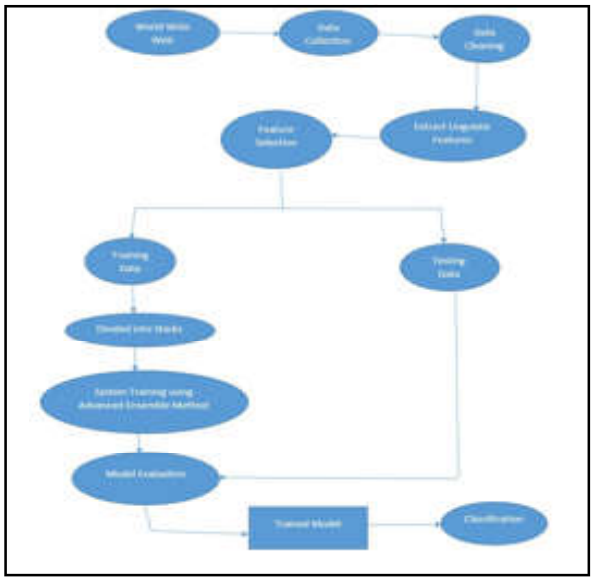

Fig.1 Proposed model architecture

4. ALGORITHMS USED IN THE SURVEY

4.1 Data Cleaning and Exploration

The process of presetting or removing incorrect, corrupted, inappropriately configured, duplicate, or incomplete data within a data file is known as data cleaning. It is the first step involved in the data analysis. Usually the data repetition and replication can be identified with this process. Also the existence of null values if any can be tracked easily and removed for achieving better accuracy. The completeness of the data, correctness of the data are ensured. It includes both manual as well as automated tools. Manually it is done using data analysis and automated tools like Trifacta, Qlikview etc,.

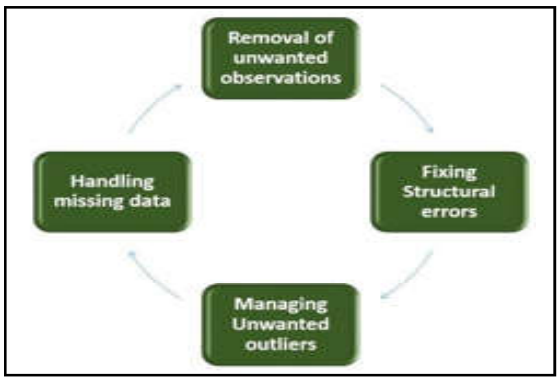

Fig.2 Data cleaning

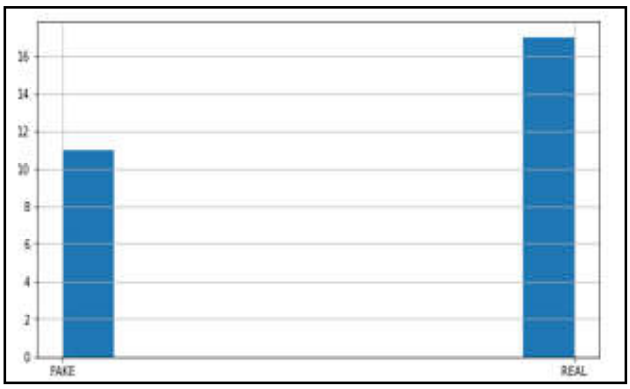

Fig.3 Data exploration of sample data

4.2 Global Vectors for Word Representation (GLoVe)

GLoVe is an unsupervised learning algorithm which is used for getting vector representations for the words (mathematical expressions for the words). Training of the system involves on the agglomerated global word-word co-occurrence on the data. The linear substructures of the word in vector space are represented in the resulted embeddings.

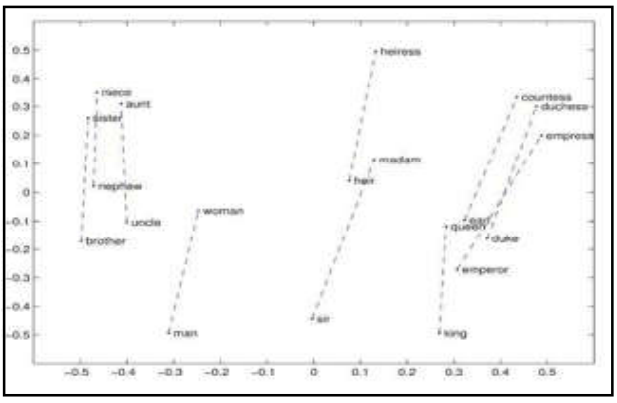

Fig.4 Linear substructures of the word

4.3 Advanced Ensemble Technique

The process of combining and using multiple models including classifiers or experts to generate strategically suitable solution to solve the intelligence problems is known as advanced ensemble method. It is specifically used to improve the (classification, prediction, function approximation, etc.) overall performance of the system, or to reduce the possibilities of choosing a poor model.

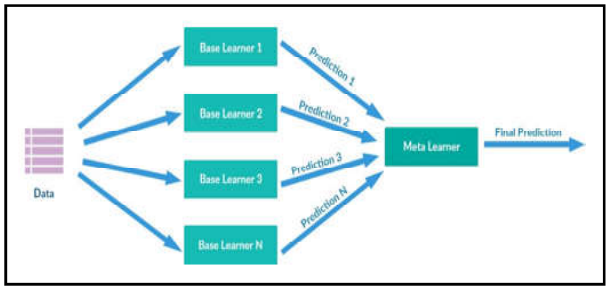

Fig.5 Advanced ensemble method

4.4 Stacking

Stacked generalization or stacking is a type of advanced ensemble techniques. The system is trained by combining the previous model predictions. In the stacking, the trained data is divided into different stacks (smallest data sets). Each stack is processed using different models. All of these models are called base models and from these predictions, we generate a final model. It is illustrated in the following figure 6.

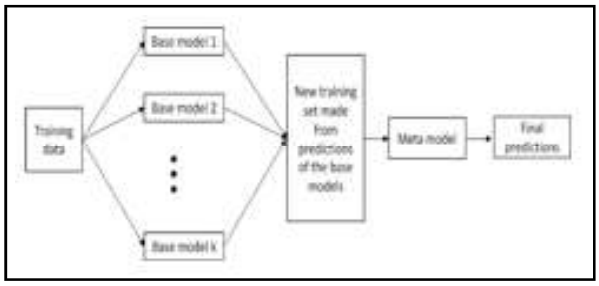

Fig.6 Stacking

4.5 Voting Classifier

The machine learning model which trains the ensemble of various algorithms and chooses the optimal methods to get the better model is known as voting classifier. It usually employs multiple classifiers to achieve high accuracy in prediction. A voting ensemble involves summing the predictions made by various classification models or averaging the predictions made by some of the regression models.

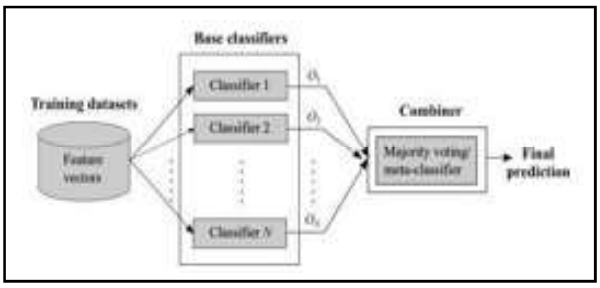

Fig.7 Voting classifier

5. RESULTS AND ANALYSIS

The results were represented in the below mentioned graphs. Initially we used the individual algorithm and then used voting classifiers which gave accuracies better than individual algorithm. In the similar way, we included advanced ensemble method, stacking into the system which could produce better accuracies. The accuracy achieved by the individual algorithms and the voting classifiers which are using combination of algorithms before the stacking of the input data is represented in the below figure8. From this figures, we can assume that using voting classifiers could get better results. We have used two voting classifiers which combined algorithms namely Logistics Regression and Random Forest and Linear SVM and K-Nearest neighbor can produce accuracy rate of 92% and 80% respectively.

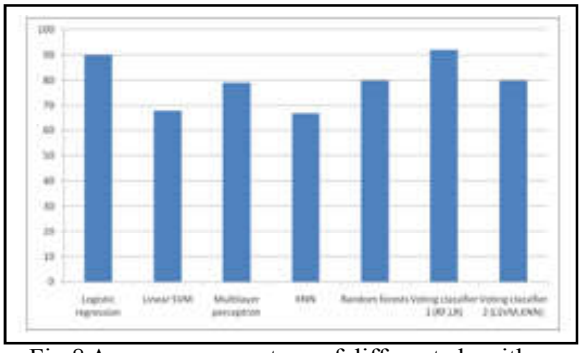

Fig.8 Accuracy percentage of different algorithm

Then we used the stacking method for the training data and compute a final model based on the individual base models. Here we can achieve accuracy rate which is better as compared to non stacked inputs. It is estimated that the using the voting classifier1 (LR, RF) on the stacked input data get the accuracy rate of 94% and using voting classifier2 (LSVM, KNN) on the stacked input data get the accuracy rate of 82%. It is represented in the figure9.

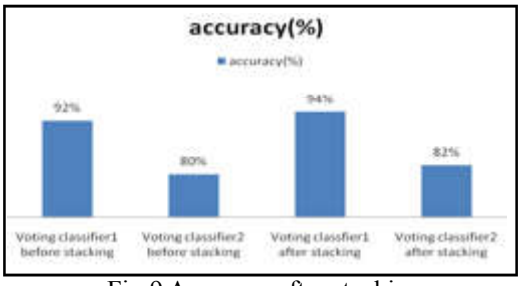

Fig.9 Accuracy after stacking

Thus the simple algorithm could be effectively used to achieve better models by the advanced ensemble machine learning technique. Similarly the voting classifier can be used for any type of learning algorithms.

6. CONCLUSION

In order to classify the news article based on their reliability requires a deep knowledge about the domain and also there is need for the experts to identify the inappropriate news articles. Around 65% of US adult population depends on the social media platforms for daily news update. Similarly the growth of social media platforms in the developing countries has been evidenced in the recent years. So the news on the digital platforms played an important role in designing people ideas and decision making. In this paper, we had implemented machine learning techniques to classify the news articles as real or fake from various domains. The process initially involves the data cleaning and extracting the linguistic features. This feature set is used as the feed to the model and the model is trained using advanced ensemble technique like stacking. In order to classify the news article based on their reliability requires a deep knowledge about the domain and also there is need for the experts to identify the inappropriate news articles. Around 65% of US adult population depends on the social media platforms for daily news update. Similarly the growth of social media platforms in the developing countries has been evidenced in the recent years. So the news on the digital platforms played an important role in designing people ideas and decision making. In this paper, we had implemented machine learning techniques to classify the news articles as real or fake from various domains. The process initially involves the data cleaning and extracting the linguistic features. This feature set is used as the feed to the model and the model is trained using advanced ensemble technique like stacking. We can thereby achieve the higher accuracy and better score on the performance metrics. We used the base models as the feed to compute the final Meta model. We can thereby achieve the higher accuracy and better score on the performance metrics.

Fake news detection is a developing research area with only few numbers of datasets which are available in the open environment. We make use of our proposed system on an existing dataset. From the performance of our system, it is evidenced that the performance of our system outperforms the other approaches which are published by the different authors. In the future, we can further increase the accuracy rate by using different leaning methods in the used voting classifiers.

REFERENCES

[1] Douglas, "News Consumption and the New Electronic Media", 7e International Journal of Press/ Politics, Vol.11, No.1, 2006, pp. 29-52.

[2] J. Wong, "Almost All the Traffic to Fake News Sites Is From Facebook, New Data Show", 2016.

[3] D. M. J. Lazer, M. A. Baum and Y. Benkler,*et al*., "The Science of Fake News", Science, Vol. 359, No.6380, 2018, pp.1094-1096.

[4] S.A.Garc´ża, G.G.Garc´ża, M.S.Prieto, A.J.M. Guerrero and C.R. Jim´enez, "The Impact of Term Fake News on the Scientific Community Scientific Performance and Mapping in Web of Science", Social Sciences, Vol.9, No.5, 2020.

[5] F.T.Asr and M.Taboada, "Misinfotext: A Collection of News Articles, With False and True Labels", 2019.

[6] S. Vosoughi, D.Roy and S. Aral, "The Spread of True and False News Online", Science, Vol. 359, No.6380, 2018, pp.1146-1151.

[7] H.Ahmed, I.Traore and S. Saad, "Detection of Online Fake News Using N-Gram Analysis and Machine Learning Techniques", in Proceedings of the International Conference on Intelligent, Secure, and Dependable Systems in Distributed and Cloud Environments, Springer, Vancouver, Canada, 2017, pp.127-138.

[8] K.Shu, A.Sliva, S.Wang, J.Tang and H. Liu, "Fake News Detection on Social Media", ACM SIGKDD Explorations Newsletter, Vol.19, No.1, 2017, pp.22-36.

[9] W. Y. Wang, Liar, Liar Pants on Fire: A New Benchmark Dataset for Fake News Detection, Association for Computational Linguistics, Stroudsburg, PA, USA, 2017.

[10] B. Riedel, I. Augenstein, G. P. Spithourakis and S. Riedel, "A Simple but Tough-To-Beat Baseline for the Fake News Challenge Stance Detection Task", 2017, https://arxiv.org/abs/1707. 03264.

CARDIO VASCULAR DISEASE PREDICTION USING FUZZY LOGIC EXPERT SYSTEM

Vaanathi, Steephan Amalraj, V.S.Raj kumar, M. Pravin savaridass and N.P. Satheesh
Bannari Amman Institute of Technology, Sathyamangalam - 638 401, Erode District, Tamil Nadu
E-mail: vaanathi@bitsathy.ac.in, rajkumarvs@bitsathy.ac.in

Abstract

Cardiovascular disease is a term used to describe a variety of heart diseases, illnesses, and events that affect the heartand circulatory system. The aim of this study is to design a fuzzy expert system for heart disease diagnosis. The neuro- fuzzy system was designed with eight input fields and one output field. The input variables are heart rate, blood pressure, age, cholesterol, chest pain type, blood sugar, exercise, and sex. The output detects patients' risk levels, which are classified into 4 different categories: very low, low, high, and very high. The data set was extracted from the UCI machine learning repository and pre-processed to make it appropriate for the training, then the initial FIS was generated. Then the network was trained with the set of training data after which it was tested and validated with the set of testing data. The output of the system was designed in a way that the patient can use it personally. The patient just needs to supply appropriate values which served as input to the system and based on the values supplied, the system will be able to predict the patient's risk level. FIS is a combination of neural networks and adaptive neuro-fuzzy. The results obtained from the system are compared with the SVM classifier. The system has been tested and the result showed over 90% accuracy, it has beenshown that neuro-fuzzy is suitable and feasible to be used as a supportive tool for disease diagnosis.

Keywords: *Cardiovascular Disease, FIS, Fuzzy Logic, FuzzyExpert System*

1. INTRODUCTION

1.1 Big Data

Big data is an emerging area, which handles large collections of voluminous complex data. Big data may be both structured and unstructured data. These data are not easily processed using traditional methods. Traditional databases handle only structured and limited amounts of data because they are centralized [1]. The unstructured data sources used for big data analytics may not fit in traditional data warehouses. Furthermore, traditional data warehouses may not be able to handle the processing demands posed by big data. As a result, a new class of big data technology has emerged and is being used in many big data analytics environments. Big data analytics is often associated with cloud computing because the analysis of large data sets in real- time requires a platform like Hadoop to store large data sets across a distributed cluster and Map Reduce to coordinate, combine and process data from multiple sources[2].

Although the demand for big data analytics is high, there is currently a shortage of data health care analytics, scientists, and other analysts who have experience working with big data in a distributed, open- source environment. Appropriate computer-based information and/or decision support systems can aid in achieving clinical tests at a reduced cost[3]. This project aims to analyze the different predictive/ descriptive analytic techniques proposed for the diagnosis of heart disease.

1.1.1 Clinical Data Analytics Using Big Data Analytics

Big data analysis can help clinicians and organizations deliver higher quality and cost-effective care to patients[4]. Big data can lead to the development of an anticipatory healthcare system, where providers can create personalized evidence-based medicine, tailored to patients' personal prevention profiles, social determinants of health, and even preferences for how, where, and when they want to receive care [5]. It can help to identify both public health threats and safety issues. Big data can help researchers to understand health more than ever before. In addition, they can also understand the factors that affect it, as well as determine what treatments are most effective for particular

conditions. Most importantly, it can help patients better understand their own health and more effectively navigate and access the healthcare systems [6].

Using big data, analysts can implement predictive models and statistical methods to predict risks or trends to help healthcare providers target core in ways that improve outcomes and save money. Some healthcare organizations are already using predictive models to help customize care in ways that improve outcomes and prevent unnecessary utilization [7]. Even though it possesses a lot of advantages, there are some barriers and challenges to the effective use of big data in health care. It includes a failure to adopt existing data standards to assure interoperability across settings, a lack of willingness to engage in information sharing, concerns about privacy and security, a lack of tools to help both clinicians and patients take advantage of data, and the need to build a culture in medicine that integrates the use of data in a practical way[8].

1.2 Cardiovascular Disease

Cardiovascular disease (CVD) is the world's leading cause of morbidity and mortality. The results of the global burden of disease study show that ischemic heart disease was the leading cause of disability-adjusted life years in 2010. In many countries, obesity is likely to overtake tobacco as the leading risk to health by 2016[9]. The ability to integrate data from multiple sources and across many variables has significant potential for the evaluation and treatment of patients. These methods enable deeper characterization of a particular patient and more precise mapping to similar patients in pertinent subpopulations. Efficient characterization of subpopulations requires data harmonization, new analytical algorithms, and analysis of heterogeneous data [10]. This approach relies on data-sharing infrastructure and high- throughput database resources in large epidemiological studies as well as in small experimental studies, which would otherwise require a large cost or effort to reproduce[11].

Heart and blood vessel diseases called cardiovascular diseases include numerous problems, many of which are related to a process called atherosclerosis. Atherosclerosis is a condition that develops when a substance called plaque builds up in the walls of the arteries[12]. When a heart attack occurs, the speed of detection and quick intervention is essential to save the heart attack patient's life and prevent heart damage. Nowadays, the use of computer technology in medicine has greatly increased[13].

1.2.1 Heart Disease Prediction

In the biomedical field data mining plays an essential role in the prediction of diseases. In biomedical diagnosis, the information provided by the patients may include redundant and interrelated symptoms and signs especially when the patients suffer from more than one type of disease of the same category [14]. The physicians may not able to diagnose it correctly.

The use of intelligent systems such as neural networks, fuzzy logic, genetic algorithm, and neuro-fuzzy systems has highly helped in complex and uncertain medical tasks such as the diagnosis of diseases [15].

A heart disease prediction system can assist medical professionals in predicting heart disease status based on the clinical data of patients. In the biomedical field data mining plays an essential role in the prediction of diseases[16]. The information provided by the patients may include redundant and interrelated symptoms and signs especially when the patients suffer from more than one type of disease of the same category [17].

Data mining with intelligent algorithms can be used to tackle the problem of prediction in medical datasets involving multiple inputs [18]. Now a day's Artificial neural network has been used for complex and difficult tasks. The neural network is trained from historical data with the hope that it will discover hidden dependencies and that it will be able to use them for prediction. The forward neural networks trained by back-propagation have become a standard technique for classification and prediction tasks[19].

1.2.2 Neuro-Fuzzy Systems

The first stage in the formation of the neuro-fuzzy system is the development of FIS which was trained using a neural network algorithm. The algorithm used in training the FIS is back propagation gradient descent in combination with least squares estimate method. When a heart attack occurs, the speed of detection and quick intervention is essential to save the heart attack patient's life and prevent heart damage. Nowadays, the use of computer technology in medicine has greatly increased [20]. The use of intelligent systems such as neural networks, fuzzy logic, genetic algorithm, and neuro- fuzzy systems has highly helped in complex and uncertain medical tasks such as the diagnosis of diseases [21].

Over the last few decades, neural networks and fuzzy systems have established their reputation as alternative approaches to intelligent information processing systems. Both have certain advantages over classical methods, especially when vague data or prior knowledge is involved. Therefore, combinations of neural networks with fuzzy systems have been proposed, where both models complement each other[19].

Neuro-fuzzy hybridization results in a hybrid intelligent system that synergizes these two techniques by combining the human-like reasoning style of fuzzy systems with the learning and connectionist structure of neural networks [20]. The basic idea of combining fuzzy systems and neural networks is to design an architecture that uses a fuzzy system to represent knowledge in an interpretable manner and the learning ability of a neural network to optimize its parameters [21].

1.3 Problem Statement

Heart disease prediction is accomplished using the FIS. The basic idea of combining fuzzy systems and neural networks is to design an architecture that uses a fuzzy system to represent knowledge in an interpretable manner and the learning ability of a neural network to optimize its parameters[22].

This can assist medical professionals in predicting heart disease status based on the clinical data of patients. and not as an independent document. Please do not revise any of the current designations[21].

2. LITERATURE SURVEY

2.1 Fuzzy Expert System for Heart Disease Diagnosis

Sanjeev Kumar *et.al.* [23] have proposed work on the Detection of Heart Disease using Fuzzy logic offering the fuzzy inference that evaluates the control rules stored in the fuzzy rule base. Defuzzification is a process to convert the fuzzy output values of fuzzy inference to real crisp values. First, a typical value is computed for each term in the linguistic variable and finally, the best compromise is determined by balancing out the results using different methods like the center of sum, the center of the area, and the mean of maximum. This system used the centroid method to process the defuzzification of the output variables. Then the designed system has been tested with domain experts. From the developed system one can check whether a person has any chance of getting a heart disease risk or not. This is one of the simple and more efficient methods for the diagnosis of heart disease analysis.

This fuzzy logic-based system performed better and produced improved results in comparison with the other systems designed for heart disease prediction [7]. The results obtained from the system are compared with the data and the observed results of the designed system are correct in 92%.

Ali Adeli. *et.al* [23] have implemented work on Fuzzy Expert System for Heart Disease Diagnosis. The aim of this study is to design a Fuzzy Expert System for heart disease diagnosis. The system has 13 input fields and one output field. Input fields are chest pain type, blood pressure, cholesterol, resting blood sugar, maximum heart rate, resting electrocardiography (ECG), details of the exercise, old peak, thallium scan, sex, and age. In the healthcare industry, data mining is mainly used for predicting diseases from datasets. The system is implemented with the main objective of getting improved performance by using a fuzzy expert system through different classification techniques available for heart disease prediction.

2.2 Data Mining Techniques Using a Neuro- Fuzzy System

A.Q. Ansari *et. al.* [19] have performed work on Automated Diagnosis of Coronary Heart Disease Using a Neuro-Fuzzy Integrated System. Computational intelligence combines fuzzy systems, neural networks, and evolutionary computing. In order to show the effectiveness of the proposed system, simulation for automated diagnosis is performed by using the realistic causes of coronary heart disease. The empirical results have revealed that this kind of hybrid system is suitable for the identification of patients with high/low cardiac risk.

A novel hybridized approach for Heart Disease Diagnosis using Data Mining and Fuzzy Logic was implemented by Nidhi Bhatla *et. al.* [20]. Cardiovascular disease is a term used to describe a variety of heart diseases, illnesses, and events that impact the heart and circulatory system. A clinician uses several sources of data and tests to make a diagnostic impression but it is not necessary that all the tests are useful for the diagnosis of heart disease. The objective of this work is to reduce the number of attributes used in heart disease diagnosis

that will automatically reduce the number of tests that are required to be taken by a patient. This work also aims at increasing the efficiency of the cardiovascular prediction system.

A.V. Senthil Kumar [21] has performed work on the diagnosis of heart disease using an Advanced Fuzzy Resolution Mechanism to represent the models in the real world the concept of a fuzzy set is used as an adaptive neuro- fuzzy inference system and the Neural network approach is used to design fuzzy inference system. The neural network uses learning and adaptation that makes the fuzzy system less dependent on the knowledge of experts. A neural network algorithm was developed with a nonlinear physiological system neural network and fuzzy logic approaches. The most common classifier technique is artificial neural networks; the reason for being common is that it uses learning from generalized capability beyond the training dataset. Granular support vector machines are a new learning model, and their accuracy rates are given as 83.04% and 84.04% for SVM and Message Digest 5 (MD5) respectively. This system is implemented to with the heart disease datasets using an artificial neural network and fuzzy neural network. This system is also tested and validated with diabetes disease data sets and the empirical results have shown that it has produced better results. To predict the parameter of numeric and categorical inputs new ANFIS was designed. Adaptive neuro- fuzzy inference system developed to estimate blood pressure. To diagnose heart patients an Adaptive Neuro-Fuzzy Inference System was also developed using the clustering technique.

2.3 Clinical Decision Support System for Heart Disease

Syed Umar Amin, *et.al* [23] have performed work on data mining technique-based Clinical Decision Support Systems for the Diagnosis, Prediction, and Treatment of Heart Disease. With the help of this study, the authors have concluded that there is a large amount of data available in medical institutions, but this data is not properly used. This medical data lacks quality and completeness. Hence, preprocessing techniques and highly sophisticated data mining techniques are required to build up an efficient decision support system. The studies have revealed the fact that the system should be built not only based on accuracy and reliability but also on reduced cost of treatment and increase patients care. In addition, the built systems should be easy to understand to enhance human decisions. The authors have also suggested that the work should be performed for proposing treatment plans for patients. Data mining techniques have shown significant success in the prediction and diagnosis of diseases. Many data mining-based systems are designed exclusively for heart disease management and have proven that they are successfully tested and validated. Hence, these techniques could be applied for diagnosis, treatment for cure, and medications.

D. P. Shukla *et. al.* [24] have performed work on data mining technique-based prediction of coronary heart disease. This system is also using Neuro-Fuzzy integrated approach in two levels. In this work, the authors have designed a system that could identify the chances of coronary heart disease. The neuro-fuzzy system divided all the parameters into two levels. According to the criticality of the parameter and assigned each level has a separate weightage. Finally, both levels are taken into consideration to arrive at a final decision. This system has a very low error rate and its work efficiency is high. The authors have concluded that this approach can be used to perform for varying data sets of different diseases.

2.4 Anfis-Based Model for Heart Disease

Allahverdi, *et.al* [22] have designed a fuzzy expert system for the determination of coronary heart disease risk the literature about the use of intelligent methods in the medicine domain has seen an enormous number of related studies in ANFIS [16]. On the other hand, fuzzy logic and neural networks are standing as good methodologies for dealing with these uncertainties. The data and prior knowledge are utilized and both of them have certain advantages over the other classical methods. At this point, neuro-fuzzy integration presents a hybrid intelligent system that combines the power of the human-like reasoning style of fuzzy logic with the structure of neural networks. Moreover, ANFIS is one of the hybrid neuro-fuzzy inference expert systems and it works with the fuzzy inference type systems. The ANFIS method provides a fuzzy modeling procedure to learn information about a data set, in order to calculate membership function parameters which allows the associated fuzzy inference system to track the given input/output data. ANFIS-based model for Heart Disease Prediction, Iman Askerzade *et.al* [15]. This work suggests a technique for the classification of heart diseases for helping patients to early predict and reliable diagnoses. Adaptive Neuro-Fuzzy Inference System has been used for classification

which has both the advantages of neural network and fuzzy logic. In the proposed model, training and average testing errors are 0.01 and 0.15 which are very satisfying. The experimental results show that the proposed technique has high accuracy, especially when compared with other studies that use the same database of heart disease. Therefore, this model is an appropriate model for the classification of heart diseases.

2.5 Classification of Heart Diseases Using Neural Networks

The application of an Artificial Neural Network can be time-consuming due to the selection of input features for the Multi-Layer Perceptron (MLP). The number of layers and the number of neurons in each layer were also determined by the input attributes. D. Shanthi [19] has proposed a neuro- genetic approach to feature selection in disease classification. Each of the input neurons connects to each of the hidden neurons, and each of the hidden neurons connects to the output neuron. The Back Propagation algorithm in particular adaptively changes the internal network. Here, free parameters are trained and a neural network can make predictions [21]. MLP is trained with the Back Propagation algorithm which suffers from the disadvantage of the high number of parameters that need to be tuned, like learning rate, number of neurons, and momentum rate.

The fuzzy neuro expert system with genetic feature reduction is used for the diagnosis of heart disease [20]. This system will help doctors to arrive at a decision about the presence or absence of heart disease in patients. The main drawback of this system is the training time and complexity. The offline training of the neural network can be performed to reduce the time complexity. In the final model, the feature subset selection process is performed in order to select the most significant attributes which are extracted to predict the results accurately [21].

3. EXISTING SYSTEM

3.1 Descripption

The heart disease data warehouse contains the clinical data of heart patients. Initially, the data warehouse is preprocessed to make the mining process more efficient. The Heart attack dataset used was obtained from the UCI machine learning repository [23]. Data preprocessing is performed to remove the number of inconsistencies that are associated with the data. This proposed work utilized improved data sharing and user identification schemes. For identification, the MD5 algorithm can be implemented to generate the signatures and used them as the identity for each user. It can be used as a cryptographic function and to produce a 128-bit hash value which can be expressed in text format as a 32-digit hexadecimal number [24]. Each user has a hash signature at the user authentication and is difficult to identify by third- party attackers.

To label the data and predict the results, the SVM classification algorithm is used. This work is intended to design and develop a diagnosis and prediction system for heart diseases based on predictive mining. The experiments have been conducted a number of times repeatedly to evaluate the performance of the system. The related techniques used for evaluation include decision trees and various predictive data mining-based Nad've Bayes algorithms [21].

3.2 Methods

In SVM, the input space is planned into a high-dimensional feature space. Then, the hyperplane that exploits the margin of separation between classes is constructed. The points that lie closest to the decision surface are called support vectors directly to involve their location. Then for data sharing, the k-anonymity techniques are used [16]. Data sharing is making for w the data which is used for scholarly research available to other investigators. An exponential growth in the number and variety of data collection containing person-specific information and collection of data is beneficial both in research and business.

K-anonymity is a framework for constructing and evaluating algorithms. In addition, this framework is responsible for the release of information and limits what can be revealed about the properties of entities to be protected[24]. Based on these results, it can be understood that the data can be used to identify the person with suppressed results for improving security. This can be implemented in this process in real-time with CVD datasets with large volumes successfully.

3.3 Drawbacks of the Existing System

- There is no security data sharing
- Authentication process becomes overhead in computation
- Only analyzed heart-related textual data

4. PROPOSED SYSTEM

4.1 System Architecture

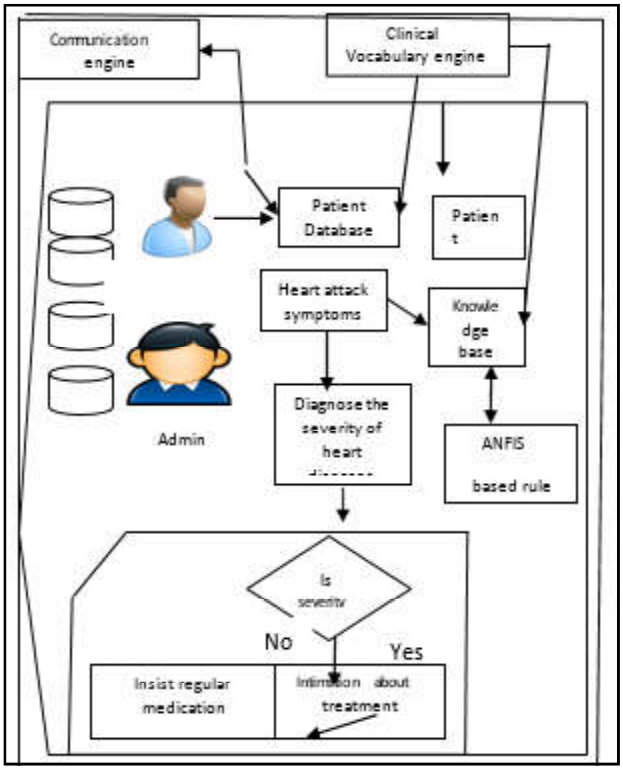

Fig.1 System Architecture

The components of this architecture are fuzzification, advanced fuzzy resolution mechanism and defuzzification. Rule base is the significant component in the fuzzy inference system. The quality of a fuzzy system depends on the fuzzy rules. Membership functions are used to retranslate the fuzzy output into a crisp value. This method is known as defuzzification. The fuzzy inference evaluates the control rules stored in the fuzzy rule base. defuzzification is a process which is used to convert the fuzzy output values of fuzzy inference to real crisp values. First, a typical value is computed for each term in the linguistic variable and finally, the best compromise is determined by balancing out the results using different methods like the center of sum, the center of the area, and the mean of maximum. But for this application, the centroid method is used to process the defuzzification of the output variable extension time. This method is the mostly used one because it has better performance and accuracy.

4.2 Mathematical model

4.2.1 Adaptive Neuro-Fuzzy Inference System

The ANFIS is a framework of adaptive techniques to assist learning and adaptation [28]. To illustrate the ANFIS architecture, two fuzzy if-then rules according to the first- order Sugeno model are considered:

Rule 1: if(x is A1) and (y is B1) then (f1=p1x+q1y+r1)

Rule 2: if(x is A2) and (y is B2) then (f2=p2x+q2y+r2)

where x and y are nothing but the inputs, Ai and Bi represent the fuzzy sets, fi represents the outputs inside the fuzzy region represented by the fuzzy rule, and pi, qi, and ri indicate the design parameters that are identified while performing the training process. The ANFIS architecture to execute these two rules is represented, in which a circle represents a fixed node and a square represents an adaptive node.

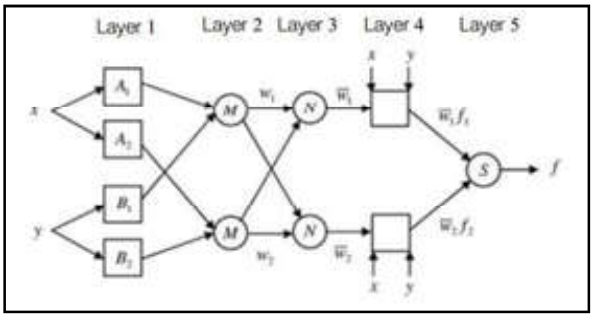

Fig.2 ANFIS architecture

Layer 1: Fuzzification layer: Every node in layer 1 is an adaptive node. The output layer 1 is the fuzzy membership grade of the inputs, which are given by:

Where can accept any fuzzy membership function?

$$\mu_{Ai}(x) = \frac{1}{x\text{-}c_{ib}} \quad (1)$$

where a_i, b_i, and c_i represent the parameters of the membership function, controlling the bell-shaped functions consequently.

Layer 2: Rule layer a fixed node labeled M which multiples the incoming signals and send the product out. Each node output represents the firing strength of the rule. The outputs of this layer can be represented as:

$$O_i^2 = W_i = \mu_{Ai}(x)\mu_{Bi}(y) i = 1,2 \quad (2)$$

Layer 3: Every node in this layer is a circle labeled N. The ith node calculates the ratio of the ith rule's firing strength to the sum of all rule's firing strengths [5]. The output of this layer is called normalized firing strengths.

$$O_i^3 = \widehat{W_i} = \frac{W_i}{W_1+W_2} \; i = 1,2 \quad (3)$$

Layer 4: In this layer, the nodes are adaptive nodes. The output of each node in this layer is simply the product of the normalized firing strength and a first-order polynomial, where ţ is the output of layer 3 and {pi, qi, ri} is the parameter set. Thus, the outputs of this layer are given by:

$$O_i^4 = \overline{W_i} f_i = \overline{W_i}(p_i x + q_i y + r_i \; i - 1,2 \quad (4)$$

Parameters in this layer will be referred to as consequent parameters

Layer 5: The single node in this layer is a circle node labeled Ó that computes the overall output as the summation of all incoming signals, i.e.,

$$O_i^5 = \text{overall output} = \sum_{i=1}^{2} \overline{W_i} f_i = \frac{\sum_{i=2}^{2} w_i f_i}{w_1 + w_2} \qquad (5)$$

4.2.2 Hybrid Learning Algorithm

The hybrid learning rule used the gradient method and the least squares estimate (LSE) to identify and update parameters [17]. Each of the hybrid learning procedures is composed of a forward pass and a backward pass.

- FORWARD PASS

In the forward pass of the hybrid learning algorithm, the functional signal goes forward until layer 4 and the consequent parameters are identified by the least squares estimate.

- BACKWARD PASS

In the backward pass, the error signals propagate backward and the premise parameters are updated by gradient descent. The chain rule is used to calculate the partial derivatives used to update the membership function parameters.

4.2.3 Neuro-Fuzzy Model Development

The first stage in the formation of the neuro-fuzzy system is the development of FIS, which was trained using a neural network algorithm [20]. During the training process, the membership function parameters were adjusted and this allowed the fuzzy system to learn from the data they were been modeled. The fuzzy rules for heart disease detection were generated using the set of input and output [24]. Because decisions are based on the testing of all of the rules in a FIS, the rules were combined in some manner in other to make a decision; this was done during the aggregation process by combining the fuzzy sets that represent the output of each rule into a single fuzzy set.

5. RESULTS AND DISCUSSION

The classification ensemble method produces better accuracy than the other classifiers which are used in medical data mining. The authors [20] have performed a comparative analysis of different algorithms. The main drawback of this algorithm is security, which arises from inpatient data.

Classification technique is the most widely used in healthcare to predict diseases. ID3, classification, and MD5 are used for cardiovascular diseases majorly [21]. They used a measurement dataset, which is retrieved from UCI machine learning. Evaluation of the actual re-identification probability of k anonymized data sets. For one of the re-identification scenarios, k-Anonymity consistently over anonymized data sets [24].

Various experiments were performed and the sizes of the training and testing data sets were determined by taking into consideration the accuracies of the system. The data set used was divided into two; the training data and the testing data, 80% of the data set were used for training while the remaining 20% was used for testing [18]. The training data set was used to train the model while the testing data set was used to verify the accuracy and the effectiveness of the trained Model for the diagnosis of a heart attack.

Table 1 Classification Accuracy of Different Classifiers

ALGORITHM	ACCURACY (in %)
MD 5	75
ANFIS	80
Fuzzy Inference	79.6
Neural Networks	83
SVM	78.8

From figure 3, it is understood that the Neural Network algorithm has shown better accuracy when compared to other classification algorithms.

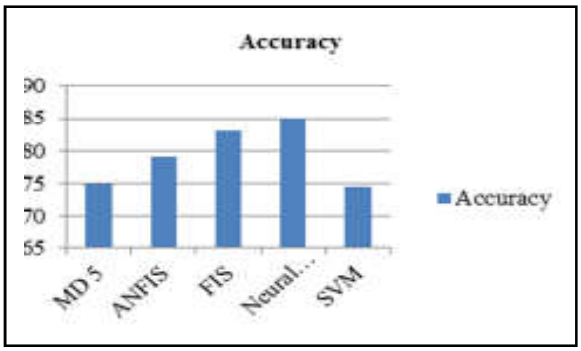

Fig.3 Classification of different classifiers

If the values of the attributes or inputs are high, then the patient has a high risk and if the values or inputs are low then the patient has a low heart risk [19]. And similarly, if the values are normal then the results show that the patient is normal. Then the system can be tested with the following values for each field and graphical result. If the values of the inputs lie in their low ranges, then the risk is also low that is the result is of minimum value. Similarly, for the high values of the input [20].

Table 2 Classification of Testing Data

Chest pain	Cholesterolmax	Heart rate	Blood pressure	Blood sugar	Old peak	Result
0	100	70	60	50	0	0.07
0.1	155	78	75	83	0.1	0.1
0.16	158	83	80	95	0.5	0.25
0.5	250	85	130	121	0.8	0.5
0.1	281	125	150	135	0.85	0.75
0.89	353	131	190	231	9	0.77
1	400	150	180	235	0.89	0.81

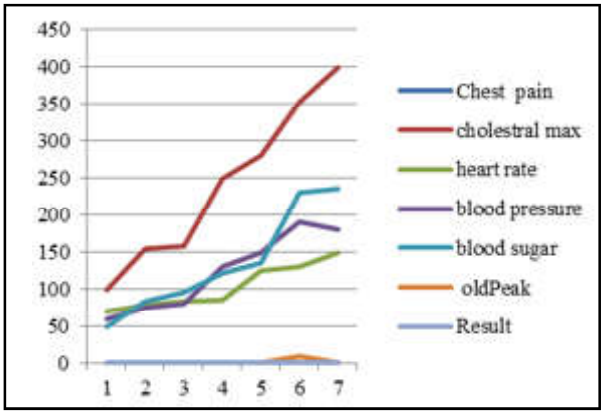

Fig.4 Results of prediction

Fuzzy Expert System for Heart Disease Diagnosis designed with follow membership functions, input variables, output variables and rule base. In this system there are 6 inputs or input variables and two output variables [21]. In this system, one can check whether a person have any heart disease risk or not. This is one of the simple and more efficient method for the diagnosis of heart diseases analysis [24]. This system was designed with fuzzy base to improved results.

6. CONCLUSION

To diagnose, the heart disease Big Data based Fuzzy Inference System for the big heart data was developed. The UCI Machine Learning heart disease dataset is used to test the developed system. Crisp values are converted into fuzzy values in the stage of fuzzification. Advanced Fuzzy Resolution Mechanism has five layers, membership function, fuzzy if-then rules, and output variables for the fuzzy model are predicted using fuzzy predicted value to improve the accuracy of the result. The outputs from the Advanced Fuzzy Resolution Mechanism are fuzzy values. By the defuzzification process, the fuzzy values are converted into crisp values of angiographic disease status. The proposed system has better performance with an accuracy of 83% which is compared with the related algorithms SVM and MD5. The problem with using these databases is there is an inaccuracy in data that makes searching for some information impossible. In the proposed fuzzy system, we use the same data to build fuzzy rules. Experimental results on real-world datasets have demonstrated that this approach has improved the scalability and privacy of data sets significantly over the other related approaches. The advantage of the developed system is that it can be used to the available data existing in the current database systems for effective decision-making and predicting the risk.

REFERENCES

[1] R. Chitra and V. Seenivasagam, "Review of Heart Disease Prediction System Using Data Mining and Hybrid Intelligent Techniques", ICTACT Journal on Soft Computing, July 2013.

[2] E.P. Ephzibah, "A Hybrid Genetic-Fuzzy Expert System for Effective Heart Disease Diagnosis", D.C. Wyld *et al.*(Eds.): ACITY 2011, ©Springer-Verlag Berlin Heidelberg 2011, CCIS, Vol.198, 2011, pp.115-121.

[3] Zhongheng Zhang, J Thorac Dis, "Big Data and Clinical Research: A Perspective from a Clinician", 2014 Dec, Vol.6, No.12.

[4] Obanijesu Opeyemi, "Development of Neuro-fuzzy System for Early Prediction of Heart Attack", International Technology and Computer Science, 2012.

[5] A.S.Vipul, "Adaptive Neuro-Fuzzy Inference System for Effect of Wall Capacitance in a Batch Reactor", Advances in Fuzzy Mathematics ISSN 0973-533X, Vol.4, 2009, pp.69-70.

[6] D.Shanthi, G.Sahoo and Dr. N.Saravanan, "Designing an Artificial Neural Network Model for the Prediction of Thrombo-embolic Stroke", International Journal of Biometric and Bioinformatics, Vol.3, No.1, 2008, pp.250-255.

[8] TaoHuangb, LiangLanc, Xuexian Fanga, Peng Ana, Junxia Mind and Fudi Wanga, "Promises and Challenges of Big Data Computing in Health Sciences".

[9] Chaitrali S. Dangare and Sulabha S. Apte, "Improved Study of Heart Disease Prediction System using Data Mining Classification Techniques", International Journal of Computer Applications, Vol.47, No.10, 2012, pp.0975-888.

[10] "Research on Big Data Analytics", www.research.com.

[11] Avan Suinesiaputra, Pau Medrano-Gracia, Brett R. Cowan and A. Alistair, "Young Big Heart Data: Advancing Health Informatics Through Data Sharing in Cardiovascular Imaging Vol 19, no.4 July 2015.

[12] Use of Big Data in Health care- Health Forum.

[13] Big Data is the future of Healthcare-cognizant solution high-quality life science," levering big data in healthcare"

[14] E.Kolɜe, N.Frasheri, "Literature Review of Data Mining Techniques Used in Healthcare Databases", Paper Presented at the ICT Innovations 2012, Ohrid, Macedonia, September 2012.

[15] A.Q. Ansari *et. al.*," Automated Diagnosis of Coronary Heart Disease Using Neuro-Fuzzy Integrated System", 2011 World Congress on Information and Communication Technologies.

[16] N. Deepika and K. Chandra Shekar, "Association Rule for Classification of Heart Attack Patients", International Journal of Advanced Engineering Science and Technologies, Vol.11, No.2, 2011, pp.253-257.

[17] K. Srinivas, B. Kavitha Rani and Dr. A. Govrdhan, "Application of Data Mining Techniques in Healthcare and Prediction of Heart Attacks", International Journal on Computer Science and Engineering, Vol.02, No.02, 2011, pp.250-255.

[18] M. Anbarasi, E. Anupriya and N.CH.S.N. Iyengar, "Enhanced Prediction of Heart Disease with Feature Subset Selection using Genetic Algorithm", International Journal of Engineering Science and Technology, Vol.2, No.10, 2010, pp. 5370-5376.

[19] D. Shanthi, G. Sahoo and Dr. N. Savanna, "Designing an Artificial Neural Network Model for the Prediction of Thrombo-embolic Stroke", International Journal of Biometric and Bioinformatics, Vol.3, No.1, 2008, pp.250-255.

[20] P. K. Anooj, "Clinical Decision Support System: Risk Level Prediction of Heart Disease Using Weighted Fuzzy Rules", Journal of King Saud University Computer and Information Sciences, Vol.11, 2011, pp.309-314.

[21] A. Ali and N.Mehdi, "A Fuzzy Expert System for Heart Disease Diagnosis", A Proceeding of the International MultiConference of Engineers and Computer Scientists, Vol.1, 2010.

[22] Syed Umar Amin, Kavita Agarwal and Dr.Rizwan Beg, "Data Mining in Clinical Decision Support Systems for Diagnosis, Prediction and Treatment of Heart Disease", International Journal of Advanced Research in Computer Engineering & Technology (IJARCET), Vol.2, Issue.1, January 2013.

[23] Ashish Kumar Sen, Shamsher Bahadur Patel and Dr. D.P. Shukla, "A Data Mining Technique for Prediction of Coronary Heart Disease Using Neuro-Fuzzy Integrated Approach Two Level", International Journal of Engineering and Computer Science ISSN:2319-7242.

[24] Novruz Allahverdi & Serhat Torun and Ismail Saritas, "Design of A Fuzzy Expert System for Determination Of Coronary Heart Disease Risk", International Conference on Computer Systems and Technologies-CompSysTech'07.

DESIGN AND FABRICATION OF AN AUTOMATED PAPER-CUTTING MACHINE FOR RE-USING WASTE PAPERS

B. Siddharthan[1], S.K.Dhinesh[2], P. Nagarajan[3], M.Raghunath[4], S. Sundar[5] and A.Prasanna[6]
[1,2,3,4&6]Department of Mechatronics, [5]Department of Electrical and Electronics Engineering
Bannari Amman Institute of Technology, Sathyamangalam-638 401, Erode District, Tamil Nadu
E-mail:siddharthan@bitsathy.ac.in

Abstract

This research paper delves into the realm of precise paper cutting, highlighting its significance in achieving uniform dimensions. The study is centred on creating an automated paper-cutting machine, capitalizing on the Geneva mechanism. This indexing tool facilitates the intermittent movement of paper, maintaining consistent intervals during cutting by transforming continuous motion. A cutting procedure involving a crank and lever mechanism is implemented, alongside a lever crank mechanism for repositioning the cutter. The core objective is to design a paper-cutting apparatus that employs the Geneva mechanism to eliminate time-consuming paper marking procedures, guaranteeing uniform paper dimensions throughout rotations. The automation aims to heighten efficiency, diminish dependence on manual labour, and reduce human errors. This versatile machine finds applicability in educational institutions, stationery and paper stores, and related domains, promising improved processes and outcomes.

1. INTRODUCTION

There is a high amount of content in the industry at the present time. Therefore, creating a new technique or procedure is needed for a well-organized, efficient manner of manufacturing. Processor techniques must completely meet the demands for accuracy and productivity. Using the Geneva mechanism, this article simulates an automatic paper-cutter. The papers can be sliced precisely using this equipment. The paper production business will majorly employ this ideation of cutting paper into large quantities. The machinery is extremely operative and is manufactured at a lesser cost. The purpose of this idea is to decrease worker tiredness and increase productivity in businesses by doing away with paper marking. The mechanism availed for this analysis was Geneva. The Geneva wheel, revolving disc, bearing, frame, and stepper motor are the components of this device.

The motive of the prototype is to reduce the marking time and to feed paper with each rotation with the same length, so this can be achieved using the Geneva mechanism. The most time-consuming process Is paper marking, to cut the papers in the desired length at the industries. Here the Geneva mechanism, convert rotational motion into intermittent motion by increasing leaps at the beginning. A spike on the rolling gear wheel penetrates into a notch on the drive shaft, causing it to move a single step.

The gear wheel additionally has an elevated circular resisting disc that holds the driven wheel in place between stages. A continuous rotation is converted into a discontinuous rotational motion via Geneva drive, also known as the Maltesecrossisa gear system. In every typical configuration. To achieve 90-degree movement for each rotation drive wheel system has been used[1]. By use of four slots in that wheel, this can be achieved. If the system has an N slot, then we can achieve 360/N movement for each rotation. Here four bar mechanism is used because of its less complex structure and its one-degree freedom[2][3]. Numerous paths are possible by randomly picking a point on the coupler curve. To find the length of four links, a mathematical model is prepared. The arrangement for the points on these paths must be calculated using the algebraic analytical formulas for these parameters. A method for calculating a 4-bar mechanism's link length that will steer the coupler curve in a specific direction. The method for creating a 4-bar mechanism described here is mathematically formulated, using a computer to create a 4-bar mechanism. This action sparked an interest in developing new analytical techniques to pinpoint mechanisms that can accomplish a particular job. It's interesting to note that three, four, or five points are frequently awarded. This path-creation process is known as a primary technique.

2. LITERATURE SURVEY

Vijay *et.al* examined the configuration and investigation of a Geneva-based paper-cutting device. By considering parameters like location, velocity, acceleration and jerk they provide differentiation from the traditional mechanism. This examination contains several analyses like kinematics to study the discontinuous motion produced by the Geneva Wheel. Its success was majorly credited to its advantageous economic aspects. By using this Geneva mechanism industries achieved the highest accuracy compared to other mechanisms and also, and they got papers at desired dimensions using this mechanism.

Han Jiguang Yu Kang the paper has examined and synthesized the elliptical crank with the use of the Geneva mechanism. It is stated that to proper Geneva mechanism, there must be equal grooves at both the internal and external wheel. The mechanism, which has a different length and variable speed along the elliptical moving crank, is the same as the Geneva wheel's driving crank. As a result, the Geneva mechanism's kinematic coefficient can be modified.

Georgata and Elena investigated the Geneva system's examination and display. The Geneva system with four openings was displayed utilizing limited component investigation and the CATIA realistic device to exhibit a few hypothetical and practical qualities. This sort of gadget changes over a nonstop revolution into an irregular alternating movement to act as an illustration of intermittent gearing. Without taking a different path, it includes substituting time periods and rest. It moreover gives different plan rules, like the considerable amount of driving cranks, slots, the diameter of the wheel, the diameter of the pin, and so on, that will permit a Geneva system to be precisely portrayed. A limited component model can be made for finite element analysis examination (FEA)(pre-handling). The core topics of the study are the development and parameter estimation study of the Geneva mechanism with 4 positions. With this technique, the Geneva component's shape can be modified without influencing its kinematic attributes.

In this paper they examine the Four-Bar Linkages, Hrones and Nelson give an outline of the 4-bar mechanism as a key 1-DOF system. By picking four-interface lengths and using a hinge joint to associate the connections into a loop, a four-bar is produced[4]. With no evident end objective in mind, while selecting a location on the connector twist, several paths are possible. Without leading an exhaustive numerical review, these unmistakable bends can be determined by building an actual replica of the instrument and noticing the direction of different points.

Madhoo et al. In this article, a solitary engine was used to drive the machine while performing a power test on the Geneva wheel and face cam. There is a separate segment describing the principle of the Geneva wheel and face Cam. The drum, which has 96 shafts, is ordered with the guide of a Geneva Wheel. Every shaft to sustain the clay body when the drum is being ordered on account of the Geneva component. Along these lines, while the cutting system's Geneva wheel is in its most extreme and least positions, a force is produced in the wheel by taking care of it through the Geneva mechanism[5].

3. METHODOLOGY

The component used to make this prototype is the Geneva wheel, Stepper motor, paper cutter, and springs. The essential distance decides the number of rollers that ought to be fitted. The belt is attached to the machines on which the material is kept. The Geneva drive is attached to the roller shaft. Since the Geneva drive shaft is associated with the stepper motor shaft, when potential is applied to the engine, the chain drive goes close by the rollers and the rollers pivot with a slight defer as per the Geneva drive. The chain sprocket is connected to the stepper motor, and the sprocket is appended to the Geneva mechanism. The engine for moving the Geneva had been turned on when the paper roll started. The Geneva wheel associates the two rollers, one of which is joined to the next. The spring that interfaces with the cutter is where the cutter is secured. The shaper wire engine is appended to the engine shaft, which has been turning. The shaper moves downwards prior to cutting the paper. The Geneva component is utilized in this mechanical paper shaper. The methods that are utilized for leading.

The crankshaft will be in the extreme position when the cam pin is in the super right position or engaged position. Accordingly, the paper cutter is completely open. The crankshaft will be in the maximum left location when the cam pin is in the extreme bottom position, or disengaged position. As a result, the cutter is partially in a cutting position. The crankshaft will be in the extremely top position when the cam pin is in the maximum left location or the disengaged position. The paper cutter is

therefore in the full cutting position. The crankshaft will be in the maximum right location when the cam pin is at the extremely top position or disengage position. Therefore, the aforementioned four steps of Geneva and the cutter enable the cutting of the paper.

4. HARDWARE DESCRIPTION

Since the operating wheel has four slots, each revolution of the gear wheel creates a 900-step advancement. Hence for 14 of the 3600, the discontinuous motion is fulfilled. A device that converts an uninterrupted revolution into an interrupted one by making use of the intermittent gear by which the driven wheel gets advanced by a single step by the drive wheel's pin entering the driven wheel's slot and the driven wheel is engaged in places between steps by a raised, circular blocking disc.

A chain wheel is an established wheel with edges, gears, or significantly varied chair wheels that interlock with a chain. The chain wheel transmits energy between two axles via the roller chain. A chain wheel is a wheel with a profile and teeth that connects to a chain, track, or other material that has holes or indentations. In contrast to a gear, chain wheels are never directly meshing together, and they are different from pulleys in that chain wheels have teeth whereas pulleys are smooth. Chainwheels are used in bicycles, motorbikes, automobiles, and other machinery to transfer rotational movements between two shafts or to provide track linear motion when gears are inefficient. Figure 1.

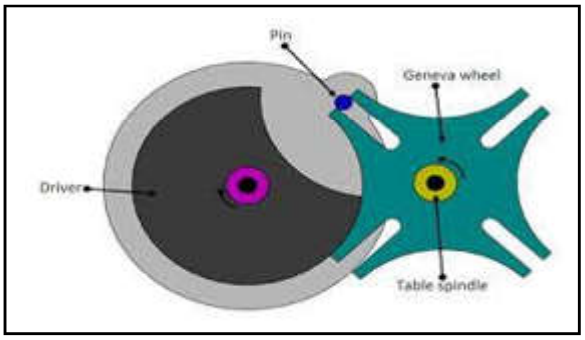

Fig.1 Geneva wheel mechanism

The most well-known sort of positive drive for moving system power between two chain wheels is a roller chain. It is comprised of a few short barrel-shaped rollers associated with side connections. It is impelled by a sprocket, a wheel with teeth. Figure 2.

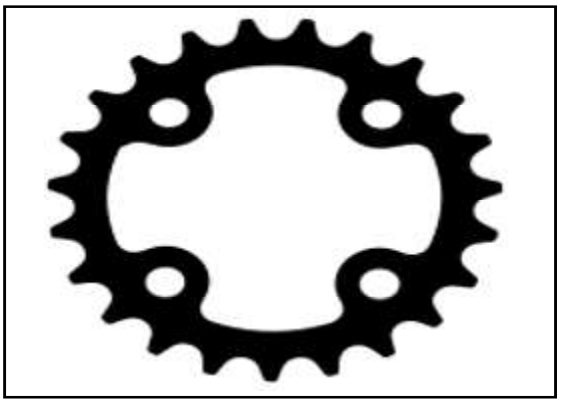

Fig.2 Sprocket

A paper cutter is a tool used to cut paper across a vertical line. The paper cutter's length may be adjusted. This paper cutter is the resonator in the four-bar crank and lever architecture. Figure 3.

Fig.3 Paper cutter or blade

The part that's been employed in the interrupted motion to feed the paper. Paper is fed causing no damage using a paper roller. Figure 4.

Fig.4 Paper roller shaft

Simple electromagnetism supports the activity of each and every electric motor. At the point when a conductor conveying current is placed in an external magnetic field, the magnetic field it produces makes it experience a force that is conversely relative to the ongoing moving through the conductor and the strength of the external magnetic

field. As you presumably review from your experience growing up exploring different types of experiments with magnets, polarities (North and North, South and South) repel whereas opposing polarities (North and South) attract. A DC motor's inner design is made to take use of the magnetic interaction that occurs when a current-conveying conductor interfaces with an external magnetic field to produce rotational motion. The motor's specifications are 12 volts, and 4.5 ampersand revolutions per minute. Figure 5.

Fig 5. Motor

Estimation and description:

30 revolutions per minute
12 Volt
18 Watt
The motor toque = (P*60)/283.14*N
= (18*60)/2*3014*30
= 5.72 Nm = 5.72*103Nmm

The shaft is composed of MS, with a maximum permissible sheer force of 42 MPa.
Torque = (3.14*fs*D3)/16
5.72*103 = (3.14*42*D3)/16
D = 8.82mm
The standard size = 9mm.

A transformer is utilized to decrease the air conditioner voltage, which is typically 220V, down to the level of the necessary dc yield. Subsequent to being at first separated by a direct capacitor channel to give a DC voltage, a diode rectifier then, at that point, produces a full-wave rectified voltage. Normally, there is some wave or ac voltage change in the subsequent DC voltage. Regardless of whether the information dc voltage differs or the heap attached to the result dc voltage changes, a controller circuit disposes of the waves and keeps up with a similar dc value. This voltage guidance is frequently performed using one of the prominent variable voltage IC circuits.

5. EXPERIMENT SETUP

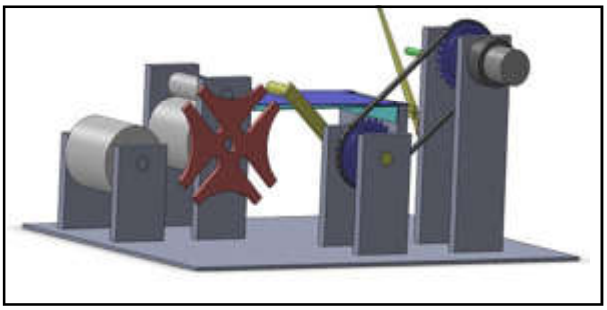

Fig.6 Paper cutting machine-front view

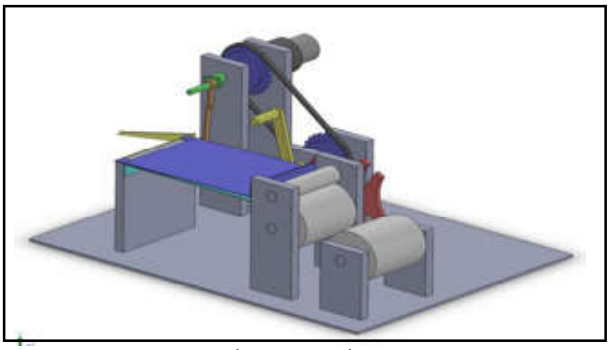

Fig.7 Rear view

6. RESULTS AND DISCUSSION

An Arduino-based paper-cutting machine is a device that uses a microcontroller, such as an Arduino, to control the movement of a cutting blade to cut paper or other materials. This type of machine is commonly used in the field of crafting and DIY projects, as it allows for the precise cutting of materials to create intricate designs and patterns.

One of the main advantages of using an Arduino-based paper-cutting machine is its flexibility. Arduino is an open-source platform, which means that users can easily modify and customize the machine to suit their specific needs. This allows for the creation of unique designs and patterns that would be difficult or impossible to achieve with traditional cutting methods. Additionally, Arduino-based machines are relatively easy to use and can be controlled by a computer or other device, making them accessible to a wide range of users, including those without extensive technical knowledge.

Another advantage of using an Arduino-based paper-cutting machine is its precision. These machines use computer-controlled motors to move the cutting blade, which allows for precise cuts and detailed designs. This is especially useful for projects that require intricate

patterns or designs, such as scrapbooking, card making, and other crafts.

Another limitation of Arduino-based paper-cutting machines is that they are not suitable for cutting thicker materials or materials that are not flexible, such as metal or plastic. This can limit their use in certain projects or industries.

An Arduino-based paper-cutting machine is a versatile and precise tool that can be used in a wide range of crafting and DIY projects. They can be easily customized and controlled by a computer or other device, allowing users to create unique designs and patterns. However, they can be relatively expensive and require a certain level of technical knowledge to build and operate. Additionally, they are not suitable for cutting thicker or non-flexible materials. With the advancements in technology and materials, it is possible that it will overcome these limitations in the future. Overall, Arduino-based paper-cutting machines hold great promise for the field of crafting and DIY projects, and further research and development are needed to fully realize their potential.

7. CONCLUSION

For limited-scope businesses, the plan and investigation of a paper-cutting gadget using the Geneva mechanism will be especially valuable. There is a paper-cutting machine, yet it has downsides, for example, being gigantic in size, costly, requiring expert labour to work, and requiring electrical information. Nonetheless, we have our own machine that will tackle this disadvantage due to its little size, decreased cost, absence of necessity for specialised labour, and nonappearance of electrical input. This machine's essential objective is to abbreviate the time expected for cutting and stamping paper. Our device is capable for accomplishing this objective.

REFERENCES

[1] U.Vijay Kumar, Ghanshyam Kumar, Dharesh Bansod, Deepak Sahu, Rishabh Bendre and Aakanksha Suryawanshi, "Design and Analysis of Paper Cutting Machine Work on the Geneva Mechanism", IJARIIE, Vol.2, No.2, 2016, pp.35-43.

[2] "Analysis and Synthesis of the Geneva Mechanism with Elliptic Crank", International Journal of Hybrid Information Technology, Vol.8, No.8, 2015, pp.253-260.

[3] Haraga and Elena Ionita, "Aspects Theoretical and Practical based on the Finite Element Analysis and Modeling of the Geneva Mechanism", IJASTR, Vol.1, No.2, 2015, pp.20-40.

[4] G. Madhoo, Mohammed Sameed, Mohsin Ali and Ashwin C.Gowda,"Force Analysis of Geneva Wheel and Face Cam Used in Automat", International Journal of Engineering Research and Applications, Vol.4, No.6, 2014, pp.73-88.

[5] Cutting Mechanism by Providing Feed through Geneva Mechanism, IJISET, Vol.2, No.4, 2015, pp.1172-1175.

A MACHINE LEARNING APPROACH FOR ANOMALY DETECTION BASED ON ONLINE OVERSAMPLING

R.Nithya[1], T.Savithadevi[2], K.Chandraprabha[3], M.Nithya[4] and A.Indirani[5]
[1]Department of Computer Science and Engineering, [3]Department of Information Technology,
[4]Department of Computer Technology, [5]Department of Artificial Intelligence and Machine Learning
Bannari Amman Institute of Technology, Sathyamangalam - 638 401, Erode District, Tamil Nadu
[2]Department of Computer Science and Engineering,
Dr.N.G.P Institute of Technology, Coimbatore - 641 048, Tamil Nadu
E-mail:nithyarangasamy03@gmail.com, csesavi@gmail.com, knaprabha@gmail.com

Abstract

In data mining and Machine Learning, anomaly detection has been a critical investigation problem. Numerous real-world uses, such as invasion detection or credit card fraud detection, as well as money transfer and mail transactions, necessitate an accurate and efficient way to identify data instances. Destructive data injections over Internet services and applications have become a most defenseless commotion which is a fragment of interruption. By means of oversampling the data instance, it outlines and depicts the accurate and adequate static form and dynamic behavior of the scheme, this is then utilised to perceive abnormal fluctuations or anomalous behaviors. Be contingent on the aberration, our system finds the destructive data and it blocks to diminish the network traffic over the web.

Keywords: *Anomaly, Data mining, Network traffic, Oversampling, Outliers*

1. INTRODUCTION

Anomaly (or outlier) detection's aim is to safeguard a small group of events that deviates from the standard. "a claim that significantly changes after being clarified, raising the possibility that it was made using a different process," according to a well-known concept of "outlier," which offers a broad definition of an outlier and supports several anomaly detection procedures. Intrusion detection, fraud and fault Detection, device health monitoring, event detection in sensor networks, and detecting ecosystem disruptions are all examples of anomaly detection. It's often used in preprocessing to get rid of erroneous data from a dataset. However, because the aforementioned real-world solicitations only provide a limited amount of characterized data, how to control anomaly of unknown data (or events) necessitates responsiveness from professionals in societies for machine learning and data mining.

An abstract definition of an anomaly is a structure that deviates from typical, expected behaviour. Three broad groups serve as classifications for anomalies [1], [2],[3].

- **Point Anomalies:** The simplest type of anomaly is a point anomaly, which happens when one data instance can be considered unusual for the remaining data.
- **Contextual Anomalies:** Nonetheless, a contextual anomaly occurs when a data instance is anomalous in one context but not another. The two characteristics of contextual abnormalities are contextual attributes and behavioural attributes.The context of an instance is determined using the first property(or neighborhood). Examples of contextual characteristics in spatial datasets include a location's longitude and latitude. In addition, time is a contextual attribute in time series data that establishes a case's placement within the overall timeline.

The second attribute is a behaviour trait that specifies the non contextual characteristics of an instance. A behavioural attribute might be, for instance, the quantity of rain that falls at any given location in a spatial dataset that shows the global average for rainfall. The significance of the contextual abnormalities in the target region determines the preference for using the contextual anomaly detection technique. Another important factor is the accessibility of qualitative characteristics. It makes sense to utilize a contextual detection method when it is simple to recognise a context. In other cases, it is not viable to create the impression that using a particular method is difficult.

- Collective anomalies: A group of related data examples that are anomalous for the overall dataset make up a collective anomaly.

One of the early strategies for discovering abnormalities is statistical anomaly detection [3]. Using statistical techniques, a statistical model is created for the typical behaviour of the supplied data. Then, a statistical inference test can be run to find a particular case that fits this model or not. Statistical anomaly spotting is carried out using a number of techniques [4]. This covers proximity-based, semi-parametric, parametric, non-parametric, and statistical techniques.

The usage of machine learning (ML) methods for anomaly detection is growing. The goal of these methods is to automate the process of learning from instances [5]. The technique is used to develop a model that distinguishes between typical classes and atypical classes.

Anomaly detection that functions on the training data function, can be split into three major classes. These categories were employed to create the model. The three major categories are [1], [13].

- Supervised anomaly detection: In this subject, labelled examples can be found in both the normal and anomalous training datasets. To create a predictive model for both the anomaly and normal classes in this model, and then to evaluate the two models. Second, it can be hard to find exact and representative labels, especially for the anomaly class.
- Semi-supervised anomaly detection: Here, only typical class instances are trained. Everything that cannot be categorised as commonplace is therefore labelled as anomalous.
- Semi-supervised methods assume that only the instances belonging to the normal class have been labelled in the dataset. They are more well-liked than supervised techniques because they do not require anomaly class labels.
- Unsupervised anomaly detection: In this situation, the methods can be implemented without training datasets. These techniques suggest that in test datasets, Anomalies are substantially less frequent than common occurrences. However, if the assumption is incorrect, this method has a high false alarm rate.

2. LITERATURE REVIEW

Detection of intrusion is a major defence-in-depth strategy. In recent years, network protection architecture has become a hot topic in computer security. A new intrusion detection method with low overhead and high effectiveness is presented based on Principle Component Analysis(PCA) [7][8]. Data related to the command sequences and system calls are the main source of information to verify the stated method. The system calls and commands count in a data block are computed. The input data will be the data column vector which shows the blocks and traces of the data. PCS is used to minimize the dimensional data vectors and space between the data vectors and it reduces the projection onto the subspace which is useful for the anomaly detection. Experimental outcomes indicate the suggested system shows better results with reference to accuracy of identification, cost of computation and instantaneous execution.

Along with finding the anomalies which are difficult to find out, the recorded anomalies must be interesting to the customer. This must be the important activity for detection software as a data analysis tool. When a customer receives a lot of points classified as candidate anomalies, the program will quickly become obsolete. Using domain awareness of the user we can ensure the advantage of the returned anomalies. There are certain environmental attributes which are not directly indicating the anomaly and often ignored by the customer. But they have a direct impact on the predicted distribution of outcome attributes, the values of which may imply an unusual observation. The suggested approach [9] takes these values into account and for the learning process it makes use of three expectation algorithms. For anomaly detection, the system compares to other methods currently in use with 13 different datasets.

Machine learning algorithms allow systems to discover from real-world data and observe behaviour. Algorithms that allow computers to view actions learned from previous experiences can be programmed based on past experiences[10]. The abnormal instances in a channel are evaluated using machine learning algorithms. The algorithms can be trained on a range of data and can track network manipulation. In terms of training and evaluating irregular behaviour in a network, supervised learning is critical. The supervised techniques implemented to discover network abnormalities are discussed in this paper.

According to the results of the literature review described in this research, the approaches for detecting network anomalies have been divided into four broad groups [11]. For each group, we established the presumptions used to distinguish between typical and abnormal data instances. These conclusions will serve as a guideline for evaluating the techniques' efficacy in a specific domain. Unlike other surveys, this paper included a discussion of network traffic dataset problems that are of particular interest to the network traffic analysis research community.

The main task of data mining is to discover the outliers from a large array of data objects, which aims to differentiate the mechanisms causing distinct classes of objects in the dataset. The currently available methods are proposed on the basis of computing distances in a full-dimensional Euclidean data space (sometimes indirectly by assuming such distributions). These methods failed with high dimensional data caused by the well known "curse of dimensionality". ABOD (Angle-Based Outlier Detection) approach [12], [13] evaluates the variance in the angles between the difference vectors of a point and the other points. In comparison to strictly distance-based methods, the effects of the "curse of dimensionality" are reduced in this method. It is not influenced by the parameter selection which has an impact on the precision of the accomplished ranking. The distance-based approach LOF performs better than ABOD on a variety of datasets with high dimensional data.

3. PROPOSED SYSTEM

The proposed system uses a systematic recognition method with existing blacklists to uncover malicious networks in a structured manner. It is implemented to create indicators This is useful for figuring out whether a network is having a significant amount of malevolent behaviour or not. This could be accustomed to identify the malevolent networks by the Inter Service Providers for examining the agreements. Also Internet Service Providers also use the metrics to monitor the effectiveness of their efforts to combat misuse and link up with other networks. Using this statistical method we can attain a lesser error rate even with a reduced number of observations.

This system allows the user to fix their own threshold range, weight and term frequency to discover the spam data. After finding the spam data the system will block them which will avoid the zombies attack and network degradation. Figure 1 shows the system architecture of the proposed anomaly detection method.

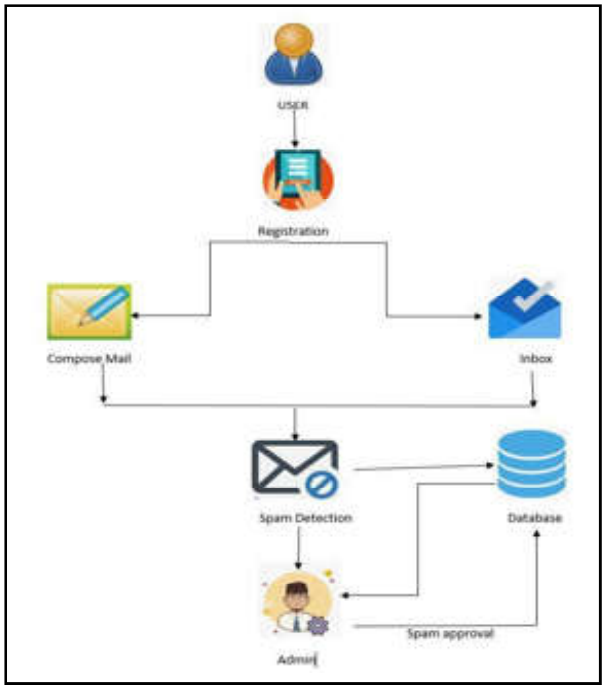

Fig. 1 System architecture

4. MODULES

4.1 Mail Server Creation and Admin

The first module of the architecture is the mail server creation. It is created to communicate with different individuals via email servers. The system includes sending email using the compose option and can receive mails from multiple recipients. Viewing sent emails and spam mails is also an option on the mail server. Admin is the vital module from both remote login and from a known machine ensuring users have total control over their accounts. The admin and server part plays an important role in the communication on the user's side. The server will respond to the queries from the user's with accessibility rights. The administrator has the evidence of the outbreaks as well as the prohibited details in this area.

After marking the message as spam, the administrator verifies which host address it originated from. If the spam messages are repeatedly sent from the spam sender, then the contents will be added to the spam database table and he will no longer be able to forward the spam messages.

4.2 Users

Users are the ones in charge of making or starting communication with the server. Users can be divided into two categories in this work: legitimate users and attackers. The intruders are mainly from remote system logins and are leveraging compromised networks - Computer that is well-known and Device that is unknown or that requires a remote login.

4.3 Web Access Security

Due to the widespread use for personal and corporate data, web services have often been the target of outbreaks. As the emphasis has changed from targeting the front end to exploiting the susceptibilities of web applications, These invasions have expanded in variety.

4.4 Accessibility and Verification

In this module, for the authenticating purpose the user details will be stored by the cookies whenever the user login from the remote system. For the first time users the cookie will save their information and they won't be capable of checking their entry.

4.5 Remote Login Limitation

Certain restrictions will be imposed on the remote login identity when the protocol detects a huge quantity of inaccurate predictions for a single and for also multiple logins.

4.6 Cookie Verification

A copy of every single user username in the remote login in addition the known computer will be saved, which helps in data verification when a mistake is made.

4.7 Spam Detection

Preprocessing is done with the existing spam documents by following methods. Stop words or other extraneous information will be removed. The words is, am, the, of, an, we, and our are examples of some of the conjunctions, verbs, disjunctions, and pronouns that are included in this list. The word "connect" is the root of words like "connect," "connected," and "link." With reference to the words or keywords specified in the text, an acceptable depiction of the content is provided.

In the information processing task, data representation techniques like term frequency and inverse document frequency are used. The server will carry out the preprocessing and clustering operation to assess whether the user is submitting any spam material. The message will be blocked by the server if it has been determined to be spam mail. This technique helps to eliminate network traffic and zombie attacks in the network.

4.8 Reports

Reports by the admin will contain restrictions to suit remote login systems and details for filtering the spam sender activity list. This is the outcome of the admin investigation and all biscuit information.

5. CONCLUSION

In this research, we suggested an oversample Principal Component Analysis-based online anomaly detection approach. We demonstrated how the osPCA with LOO approach enables us to effectively detect the existence of uncommon but anomalous data using variations of the dominant principal direction. In a similar vein, we demonstrated how to effectively detect the presence of uncommon but anomalous data using variations of the dominant principal direction. Our recommended online updating technique enables the osPCA to efficiently update the major path when oversampling a data set without having to deal with Eigenvalue disintegration difficulties.

Moreover, our strategy doesn't require keeping the entire covariance or data matrices throughout the live detection phase. Furthermore, when combined with existing anomaly detection methods, our approach can deliver acceptable results while considerably reducing computing costs and memory needs. The ideal option for problems involving large-scale or flowing data is online osPCA. In the presence of several data clusters, it might be challenging using linear models like Principle Component Analysis to predict the data distribution.

In the context of extremely high-dimensional data, several learning approaches run into the dimensionality problem. It is complicated to predict the data distribution using linear models like Principle Component Analysis when working with several clusters.

REFERENCES

[1] M. Thottan and Chuanyi Ji, "Anomaly Detection, Analysis and Prediction Techniques in IoT Environment: A Systematic Literature Review", IEEE Access, Vol.7, June 2019.

[2] V. Chandola, A. Banerjee and V. Kumar, "Anomaly Detection: A Survey", ACM Computing Surveys, Vol.41, No.3, 2009, pp.15:1-15:58.

[3] Sonali B. Wankhede, "Anomaly Detection using Machine Learning Techniques", IEEE 5th International Conference for Convergence in Technology (I2CT), March 2019.

[4] R. A.A. Habeeb, F.Nasaruddin, A.Gani, I.A T. Hashem, E. Ahmed and M. Imran, ''Real-time Big Data Processing For Anomaly Detection: A Survey'', Int. J. Inf. Manage., doi: 10.1016/ j.ijinfomgt.2018.08.006., Vol.45, Apr. 2019, pp.289-307.

[5] M. H. Bhuyan, D.K. Bhattacharyya and J. K. Kalita, ''Network Anomaly Detection: Methods, Systems and Tools'', IEEE Commun. Surveys Tuts.,[Online]. Available: http://ieeexplore.ieee.org/ document/6524462., Vol. 16, No.1, 1st Quart., 2013, pp.303-336.

[6] I. Bose and R. K. Mahapatra, ''Business Data Mining-A Machine Learning Perspective'', Inf. Manage., doi: 10.1016/S0378-7206(01)00091-X., Vol.39, No.3, 2001, pp.211-225.

[7] W. Wang, X. Guan and X. Zhang, "A Novel Intrusion Detection Method Based on Principal Component Analysis in Computer Security", Proc. Int'l Symp. Neural Networks, 2014.

[8] D.M. Hawkins, Identification of Outliers. Chapman and Hall, 1980.

[9] Bernardo A.G.Oliveira, Carlos A.P.Da S. Martins, Flavia Magalhćes and Luķs Fabrķcio W. Góes, "Difference Based Metrics for Deep Reinforcement Learning Algorithms", IEEE, Vol.7, 2019.

[10] Andrew A. Cook, Göksel Mżsżrlż and Zhong Fan, "Anomaly Detection for IoT Time-Series Data: A Survey", IEEE Internet of Things Journal, Vol.7, Issue. 7, July 2020.

[11] Mohiuddin Ahmed, Abdun Naser Mahmood and Jiankun Hu, "A Survey of Network Anomaly Detection Techniques", Journal of Network and Computer Applications, 2016.

[12] H. Anand, B.S.Sammuli, K.E.J. Olofsson and D.A. Humphreys, "Real-Time Magnetic Sensor Anomaly Detection Using Autoencoder Neural Networks on the DIII-D Tokamak", IEEE Transactions on Plasma Science, Vol.50, Issue.11, 2022.

[13] N.L.D. Khoa and S. Chawla, "Robust Outlier Detection Using Commute Time and Eigenspace Embedding", Proc. Pacific-Asia Conf. Knowledge Discovery and Data Mining, 2010.

GENERATIVE ADVERSARIAL NETWORK-BASED INTRUSION DETECTION SYSTEM FOR INDUSTRIAL INTERNET

R.Abinaya[1], N.P.Satheesh[2], K.Parvathy[3] and S.Raja Lakshmi[4]
[1]Sri Ramakrishna Institute of Technology, Coimbatore - 641 010, Tamil Nadu
[2]Bannari Amman Institute of Technology Sathyamangalam -638 401, Erode District, Tamil Nadu
[3]Dr.N.G.P Institute of Technology, Coimbatore - 641 048, Tamil Nadu
[4]Sri Eshwar College of Engineering, Coimbatore - 641 202, Tamil Nadu
E-mail: abinaya.cse@srit.org, satheeshnp@bitsathy.ac.in, parvathykrishna1808@gmail.com

Abstract

Industrial Internet or Industrial internet- of-things (IIoT) network is the cornerstone of Industry 4.0, which connects people and industrial equipment with real-time data analytics and communication systems. The appealing characteristics of the industrial internet make them alluring targets for cyberattacks, where attackers can gain access to physical and virtual resources of the network. Therefore, several organizations have experienced challenges in the adoption of the IIoT. A deep learning (DL)-based intrusion detection system (IDS) is an effective tool to recognize spiteful activities on Industrial Internet. But, they are hampered by some restrictions including increased false alarm rate and deprived classification performance owing to class imbalance problems. In this context, this study develops an IDS model using an adversarial training-based accurate (ATA- IDS) model to classify network activities as normal and malicious. This model uses a generative adversarial network (GAN) to handle the class imbalance problems effectively. Here, GAN generates several artificial data samples, and IDS gets trained on them together with the real datasets. The classification accuracy of the original GAN is increased by incorporating a quality-based feature selection (QFS) algorithm. The performance of the proposed IDS models is studied using the Cybersecurity–Distributed Denial of Service 2019 (CIC-DDoS 2019) dataset by means of MATLAB R2018b/deep learning toolbox. Additionally, we carry out Wilcoxon's rank-sum test to determine whether our proposed ATA-IDS model enables a noteworthy enhancement related to other classifiers or not. The empirical results demonstrate that the intended classification approach outdoes other approaches with superior enactment regarding the accuracy, sensitivity, specificity, precision, false positive rate, false negative rate, and ń-value of 98.92%, 99.52%, 99.31%, 97.77%, 5.3%, 0.38%, and 0.29, correspondingly.

Keywords: *Power system, Security-constraint, Stability, Transient analysis*

1. INTRODUCTION

Efficient data communication networks and digitalization are vital elements enabling industries to make a potential transformation towards smart production systems, which will effectively apply the power of new technologies (e.g., artificial intelligence, data science, machine learning, cloud technology, edge computing, Internet-of-things, etc.) for their commercial products and value. The fourth industrial revolution (i.e., Industry 4.0) is the new trend that defines the concept of "smart industry" [1]. This concept is based on the industrial internet to enable communication between processes, machinery, equipment, and people working in various industrial verticals including manufacturing, supply chain management, transportation, healthcare, etc. [2]. IIoT targets at developing smart factories by providing game-changing real-time remote services including industrial automation, production optimization, quality control, diagnosis of manufacturing, monitoring of structural health, and condition monitoring dynamically [3]. Above all, this digital technology fetches improved efficacy and responsiveness to consumers previously impractical. To accomplish these objectives, the industrial internet encompasses smart sensors, actuators, apparatuses, embedded software, and decentralized networking systems to collect, process, and analyze, huge datasets, which makes them tempting targets for cyberattacks, where the attackers can easily gain access to insecure devices [4].

The security issues reduce the progress leap of the industrial internet and the attackers may employ different methods to gain access to the network. A

cyberattack or intrusion is a malevolent activity that aims to compromise the confidentiality, integrity, and availability of the system. Therefore, the development of IIoT structures is still in its embryonic stage [5]. At the same time, defending these systems against threats cannot be inflated. Prevailing techniques such as authentication methods and firewalls cannot efficiently protect against cutting-edge cyber threats owing to heterogeneous standards and protocols. An IDS model is an important tool that has been extensively employed in IIoT systems to identify malicious events. These models detect malicious samples and develop a secure atmosphere for businesses against cyberattacks.

The application of IDSs in the industrial internet is always hindered by scarcities of suitable databases to train the classifier to recognize potential attacks. Besides, the false alarm rate of the prevailing attack detection models is high. Even if there is a database, the number of samples of each class of threat may not be sufficient for the detection models to get trained seamlessly and categorize with superior enactment. Furthermore, the number of normal records is very high as compared to the attack samples, which fetches data imbalance issues in the training process of the classifier. In this context, this study develops an ATA-IDS model using the generative adversarial network.

GAN is an efficient DL technique with the ability to recognize the data structure and generates new artificial samples. The GAN produces several artificial records, and IDS gets trained on them with real samples to improve the performance of the model. The efficiency of this proposed ATA-IDS model is increased by applying the QFS algorithm. The QFS algorithm selects significant attributes to reduce the feature space. The remaining sections of this article are structured as follows: Section 2 reviews the related works about the GAN-based IDS model. In Section 3, we take an in-depth look at the proposed ATA-IDS model to identify network intrusion in the IIoT system. Then, the implementation details and the numerical results are presented in Section 4 and Section 5, respectively. To end, conclusions are drawn in Section 6.

2. RELATED WORK

The generative adversarial network is a promising tool to identify anomalous activities in networking systems due to both their ability to recognize the data pattern and generate the new counterfeit sample. Intrusion recognition, which discriminates anomalous data, is a significant problem that can be resolved by adversarial networks with a different perspective, especially in innovative application domains such as the industrial internet. To understand an accurate representation of the rudimentary data pattern, a considerable amount of instances is indispensable for these approaches. If this data source is decentralized (e.g. warehoused at data centers of various nodes), efficient training algorithms are required to achieve similar performance to the centralized instances [6]. As a form of unsupervised learning, the adversarial network has been widely used in IDS since it can identify abnormal incidents through confrontational learning [7].

GANs are used for producing fake samples from the original one and need a robust relationship (i.e., the training of the generator and the discriminator need to be in synchronization) for the producers to create precise fake samples that can "bypass" the discriminator [6]. Schlegl et al. proposed a GAN-based abnormality detection approach (Ano-GAN) by exploiting the pattern extraction ability of confrontational training [8]. The classifier is learned from regular data and then evaluated on attack records. The producer acquired statistics about original data and, if this is anomalous, it would learn to produce a fake normal record. The key limitation is that Ano-GAN needs an arduous backpropagation method to define the mapping for anomaly ranking [8].

Shahriar *et al.,* proposed a generative adversary-based IDS model (G-IDS) where GAN generates artificial samples for the training process [9]. This approach also addresses the imbalanced data issue. The authors create a dataset and evaluate the enactment of the projected approach through different metrics. It is witnessed that this model outdoes other IDS models. Xu et al. (2022) proposed a Bidirectional GAN (Bi-GAN) approach that is an efficient tool for identifying anomalous with reduced overheads related to the learning process [10]. In Bi-GAN, the training procedure of the producer is diverse from the training procedure of the discriminator till it satisfies the constraints of the cross-entropy loss. Besides, this method introduces a novel idea of a one-class classification algorithm as a discriminator. This algorithm detects attack samples based on binary outcomes instead of applying inflated and complicated anomaly scores.

From a comprehensive review, this work identifies the issues of the proposed adversarial approaches experienced by the scholars: (i) Training of IDS models is a perplexing task owing class imbalance problem, but, some methods have been proposed for making it feasible; however, it is still an active research theme; (ii) Lack of standard evaluation measures for GAN assessment; and (iii) In some cases, the discriminator and generator do not work well due to class imbalance problem. By bearing these problems in mind, this study proposes an ATA-IDS model to classify network activities as normal and malicious. This model uses a GAN to handle the class imbalance problem effectively. Here, the adversarial network generates several artificial samples, and the classifier gets trained on them along with the real datasets. The classification accuracy of the IDS model is increased by incorporating the QFS algorithm.

3. PROPOSED ADVERSARIAL TRAINING - BASED IDS MODEL

Most of the prevailing IDS models struggle with a deficiency of databases for learning and testing processes which makes the deployment of IDS models perplexing to recognize the possible threats with anticipated performance. Even if there is a database, the number of samples of each class may not be adequate for the recognition model to learn seamlessly and detect threats with better performance. Also, imbalanced databases are fetching further difficulties to the IDS. In this study, we propose an adversarial training-based accurate recognition approach to increase classification performance. The GAN produces artificial records to train the classifier. In other words, it produces duplicate data samples, and the classifier gets trained on generated samples along with the original instances to improve the efficiency of the system. This section provides the details of the ATA-IDS model developed in this work.

3.1 Archtecture of ATA-IDS Model

The intended ATA-IDS model aims at recognizing cyber threats on the industrial internet. In the ATA-IDS model, the generator (*Gen*) and the discriminator (*Disc*) perform a two- player min-max game for producing confrontational data. To prevent the non-convergence and vagueness of traditional confrontational systems, the ATA-IDS model employs the Wasserstein GAN configuration [11].*Gen* in this proposed model controls the features to generate confrontational malicious records. The *Disc*¸ Ü is trained to learn the way to differentiate attack samples and feedback on the learning process of the *Gen*.

The intended ATA-IDS model comprises the following modules: (i) data accumulator; (ii) *Gen* and *Disc* (iii) intrusion recognition module; (iv) governor; and (v) loss function (LF) estimator.

Figure 1 illustrates the organization of the intended ATA-IDS approach to detect anomalies with higher prediction performance. It can alleviate the class imbalance issue by creating confrontational malicious instances. Primarily, the accumulator collects real-world datasets using the data accumulator (i.e., sensors). This module may also get generated data from the *Gen* of the data generation module. All of these samples are collected continuously. When preprocessing this dataset, it is added in the dataset with suitable tags to discriminate the samples (i.e., normal or attack).

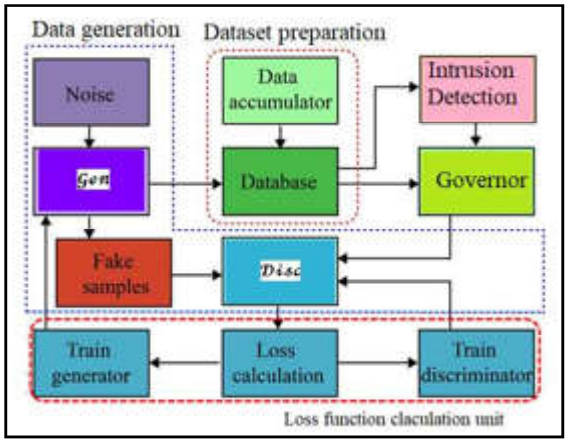

Fig.1 Architecture of ATA-IDS

The preparation module comprises two important components: data accumulator and dataset. The accumulator collects data by getting packets using sensors. The samples are preprocessed before storing into the database. The Wireshark application is used in this study to collect traffic flow and extract features from them. The communication between the actuators and the sensors of an industrial internet generates massive data, which often includes normal records. However, an assailant tries to compromise the communication system or the sensors to execute a threat. Consequently, to make the network robust against various advanced attacks, a firewall is used with the collector to label the data samples.

The data generation module comprises two DL models, *Gen* and *Disc*. The former component gets noise

input, regulates it, and gives it to the *Disc* for classification. *Gen* is employed to learn what the original data may look like, which it does by observing how the *Disc* replies to its generated data records. If the *Disc*, is not cheated, *Gen* is penalized by backpropagation. This reinforces the operation of *Gen* to create more positive differences in its noise inputs. If the *Gen* is competent at tricking the *Disc* then the *Disc* is penalized similarly. *Gen* does notwork excellently in the initial stages of the learning process,predominantly if the dataset includes complex datasets.

Since *Gen* is not aware of the statistics of the dataset, itoffers random estimation. Mainly, the *Disc* can unswervingly discriminate the feeble guesses of the *Gen* into fake and real data.Since the *Gen* assumption starts to improve and look like the original sample, the *Disc* may misclassify the *Gen* fake data.When this happens, the *Disc* faces greater losses, which enforces it to study and differentiate fake samples from the *Gen*, instead of the original data. The *Gen* reacts to the *Disc* improved performance by engendering higher-quality samples. Preferably, training halts when *Disc* is classifying the data samples with 50% efficiency. The governor selects one class and sends all the records to the data generation module, stating "1" as the label of the attack sample and "0" for the normal data. In this work, the *Gen* and *Disc*are simulated using DL networks.

Consider the original sample R and corresponding tag T_R^* are inputs. The best feature of data R* and the corresponding tag T_R^* are outputs after selecting the appropriate feature. The noise vector υ and condition vector T_{fake} are input to the *Gen* to generate the fake sample R_{fake}. It is pigeonholed by the *Disc*. The original and fake judgment loss $L_{rf}(Gen)$ and the classification loss $L_{cl}(Gen)$ are computed. Then, the training of the *Gen* is compliantly performed and R* is accepted by the *Disc*. The original and synthetic data judgment loss $L_{rf}^*(Gen)$ and the classification loss $L^*_{class}(Gen)$ for R^* are outcomes. Moreover, R_{fake} is transmitted to the *Disc*, for subsequent processing. The actual and synthetic data judgment loss $L^{fake}_{rf}(Disc)$ and classification loss $L^{fake}_{cl}(Disc)$ of R_{fake} are outcomes. *Gen* training is realized by following these LFs as defined in Equations (1) and (2).

$$L_{rf}(Disc) = E_{v\sim p_v(v),T_{fake}\sim P_t}\left[\log\left(1 - Disc\left(Disc\left(v, T_{fake}\right)\right)\right)\right] \quad (1)$$

$$L_{cl}(Disc) = E_{v\sim p_v(v),T_{fake}\sim P_t}\left[L_D\left(T_{fake} \| G\left(v, T_{fake}\right)\right)\right] \quad (2)$$

When the input is random latent vector u and tag T_{fake}, the *Gen* generates data R_{fake} as the output. The loss function L_{Gen} of *Gen* is computed from the weighted sum of loss functions. It contains the discriminant loss $L_{rf}(Gen)$ of R_{fake} that is decided by the Disc as actual or as synthetic data. The prediction loss $L_{cl}(R_{fake})$ of R_{fake} is pigeonholed and computed using Equation (3).

$$L_{Gen} = \beta L_{rf}(Gen) + \gamma L_{cl}(Gen) + \delta L_{sh}(Gen) \quad (3)$$

where $L_{sh}(Gen)$ is the shunt loss that R_{fake} is perceived as the input data. The parameters β,γ, and δ are the weights of $L_{rf}(Gen)$, $L_{ct}(Gen)$ and $L_{sh}(Gen)$, respectively.

As the *Gen* is an important module of the ATA-IDS model, it performs an important role in generating confrontational records for the threat detection model. To transform actual data into a confrontational one, the actual noise perturbation is assimilated into the actual dataset before the data conception. This work concatenated actual data and a latent vector as inputs fed to the *Gen*. The actual data is preprocessed and the constants of the noise part are standardized within [0, 1]. Figure 2 displays the configuration of the generator and discriminator in the ATA-IDS approach.

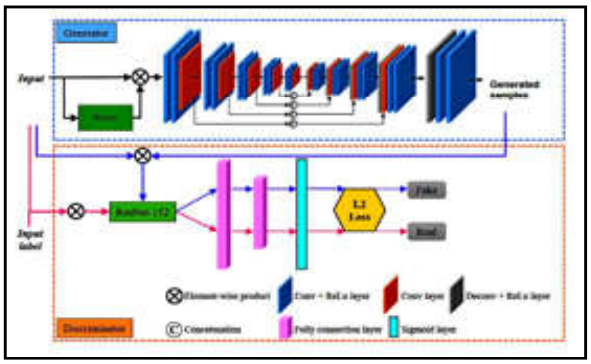

Fig.2 Generator and discriminator in ATA-IDS

A simple residual network is employed as the *Gen*. In this system configuration, deconvolutional operations are omitted, and only the basic convolution operation is executed. Moreover, this work exploits a method named dropout (skip or shortcut) links to intuitively eliminate links with relevant layers from DL models during learning, which circumvents their co-adaptation owing to the overfitting issue. The *Gen* employed in the ATA

intrusion detection approach contains five units such as convolution, activation, subsampling, dense (fully connected), and output units.

The convolution unit aims to learn attribute maps (AMs) of the dataset through various kernel functions, by which their spatial relationship can be conserved. Every pixel in AMs is mapped to an area of adjacent pixels in the earlier unit. The activation procedure adds nonlinearities to *Gen* operation which is required for multi-layer DL algorithms to classify nonlinear attributes. The subsampling (pooling) operation is employed to decrease the attribute space dimension obtained from the convolution unit. This function aims to make shift invariance by decreasing the resolution of the AMs. The subsampling unit is generally placed among two convolution layers and integrated with its equivalent AMs of the previous unit. After organizing convolutional and pooling layers, deep learners comprise one or more fully connected units which target to achieve high-quality AMs. These units take all nodes in the earlier layer and connect them to each node of the present unit to produce global semantic data. However, this operation is not always required as it can be substituted by a 1×1 convolution operation. The final unit is the output unit. The limitations analogous to a particular layer can be optimized by reducing an appropriate loss operation of the relevant layer.

During learning, the weights assigned to L_{rf} *(Gen)* and L_{cl} *(Gen)* are high and the weight of L_{sh} *(Gen)* is minimum, instigating the generated fake sample to be weak. Besides, it will cause poor performance of the detection process with deprived dependability. If the weight of L_{sh} *(Gen)* is higher and the weights of L_{rf} *(Gen)* and L_{cl} *(Gen)* are very low, the learning data pattern cannot be effectively excerpted by the *Gen*. This adds difficulties to the *Disc* to differentiate the actual samples from the generated synthetic data that disturb the performance of the *Gen*. Therefore, the weight should be set to ensure that *Gen* can raise the sternness of the fake samples. Moreover, the *Disc* is strong enough to differentiate the data. The input of the *Disc* comprises the generated data R_{fake} of the *Gen*, the ideal feature data R^*, and the corresponding accurate tag T_R. The output R^* is the feature data selected by the QFS algorithm with *R* as the input data.

In addition, some techniques are employed for processing the enhanced features. To make the value of resultant attributes within [0, 1], the attributes which are above one are set as 1 and below zero are set as 0. Similarly, the distinct features which have more than 2 values before the preprocessing are only present in "intrinsic" features. After generating fake samples using *Gen*, the values of these enhanced features will be transformed into binary values with 0.5 as the preset value. The values above/below 0.5 will be transformed into 1/0. ATA-IDS approach uses a binary classification algorithm as a *Disc* that calculates the probability that a sample is fit into a specified class. As an adversarial IDS approach, the *Disc* helps *Gen* learn data patterns and generate synthetic samples. The losses defined in Equations (1) – (3) are calculated by recognizing the outcomes of the *Disc* and the gradient is backpropagated to the *Gen*. By making the *Disc* handle confrontational data and updating the parameters by the loss from the *Disc*, the *Gen* analyzes an improved attack approach to improve actual malicious data.

3.2 Quality-based Feature Selection

Feature engineering is the process of identifying and excluding irrelevant and redundant attributes from the dataset. This reduces the feature space and may facilitate training procedures to run quicker and more proficiently. A feature is important if its values change steadily with the class association. That is, a feature is significant if it is correlated to the label; or else it is unrelated.

Algorithm 1: QFS algorithm
A ← number of attributes
n ← number of iterations
for i=1 to n do
execute RelieF and compute feature quality
measure sort attributes by quality measure
remove features with the lowest measure
end for
return quality measure for other features

Weak significance designates that the feature can increase the performance of the detection model rarely. Features are germane if they are either strongly or feebly related, and are irrelevant or else. Unrelated features can never increase the performance of the system. Attribute quality defines the variation that presents in the dataset associated with the certain attribute value. Therefore, they are known as impurity functions. This work uses a technique named Optimized RelieF (ORelieF) to calculate the attribute quality.

ORelieF is a variant of the basic Relief algorithm. ORelieF is a recursive feature elimination technique and the lower-ranking feature is eliminated based on feature quality in every iteration. Alternatively, selecting the number of iterations (n) is also important. Attribute engineering selects the subsection of descriptive attributes indispensable to create an alarm when an invasion is detected. This procedure uses the quality-based assessment to compute the quality of the relationship between attributes of the samples in the dataset.

4. PERFORMANCE EVALUATION

The developed ATA-IDS model with 5Ř˜Ü/!5ŘĂÜ (generative model) and a *Disc* (binary classifier) is implemented in a test bed successfully. The learning process of ATA-IDS includes two added modules including a preprocessor and QFS algorithm, which accomplish preprocessing and feature selection, correspondingly. The data preprocessor parses data packets, selects significant features based on quality, transform the data, and generates tags for each sample. The attribute selection unit chooses important attributes by applying our proposed QFS algorithm. The intended ATA-IDS approach is realized by MATLAB R2018b/ Deep learning toolbox on an Intel Core i7-4790 CPU, and Windows 10 operating system. This work trains the proposed ATA-IDS model with normal and attack data; 70% of the dataset is used for training, and 30% is used for testing.

4.1 Real Dataset

The CIC-DDoS dataset encompasses 50063112 records, with 50006249 attack samples and 56863 normal samples [12]. The dataset has 84 features and twelve cyber threats as given in Table 1.

Table 1 Statistics of the CIC-DDoS Dataset

Class	Number of Instances	Distribution (%)
Normal	56863	0.11
DdoS-TFTP	20082580	40.11
DdoS-SNMP	5159870	10.31
DdoS-DNS	5071011	10.13
DdoS-MSSQL	4522492	9.03
DdoS-NetBIOS	4093279	8.18
DdoS-UDP	3134645	6.26
DdoS-SSDP	2610611	5.21
DdoS-LDAP	2179930	4.35
DdoS-SYN	1582289	3.16
DdoS-NTP	1202642	2.40
DdoS-UDP-Lag	366461	0.73
DdoS-WebDDoS	439	0.01
Total	50063112	100

Table 2 Distribution of data samples in CIC-DDoS Before and After using Generative Network

Type	Original Data Samples in the Dataset	Data Samples after adding the Synthetic dataset
Normal	56,863	10,56,863
DDoS_DNS	50,71,011	50,71,011
DDoS_LDAP	21,79,930	21,79,930
DDoS_MSSQL	45,22,492	45,22,492
DDoS_NetBIOS	40,93,279	40,93,279
DDoS_NTP	12,02,642	12,02,642
DDoS_SNMP	51,59,870	51,59,870
DDoS_SSDP	26,10,611	26,10,611
DDoS_SYN	15,82,289	15,82,289
DDoS_TFTP	200,82,580	200,82,580
DDoS_UDP	31,34,645	31,34,645
DDoS_UDP-Lag	3,66,461	13,66,461
DDoS_WebDDoS	439	10,00,439
Total	500,63,112	530,63,112

4.2 Generated Dataset Using GAN

Table 2 lists the increased records produced by the ATA- IDS model for the database employed in this work. The proposed model is implemented and data samples are generated to evade the class imbalance proble.

4.3 Evaluation Measures

To assess the efficiency of the intended ATA-IDS, this work exploits seven performance indicators such as accuracy (ACC), sensitivity (SEN), specificity (SPE), precision (PRE), false negative rate (FNR), false positive rate (FPR), and ń-values. These indicators, excluding FPR, FNR, and ń-values are essential to be bigger to improve the effectiveness of the detection process. The efficacy is calculated regarding ACC of an intrusion detection model and it is calculated using Equation (4).

$$ACC = \frac{T_- + F_+}{T_- + T_+ + F_- + F_+} \quad (4)$$

where true positive (T_+) is the number of records that are properly categorized as malevolent records; false negative (F_-) is genuine of malevolent records that are incorrectly categorized as genuine records; true negative (T_-) is the number of records that are properly categorized as genuine records; and false positive (F_+) indicates the number of genuine records that is incorrectly categorized as a malevolent. Sensitivity and specificity define how well the model differentiates malevolent and genuine labels. The SEN and SPE of a classifier are computed using Equation (5) and Equation (6), correspondingly. Precision is the proportion of the 5ŘGÜ> of a particular label to the number of malevolent records categorized as the related label as given in Equation (7). The FPR and FNR are also significant metrics to evaluate the efficiency of the intended ATA detection approach. These measures are computed using Equations (8) and (9).

$$SEN = \frac{T_+}{T_+ + F_-} \quad (5)$$

$$SPE = \frac{T_-}{T_- + F_+} \quad (6)$$

$$PRE = \frac{T_+}{T_+ + F_+} \quad (7)$$

$$FPR = \frac{F_+}{F_+ + T_-} \quad (8)$$

$$FNR = \frac{F_-}{F_- + T_+} \quad (9)$$

Wilcoxon's statistical analysis is a nonparametric used to decide whether the developed ATA detection approach delivers a noteworthy improvement related to other approaches or not. This test is conducted to examine the impacts of the developed detection approach and related to each of the other models at a 5% significance level. The p-values less than 5% indicate that there is a remarkable difference at a level of 5%. Similarly, the p-values > 5% denoted that there is no remarkable difference amongst the related values.

5. RESULTS AND DISCUSSION

5.1 Experimental Results and Discussion

We evaluate the performance of the ATA-IDS model in terms of evaluation metrics. The intended model can achieve better results as compared to other related models when it is applied to the CIC-DDoS database. This work assesses the enactment of the intended ATA-IDS by relating its outcomes with some advanced classifiers including Ano-GAN [8], IDS-GAN [10], GAN [13], multilayer perceptron with GAN (MLP-GAN) [14], long short-term memory with GAN (LSTM-GAN) [15], and GAN-based support vector machine (GAN-SVM) [16]. Our QFS algorithm selects 7 attributes as significant to reduce the feature space. The experimental outcomes gained by our ATA-IDS model for different folding are recorded in Table 3. From these results, it is found that the ATA-IDS has realized 98.92% ACC, 99.52% SEN, 99.31% SPE, and 97.77% PRE, by adding synthetic records with the actual samples in the database. Besides, it realizes an improved false alarm rate (i.e., 5.30% FPR and 0.38% FNR).

Table 3 Results Obtained by ATA-IDS for Different Folding

Fold	ACC	SEN	SPE	PRE	FPR	FNR	p-value
#1	97.20	99.30	98.80	97.30	5.20	0.47	0.10
#2	98.60	99.70	99.20	97.70	5.60	0.67	0.41
#3	99.00	99.80	99.60	98.10	5.00	0.07	0.10
#4	99.90	99.90	99.40	97.90	4.80	0.09	0.10
#5	99.90	99.50	99.60	98.10	5.00	0.07	0.11
#6	97.20	99.30	97.80	96.30	5.50	0.27	0.10
#7	99.90	99.60	99.50	98.00	4.90	0.63	1.51
#8	98.90	99.70	99.90	99.00	5.90	0.70	0.10
#9	99.00	99.20	99.60	98.10	5.00	0.67	0.10
#10	99.60	99.20	99.70	97.20	6.10	0.17	0.31
Mean	98.92	99.52	99.31	97.77	5.30	0.38	0.29
S.D	1.02	0.26	0.61	0.72	0.45	0.27	0.44

The ATA-IDS model also provides 0.29% of Á-value which specifies that the results gained by the proposed model are noteworthy. Additionally, the ATA-IDS model realizes minimum standard deviation (SD) values in the detection process with ACC of 1.02%, SEN of 0.26%, SPE of 0.61%, PRE of 0.72%, FPR of 0.0.45%, FNR of 0.27%, and Á-value of 0.44%. Figures 4 and 5 illustrate the complete results achieved by the ATA-IDS for different folds in terms of the mean value of evaluation measures.

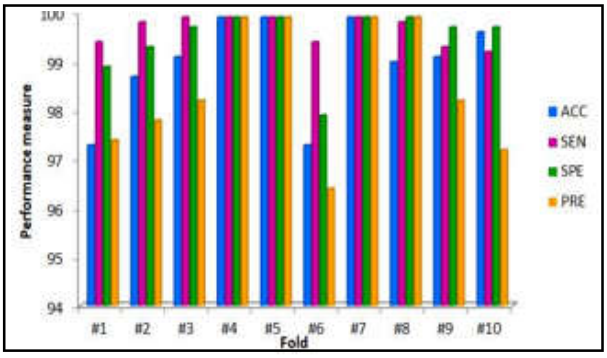

Fig.4 Results of ATA-IDS in terms of ACC, SEN, SPE, and PRE

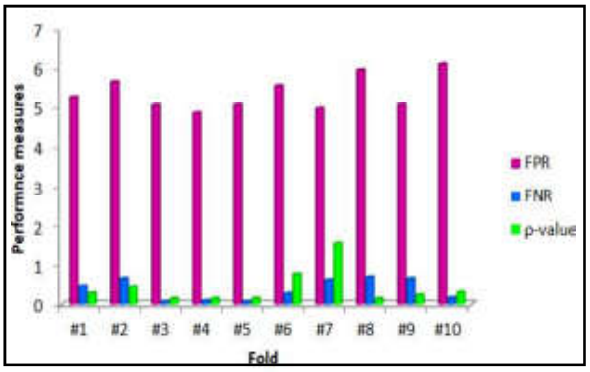

Fig.5 Results of ATA-IDS in terms of FPR, FNR, and ń-value

The mean and SD value of performance measures gained from the CIC-DDoS database by various IDS models including ATA-IDS is shown in Table 4. From these results, it is witnessed that the basic GAN model has achieved 83.89% ACC, 85.09% SEN, 90.59% SPE, 78.59% PRE, 12.17% FPR, 1.25% FNR, and 8.12% ń-value. MLP-GAN has achieved detection performance with an ACC of 72.39%, SEN of 83.89%, SPE of 85.99%, PRE of 79.19%, FPR of 14.23%, FNR of 2.97%, and ń-value of 6.75%. The LSTM-GAN classification network provides better results regarding ACC, SEN, SPE, PRE, FPR, FNR, and ń-value, It revealed 78.22%, 93.22%, 90.02%, 74.72%, 13.72%, 2.41%, and 3.24%, respectively.

Table 4 Mean Value of Performance Measures Obtained by ATA-IDS

Method	ACC	SEN	SPE	PRE	FPR	FNR	P-value
GAN	83.89	85.09	90.59	78.59	12.17	1.25	8.12
MLP-GAN	72.39	83.89	85.99	74.19	14.23	2.97	6.75
LSTM-GAN	78.22	93.92	90.02	74.72	13.72	2.41	3.24
Ano-GAN	80.82	94.59	87.79	79.09	10.69	2.18	5.18
IDS-GAN	82.63	96.34	93.35	79.95	18.25	1.65	7.06
GAN-SVM	87.07	97.20	95.27	84.27	17.06	1.20	5.56
IGAN-IDS	98.92	99.52	99.31	97.77	5.30	0.38	0.29

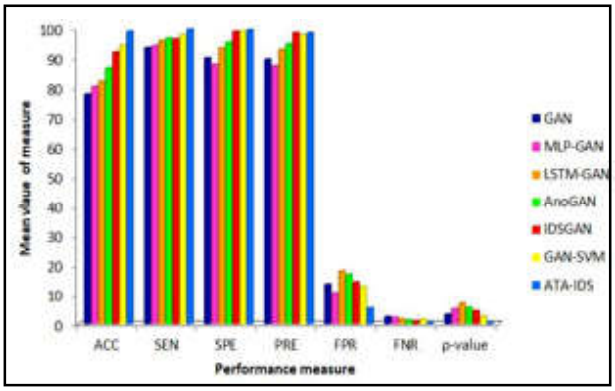

Fig.6 Mean value of measures in ATA-IDS and other models

By exploiting the interpretation learning ability of deep convolutional adversarial networks, Ano-GAN offers improved detection enactment regarding ACC (80.82%), SEN (94.59%), SPE (87.79%), PRE (79.09%), with reduced false alarm rate (10.69% FPR and 2.18% FNR), and Á-value (5.18). IDS-GAN executes the black-box attacks against the IDS by means of ML techniques where most of the confrontational malevolent data circumvented the recognition of the IDS. It offers better outcomes with respect to ACC, SEN, SPE, PRE, FPR, FNR, and Á-value, this model shows 82.63%, 96.34%, 93.35%, 79.95%, 18.25%, 18.25%, 1.65%, and 7.06%, respectively. The GAN-SVM model delivers related results as IDSGAN. It provides detection enactment regarding ACC (87.07%), SEN (97.20%), SPE (95.27%), and PRE (84.27%). However, it shows a considerable false alarm rate (17.06% FPR and 1.2% FNR), and *p*-value (5.56%) in the intrusion detection process. To minimize the FAR, this work suggests the ATA-IDS. It can be found that the ATA-IDS model outdoes all other state-of-the-art IDS models in terms of performance measures. The key reason for the greater enactment of ATA-IDS is that the proposed ResNet- based *Gen* and *Disc,* as well as the attribute selection approach, can increase the performance of the IDS model in the IIoT environment.

Table 5 shows the outcomes gained by ATA-IDS regarding the SD value of enactment indicators. By considering these SD values, the intended approach provides very less SD values in the detection process with ACC of 1.52%, SEN of 0.76%, SPE of 1.11%, PRE of 1.22%, FPR of 0.95%, FNR of 0.77%, and ń-value of 0.44%. From Figure 7, it can be observed that the SD of the ATA-IDS is less than all other approaches with respect to the performance indicators. Therefore,

Table 5 SD Value of Performance Measures Obtained By ATA- IDS

Method	ACC	SEN	SPE	PRE	FPR	FNR	ρ-value
GAN	3.17	3.08	3.21	2.26	2.37	1.83	2.03
MLP- GAN	3.03	3.08	3.26	3.04	0.94	1.29	2.58
LSTM-GAN	6.33	1.64	5.79	6.04	4.58	1.03	1.94
Ano-GAN	5.20	2.68	4.82	5.06	4.89	0.89	2.23
IDS- GAN	4.74	2.51	1.52	4.30	2.88	0.72	2.51
GAN- SVM	5.49	2.64	2.82	2.72	3.16	3.45	2.58
IGAN- IDS	1.52	0.76	1.11	1.22	0.95	0.77	0.44

the ATA-IDS model delivers much more reliable results for recognizing anomalies than the others. Thus, ATA-IDS is a more feasible model for detecting intrusion in the industrial internet.

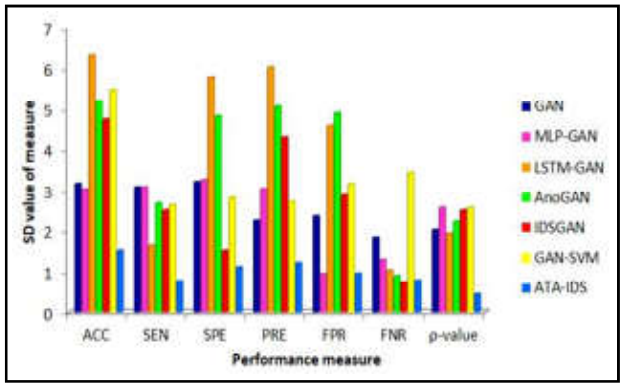

Fig.7 SD value of measures in ATA-IDS and other models

6. CONCLUSION

The industrial internet is the imminent technology of various industries. However, security is one of the major concerns in this network that needs constant observation to prevent malevolent threats from distressing the genuine activity of the system and to evade its shattering concerns. In this context, we develop an intrusion detection model using the ATA-IDS model to classify network activities as genuine and malicious. This model uses a GAN to handle the class imbalance problem effectively. It generates several artificial records, and IDS gets trained on them along with the real datasets. The classification accuracy of the original GAN is increased by incorporating the QFS algorithm. The performance of the proposed IDS models is studied using CIC-DDoS 2019 dataset by means of MATLAB R2018b/deep learning toolbox. Additionally, we carry out Wilcoxon's rank-sum test to determine whether our proposed ATA-IDS model enables a noteworthy enhancement related to other classifiers or not. The empirical results demonstrate that the intended classification approach outdoes other approaches with superior enactment regarding the accuracy, sensitivity, specificity, precision, false positive rate, false negative rate, and ń-value of 98.92%, 99.52%, 99.31%, 97.77%, 5.3%, 0.38%, and 0.29, correspondingly. Additionally, the ATA-IDS model realizes minimum SD values in the detection process with ACC of 1.02%, SEN of 0.26%, SPE of 0.61%, PRE of 0.72%, FPR of 0.0.45%, FNR of 0.27%, and ń-value of 0.44%.

REFERENCES

[1] A.Jamwal, R.Agrawal, M.Sharma and A.Giallanza, "Industry 4.0 Technologies for Manufacturing Sustainability: A Systematic Review and Future Research Directions", Applied Sciences, Vol.11, No.12, 2021, pp.5725.

[2] M. Javaid, A. Haleem, RP. Singh, S. Rab and R. Suman, "Upgrading the manufacturing sector via applications of Industrial Internet of Things (IIoT)", Sensors International, Vol.2, 2021, pp.100129.

[3] AN. Jahromi, H.Karimipour, Dehghantanha and KKR Choo, "Toward Detection and Attribution of Cyber-Attacks in Iot-Enabled Cyber–Physical Systems", IEEE Internet Things Journal, Vol.8, No.17, 2021, pp.13712-13722.

[4] S. Pal and Z. Jadidi, "Analysis of Security Issues and Countermeasures for the Industrial Internet of Things", Applied Sciences, Vol.11, No.20, 2021, pp.9393.

[5] N. Abosata, S. Al-Rubaye, G. Inalhan and C. Emmanouilidis, "Internet of Things for System Integrity: A Comprehensive Survey on Security, Attacks and Countermeasures for Industrial Applications", Sensors, Vol. 21, 2021, pp.3654.

[6] X. Xia, X. Pan, N. Li, X. He, L. Ma, X.Zhang and N.Ding, "AN-based Anomaly Detection: A Review", Neurocomputing, Vol.493, 2022, pp. 497-535.

[7] M. Katzef, AC.Cullen, T. Alpcan and C.Leckie, "Generative Adversarial Networks for Anomaly Detection on Decentralized Data", Annual Reviews in Control, Vol.53, 2022, pp. 329-337.

[8] T. Schlegl, P. Seeböck, SM. Waldstein, U.Schmidt-Erfurth and G. Langs, "Unsupervised Anomaly Detection with Generative Adversarial Networks to Guide Marker Discovery", Proceedings of Information Processing in Medical Imaging, Cham, Switzerland: Springer, 2017, pp.146-157.

[9] MH. Shahriar, NI. Haque, MA. Rahman and M. Alonso, "G-IDS: Generative Adversarial Networks Assisted Intrusion Detection System", IEEE 44th Annual Computers, Software, and Applications Conference, 2020 pp. 376-385.

[10] W. Xu, J. Jang-Jaccard, T. Liu, F. Sabrina and J. Kwak, "Improved Bidirectional GAN-Based Approach for Network Intrusion Detection Using One-Class Classifier', Computers, Vol.11, 2022, pp.85.

[11] J. He, "CWGAN-DNN: A Method of Conditional Wasserstein Generation against Network Intrusion Detection", Journal of Air Force Engineering University, Vol.22, No.5, 2021, pp. 67-74.

[12] I. Sharafaldin, AH. Lashkari and AA. Ghorbani, "Toward Generating a New Intrusion Detection Dataset and Intrusion Traffic Characterization", In Proceedings of the ICISSP 2018, Madeira, Portugal, 2018, pp.108-116.

[13] I. Goodfellow, J. Pouget-Abadie, M. Mirza, B. Xu, D.Warde-Farley, S. Ozair, A. Courville and Y. Bengio, "Generative Adversarial Nets", Advances in Neural Information Processing Systems, 2014, pp.2672-2680.

[14] I. Yilmaz, R. Masum and A.Siraj, "Addressing Imbalanced Data Problem with Generative Adversarial Network for Intrusion Detection", Proceedings of the 2020 IEEE 21st International Conference on Information Reuse and Integration for Data Science, IEEE, Las Vegas, NV, USA, 2020, pp.25-30.

[15] IO. Lopes, D. Zou, IH.Abdulqadder, FA. Ruambo, B.Yuan and H.Jin, "Effective Network Intrusion Detection via Representation Learning: A Denoising Auto Encoder Approach", Computer Communications, Vol.194, 2022, pp.55-65.

[16] PH. Huynh, VH. Nguyen and Do, "Enhancing Gene Expression Classification of Support Vector Machines with Generative Adversarial Networks", Journal of Information and Communication Convergence Engineering, TN 2019.

TRANSFORMER ENSEMBLE METHOD FOR HATE SPEECH DETECTION

P.R. Rupashini and K.Premalatha
Department of Computer Science and Engineering
Bannari Amman Institute of Technology, Sathyamangalam - 638 401, Erode District, Tamil Nadu

Abstract

Because of the Internet's accessibility and anonymity, there has been growing concern about the spread of hate speech for many years. The social fabric of our society is harmed by rhetoric that dehumanizes, disparages, or threatens individuals and oppressed groups in addition to posing a threat to the targets' mental health and democratic access to the Internet. As a result, manual moderation has received a lot of attention. Yet, this is a Sisyphean process due to the volume of data generated every day, especially on social media sites like Facebook and Twitter. The need for automated tools to identify hate speech has grown as a result.

Here, we tackled the problem of hate speech detection by analyzing a benchmark of hate speech from Twitter using a simple ensemble of transformer models. We used this approach to arrive at a weighted F1 score of 0.8426, which we were able to raise by using more training data, leading to a weighted F1 score of 0.8504. This notably outperforms the system with the best performance in the literature.

Keywords: *Ensemble, Hate speech detection, Natural language processing, Transformers, ROBERTa*

1. INTRODUCTION

The subject of hate speech still raises a lot of questions. One major point of contention is whether hate speech should be criminalized or whether it should be covered by the free speech guarantee [1,2,3].

Another topic of discussion is the proper countermeasure to use. Experts disagree on whether to use tactics that attack the problem's source, such as counter-speech and education, or whether to suppress (via legal action, banning, or blocklists). Yet, without the ability to identify hate speech in bulk, these arguments are useless.

Even though manual detection may seem like a simple (though hardly scalable) option, the difficulty of manual moderation [4] and the enormous volume of data generated online also make an automatic approach to detecting hostile and offensive content necessary.

1.1 Related Work

The recent increase in offensive and hostile content may have been influenced by the simplicity of obtaining quick, dependable Internet access, which allowed ideas and information to spread at an unheard-of rate and provided the option of anonymity[5]. The identification of hate speech has thus been the subject of extensive research. These initiatives go back to Microsoft research in the late 1990s and the suggestion of a rule-based system by the name of Smokey. There have been other ideas for rule- based, template-based, or keyword-based systems that are comparable to our one [6].

Many academics have since attempted to solve this problem using conventional machine learning techniques. Following feature extraction using the Bag-of-Words (BoW) method, Kwok and Wang [7] used a Naive Bayes classifier to identify racism directed at black people on Twitter. Vector Machines (SVMs) on BoW characteristics to categorize racist writings[8]. Others, however, used more advanced feature extraction techniques to obtain input for the traditional machine learning methods (such as SVM, Naive Bayes, and Logistic Regression [9,10]) deployed for the detection of hateful content because the BoW approach was shown to have high false-positive rates [11].

Deep learning's acceptance in natural language processing (NLP), which came after its success in pattern recognition and computer vision, contributed to the advancement of the field of hate speech identification Embeddings' introduction played a significant part in this procedure. For starters, by adding beneficial features to the same traditional machine learning algorithms for hate speech identification, the BoW technique achieves much

superior complexity, and classification scores [12]). Convolutional neural networks [13], recurrent neural networks [14,15,16], and techniques that combined the two [17] were other well-liked deep learning approaches for the task.

The introduction of transformers was another important development, particularly because BERT's text categorization performance significantly improved [18]. Additionally, transformer models have excelled in contests for identifying hate speech, with the majority of the top ten teams employing one in a recent challenge [19]. The identification of hate speech has also been achieved using transformer ensembles [20]. In a recent competition with more than fifty participants, such a solution recently received the best performance or the best performance on average across a number of subtasks. For this reason, we also chose to use a collection of transformer models in this instance.

1.2 Contribution

Here, to achieve cutting-edge performance on the HASOC benchmark, we combine the RoBERTa model with a 5-fold ensemble training strategy. Additionally, we propose additional fine-tuning, which significantly enhances the performance of models trained on different folds.

Table 1 Example Tweets from the HASOC Dataset [22]

Tweet	Label
@piersmorgan Dont watch it then. #dickhead	NOT
This is everything. #fucktrump https://t.co/e2C48U3pss	HOF
I stand with him ...He always made us proud □□□#DhoniKeepsTheGlove	NOT
@jemelehill He's a cut up #murderer #fucktrump #impeachtrump	HOF
□□□□□□□□□□□□□□□ @ Houston, Texas https://t.co/8QGgbWtOAf	NOT

2. EXPERIMENTAL MATERIALS

The benchmark challenge in this part. Many competitions have been held to develop solutions because of how important the issue is. We are confident that our approaches can be applied to the problem raised by the HASOC data for this study, especially the English language data. Here, 6712 tweets were annotated into the following categories, with 860 tweets in the test set and 5852 in the training set, respectively.

NOT: tweets not considered to contain hateful or offensive content
HOF: tweets considered to be hateful, offensive, or profane

Whereas in the training set, 2261 tweets were classified into the second group in almost 39% of all cases, in the test set, this ratio was only 28% (240 tweets). Table 1 contains a selection of sample tweets from the training set. As can be seen, there are some instances where it is not entirely clear why one tweet was branded as hateful while others were not (#fucktrump). The system description papers from the first HASOC competition include a list of additional examples with disputed labeling. This may be the reason why Ross et al. advised that hate speech detection be seen as a regression job rather than a classification task .

2.1 OffensEval

Table 2 below demonstrates that the training data published by Zampieri et al. for the 2020 OffensEval competition were scores rather than class labels in accordance with the aforementioned advice. Due to time constraints, we only used the first million tweets from the training set's total of 9,089,140.

Table 2 Example tweets from the OffensEval corpus [47]

Tweet	Score
@USER And cut a commercial for his campaign.	0.2387
@USER Trump is a fucking idiot his dementia is getting worse	0.8759
Golden rubbers in these denim pockets	0.3393
Hot girl summer is the shit!!! #period	0.8993

3. EXPERIMENTAL METHODS

The processing pipeline we utilized to categorize HASOC tweets are covered in this section. This includes the procedures we took to pre-process the text, a brief explanation of the machine learning models we employed, and the training strategy we performed on those models.

3.1 Text Pre-processing

Content from social media platforms, and Twitter in particular, frequently contains a lot of paralinguistic components and lacks correct grammar and punctuation (e.g. URLs, emoticons, emojis, hashtags). Before being given to our model, tweets underwent pre-processing to help mitigate any potential issues brought on by this variable. Prior to adding more white space characters between words and punctuation, consecutive white space characters were first substituted by a single occurrence. Then the character series @USER and URL respectively took the place of @-mentions and links.

Also, all emojis and emoticons were eliminated because our initial study of the more than nine million tweets in the OffensEval dataset failed to detect a significant association between emojis and hatefulness scores.

3.2 RoBERTa

In this work, we employed a RoBERTa [20] variation of BERT [8] from the Simple Transformers library for tweet classification and regression (for a detailed description of transformers in general, as well as BERT and RoBERTa in particular, please see the sources cited in this paper). We did so with encouragement thanks to BERT's text categorization performance and our initial RoBERTa experiments. With the exception of the learning rate, for which we chose 1e5, we followed when choosing values for our meta-parameters during the training of the aforementioned model.

3.3 5-fold Ensemble Training

The training scheme below was employed in our experiments. In the beginning, we divided the HASOC train set into five equal halves, each with 1170 tweets (Dev1 , Dev2 , Dev3 , Dev4 , Dev5). This division was done in such a way that the ratio of the two separate classes was the same in each subset as it was in the entire division. Finally, using the leftover tweets from the initial training set, we built a training set for each development set (Train1, Train2, Train3, Train4, Train5). We utilised each fold to train a different RoBERTa model after building the five folds in this way.

The ensemble of the five separate models, which comprised the final model, was then developed. The ensemble model's predictions were produced by averaging the predicted scores of the five individual models.

Table 3 F1-scores of Different Models on the Test Set of the HASOC Benchmark. For each model and each F1-score, the best result is emphasized in bold

Model	Fold	H	HASOC (Off)
Macro F1 -score	1st	0.7586	0.7964
	2nd	0.7681	0.7855
	3rd	0.7688	0.7943
	4th	0.7914	0.7929
	5th	0.7758	0.8029
	Ensemble	**0.7945**	0.7976
Weighted F1 -score	1st	0.8125	0.8507
	2nd	0.8165	0.8402
	3rd	0.8244	0.8474
	4th	0.8415	0.8485
	5th	0.8327	0.8537
	Ensemble	**0.8426**	0.8504

Here, we looked at two distinct ensembles. We used a pretrained RoBERTa model for one (HASOC only), tweaked it on various folds, and produced five variants of the model. The predictions from various models were then averaged for the final classification. We first improved the RoBERTa model using one million tweets from the OffensEval competition for training and ten thousand tweets for validation to see how further improvement might affect the outcomes. The model that was created was then further adjusted in the way outlined above. However, since the initial fine-tuning produced a regression model, we first substituted the NOT and HOF labels with values of 0 and 1, respectively, before further refining these models.

In this instance, min-max normalisation was used to first rescale the projected scores prior to and each F1 -score, the best result is emphasized classification to the 0-1 range (HASOC in bold. OffensEval)

4. RESULTS AND DISCUSSION

On the HASOC test set, we assessed the produced ensembles. Table 3 is a list of the findings from these tests. As shown in Table 3, the performance of individual models significantly improved as a result of further fine-

tuning utilising OffensEval data (using the paired t-test, we find that the change is significant at p 0.05 for both the macro and the weighted F1 -score). Yet, there is a significantly smaller gap between the ensembles' performances. The five models in the HASOC OffensEval example may be more comparable to one another, which could be one explanation for this (given that here the original model went through more fine-tuning with the same data).

However, while the ensemble achieves greater F1 scores using both metrics in the case of the HASOC only model, this is not the case with the HASOC OffensEval model, where the best performance is obtained using the model trained on the fifth fold. Despite this, in all F1 -score metrics, both ensemble approaches surpass the HASOC competition winner. (The winning team achieving a score of 0.7882 and 0.8395 in terms of macro F1-score, and weighted F1-score respectively).

REFERENCES

[1] E. Barendt, What is the Harm of Hate Speech? Ethic Theory, Moral Prac., https://doi.org/10.1007/s10677-019-10002-0, Vol.22, 2019, pp. 759-760.

[2] R. Dworkin, "A New Map of Censorship, Index on Censorship", https://doi.org/10.1080/03064220500532412, Vol.35, No.1, 2006 pp.130-133.

[3] V. Basile, C. Bosco, E. Fersini, D. Nozza, V. Patti, F.M. Rangel Pardo, P. Rosso and M.Sanguinetti, "SemEval-2019 task 5: Multilingual Detection of Hate Speech against Immigrants and Women in Twitter", in Proceedings of the 13th International Workshop on Semantic Evaluation. https://doi.org/10.18653/v1/S19-2007., 2019, pp.54-63.

[4] A. Hern, "Revealed: Catastrophic Effects of Working as a Facebook Moderator", The Guardian 2019, https://www.theguardian.com/technology/2019/sep/17/revealed-catastrophic-effects-working- facebook-moderator, accessed on 2020-pp.04-26.

[5] S. Heyman, "Hate Speech, Public Discourse, and the First Amendment", in I.Hare, J. Weinstein, J. (eds.) Extreme Speech and Democracy. Oxford Scholarship Online, https://doi.org/10.1093/acprof:oso/9780199548781, 2009.

[6] T. GrØondahl, L. Pajola, M. Juuti, M. Conti and N. Asokan, "All you need is "love", Evading Hate Speech Detection, in Proceedings of the 11th ACM Workshop on Artificial Intelligence and 26 Security. AISec '18, Association for Computing Machinery, New York, NY, USA (2018). https://doi.org/10.1145/3270101.3270103, pp.2-12.

[7] S. MacAvaney, H.R. Yao, E. Yang, K. Russell, N.Goharian and O.Frieder, "Hate Speech Detection: Challenges and Solutions", PLOS ONE, https://doi.org/10.1371/journal.pone.0221152, Vol.14, No.8, 2019, pp.1-16.

[8] Greevy, E., Smeaton, A.F.: Classifying racist texts using a support vector ma- chine. In: Proceedings of the 27th Annual International ACM SIGIR Confer- ence on Research and Development in Information Retrieval. SI- GIR '04, Association for Computing Machinery, New York, NY, USA, https://doi.org/10.1145/1008992.1009074, 2004, pp.468-469.

[9] P. Burnap and M.L. Wiliams, Cyber Hate Speech on Twitter: An Application of Machine Classification and Statistical Modeling for Policy and Decision Mak- ing", Policy & Internet, https://doi.org/10.1002/poi3.85,https://onlinelibrary.wiley.com/doi/abs/10.1002/po i3.85., Vol.7, No.2, 2015, pp.223-242.

[10] T. Davidson, D. Warmsley, M. Macy and I.Weber, "Automated Hate Speech Detection and the Problem of Offensive Language", in Proceedings of the 11th International AAAI Conference on Web and Social Media.ICWSM '17, 2017, pp. 512–515.

[11] J. Devlin, M.W. Chang, K. Lee, K.Toutanova, "BERT: Pre-training of deep bidirectional transformers for language understanding. In: Proceedings of the 2019 Conference of the North American Chapter of the Association for Computational Linguistics: Human Language Technologies, Association for Computational Linguistics,
Minneapolis, 12 Minnesota (Jun2019). https://doi.org/10.18653/v1/N19-1423, Vol.1(Long and Short Papers). pp. 4171-4186.

[12] N. Djuric, J. Zhou, R. Morris, M. Grbovic, V. Radosavljevic and N. Bhamidipati, "Hate speech detection with comment embeddings", in Proceedings of the 24th International Conference on World Wide Web. WWW '15 Com- panion, Association for Computing Machinery, New York, NY, USA, https://doi.org/10.1145/2740908.2742760, 2015, pp.29-30.

[13] B. Gamback and U.K.Sikdar, "Using Convolutional Neural Networks to Classify Hate-Speech", in Proceedings of the First Workshop on Abusive Language Online. Association for Computational

Linguistics, Van-couver, BC, Canada, https://doi.org/10.18653/v1/W17-3013, https://www.aclweb.org/anthology/W17-3013, August.2017, pp.85-90.

[14] F. Del Vigna, A. Cimino, F. Dell'Orletta, M. Petrocchi and M.Tesconi, "Hate Me, Hate Me Not: Hate Speech Detection on Facebook", in ITASEC, 2017.

[15] H.T.T.Do, H.D. Huynh, K.V. Nguyen, N.L.T. Nguyen and A.G.T. Nguyen, "Hate Speech Detection on Vietnamese Social Media Text Using the Bidirectional -LSTM model, http://arxiv.org/abs/1911.03648, 2019.

[16] P. Badjatiya, S. Gupta, M. Gupta and V. Varma, "Deep Learning For Hate Speech Detection in Tweets", in Proceedings of the 26th International Conference on World Wide Web Companion. WWW '17 Companion (2017).

[17] I. Kwok and Y. Wang, "Locate the hate: Detecting tweets against blacks", in Proceedings of the Twenty-Seventh AAAI Conference on Artificial Intelligence. AAAI'13, AAAI Press, 2013, pp.1621–1622.

[18] Y. Liu, M. Ott, N. Goyal, J. Du, M. Joshi, D. Chen, O. Levy, M. Lewis, L. Zettlemoyer and V. Stoyanov, "Roberta: A Robustly Optimized Bert Pertaining Approach, 2019.

[19] Brown, A.: What is so special about online (as compared to offline) hate speech? https://doi.org/10.1177/1468796817709846., Ethnicities, Vol.18, No.3, 2018, pp.297-326.

[20] T. Mandl, S. Modha, C. Mandlia, D. Patel, A. Patel and M.Dave, "HASOC-Hate Speech and Offensive Content Identification in Indo-european Languages", https://hasoc2019.github.io, accessed on 2019-09-20.

DRYING CHARACTERISTICS OF HOT AIR ASSISTED MICROWAVE DRYING ON MORINGA LEAVES, SPINACH LEAVES, LEMONGRASS, BANANA, AND GINGER

E. Tamilan, K. Sivakrishnan, P. Nithishkumar and J. Balaji
Bannari Amman Institute of Technology, Sathyamangalam - 638 401, Erode District, Tamil Nadu

Abstract

Moringa leaves, spinach, lemongrass, banana, and ginger have various bioactive phytochemicals, micronutrients, and health-improving pharmacological properties. The objective of the present study is to dry moringa leaves, spinach, lemongrass, banana, and ginger using a hot air-assisted microwave drier and study the effect of microwave power on drying rate, effective moisture diffusivity, activation energy, and antioxidant activity. To get the best fit model, MTLAB was used. At 0.6 kW microwave power, drying rate, effective moisture diffusivity, and antioxidant activity increased while drying time and activation energy decreased. The best fit model was evaluated by using an increased co-efficient of determination and reduced root mean square error was also determined. From the result, the study concluded that hot air-assisted microwave drying is one of the potential driers for drying moringa leaves, spinach, lemongrass, banana, and ginger.

Key words: *Activation Energy, Thin Layer Model, Antioxidant Activity, Effective Moisture Diffusivity, Hot Air Assisted Microwave Drying, Microwave Power*

1. INTRODUCTION

Moringa oleifera belongs to the Moringaceae family. It contains calcium, protein, iron, and amino acids, which help human body heal and build muscle. The leaves of M. oleifera are also excellent sources of phytonutrients like ascorbic acid, tocopherols, and carotenoids. Oyeyinka, A.T and Oyeyinka, S.A.[1]. Leaves are used to cure gastric ulcers, conjunctivitis, tuberculosis, bronchitis, asthma, dysentery, jaundice, inflammation, diabetes, and fatigue. Jesuthasan, A.S and Uluwaduge, D.I.[2]. Spinach(Spinacia oleracea) belongs to Amaranthaceae family. Spinach is a good source of vitamin C, calcium, iron phosphorus, sodium, and potassium in addition to being high in beta carotene (provitamin A) and folate. Spinach contains folate, which prevents neural tube defects. El "Sayed S.M.[3]. Banana belongs to the Musaceae family. It is one of the oldest cultivated plants known for its dietary and medicinal properties. Vitamins (riboflavin, folate, and vitamin C), carotenoids (-carotene, lutein, and zeaxanthin), and minerals (P,K, Ca, Mg, Na, Fe, Mn, Zn, Cu, and B) have been found to vary widely among various banana cultivars. Ashokkumar, K *et al.*[4]. Lemongrass belongs to Gramineae family. All parts of lemongrass contain a lot of antioxidant chemicals like vitamins,minerals, electrolytes, and others [5]. It controls dandruff, improves anemia, promote mental health, decreases risk of cardiovascular disease by lowering cholesterol, Works as a strong anti-viral agent. Megan Wochnick. R.D. N.[6]. Ginger belongs to the Zingiberaceae Family. It is used for arthritis Shahrajabian, M. H. Sun, W and Cheng, Q[7], stomach problems, asthma Kardan M *et al*[8], diabetes, and irregular menstruation. There is suggestive evidence that ginger reduces inflammation and pain, and there is scientific support that ginger can alleviate the symptoms of nausea and vomiting following pregnancy, surgery, cancer therapy, or motion sickness Jesuthasan A.S. and D.I. Uluwaduge [9].

2. MATERIALS AND METHODS PURCHASING OF RAW MATERIAL

Fresh Moringa leaves, spinach, banana, lemongrass, and ginger were procured from the local available market in Perundurai.

2.1 Prepartion of Raw Material

Cleaning should be done for the removal of sand particles and other foreign particles from the purchased products.

3. EQUIPMENT USED MICROWAVE DRYER

In the field of processing fruits and vegetables, microwave drying has become widely used as a clean and effective method since the maturation of high-power magnetron production. Fruits and vegetables' uniformity, moisture and heat dissipation efficiency, and uniformity

are all enhanced by microwave fluidization drying (MFD) Lv, W., Li, D[10].

3.1 Drying Process

Moringa and spinach leaves, lemongrass, banana, ginger was purchased and they were sorted and washed. They were peeled and cut at a uniform size using a clean sharp knife. The samples are subjected to microwave drying at various powers (0.2,0.4,0.6,0.35,0.45,0.55 kw). Then dried samples are stored and utilized for further analysis.

3.2 Determination of Drying Characteristics

The various drying characteristics are determined by the following techniques.

3.3 Drying Rate

Removal of water from the sample at a particular time is known as the drying rate. The overall drying rate was calculated using the equation.

$$\text{Drying rate, g } H_2O/\text{ g solids/min} = \frac{\text{Amount of water removed, g}}{\text{dry solids, g} * \text{Time, min}}$$

4. EFFECTIVE MOISTURE DIFFUSIVITY

The effective moisture diffusivity (D_{eff}) was calculated at each corresponding moisture content and time in this study. The average effective moisture diffusivity (D_{eff}) (Avg) was calculated by using equation.

$$MR = \frac{8}{\pi^2}\exp\left(\frac{-D_{eff}\pi^2 t}{4L^2}\right)$$

Where,
MR – Moisture ratio
L – Half thickness of the sample, m t – Time taken for drying, s-Activation energy.
The activation energy was also calculated by using the Arrhenius relation which is presented as equation

$$D_{eff} = D_0\exp\left(\frac{-E_a}{RT}\right)$$

Where,
T - Temperature (C)
R - Gas constant (kJ/mol-1 K-1)
Do - Effective moisture diffusivity
E_a - Activation energy (kJ/mol)

5. MATHEMATICAL MODELING

In this study, the experimental drying data of moringa leaves, spinach,lemongrass, banana, and ginger at different microwave powers were fitted into commonly used thin-layer drying models, listed in below Table. For mathematical modelling MATLAB software version 11 was used.

Sl.No.	Model Name	Model	Reference
1	Henders on and Pabis	MR=a.exp(-k.t)	(Henderson and pabis 1961)
2	Page	MR=ex p(-k.t*n*)	(page 1949)
3	Two term exponent ial	MR =a. exp (-k.t) + (1-a) exp(- k.a.t)	(Sharaf- Eldeen et al. 1980)
4	verma	MR =a. exp (-k.t) + (1-a) exp(- g.t)	(Mujaffar and john 2018)
5	Diffusio n model	MR =a. exp (-k.t) + (1-a)exp(- k.a.t)	(Mujaffar and john 2018)
6	Three paramete r model	MR=a.exp((-k.t)*)	(Potisate and Phoungchan dang 2015)
7	Midilli- Kucuk	MR=a.exp(- k.tn)+b. t	(Midilli et al. 2002)
8	Logarith mic	MR =a.exp(-k.t)+c	(Togrul and Pehlivan 2003)

6. RESULTS AND DISCUSSION

The microwave drying of moringa and spinach leaves, lemongrass, ginger carried out at different power levels such as 0.2, 0.4, and 0.6 kW and banana is carried out at 0.35, 0.45, and 0.55 kW which is used to determine the drying rate. At 0.2, 0.4, and 0.6 kW, the drying of moringa leaves took 24, 22, 20 minutes; spinach leaves took 46, 38, 34 minutes; lemongrass took 20, 16, 14 minutes; ginger took 34, 28, and 20 minutes; and at 0.35, 0.45, and 0.55 kW, the drying of banana took 38, 36, 34 minutes. The drying time was directly proportional to the microwave power levels i.e the higher power consumes more time. Similar findings have been reported for spinach, moringa and banana leaves microwave dried at 180-900 W, 150-900 W and 350 W. By working at 900 W instead of 300 W, the drying time could be shortened by 3.1- fold for ginger slices. For moringa leaves, Drying rate increased with decrease in drying time. The higher microwave

power resulted in greater rates of moisture removal and an enhancement of drying potential

Potisate Y. and S. Phoungchandang [11]. Total drying time for spinach leaves is from 7.7 min to 25 min Dadali G., *et al*[12]. The drying of banana slices took place in the falling rate drying period with convection drying taking the longest time. Higher drying rates were observed with the higher power level Maskan M[13]. Similar results were obtained by Ganesapillai.M.,*et al*[14] for microwave drying ginger.

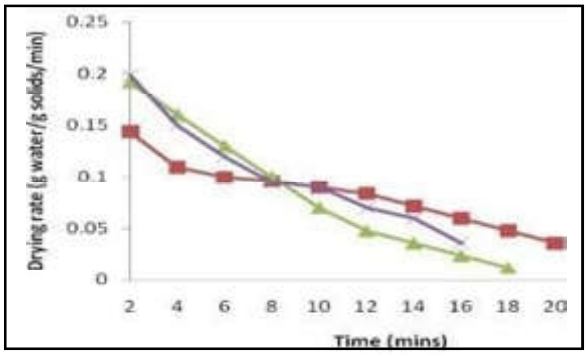

Fig.1 Drying rate Vs time of moringa leaves at different power level

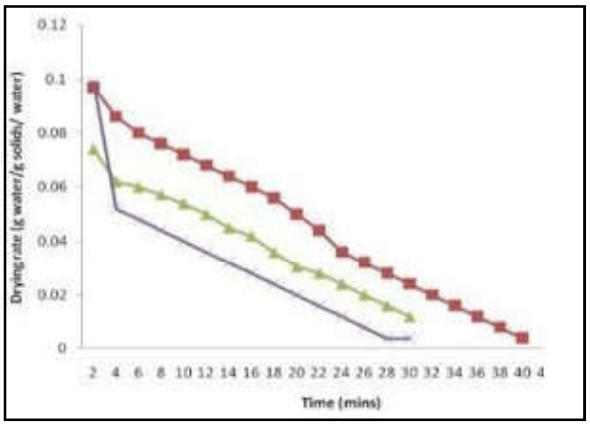

Fig.2 Drying rate Vs time of spinach leaves at different power level

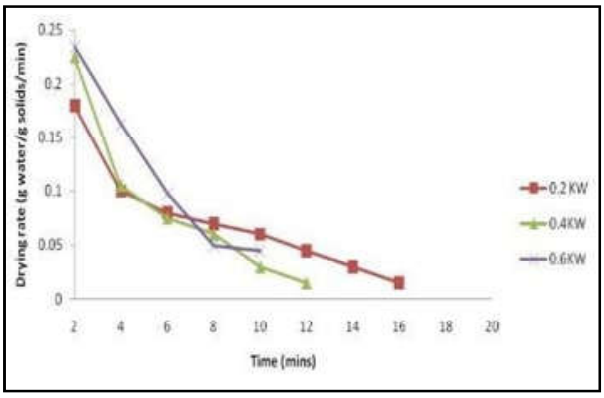

Fig.3 Drying rate Vs time of lemongrass at different power level

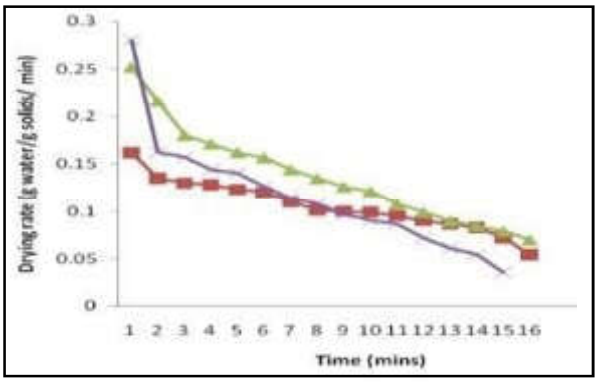

Fig.4 Drying rate Vs time of ginger at different power level

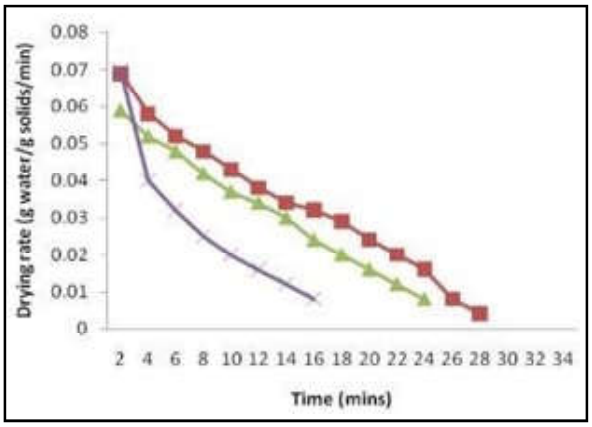

Fig.5 Drying rate Vs time of banana at different power level

7. EFFECTIVE MOISTURE DIFFUSIVITY

Effective moisture diffusivity (D_{eff}) is the rate of moisture movement. D_{eff} increases with increase in microwave output power Potisate Y. and S. Phoungchandang [11]. High D_{eff} for moringa leaves, spinach leaves, ginger, and lemongrass was observed at 0.6 kW, except banana. For banana, high D_{eff} was observed at 0.55 kW. For optimizing best drying conditions, the Deff value should be higher. The effective moisture diffusivity values (D_{eff}), obtained from this study were within the general range of 10-11 to 10-9 m2.s-1 for food materials Madamba, P. S. , et al[15].

8. ACTIVATION ENERGY

Activation Energy (E_a) is the minimum amount of energy required to start a reaction. E_a decreases with increase in microwave output power. Low E_a for moringa leaves, spinach leaves, ginger, and lemongrass was observed at 0.6 kW, except banana. For banana, low E_a was observed at 0.55 kW. For optimizing best drying conditions, the E_a value should be lower Maskan M[13] and Ganesapillai.M., *et al*[14]. Because increase in effective moisture diffusivity and decrease in activation

energy corresponding with increase in microwave 38 output power increase the diffusivity and moisture transfer rate which in terms decrease the drying time Potisate Y. and S. Phoungchandang [11].

Table 1 Effective Moisture Diffusivity and Activation Energy of the Samples

Sample	*Deff*(m2/s)	*Ea*(KJ/mol.(K)
Moringa (0.2 kW)	1.18±0.0416a* 10-11	135.506±0.245e
Moringa (0.4kW)	1.358±0.026b* 10-11	135.130±0.112e
Moringa (0.6kW)	1.57±0.036c* 10-11	134.727±0.039e
Spinach (0.2 kW)	1.02±0.058a*10-11	160.937±0.027f
Spinach (0.4 kW)	1.3±0.01b*10-11	160.292±0.06f
Spinach (0.6 kW)	1.36±0.0152b* 10-11	160.158±0.081f
Lemongrass (0.2kW)	2.21±0.0264 e* 10-11	132.257±0.146d
Lemongr ass (0.4kW)	2.61±0.05e*10-11	131.8±0.088d
Lemongr ass(0.6kW)	3.22±0.0757f* 10-11	131.236±0.07d
Ginger(0.2 kW)	1.176±0.0313d * 10-9	112.236±0.005c
Ginger (0.4 kW)	1.392±0.01b* 10-9	110.77±0.036c
Ginger (0.6 kW)	2.014±0.01e* 10-9	109.78±0.0435b
Banana (0.35kW)	1.568±0.054c* 10-9	109.05±0.0288b
Banana (0.45kW)	1.542±0.005c* 10-9	109.11±0.0463b
Banana (0.55kW)	1.73±0.035d* 10-9	108.78±0.005a

9. THIN LAYER DRYING MODEL

The moisture ratio (MR) is approximately proportional to the difference in moisture content between the material being dried and the equilibrium moisture content at the drying conditions. The mathematical drying models for thin- layer drying was fitted by moisture ratio(MR) and drying time. Normally, for microwave drying, the equilibrium moisture content was assumed to be zero.

The obtained microwave drying curves were analyzed using eight different empirical and semi-empirical drying models through regression analyses. Although the coefficient of determination (R2) was one of the primary criteria for selecting the best equation to account for the variation in the drying curves, other statistical parameters such as root mean square error (RMSE) values were determined to validate the consistency of the fit. The highest value of R2 and the lowest values of RMSE were used to determine the best fit.

Table 2 Thin Layer Drying Model of Dried Moringa Leaves

Model	0.2kW			0.4kW			0.6kW		
	R2	RMSE	Co- efficient of parameter	*R2*	RMSE	Co- Efficient of parameter	*R2*	RMSE	Co- efficient of parameter
Hendersn and Pabis	0. 9871	0.03082	a=0.9784 k=0.0823	0. 9379	0.06822	a=0.9199 k=0.1143	0. 9709	0.05363	a=1.012 k=0.1252
Page	0.9913	0.02524	k=0.1119 n=0.8855	0.987	0.03122	k=0.2682	0.9706	0.053	k=0.1275 n=0.641
MidilliKucuk	0.9961	0.01764	a=1.008 b=0.005276 k=0.1041	0.9968	0.01876	a=0.9901 b=0.0127 k=0.1853	0. 9793	0.04952	a=1.036 b=0.00715 k=0.1538
Newton	0.9858	0.03062	k=0.08519	0.9207	0.0721	k=0.1272	0.9705	0.04984	k=0.1234
Two-term	0.9986	0.01157	a=0.9987 b=0.09062 c=0.00014 d=0.3274	0.9969	0.01804	a=0.8863 b=0.2018 c=0.1051 d=0.04562	0 9863.	0.04984	a=1.032 b=0.1372 c=5.26*105 d=0.5446
Logarithmic	0.9954	0.01955	a=0.8663 c=0.1426 k=0.1171	0.9962	0.01821	a=0.7718 c=0.2245 k=0.2433	0. 9776	0.04501	a=0.9102 c=0.1238 k=0.1668

Table 3 Thin Layer Drying Model of Dried Spinach Leaves

Model	0.2kW			0.4kW			0.6kW		
	R2	RMSE	Co- efficient of parameter	*R2*	RMSE	Co- Efficient of Parameter	*R2*	RMSE	Co- efficient of Parameter
Hendersn and Pabis	0.9273	0.08274	a=1.067 k=0.07658	0. 9178	0.07679	a=0.9187 k=0.08854	0. 9907	0. 02793	a=1.001 k=0.09212
Page	0.9216	0.08593	k=0.05608 n=1.091	0.914 2	0.06328	k=0.1946 n=0.7111	0.991	0. 02744	k=0.09871 n=0.97
Three Parameter Model	0.9273	0.08678	a=1.067 k=0.2993 n=0.2559	0.917 8	0.08094	a=0.9187 k=0.2391 n=0.3703	0. 9907	0.02962	a=0.934 k=0.09212 n=1.072

Table 4 Thin Layer Drying Model of Dried Lemongrass

Model	0.2kW			0.4kW			0.6kW		
	R2	RMSE	Co- efficient of parameter	*R2*	RMSE	Co- Efficient of Parameter	*R2*	RMSE	Co- efficient of Parameter
Hendersn and Pabis	0.992	0.0275	a=1.063 k=0.0637	0. 9573	0.07384	a=1.167 k=0.06914	0. 9908	0. 0301	a=1.052 k=0.1004
Page	0.9961	0.1928	k=0.03456 n=1.188	0.991 9	0.03217	k=0.008263 n=1.692	0.9909	0. 0289	k=0.0717 n=1.115
Midilli–Kucuk	0.9924	0.02742	a=1.126 k=0.5466 n=0.000362	0.97	0.06367	a=1.126 k=0.5466 n=0.000362	0. 9992	0.0288	a=1.063 k=0.1055 b=0.00076

Table 5 Thin Layer Drying Model of Dried Banana

Model	0.35kW			0.45kW			0.55kW		
	R2	RMSE	Co- efficient of parameter	*R2*	RMSE	Co- Efficient of Parameter	*R2*	RMSE	Co- efficient of Parameter
Hendersn and Pabis	0.964	0.04278	a=0.9799 k=0.03483	0. 9861	0.0253	a=0.9926 k=0.03131	0. 9919	0.02041	a=1.01 k=0.03553
Page	0.9734	0.03681	k=0.05544 n=0.8388	0.9871	0..0244	k=0.03716 n=0.9485	0.9916	0. 02086	k=0.03483 n=1.001
Two term exponential	0.9784	0.03317	a=2.612 k=0.0978	0.9873	0.0242	a=0.4075 k=0.05289	0. 987	0.02592	a=0.03309 k=1

Table 6 Thin Layer Drying Model of Dried Ginger

Model	0.2kW			0.4kW			0.6kW		
	R2	RMSE	Co- efficient of parameter	*R2*	RMSE	Co- Efficient of Parameter	*R2*	RMSE	Co- efficient of Parameter
Hendersn and Pabis	0.9538	0.07611	a=1.152 k=0.06775	0. 9092	0.03184	a=1.045 k=0.09208	0. 9786	0.05568	a=1.068 k=0.1552
Page	0.9988	0.01245	k=0.00735 n=1.729	0.9741	0..01637	k=0.05239 n=1.204	0.9951	0.02665	k=0.0726 n=1.344
Verma	0.9266	0.09906	a=115.4 k=0.05198 g=0.05192	0.9977	0.0162	a=3.494 k=0.1352 g=0.1666	0.9794	0.05144	a=3.933 k=0.08549 g=0.09521
Diffusion	0.9975	0.01825	a=13.32 c=0.9184 k=0.144	0.9794	0.01617	a=2.983 b=0.8349 k=0.1643	0.992	0.03211	a=0.4369 b=0.2771 k=0.7125

10. CONCLUSION

Microwave drying of moringa leaves, spinach, lemongrass, ginger, and banana retained more bioactive phytochemicals. Microwave heating results in rapid mass transfer within the sample because heat generated by the microwave creates a large vapor pressure difference between the centre and surface of the product. So, increase in microwave output power increases the effective moisture diffusivity and decreases activation energy

REFERENCES

[1] A.T.Oyeyinka and S.A.Oyeyinka, "Moringa Oleifera as a Food Fortificant: Recent Trends and Prospects", Journal of the Saudi Society of Agricultural Sciences, Vol.17, No.2, 2018, pp.127-136.

[2] A.S.Jesuthasan and D.I.Uluwaduge, "Ethnobotanics Used In Folk Medicine of Tamil Culture in Sri Lanka: A Scientific Review", Journal of Integrative Medicine, Vol.15, No.1, 2017, pp.19-26.

[3] S.M.El-Sayed, "Use of Spinach Powder as Functional Ingredient in the Manufacture of UF-Soft cheese", Heliyon Vol.6, 2020, pp.e03278.

[4] K.Ashokkumar, S.Elayabalan, V.G. Shobana, P. Sivakumar and M.Pandiyan, "Nutritional Value of Cultivars of Banana (Musa spp.) and its Future Prospects", Journal of Pharmacognosy and Phytochemistry, Vol.7, No.3, 2018, pp.2972-2977.

[5] Food Data Central Search Results. Food Data Central, https://fdc.nal.usda.gov/fdc- app.html#/food-details/168573/nutrients, 2019.

[6] R.D.N. Megan Wochnick, "Health Benefits of Lemongrass and How to Use It", 2020.

[7] M.H. Shahrajabian, W. Sun and Q.Cheng, "Clinical Aspects and Health Benefits of Ginger (Zingiber Officinale) in Both Traditional Chinese Medicine and Modern Industry", Acta Agriculturae Scandinavica, Section b-Soil & Plant Science, Vol.69, No.6, 2019, pp.546-556.

[8] M.Kardan, A.Rafiei, J.Ghaffari, R. Valadan, Z. Morsaljahan and S.T.Haj-Ghorbani, "Effect of Ginger Extract on Expression of GATA3, T-bet and ROR-ăt in Peripheral Blood Mononuclear Cells of Patients with Allergic Asthma", Allergologia et Immunopathologia, Vol.47, No.4, 2019, pp.378-385.

[9] A.S. Jesuthasan and D.I.Uluwaduge, "Ethnobotanics Used in Folk Medicine of Tamil Culture in Sri Lanka: A Scientific Review", Journal of Integrative Medicine Vol.15, 2017, pp.19-26.

[10] W. Lv, D. Li, H. Lv, X. Jin, Q. Han, D.Su and Y.Wang, "Recent Development of Microwave Fluidization Technology for Drying Of Fresh Fruits and Vegetables", Trends in Food Science & Technology, Vol.86, 2019, pp.59-67.

[11] Y. Potisate and S.Phoungchandang, "Microwave Drying of Moringa Oleifera (Lam.) Leaves: Drying Characteristics and Quality Aspect", Asia- Pacific Journal of Science and Technology, Vol. 20, 2015, pp.12-25.

[12] G. Dadali, *et al.*, "Effect of Drying Conditions on Rehydration Kinetics of Microwave Dried Spinach", food and bioproducts processing, Vol.86, 2008, pp.235-241.

[13] M.Maskan, "Microwave/air and Microwave Finish Drying of Banana", Journal of Food Engineering Vol.44, 2000, pp.71-78.

[14] M. Ganesapillai, *et al.,* "Experimental Analysis of Microwave Drying Kinetics and Characterization of Ginger Rhizomes", Journal of Food Processing and Preservation, Vol.36, 2012, pp.401-411.

[15] P.S.Madamba, *et al.,* "The Thin-Layer Drying Characteristics of Garlic Slices", Journal of Food Engineering, Vol.29, 1996, pp.75-97.

SYNCHRONIZATION OF CHAOTIC NEURAL NETWORKS VIA MEMORY BASED SAMPLED-DATA CONTROL

R. Preetha and M. Parimala
Department of Mathematics,
Bannari Amman Institute of Technology, Sathyamangalam-638 401, Erode District, Tamil Nadu
E-mail: preetha@bitsathy.ac.in, rishwanthpari@gmail.com

Abstract

This paper investigates the synchronization issue of chaotic neural networks (NNs) with time delays under the memory-based sampled-data control (MSDC) scheme. To do this, MSDC is designed in the slave-delayed chaotic NNs, where a transmission delay is considered in the sampling time tk. The synchronization criterion is derived based on suitable Lyapunov functions, which include the information of e(t) to e(tk+1) and e(t) to e(tk+1). The derived criterion ensures the synchronization between the master and slave delayed chaotic NNs under the MSDC scheme, which means that the error system is globally asymptotically stable. Finally, a numerical example and their simulation results are given to show the effectiveness of the derived criterion and the proposed control scheme.

Keywords: *Chaotic neural networks, Lyapunov functional, Linear matrix inequality, Synchronization.*

1. INTRODUCTION

Past decades, chaotic nonlinear system has received much attention among the researchers due to various applications in the field of secure communication, image encryption, infor- mation science and so on. The analysis of the synchronization issue between two non-linear systems is challenging topic among the researchers. On the other hand, time-delay is an unavoidable factor in the NNs due due to the finite switching speed of the neuron amplifiers [1]. This can make the entire network as a poor performance or instability. Therefore, the time-delay is play an important role in the investigation of the qualitative analysis. Also, the synchronization analysis of master and slave NNs has paid great attention in the literature based on Lyapunov functional / looped Lyapunov functional and the linear matrix inequality approach [2]. As an example, the authors in [3] have investigated the finite-time synchronization of inertial NNs with time-delays using integral inequalities. In [4], the synchronization problem of chaotic inertial NNs has been addressed and the chaotic nature of the master delayed inertial NNs has implemented in the secure communications. The fractional-order-based sufficient condi- tions have been derived for analyzing the synchronization of delayed NNs with fractional order derivatives in [5]. Moreover, the fixed-time synchronization of NN without delays has been investigated in [6] based on an upper bound estimate formula. From the above discussion, we can observe that the globally synchronization conditions of delayed NNs have been derived by many researchers with the help of the Lyapunov functional approach.

To achieve the synchronization criteria, various control schemes have been proposed in the literature, such as state- feedback control, adaptive, observed-based feedback, and event-triggered control. Recently, the sampled-data control scheme has been commonly used in control systems where the continuous-time signal is converted into a digital signal and then processed by a digital controller. The digital controller generates control signals that are then converted back into continuous-time signals using a digital-to-analog converter and applied to the plant. The key advantage of using a sampled- data control scheme is that it allows for the use of digital signal processing techniques to design and implement the controller. Hence, the sampled-data control scheme received much attention among the researchers. As an example, in the presence of time-delays, the authors in [7] have derived the exponential synchronization criteria based on Lyapunov functional under the SDC scheme. The proposed control can achieve the synchronization criteria between two delayed NNs. In [8], quantized-based SDC has been introduced for addressing the

synchronization issues of inertial NNs under heterogenous delays. Moreover, the stochastic switched-based SDC has been proposed in [9] for analyzing chaotic NNs with packet dropout, where a stochastic variable was introduced and the resulting distribution satisfied the Bernoulli distribution. The stochastic synchronization criteria have been derived based on a novel loop-delay-product-type Lyapunov functional and numerical simulation results that show the effectiveness of the synchronization conditions under the proposed control scheme.

Recently, memory-based SDC has received much attention among researchers than the SDC scheme, where a trans- mission delay term is introduced in the sampling time and modelled as a memory-based SDC scheme. One advantage of memory-based SDC is that it can reduce the effects of the sampling delay and improve the performance of the control system. Therefore, memory-based SDC has been utilized for the stability and stabilization of nonlinear systems. As an example, in [10], memory-based SDC has been introduced for solving the stabilization issue of nonlinear chaotic systems with a fuzzy approach, where the memory-based Lyapunov functional is introduced to derive the stabilization condition. The authors in [11] have introduced memory-based SDC for analyzing the synchronization issue of delayed complex dy- namical networks, and the transmission delay and uncertainty are considered in the control input. The exponential stability conditions have been derived based on the piecewise Lyapunov function and some integral inequalities. The synchronization of the semi-Markov jump-based complex dynamic networks has been investigated under the memory SDC scheme, and the sufficient conditions of the dissipative synchronization have been derived based on the double integral and triple integral based Lyapunov functionals. Therefore, the memory- based SDC plays an important role in analyzing the stability, stabilization, and synchronization of nonlinear systems with uncertainty and time delays.

In the above discussion, the synchronization problem of master and slave chaotic NNs with time delay is addressed.We designed memory-based SDC in the slave chaotic NNs, and an error NNs model is derived between the master and slave systems. Then, a looped-type Lyapunov function is introduced, which includes the information of x(t)and x(t-·). The synchronization criterion is derived in terms of LMIs. The criterion ensures the asymptotical stability of the error states when time tends to be large, and this implies that master and slave states are synchronized with each other's under the proposed memory-based SDC scheme. Finally, a numerical example and simulation results are given to illustrate the effectiveness of the proposed work.

Notations: This paper uses standard notation throughout. He{M} = M + M and the matrices are assumed to have appropriate dimensions.

2. PROBLEM FORMULATION

Consider the master system in the following form:
Łx(t) = - Ax(t) + Bf(x(t)) + Wf(x(t - t)) + u(t) (1)
(t), t " [-t, 0]where x(t) = [xx(t) = Õ11(t), x2(t), . . . , x n(t)] T " Rn, f(x(t)) =[f(x(t) and u(t) representsthe neural state vector, neurons activation function, initial condition, control input respectively. Time-delay has the condition is that t = 0. A = diag{a 1(t)), f(x2(t)), . . . , f(xn1(t))], Õ , a21is aknown diagonal matrix , B " R, . . . , an×n n} > 0 " R is the connection weight matrix (CWM) , W " R is the delayed CWM. Consider the slave system as follows:
n×n Ły(t) = - Ay(t) + BĒ(y(t)) + WĒ(y(t - t)) + u(t) (2)
y(t) = Õ (t), t " [-t, 0]
Error system has the following representation
by denoting 2
error signal e(t) = y(t) - x(t) with g(e(t)) = Ē(y(t)) f(x(t)).
From the equation (1) and (2) the error system as follows:
Łe(t) = - Ae(t) + Bg(e(t)) + Wg(e(t - t)) + Ku (tAssumption 1. The activation functions in (1) is continuous, bounded and satisfy l Where L L 2 = n i = f 11i(³1) - fi(³)³1= diag(l+l2+1,l2+l2- ³1+2l2+1, l, . . . ,22ll= +2n+i, f, . . . , l+l2+no.ni(0) = 0, ³, l+n),18 = ³n×nk2.- ·) (3)

Assumption 1. The activation functions in (1) is continuous, bounded and satisfy-

$$l_i^- \le \frac{f_i(\gamma_1) - f_i(\gamma_2)}{\gamma_1 - \gamma_2} \le l_i^+, \ f_i(0) = 0, \gamma_1 \ne \gamma_2.$$

Where $L_1 = diag(l_1^- l_1^+, l_2^- l_2^+, \ldots, l_n^-, l_n^+)$,

$$L_2 = \left\{ \frac{l_1^- + l_1^+}{2}, \frac{l_2^- + l_2^+}{2}, \ldots, \frac{l_n^- + l_n^+}{2} \right\}.$$

The state of (2) is sampled when t = tk, where {t} satisfies the condition for tk" R+" 0 = t0< t< . . . <tk. . . , "k " N. At t = t, define a SDC:u(t) = Ke(tk- ·) (4)
where K is a gain matrix. The sampled data period d k takes the form d k= tk+1- tkand satisfies 0 < d

3. MAIN RESULTS

3.1 Preliminaries

The following lemma is useful to derive the Main Result.

Lemma 1. [10] Given constant matrices N, L, Q of appropriate dimensions where N and Q are symmetric and Q > 0, then N + L QL < 0 if and only if "T # "1kk= d#Mk

$$\begin{bmatrix} N & L^T \\ L & -Q^{-1} \end{bmatrix} < 0, \text{ or equivalently } \begin{bmatrix} -Q^{-1} & L \\ L^T & N \end{bmatrix} < 0.$$

3.2 New Synchronization Criteria

This section provides stability conditions for the error system (3), based on looped LKF and integral inequalities.Some vector notations are defined to give a clear understanding of the proof of the theorem as follows:

$$\zeta^T(t) = \Big[e^T(t) \quad e^T(t-\tau) \quad e^T(t_k-\tau) \quad \dot{e}^T(t) \quad e^T($$
$$e^T(t_{k+1}) \quad f^T(e(t)) \quad f^T(e(t-\tau)) \quad e^T(t-$$
$$\varsigma = \left[0_{n\times(m-1)n} \; I_{n\times n} \; 0_{n\times(9-m)n}\right] \in \mathbb{R}^{n\times 9n}, \; m = 1,$$

Theorem 1. For known scalars t, a, the error system (3) is said to be globally asymptotically stable if there exist symmetric matrices P¹> 0, Qi> 0, Ri> 0, T> 0(i =1, 2, 3), S> 0, and any appropriate dimension matrices M1> 0, S2> 0, H1> 0, H1, M2, Y2, real matricesJ1, J2, Z1, Z2and dk" {dm, dM1, Y2i}, the following LMIs holds:

$$\Upsilon_1 = \Omega + d_k\Gamma_5, \; \Upsilon_2 = \Omega + d_k\Gamma_6, \qquad (5)$$

where

$$\Omega = \Gamma_1 + \Gamma_2 + \Gamma_3 + \Gamma_4 + \Gamma_7 + \Gamma_8 + \Gamma_9$$
$$\Gamma_1 = He\{\varphi_1^T P\varphi_4\}$$
$$\Gamma_2 = \varphi_7^T R_1\varphi_7 - \varphi_8^T R_1\varphi_8$$
$$\Gamma_3 = h^2\varphi_4^T Q_2\varphi_4 - \frac{\pi^2}{4}(\varphi_9 - \varphi_3)^T Q_2(\varphi_9 - \varphi_3)$$
$$\Gamma_4 = \varphi_1^T Q_3\varphi_1 - \varphi_2^T Q_3\varphi_2$$
$$\Gamma_5 = 2\varphi_4^T R_2(\varphi_1 - \varphi_5) + \varphi_4^T R_4\varphi_4 + 2[(\varphi_1 - \varphi_5)^T Q_4 + \varphi_3^T Q_5]\varphi_4 + \zeta^T(t)\chi_2 R_5^{-1}\chi_2\zeta(t)$$
$$\Gamma_6 = -2(\varphi_6 - \varphi_1)^T R_3\varphi_4 + \varphi_4^T R_5\varphi_4 + 2\varphi_1^T Q_1\varphi_6 + \zeta^T(t)\chi_1 R_4^{-1}\chi_1\zeta(t)$$
$$\Gamma_7 = -(\varphi_1 - \varphi_5)^T R_2(\varphi_1 - \varphi_5) + (\varphi_6 - \varphi_1)^T R_3(\varphi_6 - \varphi_1) + 2(\varphi_1 - \varphi_6)^T Q_1\varphi_6 - (\varphi_1 - \varphi_5)^T[Q_4(\varphi_1 - \varphi_5) + 2Q_5\varphi_3] + [\varphi_1^T M_1 + \varphi_5^T M_2](\varphi_1 - \varphi_5) + [\varphi_6^T N_1 + \varphi_1^T N_2](\varphi_6 - \varphi_1)$$
$$\Gamma_8 = He\left\{\varphi_1^T L_2 M_1\varphi_7 - \varphi_1^T L_1 M_1\varphi_1 - \varphi_7^T M_1\varphi_7 - \varphi_2^T L_1 M_2\varphi_2 + \varphi_2^T L_2 M_2\varphi_8 - \varphi_8^T M_2\varphi_8\right\}$$
$$\Gamma_9 = He\left\{[\varphi_1 + \alpha\varphi_4]X[-A\varphi_1 + B\varphi_7 + W\varphi_8 + k\varphi_3 - \varphi_4]\right\}$$
$$\chi_1 = [M_1 \; 0\;0\;0 \; M_2 \; 0\;0\;0\;0], \; \chi_2 = [N_1 \; 0\;0\;0\;0 \; N_2 \; 0\;0\;0],$$
$$\varphi_i = [0_{n\times(i-1)n} \; I_{n\times n} \; 0_{n\times(9-i)n}] \in \mathbb{R}^{n\times 9n}, \; i = 1, 2, \ldots, 9.$$

Then, the gain matrix, $K = Y_1^{-1}F$

Proof. Mode-dependent LKF candidate is considered as follows:

$$V(e(t), t) = \sum_{m=1}^{4} \mathcal{V}_j(e(t), t) + \sum_{m=1}^{4} \mathfrak{V}_j(e(t), t) \qquad (6)$$

where

$$\mathcal{V}_1(e(t), t) = e^T(t)P_i e(t)$$
$$\mathcal{V}_2(e(t), t) = \int_{t-\tau}^{t} f^T(e(s))R_1 f(e(s))ds$$
$$\mathcal{V}_3(e(t), t) = h^2\int_{t_k-\eta}^{t} \dot{e}^T(s)Q_2\dot{e}(s)ds - \frac{\pi^2}{4}\int_{t_k-\eta}^{t-\eta}(e(s) - e(t_k-\eta))^T Q_2(e(s) - e(t_k-\eta))ds$$
$$\mathcal{V}_4(e(t), t) = \int_{t-\tau}^{t} e^T(s)Q_3 e(s)ds$$
$$\mathfrak{V}_1(e(t), t) = (t_{k+1} - t)(e(t) - e(t_k))^T R_2(e(t) - e(t_k)) + (t - t_k)(e(tk+1) - e(t))^T R_3(e(tk+1) - e(t))$$
$$\mathfrak{V}_2(e(t), t) = (t_{k+1} - t)\int_{t_k}^{t} \dot{e}^T(s)R_4\dot{e}(s)ds - (t - t_k)\int_{t}^{t_{k+1}} \dot{e}^T(s)R_5\dot{e}(s)ds$$
$$\mathfrak{V}_3(e(t), t) = 2(t - t_k)\{(e(t) - e(t_{k+1}))^T Q_1 e(t_{k+1})\}$$
$$\mathfrak{V}_4(e(t), t) = (t_{k+1} - t)(e(t) - e(t_k))^T [Q_4(e(t) - e(t_k)) + 2Q_5 e(t_k - \eta)]$$

By computing the derivative as

$$\dot{V}(e(t), t) = \sum_{m=1}^{4} \dot{\mathcal{V}}_j(e(t), t) + \sum_{m=1}^{4} \dot{\mathfrak{V}}_j(e(t), t) \qquad (7)$$

$$\dot{\mathcal{V}}_1(e(t), t) = 2e^T(t)P\dot{e}(t) = \zeta^T(t)\Gamma_1\zeta(t) \qquad (8)$$
$$\dot{\mathcal{V}}_2(e(t), t) = f^T(e(t))R_1 f(e(t)) - f^T(e(t\tau))R_1 f(e(t-\tau)) \qquad (9)$$
$$= \zeta^T(t)\Gamma_2\zeta(t) \qquad (10)$$
$$\dot{\mathcal{V}}_3(e(t), t) = h^2\dot{e}^T(t)Q_2\dot{e}(t) - \frac{\pi^2}{4}(e(t-\eta) \qquad (11)$$
$$- e(t_k - \eta))^T Q_2(e(t-\eta) - e(t_k - \eta)) \qquad (12)$$
$$= \zeta^T(t)\Gamma_3\zeta(t) \qquad (13)$$
$$\dot{\mathcal{V}}_4(e(t), t) = e^T(t)Q_3 e(t) - e^T(t-\tau)Q_3 e(t-\tau) \qquad (14)$$
$$= \zeta^T(t)\Gamma_4\zeta(t) \qquad (15)$$
$$\dot{\mathfrak{V}}_1(e(t), t) = -(\varphi_1 - \varphi_5)^T R_2(\varphi_1 - \varphi_5) + 2(t_{k+1} - t)\varphi_4^T R_2(\varphi_1 - \varphi_5) + (\varphi_6 - \varphi_1)^T R_3(\varphi_6 - \varphi_1) - 2(t - t_k)(\varphi_6 - \varphi_1)^T R_3\varphi_4$$
$$\dot{\mathfrak{V}}_2(e(t), t) = (t_{k+1} - t)\varphi_4^T R_4\varphi_4 + (t - t_k)\varphi_4^T R_5\varphi_4 - \int_{t_k}^{t} \dot{e}^T(s)R_4\dot{e}(s)ds - \int_{t}^{t_{k+1}} \dot{e}^T(s)R_5\dot{e}(s)ds$$

$$\mathfrak{V}_3(e(t),t) = 2(\varphi_1-\varphi_6)^T Q_1\varphi_6 + 2(t-t_k)\varphi_4^T Q_1\varphi_6$$
$$\dot{\mathfrak{V}}_4(e(t),t) = -(\varphi_1-\varphi_5)^T[Q_4(\varphi_1-\varphi_5)+2Q_5\varphi_3]$$
$$+2(t_{k+1}-t)[(\varphi_1-\varphi_5)^T Q_4+\varphi_3^T Q_5]\varphi_4$$

The following inequality is holds with $R_4 \geq 0, R_5 \geq 0$, $-\int_{t_k}^{t}\dot{e}^T(s)R_4\dot{e}(s)ds, -\int_{t}^{t_{k+1}}\dot{e}^T(s)R_5\dot{e}(s)ds$, we can obtain hat

$$\int_{t_k}^{t}\dot{e}^T(s)R_4\dot{e}(s)ds \leq (t-t_k)\zeta^T(t)\chi_1 R_4^{-1}\chi_1\zeta(t) + [\varphi_1^T M_1+\varphi_5^T M_2](\varphi_1-\varphi_5)$$
$$\int_{t}^{t_{k+1}}\dot{e}^T(s)R_5\dot{e}(s)ds \leq (t_{k+1}-t)\zeta^T(t)\chi_2 R_5^{-1}\chi_2\zeta(t) + [\varphi_6^T N_1+\varphi_1^T N_2](\varphi_6-\varphi_1)$$

$$\sum_{n=1}^{4}\dot{\mathfrak{V}}_j(e(t),t) = \zeta^T(t)((t_{k+1}-t)\Gamma_5+(t-t_k)\Gamma_6+\Gamma_7)\zeta(t) \quad (16)$$

From Assumption 1, we have

$$0 \leq -2\sum_{j=1}^{n}M_{1j}[f_j(\mathfrak{K}_j(t))-l_j^-\mathfrak{K}_j(t)][f_j(\mathfrak{K}_j(t))-l_j^+\mathfrak{K}_j(t)]$$
$$-2\sum_{j=1}^{n}M_{2j}[f_j(\mathfrak{K}_j(t-\mathfrak{h}(t)))-l_j^-\mathfrak{K}_j(t-\mathfrak{h}(t))]$$
$$\times[f_j(\mathfrak{K}_j(t-\mathfrak{h}(t)))-l_j^+\mathfrak{K}_j(t-\mathfrak{h}(t))] = \zeta^T(t)\Gamma_8\zeta(t) \quad (17)$$

For any matrix X, the zero equations are defined as follows:

$$0 = 2[e^T(t)+\alpha\dot{e}^T(t)]X[-Ae(t)+Bf(e(t))+Wf(e(t-\tau)) + Ke(t_k-\eta)-\dot{e}(t)] \quad (18)$$

$$\zeta^T(t)\Gamma_9\zeta(t) \quad (19)$$

Form (8) - (16), adding (17) - (18) into (6) yields

$$\dot{V}(e(t),t) = \zeta^T(t)\Upsilon\zeta(t) \quad (20)$$

where

$$\Upsilon = \frac{t_{k+1}-t}{d_k}\Upsilon_1+\frac{t-t_k}{d_k}\Upsilon_2,$$
$$\Upsilon_1 = \Omega+d_k\Gamma_5, \Upsilon_2 = \Omega+d_k\Gamma_6,$$
$$\Omega = \Gamma_1+\Gamma_2+\Gamma_3+\Gamma_4+\Gamma_7+\Gamma_8+\Gamma_9$$

Therefore for $t \in \{t_k, t_{k+1}\}$, from $\Upsilon_1 < 0$ and $\Upsilon_2 < 0$, one can get $\dot{V}(e(t),t) < 0$. This implies that $\Upsilon < 0$. This completes the proof. □

4. NUMERICAL EXAMPLE

Two numerical examples are given in this section to highlight the proposed result's effectiveness.

Example 1. The NNs (3) is considered with the p

$$B = \begin{bmatrix}1 & -1\\ -1 & -1\end{bmatrix}, W = \begin{bmatrix}0.88 & 1\\ 1 & 1.5\end{bmatrix}, A = \mathrm{diag}\{2,2\},$$
$$L_1 = \mathrm{diag}\{0,0\}, \; L_2 = \mathrm{diag}\{0.4,0.8\}.$$

Let us denote a1= 0.15, a2= 0.0015, t = 1, d=10= 0.01 and solving the LMIs in Theorem 1, the obtained positive definite matrices are listed here

$$F = \begin{bmatrix}0.0092 & -0.0018\\ -0.0020 & 0.0123\end{bmatrix},$$

$$X = 1.0*e^{+06}*\begin{bmatrix}1.5945 & -0.3080\\ -0.3067 & 1.7639\end{bmatrix},$$

$$P = 1.0*e^{+05}*\begin{bmatrix}2.3948 & -0.4700\\ -0.4700 & 2.6564\end{bmatrix},$$

$$R_1 = 1.0*e^{+05}*\begin{bmatrix}1.8045 & 1.8198\\ 1.8198 & 4.2093\end{bmatrix},$$

$$R_2 = 1.0*e^{+05}*\begin{bmatrix}-2.1107 & 0.0270\\ 0.0270 & -2.2014\end{bmatrix},$$

$$R_3 = 1.0*e^{+05}*\begin{bmatrix}2.0047 & -0.1043\\ -0.1043 & 1.9086\end{bmatrix},$$

$$R_4 = 1.0*e^{+05}*\begin{bmatrix}3.1296 & -0.4898\\ -0.4898 & 3.3561\end{bmatrix},$$

$$R_5 = 1.0*e^{+05}*\begin{bmatrix}3.1175 & -0.4975\\ -0.4975 & 3.3637\end{bmatrix},$$

$$Q_1 = 1.0*e^{+05}*\begin{bmatrix}2.7924 & -0.0449\\ -0.0449 & 2.8557\end{bmatrix},$$

$$Q_2 = 1.0*e^{+05}*\begin{bmatrix}1.6953 & 0.0050\\ 0.0050 & 0.4940\end{bmatrix},$$

$$Q_3 = 1.0*e^{+05}*\begin{bmatrix}1.8391 & -0.2528\\ -0.2528 & 2.3443\end{bmatrix},$$

$$Q_4 = 1.0*e^{+05}*\begin{bmatrix}2.9255 & -0.0000\\ -0.0000 & 2.9255\end{bmatrix},$$

$$Q_5 = 1.0*e^{+05}*\begin{bmatrix}0.0020 & -0.0001\\ -0.0001 & 0.0022\end{bmatrix}$$

with the control gain matrix K is

$$1.0*e^{+05}*\begin{bmatrix}0.5727 & 0.0226\\ -0.0122 & 0.7024\end{bmatrix}.$$

By using the above gain matrix K, the state trajectory of the error system are converges to the equilibrium point which is given in Figure 1.

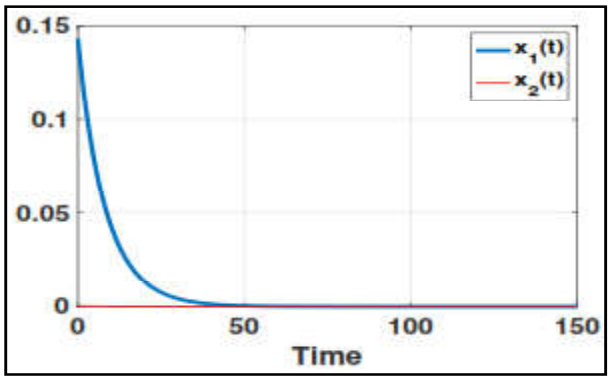

Fig. 1 State trajectory of NNs

5. CONCLUSION

In this work, the synchronization of chaotic NNs with time delays was addressed under memory-based SDC. In the sampling time t, the memory term was taken into account, and memory-based SDC was used in the control input of slave chaotic NNs. By using looped Lyapunov functionals, the synchronization criterion was derived and expressed in terms of LMIs. The criterion ensures that the error states are inconvergence with the origin, and this means that master states and slave states of the chaotic NNs are synchronized with each other's. Finally, a numerical example was given to illustrate the superiority of the derived synchronization criterion.

REFERENCES

[1] C.Chen, L. Li, H. Peng, Y. Yang, L. Mi and H. Zhao, "A New Fixed-Time Stability Theorem and its Application to the Fixed-Time Synchronization of Neural Networks", Neural networks, Vol.123, 2020, pp.412-419.

[2] B.Ganesan, P.Mani, L.Shanmugam and M.Annamalai, "Syn-chronization of Stochastic Neural Networks Using Looped-Lyapunov Functional and its Application to Secure Communication", IEEE Transactions on Neural Networks and Learning Systems, DOI:10.1109/TNNLS.2022.3202799., 2022.

[3] C.Ge, B. Wang, X.Wei and Y.Liu, "Exponential Synchronization of a Class of Neural Networks with Sampled-Data Control", Applied Mathematics and Computation, Vol.315, 2017, pp.150-161.

[4] R.Kiruthika, R.Krishnasamy, S.Lakshmanan, M.Prakash and A.Manivannan, "Non-fragile Sampled-Data Control for Synchronization of Chaotic Fractional-Order Delayed Neural Networks via LMI Approach", Chaos, Solitons & Fractals, Vol.169, 2023, pp.113252.

[5] S. Lakshmanan, M. Prakash, C.P. Lim, R.Rakkiyappan, P.Balasubramaniam and S.Nahavandi, "Synchronization of an Inertial Neural Network with Time-Varying Delays and its Application to Secure Communication", IEEE Transactions on Neural Networks and Learning Systems, Vol.29, 2016, No.1, pp.195-207.

[6] Y. Liu, B.-Z. Guo, J. H. Park and S.-M. Lee, "Nonfragile Exponential Synchronization of Delayed Complex Dynamical Networks with Memory Sampled-Data Control", IEEE Transactions on Neural Networks and Learning Systems, Vol.29, No.1, 2016, pp.118-128.

[7] Y. Liu, J. H. Park, B.-Z. Guo and Y. Shu, "Further Results on Stabilization of Chaotic Systems Based On Fuzzy Memory Sampled-Data Control", IEEE Transactions on Fuzzy Systems, Vol.26, No.2, 2017, pp.1040-1045.

[8] R. Suresh and A.Manivannan, "Robust Stability Analysis of Delayed Stochastic Neural Networks via Wirtinger-Based Integral Inequality", Neural Computation, Vol.33, No.1, 2021, pp.227-243.

[9] J. Wang, K.Shi, Q. Huang, S. Zhong and D. Zhang, "Stochastic Switched Sampled-Data Control for Synchronization of Delayed Chaotic Neural Networks with Packet Dropout", Applied Mathematics and Computation, Vol.335, 2018, pp.211-230.

[10] L. Xie, Output Feedback hq Control of Systems with Parameter Uncertainty", International Journal of Control, Vol.63, No.4, 1996, pp.741-750.

[11] R. Zhang, D. Zeng, J.H. Park, Y.Liu and S.Zhong, "Quantized Sampled-data Control for Synchronization of Inertial Neural Networks with Heterogeneous Time-Varying Delays", IEEE Transactions on Neural Networks and Learning Systems, Vol.29, No.12, 2018, pp.6385-6395.

[12] Z. Zhang, M.Chen and A. Li, "Further Study on Finite-Time Syn- Chronization for Delayed Inertial Neural Networks via Inequality Skills", Neurocomputing, Vol.373, 2020, pp.15-23.

COMMON FIXED POINT THEOREMS IN COMPLETE INTUITIONISTIC FUZZY METRIC SPACES USING WEAKLY COMPATIBLE MAPPINGS

S. Krishnaveni and D. Umamageswari
Department of Mathematics,
Bannari Amman Institute of Technology, Sathyamangalam - 638 401, Erode District, ,Tamil Nadu
E-mail: krishnaveni.venus@gmail.com, umamageswarid@bitsathy.ac.in

Abstract

The purpose of this article is to prove some common fixed point theorem in complete intuitionistic fuzzy metric space by using the weaker conditions such as Reciprocally continuous, Compatible mappings, Weakly compatible and Associated sequence. The aim of this note is to generalized the results for complete intuitionistic fuzzy metric space space (X , M , N.?, ?). (X , M , N.?, ?) in place of complete metric.

Keywords: *Associated sequence, Complete Intuitionistic Fuzzy Metric Space, Common Fixed Point, Reciprocally Continuous, Self-mapping, Weakly compatible*

1. INTRODUCTION

Since the introduction of the concept of fuzzy sets by Zadeh [1] in 1965, Atanassov [2] introduced and studied the concept of intuitionistic fuzzy sets as a generalization of fuzzy sets. many authors have introduced the concept of fuzzy metric in different ways [3], [4]&[5]. Grabiec [6] extend two fixed point theorems of Banach and Edelstein to contractive mappings of complete and compact fuzzy metric spaces in the sense of Kramosil and Michalek [7]. George and Veeramani [8], [9] modified the concept of fuzzy metric space introduced by Kramosil and Michalek [7] and defined a Hausdorff topology on this fuzzy metric space. Many authors [10,11,12,13,14] obtained common fixed point theorems for weakly commuting maps and R-weakly commuting mappings.

The purpose of this article is to prove some common fixed point theorem in complete intuitionistic fuzzy metric space by using the weaker conditions such as Reciprocally continuous, Compatible mappings, Weakly compatible and Associated sequence. The aim of this note is to generalized the results for complete intuitionistic fuzzy metric space (X, M, N.*,◊) in place of complete metric space(X, M, N.*,◊).

2. PRELIMINARIES

2.1 Definition: Let S and T be self-mappings of an intuitionistic fuzzy metric space (X, M, N.*,◊) Then S and T are to be weakly commuting if M(*STx, TSx, kt)>M(Sx, Tx, t*) and N(*STx, TSx, kt)<N(Sx,Tx,t)* for all $x \in X$.

2.2 Definition: A pair of self-mappings (S,T) of an intuitionistic fuzzy metric space (X, M, N.*,◊) is said to be compatible if $\lim$ M (*STx,TSx,kt) =1 and* $\lim$ N (*STx, TSx, kt)=0* for all *t>0*, whenever {x_n} is a sequence in X such that $\lim_{n\to\infty} Sx_n = \lim_{n\to\infty} Tx_n = u$ for some $u \in X$.
Clearly commuting mappings are weakly commuting, but the converse is not necessarily true.

2.3 Definition: Two self-maps S and T of a an intuitionistic fuzzy metric space (X, M, N.*,◊) are said to be weakly compatible if they commute at their coincidence point. i.e if $Su=Tu$ for some $u \in X$ then STu=TSu.

It is clear that every compatible pair is weakly compatible but its converse need not be true.

2.4 Definition: Two mappings S and T of an intuitionistic fuzzy metric space (X, M, N.*,◊) are called reciprocally continuous if $STu_n \to TSu_n \to T_z$, whenever {u} is a sequence such that $Su_n \to_z$, $Tu_n \to z$ for some z in X. If S and T are both continuous, then they are obviously reciprocally continuous, but converse is not true.

2.5 Theorem: Let P,Q,S and T be self-mappings from complete intuitionistic fuzzy metric space (X, M, N.*,◊) into itself satisfying the follwoing conditions

$$S(X) \subset Q(X) \text{ and } T(X) \subset P(X) \qquad (1)$$

$$M(Sx,Ty,kt) \geq \alpha \frac{M(Qy,Ty,t)[1+M(Px,Sx,t)]}{[1+M(Px,Qy,t)]} + \beta M(Px,Qy,t)$$

$$N(Sx,Ty,kt) \leq \alpha \frac{N(Qy,Ty,t)[1+N(Px,Sx,t)]}{[1+N(Px,Qy,t)]} + \beta N(Px,Qy,t) \qquad (2)$$

for all x, y in X where $\alpha, \beta \geq 0, \alpha + \beta < 1$.
one of P,Q,S and T is continuous (3)
Pairs (S,P) amd (T,Q) are compatible on X (4)
then, P,Q,S and T have a unique common fixed point in X.

2.6 Associated Sequence: Suppose P,Q,S and T are self-maps of an intuitionistic fuzzy metric space (X, M, N.*,◊) satisfying the condition (1). Then for an arbitrary $X_o \in X$ such that $Sx_0 = Qx_1$ and for this point x_1, there exists a point x_2 in X such that $Tx_1 = Px_2$ and so a sequence $\{y_n\}$ in X such that $y_{2n} = Sx_{2n} = Qx_{2n+1}$ $y_{2n+1} = Px_{2n+2} = Tx_{2n+1}$ for n>0.We shall call this sequence as an "Associated sequence of x_0 "relative to the four self-maps P,Q,S and T.

2.7 Lemma: Let P,Q,S and T be selfmappings from a complete intuitionistic fuzzy metric space (X, M, N.*,◊) into itself satisfying the conditions (1) and (2). Then the associated sequence $\{y_n\}$ relative to four selfmaps is a Cauchy sequence in X.

Proof: From the definition of associated sequence (2.6), we have

$$M(y_{2n}, y_{2n+1}, kt) = M(Sx_{2n}, Tx_{2n+1}, kt)$$
$$\geq \alpha \frac{M(Qx_{2n+1}, Tx_{2n+1}, t)[1+M(Px_{2n}, Sx_{2n}, t)]}{[1+M(Px_{2n}, Qy_{2n+1}, t)]} + \beta M(Px_{2n}, Qy_{2n+1}, t)$$

$$= \alpha \frac{M(y_{2n}, y_{2n+1}, t)[1+M(y_{2n-1}, y_{2n}, t)]}{[1+M(y_{2n-1}, y_{2n}, t)]} + \beta M(y_{2n-1}, y_{2n}, t)$$

$$M(y_{2n}, y_{2n+1}, kt) = \alpha M(y_{2n}, y_{2n+1}, t) + \beta M(y_{2n-1}, y_{2n}, t)$$

$$(1-\alpha) M(y_{2n}, y_{2n+1}, t) \geq \beta M(y_{2n-1}, y_{2n}, t$$

$$M(y_{2n}, y_{2n+1}, t) \geq \frac{\beta}{(1-\alpha)} M(y_{2n-1}, y_{2n}, t)$$

$$N(y_{2n}, y_{2n+1}, kt) = N(Sx_{2n}, Tx_{2n+1}, kt)$$
$$\leq \alpha \frac{N(Qx_{2n+1}, Tx_{2n+1}, t)[1+N(Px_{2n}, Sx_{2n}, t)]}{[1+N(Px_{2n}, Qy_{2n+1}, t)]} + \beta N(Px_{2n}, Qy_{2n+1}, t)$$

$$= \alpha \frac{N(y_{2n}, y_{2n+1}, t)[1+N(y_{2n-1}, y_{2n}, t)]}{[1+N(y_{2n-1}, y_{2n}, t)]} + \beta N(y_{2n-1}, y_{2n}, t)$$

$$N(y_{2n}, y_{2n+1}, kt) = \alpha N(y_{2n}, y_{2n+1}, t) + \beta N(y_{2n-1}, y_{2n}, t)$$

$$(1-\alpha) N(y_{2n}, y_{2n+1}, t) \leq \beta N(y_{2n-1}, y_{2n}, t)$$

$$N(y_{2n}, y_{2n+1}, t) \leq \frac{\beta}{(1-\alpha)} N(y_{2n-1}, y_{2n}, t)$$

$$M(y_{2n}, y_{2n+1}, t) \geq h M(y_{2n-1}, y_{2n}, t),$$

$$N(y_{2n}, y_{2n+1}, t) \leq N(y_{2n-1}, y_{2n}, t)$$

where $h = \frac{\beta}{(1-\alpha)}$

Now

$$M(y_n, y_{n+1}, t) \geq h M(y_{n-1}, y_n, t) \geq$$
$$h^2 M(y_{n-2}, y_{n-1}, t) \geq \ldots\ldots \geq h^n M(y_0, y_1, t)$$

$$N(y_n, y_{n+1}, t) \leq h N(y_{n-1}, y_n, t) \leq$$
$$h^2 N(y_{n-2}, y_{n-1}, t) \leq \ldots\ldots \leq h^n N(y_0, y_1, t)$$

For every integer p > 0 , we get

$$M(y_n, y_{n+p}, t) \geq M(y_n, y_{n+1}, t) + M(y_{n+1}, y_{n+2}, t) + \ldots\ldots + M(y_{n+p-1}, y_{n+p}, t)$$
$$\geq h^n M(y_0, y_1, t) + h^{n+1} M(y_0, y_1, t) + \ldots\ldots\ldots + h^{n+p-1} M(y_0, y_1, t)$$
$$\geq (h^n + h^{n+1} + \ldots\ldots\ldots + h^{n+p-1}) M(y_0, y_1, t)$$
$$\geq h^n (1 + h + h^2 + \ldots\ldots + h^{p-1}) M(y_0, y_1, t)$$

$$N(y_n, y_{n+p}, t) \le N(y_n, y_{n+1}, t)$$
$$+ N(y_{n+1}, y_{n+2}, t) + \ldots\ldots + N(y_{n+p-1}, y_{n+p}, t)$$
$$\le h^n N(y_0, y_1, t) + h^{n+1} N(y_0, y_1, t)$$
$$+ \ldots\ldots + h^{n+p-1} N(y_0, y_1, t)$$
$$\le (h^n + h^{n+1} + \ldots\ldots + h^{n+p-1}) N(y_0, y_1, t)$$
$$\le h^n (1 + h + h^2 + \ldots\ldots + h^{p-1}) N(y_0, y_1, t)$$

Since $h < 1$, $h^n \to 0$ as $n \to \infty$, so that

$M(y_n, y_{n+p}, t) \to 0, N(y_n, y_{n+p}, t) \to 0.$

This shows that the sequence $\{y_n\}$ is a Cauchy sequence in X and since X is a complete metric space, it converges to a limit, sayz $z \in X$. The converse of the Lemma is not true, that P, Q, S and T are self-maps of a complete intuitionistic fuzzy metric space (X, M, N.*,◊) satisfying (1) and (2), even if for $x_0 \in X$ and for associated sequence of x_0 converges, the complete intuitionistic fuzzy metric space (X, M, N.*,◊) need not be complete.

3. MAIN RESULT

3.1 Theorem: Let *P,Q,S* and *T* are self-maps of a complete intuitionistic fuzzy metric space (X, M, N.*,◆) satisfying the (1),(2) and the conditions:

The pair *(S,P)* is reciprocally continuous and compatible and the pair *(T,Q)* is weakly compatible (5)
Also The associated sequence relative to four self-maps *P,Q,S* and *T*such that the sequence

$Sx_0, Tx_1, Sx_2, Tx_3 \ldots\ldots Sx_{2n}, Tx_{2n+1} \ldots\ldots$

converges to $z \in X$ as $n \to \infty$ (6)
then *P,Q,S* and *T* have a unique common fixed point *z* in *X*.

Proof: From the condition (6), $Sx_0, Tx_1, Sx_2, Tx_3 \ldots\ldots Sx_{2n}, Tx_{2n+1} \ldots\ldots$ converges to $z \in X$ as $n \to \infty$
First suppose that the pair *(S,P)* is reciprocally continuous and compatible, then from the definition of reciprocally continuity of *(S,P)* if $Sx2n \to z$, $Px2n \to z$ as then $SPx_{2n} \to S_z$, $PSx_{2n} \to Pz$ (7)
From the compatibility of the pair *(S,P)* we get

$$\lim_{n\to\infty} M(SPx_{2n}, PSx_{2n}, kt) = 0,$$
$$\lim_{n\to\infty} N(SPx_{2n}, PSx_{2n}, kt) = 1 \text{ or}$$
$$\lim_{n\to\infty} SPx_{2n} = \lim_{n\to\infty} PSx_{2n}$$

Using (7) this gives that $S_x = P_z$.
Since $S(X) \subset Q(X)$ there exists $u \in X$ such that $Sz = .Qu$.
we consider

$$M(Sz, z, kt) = \lim_{n\to\infty} M(Sz, Tx_{2n+1}, kt) \ge$$
$$\lim_{n\to\infty} \left\{ \alpha \frac{M(Qx_{2n+1}, Tx_{2n+1}, t)[1 + M(Pz, Sz, t)]}{[1 + M(Pz, Qx_{2n+1}, t)]} + \beta M(Pz, Qx_{2n+1}, t) \right\}$$
$$N(Sz, z, kt) = \lim_{n\to\infty} N(Sz, Tx_{2n+1}, kt) \le$$
$$\lim_{n\to\infty} \left\{ \alpha \frac{N(Qx_{2n+1}, Tx_{2n+1}, t)[1 + N(Pz, Sz, t)]}{[1 + N(Pz, Qx_{2n+1}, t)]} + \beta N(Pz, Qx_{2n+1}, t) \right\}$$

this gives $M(Sz,z,kt) > \beta M(Sz,z,kt)$, $N(Sz,z,kt) < \beta N(Sz,z,kt)$ since $\beta > 0$. $\alpha+\beta<1$ giving that $M(Sz,z,kt) = 0$, $N(Sz,z,kt)$. Thus $Sz=z$.
Hence $Sz = Pz = z = Qu$. This shows that '*z*' is a common fixed point of *P* and *S*.
Now we prove $Qu=Tu$.
Consider

$M(z,Tu,kt) = M(Sz,Tu,kt) >$

$$M(z, Tu, kt) = M(Sz, Tu, kt) \ge$$
$$\left\{ \alpha \frac{M(Qu, Tu, t)[1 + M(Pz, Sz, t)]}{[1 + M(Pz, Qu, t)]} + \beta M(Pz, Qu, t) \right\}$$

$$= \alpha M(z, Tu, t)$$
$$N(z, Tu, kt) = N(Sz, Tu, kt) \le$$
$$\left\{ \alpha \frac{N(Qu, Tu, t)[1 + N(Pz, Sz, t)]}{[1 + M(Pz, Qu, t)]} + \beta N(Pz, Qu, t) \right\}$$
$$= \alpha N(z, Tu, t)$$

this gives $M(z,Tu,kt) > \alpha M(z,Tu,kt)$, $N(z,Tu,kt) < \alpha N(z,Tu,kt)$ since $\alpha > 0$.
$\alpha+\beta<1$ giving that $M(z,Tu,kt) = 0$, $N(z,Tu,kt)$.
Thus $Tu=z$, we get $TQu = Qtu$ or $Tz=Qz$.

Again we consider

$$M(z,Tz,kt) = M(Sz,Tz,kt) \geq$$
$$\left\{ \beta \frac{M(Qz,Tz,t)[1+M(Pz,Sz,t)]}{[1+M(Pz,Qz,t)]} \right\}$$
$$+ \beta M(Pz,Qz,t)$$
$$= \beta M(z,Tz,t)$$
$$N(z,Tz,kt) = N(Sz,Tz,kt) \leq$$
$$\left\{ \beta \frac{N(Qz,Tz,t)[1+N(Pz,Sz,t)]}{[1+M(Pz,Qz,t)]} \right\}$$
$$+ \beta N(Pz,Qz,t)$$
$$= \beta M(z,Tz,t)$$

this gives $M(z,Tu,kt) > \beta M(z,Tu,kt)$, $N(z,Tu,kt) < \beta N(z,Tu,kt)$ since $\beta > 0$. $\alpha+\beta < 1$ giving that $M(z,Tz,kt) = 0$, $N(z,Tz,kt) = 0$. Thus $Tz=z$.

Hence $Qz = Tz = z$. Therefore $Pz=Qz=Sz=Tz= z$, showing that 'z' is a common fixed point of P,Q,S, and T. The uniqueness of the fixed point can be easily proved.

Remark 3.2. Theorem 3.1 is a generalization of Theorem 2.5 by virtue of the weaker conditions such as the reciprocal continuity and compatibility of the pair *(S,P)* in place continuity of one of the mappings; weakly compatibility of the pair *(T,Q)* in place of compatibility; and associated sequence relative to four self-maps P,Q,S and T in place of the complete metric space.

REFRENCES

[1] L. A. Zadeh, "Fuzy Sets", Information and Control, Vol.8, 1965, pp.338-353.

[2] Deng Zi-Ke, "Fuzzy Pseudo-metric Spaces", J. Math. Anal. Appl., Vol.86, 1982, pp.74-95.

[3] O. Kaleva and S. Seikkala, "On Fuzzy Metric Spaces", Fuzzy Sets and Systems, Vol.12, 1984, pp.225-229.

[4] K. Menger, "Statistical Metrics", Proc. Nat. Acad. Sci., Vol.28, 1942, pp.535-537

[5] Grabiec, "Fixed Points in Fuzzy Metric Spaces", Fuzzy Sets and Systems, Vol.27, 1988, pp.385-389.

[6] O. Kramosil and J. Michalek, "Fuzzy Metric and Statistical Metric Spaces", Kybernetica, Vol.11, 1975, pp.326-334.

[7] A. George and P. Veeramani, "On Some Results in Fuzzy Metric Spaces", Fuzzy Sets and Systems, Vol.64 1994, pp.395-399.

[8] A. George and P. Veeramani, "On Some Results of Analysis for Fuzzy Metric Spaces", Fuzzy Sets and Systems , Vol.90, 1997, pp.365-368.

[9] S. Sessa, "On A Weak Commutativity Condition of Mappings in Fixed Point Considerations", Publ. Inst. Math. Vol.32, No.32, 1982, pp.149-153.

[10] S. L. Singh, "On Common Fixed Points of Commuting Mappings", Math. Seminar Notes Kobe Univ. Vol.5, 1977, pp.131-134.

[11] P. V. Subrahmanyam, "A Common Fixed Point Theorem in Fuzzy Metric Spaces", Inform. Sci., Vol.83, 1995, pp.109-112.

[12] R. Vasuki, "Common Fixed Points for R-Weakly Commuting Maps in Fuzzy Metric Spaces", Indian J. Pure Appl. Math., Vol.30, 1999, pp.419-423.

[13] K. Atanassov, "Intuitionistic Fuzzy Sets", Fuzzy Sets and Systems, Vol.20, 1986, pp.87-96.

[14] R. Umamaheshwar Rao and V. Srinivas, "A Common Fixed Point Theorem Under Certain Conditions", Gen. Math. Notes, Vol. 8, No.2, 2012, pp.28-33.

PESTER POWER AND ADVERTISEMENT INFLUENCE ON PURCHASE OF FOOD PRODUCT BY KIDS IN COIMBATORE REGION

B. Nandhini
Department of School of Management Studies
Bannari Amman Institute of Technology, Sathyamangalam - 638 401, Erode District, TamilNadu
Email : nandhinib@bitsathy.ac.in

Abstract

The aim of this study is to determine the extent to which Pester Power influences parents' food buying decisions in a convenience store setting. This research is significant because marketers should be aware of how they can better exploit the factors that lead to Pester Power, thus encouraging purchasing decisions in their favour. Children use their controlling power in the form of nagging actions to influence their parents' or others' purchasing decisions. Since marketers concentrate on children in their promotional campaigns, children have rationalised their ability to influence their parents' decision-making processes. SPSS was used to analyse the results. Pester Power influences purchasing decisions on categories of food items, and attributes added to influence kids, which in turn cause Pester Power, are addressed in the research questions. The findings have implications for the creation of children's marketing strategies, and future studies can look at how peer groups and other socialising agents influence children's knowledge sources, which impacts.

Keywords: *Child influence, Pester Power, Purchase Decision,Convenience store, Food products, Marketing strategies*

1. INTRODUCTION

The aim of this study is to determine the degree to which Pester Power influences parents' food purchasing decisions in a convenience store setting. This research is significant because marketers should be aware of how to better leverage the factors that lead to Pester Power, thus encouraging purchasing decisions in their favour. Pester influence marketing is aimed at children who, when they are unable to buy things for themselves, nag, pester, and beg their parents to buy unhealthy food for them.Children have a stronger hold on society than their parents ever did. They are not only customers in and of themselves, but they also have a significant impact on the family's buying power. "Kid fluence" refers to the overt or indirect impact that children have on family transactions. When parents make a buying decision, parents give priority and consideration to their children. Pester influence is widely used by marketing campaigns to reach the 4 to 6-year-old demographic, since they have little disposable income and hence are unable to purchase products on their own.The rise of child ads is directly linked to the growth of the issue of pesters control. Mr. Potato Head was the first children's toy to be sold on television, airing in 1952 and paving the way for pester control, as pitching to children was seen as a novel concept. It is now standard practice to sell children's goods directly to children. Because of the way they continually nag their parents, children have assumed the role of being the "absolute tool" in controlling family spending. As a result, marketing agencies have compared children to a "Trojan horse" inside the modern household.

2. OBJECTIVES OF STUDY

- To assess the effect of Pester Power and Advertising on Food product purchasing decisions in a convenience store environment.
- To know which product categories exhibited more pester power.
- To understand the role of advertisements and Product's taste, colour play in fostering pester power

3. SCOPE OF STUDY

This study covers the shopping behavior of people with Pester Power (the level of acceptance of food items upon Pestering) and the factors that facilitate buying decision. The demographic profile of respondents was studied in detail.

4. REVIEW OF LITERATURE

There is two forms of influence that children have; active and passive influence, according to the report[1]. Children have an effect on all stages of the family decision-making process, but particularly on instigation and choice, according to previous research. The study also backs up previous results that show how children's impact differs depending on the decision areas they are involved in. Children have the most impact on small and uncomplicated cooked meals, food that is easy to cook, harmful food (e.g. sweets) versus nutritious goods (e.g. fruit, vegetables, and fish) and fruit has more influence than vegetables when it comes to healthy food. The research also adds to our understanding of how children engage in and assist with different activities.

It was discovered that children had various effects on product purchases[2]. Women believed that their children had a greater influence on Lay selection. The impact of a child on a parent's purchasing decision is influenced by certain demographic characteristics of the child's mother and family. When it comes to imported chocolates and branded juice, girls have a lot of control on their parents' decisions. As children get older, their effect on their parents' choice of different things grows. Finally, the monthly income of the family was found to have an effect on the product preferences of the parents. It has been noted that mothers from higher-income families pay less attention to the price of goods and include their children in such practices.

Children's purchase demands and their parents' subsequent purchases are influenced by a number of factors[3]. The independence of a child's movements, the product's exposure, and the child's developmental stage were found to be factors affecting the amount of children's purchase requests. The number of transactions made in response to a child's request is determined by this variable, as well as the suitability of the good for use on the premises, the linguistic form of the child's request, the parent's household income, and the price of the good.

Children have a significant influence on the purchasing decisions made by their families[4]. To objectively examine all of the factors that role children's influence in family decision-making in India, which has always retained its traditional values but has undergone metamorphosis as a result of changes in family structure, an increase in the number of working couples, and delegation of authority.

Packaging and colors play an important role in attracting children's interest and gaining parental approval[5]. Investing more time and money on it, as well as deploying different experts in the direction of creating, various packages, and more suitable packaging, may be of particular significance. Children adore cartoon characters and pictures and are always on the lookout for them, and they prefer packages that are brightly colored and distinct from other items. According to the location of game and entertainment in a store has a positive impact on children's interest, it is more relevant in stores. Giving gifts to children, for example, has an effect on their loyalty.

This research is significant because marketers should be aware of how they can better exploit the factors that lead to Pester Control[6], thus encouraging purchasing decisions in their favor. Pester Power influences purchasing decisions on food product types, and attributes are added to influence kids, who in turn cause Pester Power. The paper offers empirical evidence on how retailers and marketers benefited from pester power patterns, as well as the importance of children as consumers. This study is about, primary target is on young children for Advertising and Marketing[7]. Due to nagging parents spends money for children, which they are influenced. Mainly, advertisement is used for nag factor and targets parents. A young child uses various techniques so Pester Power is used for children's act of nagging their parents to buy advertised products.

The purpose of this study is children influence in purchase decision that signifies the interest to marketers across the globe[8]. This explores how different family communication structures influence Pester Power in children. There are different types of family likely; Laissez-Faire family, Protective family, Pluralistic family and consensual family have lots of bearing on different types of Pester Power. It plays major role of Persuasive and Emotional strategies or behavior at market place.

This study is about role of children purchase decision[9]. Now-a-days in family purchase decision child plays major role directly or indirectly within family purchase compared to earlier generations. Children became major purchasers' easy access to money and self determination to make own decision. They signify the influential and future market. Sometimes, they themselves purchase the product or choose the product before consulting parents or family members.

5. RESEARCH METHODOLOGY

To carry out the research, Coimbatore City in TamilNadu state was chosen at the convenience of the researcher. A sample of 211 respondents, who were parents of children under the age of 12 Years were chosen as sample frame. A structures questionnaire prepared exclusively for this study was circulated among the respondents and the responses were received electronically. The collected responses were cleaned, coded and entered into SPSS software for further analysis.

6. ANALYSIS AND INTERPRETATION

The demographic data of the respondents are given below. 54% of the respondents were Female and 46% were Male Parents. Majority of the parents belonged to the age group of 26 to 30 Years (31.8%), followed by Above 35 Years (27%) and 31 to 35 Years (25.6%) Age Groups. Most of the Parents (42.7%) are Private employees working in various sectors with the annual package of 3 Lakhs to 5 Lakhs Salary. Most of the respondents (64.9%) live as nuclear families with only 1 Child (62.1%).Most of the parents (54%) buy the products for their kids even before they ask for it, while remaining parents buy them immediately after asking.

It has been revealed from the analysis that, the type of family they belong to affects the acceptance of the purchase of junk foods, fast foods, soft drinks, healthy food items for the kids and the use of elder strategy by the kids to purchase products for them. The product categories that are being influenced by the kids in decision making of purchase are Ice creams, Chocolates, Bakery items, Junk foods and Biscuits. The factors that are most influential among the kids to choose a particular product or brand were Freebies, Cartoon, Color of product, Taste of product and Package of product. The major strategies used by the kids to make their parents buy the products they want are telling about deals and offers available, describing about the product, plain statement of wanting of the product, begging to make them buy and pretending to be ill to get sympathy.

7. CONCLUSION

According to the study carried out, the most important product attributes that influence the kids to demand a product are "freebies followed by the product," "cartoon characters on the packaging of the product," "color of the product," "taste of the product," and "packaging of the product." The chocolates, cakes, and chips categories of items tend to have the highest levels of pester strength. Advertisement and celebrity endorsements were not found to be significant factors in pester strength. According to the results, there is a clear correlation between the amount of time a child spends watching television and their desire to pester for items they have seen advertised on television.

REFERENCES

[1] M.K. Norgaard, "Family Decision-making During Food Buying", Handelshųjskolen, Aarhus University, 2009.

[2] D.K. Batra and A.Ali, "Parent's Opinion of Children's Influence in Purchase Decisions: A Comparative Analysis , between Rural and Urban Delhi", Global Business Review, https://doi.org/10.1177/0972150915597612, Vol.16, No.6, 2015, pp.1100-1111.

[3] C.Ebster, U.Wagner and D. Neumueller, "Children's Influences on in-store Purchases", Journal of Retailing and Consumer Services, Vol.16, No.2, 2009, pp.145-154.

[4] A. Ali, N. Ravichandran and D.K. Batra, "Children's Choice of Influence Strategies in Family Purchase Decisions and the Impact of Demographics", Vision, https://doi.org/10.1177/0972262912469561, Vol.17, No.1, 2013, pp.27- 40.

[5] H. Ganjinia, S. Gilaninia and E.Maleknejad, "Children's Influence in Family Purchasing Decision", Kuwait Chapter of Arabian, Journal of Business and Management Review Vol. 2, No.7, 2013.

[6] Kumar, Rupesh, "Pester Power and Advertisements Influence on Purchase of Food Products in a Convenience Store", Asian Journal of Management, 10.5958/2321-5763.2017.00032.4., Vol.8, 2017, pp.204-214.

[7] F. Baldassarre, R. Campo and A. Falcone, "Attitude Towards Food Products for Children: A Parental Viewpoint", Italy: Amedeo Falcone, 2015.

[8] P. Anitha and B.C. Mohan, "Influence of Family Structures on Pester Power and Purchase Outcomes - A Conceptual Framework", Procedia Economics and Finance, Vol.37, 2016, pp.269-275

[9] A.J. Nicholls and P.Cullen, "The Child–parent Purchase Relationship:'Pester Power", Human Rights and Retail Ethics. Journal of Retailing and Consumer Services, Vol.11, No.2, 2004, pp.75-86.

DESIGN AND ANALYSIS AQUA BIKE FOR FLOATING WASTE CLEANING

D.Selvamuthukumaran, M.Jaswanthkumar, E.Kavin and S.Balaganesh
Department of Mechanical Engineering,
Bannari Amman Institute of Technology, Sathyamanagalam - 638 401, Erode District, Tamil Nadu
E-mail:selvamuthukumaran@bitsathy.ac.in

Abstract

Water pollution has become a major environmental concern, with the presence of waste in water bodies being a significant contributor. This paper explores the potential of using aqua bikes as a means of cleaning waste from water bodies. Aqua bikes are stationary bikes designed to operate in water, and their unique features make them ideal for cleaning waste. The paper discusses the benefits of using aqua bikes for waste cleaning, including their ability to target hard-to-reach areas, their low environmental impact, and their cost-effectiveness. The study examines the technical aspects of aqua bikes, including the equipment required, the cleaning process, and the disposal of waste. The research suggests that aqua bikes can be a highly effective tool for cleaning waste in water bodies, offering an innovative solution for environmental preservation. The use of aqua bikes for waste cleaning has the potential to significantly reduce pollution levels in water bodies and promote the sustainability of aquatic ecosystems. Therefore, this report concludes that aqua bikes have the potential to become a valuable tool for environmental preservation and conservation efforts.

Keywords: *Aqua bike, Cost-effective, Environment, Ecosystem, Pollution, Waste.*

1. INTRODUCTION

Water is essential to all living things on this planet, and water resources are used more than other resources. According to the World Health Organization (WHO), polluted water is whose composition has been altered to the point where it is no longer useful. Nowadays the supply of water and the quality of beneficial water is getting worse due to water pollution[1,2]. The primary cause of water pollution is that water is uniquely vulnerable to pollution. Water is known as "universal solvent" because water is able to dissolve more substance compared to any other liquid in the earth. There are different types of water pollution groundwater pollution, surface water pollution, ocean water pollution, point source pollution, non-point source pollution, etc. Ocean water pollution is mainly due to plastic that is blown in by wind or washed in via storm drains and sewer, so this paper aims to solve this problem by collecting floating waste. Water pollution is not a new issue; it has been a problem for decades due to the fact that we have been dumping waste into bodies of water[3]. Water pollution is primarily caused by urbanisation, agriculture, and an increase in human population, all of which have begun to cause changes in the ecosystem. Every year, more people die as a result of a lack of freshwater. Consumption of contaminated water causes life-threatening diseases such as cholera, typhoid, jaundice, and others, killing over 500,000 people each year[4]. Furthermore, contaminated water may contain chemicals such as mercury or nitrates, which can lead to the development of cancer.

Currently, sanitation workers and volunteers are cleaning the lakes manually without the use of technology, which may raise concerns about human safety in a hostile environment. This project aims to provide an alternative solution by cleaning the garbage with Aqua bike[5]. An aqua bike is a human-powered vehicle which offers an effective means to move around, clean, and transport in water bodies. The idea of a water velocipede was first introduced in the 1870s; typically, people ride one for entertainment or exercise. In water, it functions like a bicycle. The propeller attached to the pedal will move the water bike forward as long as people keep cycling the pedal. So, this vehicle is not only used by the tourists, also it can be used for cleaning the floating waste, help the people during flood times by supplying medicines and foods and it is also cost-efficient comparing to existing vehicles[6].

2. LITERATURE SURVEY

This literature review is the summary of studies related to River Cleaning machines developed in recent

years. We identified and summarizes some the relevant research conducted on this machine. This literature review helped accomplishing relevant resources about the research that has already been done to avoid duplications.

The author Shubham Awasthi have developed an amphibious cycle which means the vehicle can have used in both water and land[7]. Design of the model for amphibious bicycle was done by making some attachments in the normal bicycle. He has designed the vehicle with four different sections like Front float, Rear float, Frame and Blades. He has used triangular shaped floaters in front of cycle which splits the water easily and reduces drag force due to air while riding on the land.

A water bike and introduced an idea to solve the power transmission problem[8]. The power transmission system has always been considered critical for a human powered boat (or water bicycle) since it originally appeared at Human Controlled Vessel Celebration. Mechanical issues, like scraped spots and different harms of the stuff framework for the power transmission, lead to unfortunate solidness and low proficiency of a boat. This paper depicted mechanical issues and a plan interaction of power transmission framework and afterward proposed the technique to tackle the issues. It is chosen a module and a sort of cog wheels that are fundamentally steady subsequently can send the power strong. Particularly the lower gear box is applied to CRP (contra pivoting propeller) framework for working on the underlying steadiness and the propeller effectiveness too. As the outcomes, the upper and lower gear box are planned and fabricated. What's more, from the preliminary test, it is affirmed that the power transmission framework is solid.

A vehicle and given a solution for static stability of vehicle[9]. The paper examines longitudinal static stability, a crucial prerequisite for the human-powered hydrofoil boat's performance and safety (HPHB). The derivative of the moment about the centre of gravity must be negative for the boat to be stable in the event that a disturbance modifies the trim angle. The height controlling system (HCS) of the EPISODE, an HPHB of Chungnam National University, is used to generate the equation to assess the longitudinal static stability. It is proven by the derivative that an HPHB needs a centre of gravity that is both longitudinal and vertical. A HCS was used to determine the range of a trim angle while the boat is foil-born. Using an HCS and mechanical restraint, the trim angle's range was discovered when the boat was foil-born. Also, it has been established that EPISODE is in a specific range of a trim angle where the longitudinal static stability is satisfied. Additionally, it is demonstrated that the longitudinal static stability and a range of the trim angle can be calculated from an HPHB's principal dimensions; as a result, it may be used from the conceptual design stage of an HPHB[10].

A paper related to waste management treatment[10]. The Unified Countries gauges that 40% of the 300 million tons of plastic created every year are discarded soon. At that rate there could be more plastic than fish in the ocean by 2050. Emerging nations like China, Indonesia, the Philippines, Thailand, and Vietnam contribute up to 60% of the plastics squander floating on the planet's ocean. A significant part of the plasticis caught in the South China Ocean for quite some time prior to floating out to the Pacific Sea. The plastic issue has expanded as Chinese recyclers have moved to Southeast Asia and started bringing in squander from everywhere the world. The imported plastics are modest and clean, outcompeting the messy plastics gathered locally from the tides. The reused plastic cost dropped to extraordinary level in 2017, beating plastic down searching by local people. This proposal engages the waste pickers by planning structures that boost plastic reusing. The proposition suggests that the plastic tides can be mined, destroyed, cleaned, dried, heated, and cooled in an effective and all-encompassing scene framework.

A waste cleaning machine[11]. The paper accentuation on plan and manufacture subtleties of the waterway squander cleaning machine. The work has done taking a gander at the ongoing circumstance of our public waterways which are dump with crore litters of sewage and stacked with poisons, poisonous materials, garbage and so on. The public authority of India has assumed responsibility to clean streams and put gigantic capital in numerous waterway cleaning projects like "NamamiGange", "Narmada Bachao'' and many major and medium activities in different urban areas like Ahmadabad, Varanasi and so on. By thinking about this, this machine has intended to clean stream water surface. This paper had helped us for calculations and design according to that.

3. METHODOLOGY

The methodology provides glimpses of learning process from beginning to the end.

- Design it on suitable software like Solid works.
- ANSYS analysis were carried out to analysis and verify calculation.
- Manufacturing was completed, and model testing was performed to ensure performance.

4. DESIGN CALCULATIONS

4.1 Center of Gravity of Machine

The center of gravity is the point through which the force of gravity acts on a body. the below Figure gives an idea about the center of gravity of the body which is calculated from Solid Works and found to be 0.48 from the base by giving the whole estimated weight of the full body as around 30 kg.

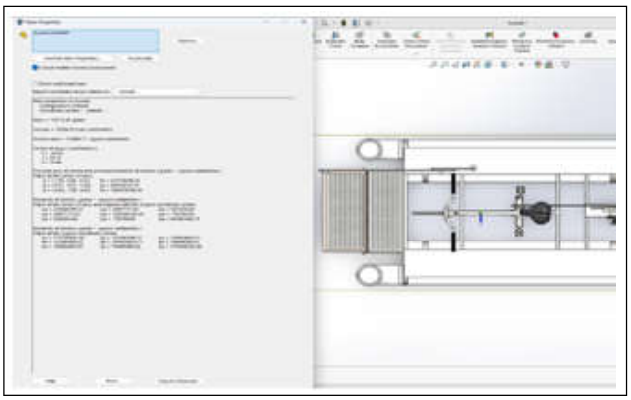

Fig.1 Centre of mass

4.2 Buoyancy

According to Archimede's Principle "The upward buoyant force that is exerted on a body immersed in a fluid, whether partially or fully submerged, is equal to the weight of the fluid that the body displaces and acts in the upward direction at the center of mass of the displaced fluid"

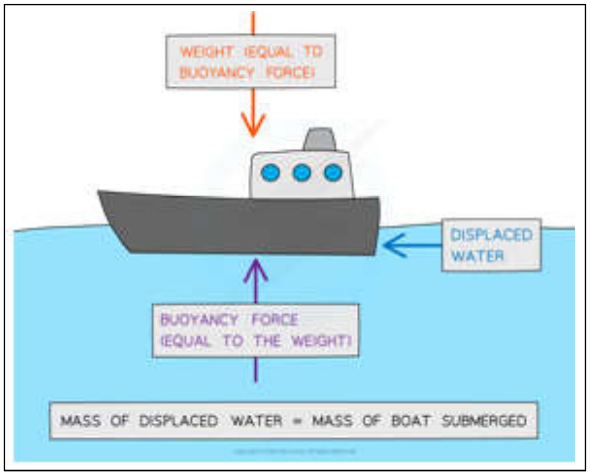

Fig.2 Buoyant force acting on floating body

The notion of the buoyant force is discussed in the above figure 2 to compute mass of fluid displaced.

For the calculation of buoyancy, some assumptions for the length, breadth, and height of floaters are made to check whether the body will float or not.The free body diagram of a floater is shown in below figure 3 to determine buoyancy.

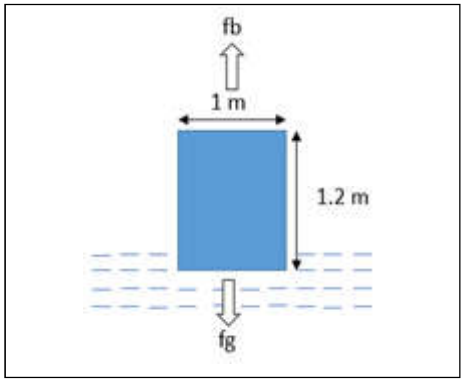

Fig.3 Buoyancy of floating body

Volume (V) = $\pi r^2 l$

V = $3.14x7.5^2x390$

V = 68883.75 cm^3

V = 0.06888375 m^3

Where L is the length and r is radius of pipe

The density of the material (Polyethylene) is taken as 955 kg/m^3

Further weight of water displaced can be calculated by the formula

Weight of water displaced = $p \times V \times g$
= 997 × 0.06888375 × 9.81
= 673.72 N

Where p is density, V is volume and g are the acceleration due to gravity
Weight of water displaced > Weight of the material
The volume of the body in water = Volume of water displaced 2.5 × 1.2 × □ = 0.137

□ = 0.045 *mfrombase*

Depth of immersion of vehicle (h) = 0.0225 m
Buoyancy Force = $\rho \times V \times g$
= 997 x 9.81 x 0.06888375
= 673.72 N
=68.70 kg
Total buoyancy = 68.70 x 2
=137.4 kg

Hence, by using Archimedes' principle buoyant force along with other parameters have been found.

4.3 Garbage Collecting Bin

The garbage collecting bin is used to store the garbage collected through the conveyor.
Length(L) = 0.64
Width(W) = 0.239 m
Height(H) = 0.2m

Volume = L × B × H
= 0.64 x 0.239 x 0.2
= 0.03 m^3

Capacity = Volume × Density of material to be collected
= 0.03 x 900
= 27 kg

5. MODELLING OF WATER BIKE

SolidWorks is a product designing tool used for sharing representations of both 2D drawings and 3D models, we have used this software to design because it is a standard tool and it could calculate various parameters like forces due to motion, flow, part stress, and deflection as well as vibration, and effects of temperature[12].

Fig.4 3D Model of Aqua Bike

The product's domain includes the design and development of the static structure and mechanisms. The design and development of the respective domains are detailed below.

5.1 Base Structure

The main role of the base structure is to provide stability for the Aqua bike[7,9]. The Aqua bike floats on the water and performs the stipulated tasks provided with the help of the buoyancy provided by the base structure. The base of the Aqua bike is developed with PVC pipes of length of 250 cm and diameter 15.24cm which is cut as per the measurements. The mild steel pipe of 20x20 mm cross section is joined in a rectangular shape using arc welding. The rectangular structure is connected to the pipes with the help of clamps. The further structures are developed on the base structure consisting of pipes and mild steel rectangular structure.

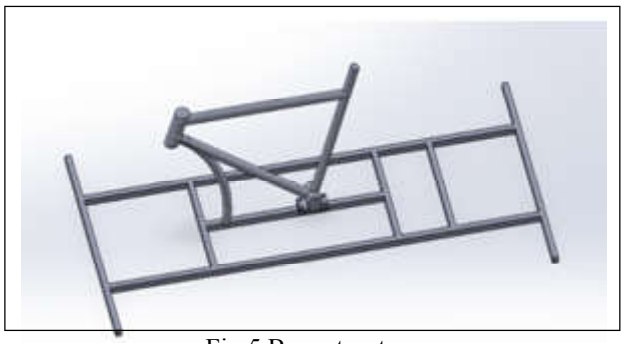

Fig.5 Base structure

5.2 Scooper Assembly

The scooper assembly is the primary and pivotal structure of the Aqua bike facilitating the continuous waste collection and uninterrupted water body maintenance. The scooper is made of stainless-steel sheet metal so that Environmentally Friendly, Stainless steel is a hygienic material, Durability and Comparatively

less weight. The scooper is attached at the front of the vehicle and it is mounted on the base frame. The scooper is connected to the handle which is operated by driver. The collected waste from water is stored on the collecting bin.

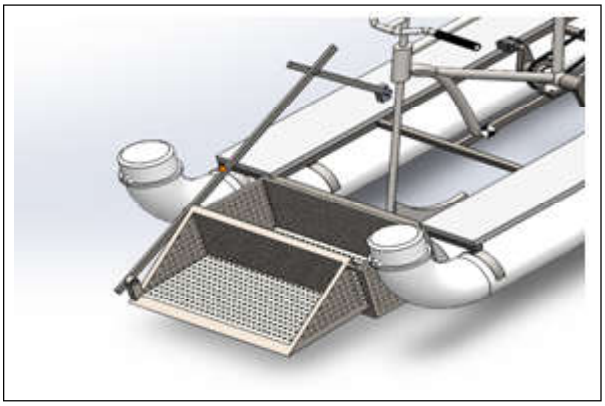

Fig.6 Scooper assembly

5.3 Propulsion System

The propulsion system facilitates the manoeuvring of the Aqua bike. The system makes use of propeller which is connected to the pedalling system of cycle with help of connecting shaft and bevel gears. The propeller is made of aluminium so the weight of the propeller is less compared to other materials and it is also corrosion resistance and cost-effective. Since it is made up of aluminium material the heat will get dissipated to water.

Fig.7 Propulsion system

6. DESIGN ANALYSIS

The ANSYS software to determine the force acting on the ROV and calculate Static Structural Analysis in various environments.

6.1 Base Frame Analysis

We have ensured the strength of base frame by running simulation on Ansys static structural. Stress and strain analysing is used to choose the material of base frame. Finite element analysing is used to check the deformation of base frame when 130 kg load is applied.

LOAD

- Load Applied: 1274 N

MESH

- Element Size: 10mm
- Element Order: Quadratic
- Number of Elements: 2586
- Number of Nodes: 19227

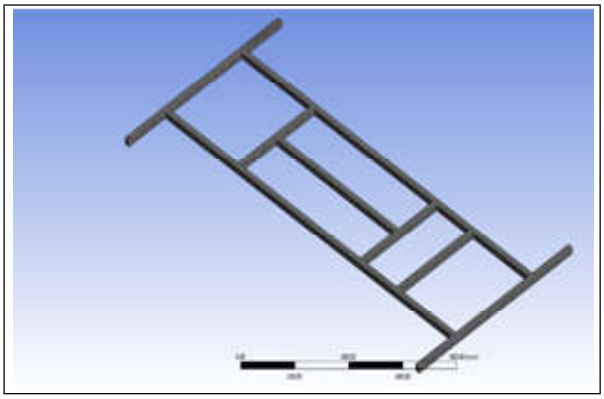

Fig.8 Base frame analysis

EQUIVALENT (VON-MISES) STRESS RESULT:
MINIMUM:0.0052356 MPa
MAXIMUM: 0.01442 MPa

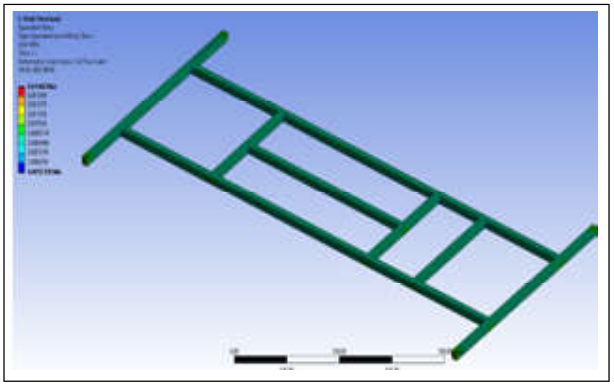

Fig.9 Equivalent (Von-Mises) stress

EQUIVALENT ELASTIC STRAIN RESULT:
MINIMUM: 2.6224×10^{-8}
MAXIMUM: 7.2098×10^{-8}

TOTAL DEFORMATION RESULT:
MINIMUM: 0 mm
MAXIMUM: 1.1658 mm

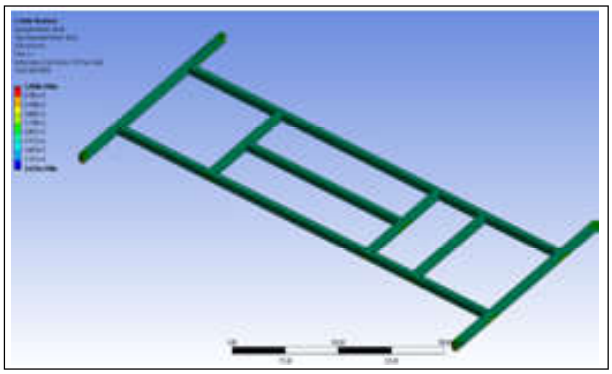

Fig.10 Equivalent elastic strain

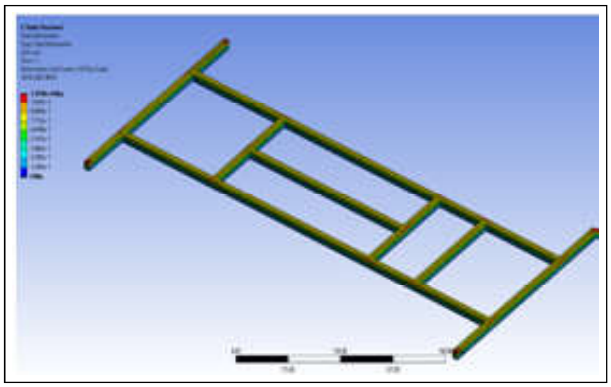

Fig.11 Total Deformation

6.2 Cycle Frame Analysis

We have ensured the strength of cycle frame by running simulation on Ansys static structural. Stress and strain analysing is used to choose the material of base frame. Finite element analysing is used to check the deformation of base frame when 100 kg load is applied.

LOAD

- Load 1 Applied: 588 N
- Load 2 Applied: 196 N

MESH

- Element Size: 10mm
- Element Order: Quadratic
- Number of Elements: 13010
- Number of Nodes: 24415

Fig.12 Cycle frame analysis

EQUIVALENT (VON-MISES) STRESS RESULT:
MINIMUM:0.000349 MPa
MAXIMUM: 9.1795 MPa

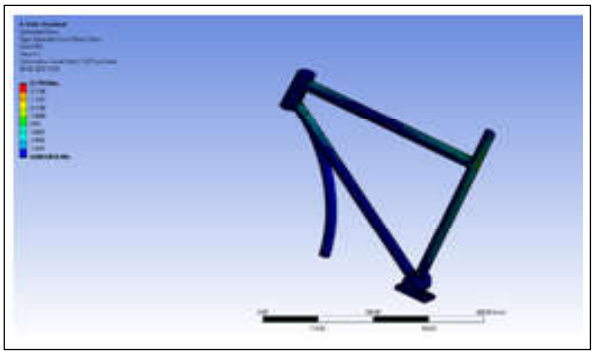

Fig.13 Equivalent (Von-Mises) stress

EQUIVALENT ELASTIC STRAIN RESULT:
MINIMUM: 3.5977×10^{-9}
MAXIMUM: 4.8935×10^{-5}

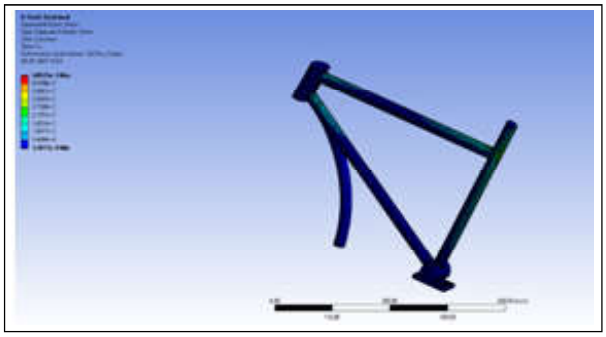

Fig.14 Equivalent elastic strain

TOTAL DEFORMATION RESULT:
MINIMUM: 0 mm
MAXIMUM: 0.037255 mm

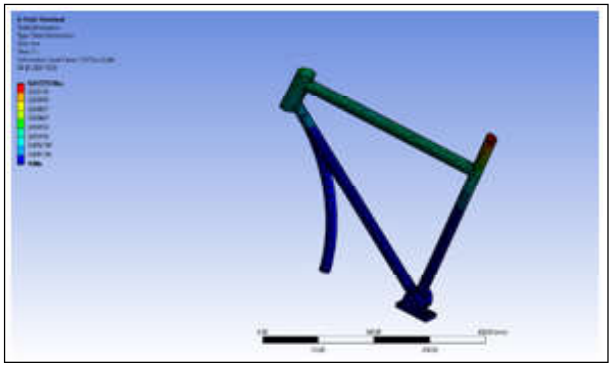

7. RESULTS AND DISCUSSION

The Aqua bike design and using the determined necessary design parameters. Using virtual tools, the Aqua bike is fully assembled and analysed. The design is simulated and tested to ensure that the Aqua bike's stability and center of mass fall within the expected range.

It had been clear that the frame can withstand up to 130kg so a man can easily can drive the vehicle which also includes medic kid and scooper assembly. The Aqua bike is expected to be used in lake, big scale water storage, pond etc.

7.1 Model Testing Result

The capacity of the collecting bin is around 27 Kgs.Different types of garbage like water bottles, plastics, leaves. etc.It can be used for tourism, collect floating waste, help people during flood times and small size cargo transport.

7.2 Result Analysis

The design and calculation for the model have been performed.According to the analysis and finding the center of gravity and buoyancy force, the model had better stability[13,14]. Overall, the working model functioned properly, as it collected the garbage through the scooper that was dumped in the collecting bin.

8. CONCLUSION

As cleaning the water bodies is a very serious issue in today's time. With the help of customer survey, there were few issues that they encountered while cleaning the river. From this innovative project "Design and Development of Aqua Bike for floating waste cleaning" is designed specifically considering the Indian rivers with the hope that it is very much economical and helpful for river cleaning. Based on the research papers and the above-mentioned problems, the conceptual design of the machine was done foremost. After which the design calculations were performed for its buoyancy and center of gravity, also the calculations of major parts such as collecting bin, scooper, etc, were done. After analysing the value for the centre of gravity was 0.045 from the base and in the middle of the machine which shows better stability.

Also, the buoyancy force calculated was 673.72 N which shows the volume displaced by the fluid body. The weight carrying capacity of the prototype is 130 kgs. Hence, with this machine, it will be very useful in cleaning the pond or any other static water body and the time taken will reduce drastically. Based on its design and estimation of the cost and availability it is very cheap and very useful for society.

REFERENCES

[1] JK. Adarsh, OS. Anush, R. Shrivarshan, S.Mithulesh Krishnan, JK. Akash, R.Arul and S. Angaleswari, "Ocean Surface Cleaning Autonomous Robot using Object classification Technique and Path Planning Algorithm", Journal of Physics: Conference Series: Vol.2115, 2021, pp.012021.

[2] AniketPuthran, K.V. Adithya, Harish Balkunde and Hemanth Kumar, "Review on Design and Fabrication of Floating Waste Collector", Vol.5, Issue-2, 2019.

[3] Ashwini jayawant and Akash Sakpal, "Aqua Skimmer for Trach Collection", International Journal of Applied Engineering Research ISSN 0973-4562, Vol.13, No.5, 2018, pp.5-8.

[4] Benjamin Carter Locher, "Amphibious Bicycle", U.S. Patent 3, Vol.844, No.246, Oct. 29, 1974.

[5] DariuszDuda and WojciechLitwin, "The Catamarans George and Energa Solar", Polish Maritime Research, No.3, 2007.

[6] Jung-Kyu Choi and Hyoung-Tae Kim, "Evaluation of Longitudinal Static Stability of Human Powered Hydrofoil Boat", Journal of the Society of Naval Architects of Korea Vol. 46, No. 4, 2009, pp. 391-397.

[7] Dr. R. K. Bansal, "Fluid Mechanics and Hydraulic Machines", Vol.4, pp.113-144, Vol.11, 2007, pp.410-468.

[8] Erin Flynn, Patrick Grindel, Nicholas Payne and Ryan Allin, "The Water Bike", 2021.

[9] Chi-Wai NG, "Mining Floating Plastic Waste Through Landscape Processes", 2018.

[10] Jung-Kyu Choi and Hyoung-Tae Kim, "A Design of Power Transmission System of a Water Bike", Journal of the Society of Naval Architects of Korea Vol.50, No.3, June 2013, pp. 153-159.

[11] Mr. P. M. Sirsat, Dr. I. A. Khan, Mr. P. V. Jadhav and Mr. P. T. Date, "Design and Fabrication of River Waste Cleaning Machine", International Conference on Science and Engineering for Sustainable Development (ICSESD-2017), 2017.

[12] Roberto Siviero, "Land Vehicle Floatable and Steerable in Water", US patent 5415574, May 16, 1995.

[13] R. Raghavi, K. Varshini and L.Kemba Devi, "Water Surface Cleaning Robot", JAREEIE, Website: www.ijareeie.com, Vol.8, Issue.3, March 2019, ISSN (Print):pp.2320-3765, ISSN (Online): pp.2278-8875.

[14] Shubham Awasthi, "Design and Fabrication of Amphibious Bicycle", International Journal of Applied Engineering Research ISSN 0973-4562, Vol.14, No.2, 2019.

OPTICAL PROPERTIES OF PULSE ELECTRODEPOSITED CuALSe2 THIN FILMS

M.Thirumoorthy[1], K.Ramesh[2] and K.Vanitha[3]
[1&3]Department of Physics,[2]Department of Physics,
[1&3]Bannari Amman Institute of Technology, Sathyamangalam-638 401, Erode District, Tamil Nadu
[2]Government Arts College, C-Mutlur, Chidambaram-608 102, Tamil Nadu
E-mail: thirumoorthy@bitsathy.ac.in

Abstract

Optical constants of pulse-plated CuAlSe2 thin films at various duty cycles were determined in the 550-1800 nm spectral range using optical absorption and transmittance measurements. Tauc's plot was used to determine the energy band gap values of the deposited films and is estimated to be between 2.45 eV and 2.66 eV. Their optical constants like refractive index, average excitation energy (E0), oscillator strength (Ed), effective mass (m), plasma frequency (ůp), and static and carrier concentration (N/m*) were estimated and reported.*

Keywords: *CuAlSe2, Thin films, Semiconductor, Electronic material*

1. INTRODUCTION

CuAlSe2 (CASe) has been widely studied owing to the wide band gap (Eg = 2.67 eV) and relative stability for the application as a buffer layer in thin-film solar cells and detectors. As a semiconductor of chalcopyrite structure, CASe exhibits a tetragonal crystal system with similar cell parameters to CuInSe2 [1,2]. Therefore, it is feasible to fabricate either n-type or p-type CuAlSe2 on suitable substrates. Therefore, CASe has been growing in popularity recently in search of an excellent window layer or buffer layer for photovoltaic cells [3]. Techniques of elemental co-evaporation [4], chemical vapour transport (CVT) [5], metal-organic chemical vapour deposition (MOCVD) [6], selenization of metallic precursors [7], and molecular beam epitaxy (MBE) [8] have been proposed for preparing CuAlSe2 thin films. Apart from these methods, the approach of pulse electrodeposition for CuAlSe2 is rarely proposed to date; however, due to the regular features of cost-effectiveness, time-saving, and displaying high-quality fabrication with appropriate parameters. This is the first report on the optical properties of pulse electrodeposited CASe films. In our earlier paper, we reported on the photoelectrochemical properties of CASe [9].

The pulse plating (PP) technique swiftly alternates the potential between different values as the plating is interrupted by a zero current. The PP technique gives high instantaneous currents due to the periodic discharge of the electric double layer, which decreases the concentration polarisation of the metal ions in the electrolyte and facilitates the passage of the ions. At the same time, the conventional DC electrodeposition method offers lower deposition rates and higher coating defects [10]. Therefore, the electron crystallization process can be controlled more accurately [11]. Furthermore, it has been reported that the PRP technique improves the quality of the deposits better than the PP method [12]. In the PRP technique, the stripping cycles applied between the sequence of cathodic pulses lead to a partial dissolution of the previously deposited layer, yielding a more homogenous deposit with enhanced particle incorporation [13–15].

2. EXPERIMENTAL METHODS

The pulse electrodeposition technique deposited CuAlSe2 thin films with different duty cycles using a non-aqueous ethylene glycol solution. 0.4 M Al2(SO4)3, 0.1 M CuSO4, 0.1 M SeO2. The films were deposited at 80°C and different duty cycles at a constant current density of 5 mA cm-2. Tin oxide-coated glass (5 ohms/sq) was used as substrate. Details of the use of non-aqueous electrolytes are given in our earlier paper [9]. The thickness of the films measured using the Mitutoyo surface profilometer was in the range of 800 nm – 1400 nm with the increase of duty cycle from 6 – 50 %. Optical transmission spectra were recorded using Hitachi UV 3400 UV –VIS-NIR spectrophotometer. The optical data were analyzed to obtain band gap, refractive index, extinction coefficient and dispersion energy, as well as the oscillator energy were obtained.

3. RESULTS AND DISCUSSION

The X-ray diffraction (XRD) pattern of CASe films formed at different duty cycles was polycrystalline, exhibiting the peaks corresponding to the single-phase chalcopyrite CASe. Peaks matching to (220), (204), (312), (112) and (116) orientations of the chalcopyrite arrangement were observed (JCPDS No.44-1269). Microstructural parameters and the XRD patterns are given in our earlier paper [9].

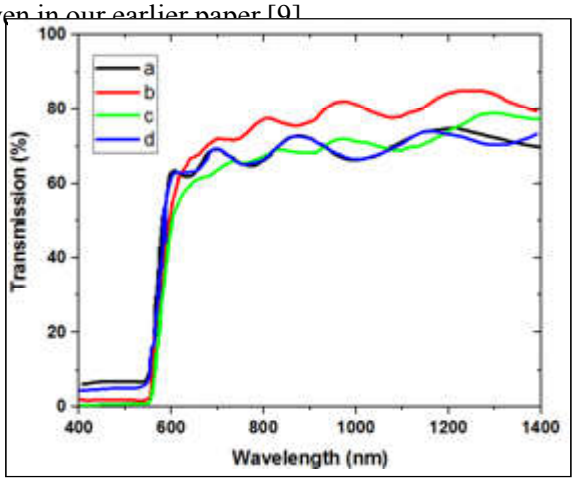

Fig.1 Transmission spectra of CuAlSe2 films deposited at different duty cycle (a) 9 % (b) 15 % (c) 33 % (d) 50 %

Figure 1 shows the transmission spectra of the CuAlSe2 films deposited at a 50% duty cycle. The spectrum exhibits interference fringes, and the value of the refractive index was estimated by the envelope method [16] as follows:

$$n = [N + (N^2 - n_s^2)]^2 \quad \ldots\ldots\ldots\ldots\ldots\ldots \quad (1)$$

$$N=(n_s^2+1)/2+2n_s[(T_{max}-T_{min})/(T_{max}T_{min})] \quad \text{----------} \quad (2)$$

Where the substrate's refractive index is denoted as ns, Tmin and Tmax are the minimum and maximum transmittances at the same wavelength in the fitted envelope curve on a transmittance spectrum. The refractive index value calculated from the above equations was 2.90–3.10 at 550 nm for the films deposited at different duty cycles. The refractive index decreases with wavelength (Figure.2).

The value of the absorption coefficient (į) was calculated using the relation

$$į = 1/d \ln \{(n-1)(n-n_s)/(n+1)(n-n_s)\} [(T_{max}/T_{min})|^2 + 1]/[(T_{max}/T_{min})^2 - 1] \quad \ldots\ldots \quad (3)$$

where "d" is the thickness of the film, and the other parameters have the usual meaning as given for equation (2). The band gap of the films increased from 2.45–2.66 eV as the duty cycle increased (from Tauc's plot) (Figure.3).

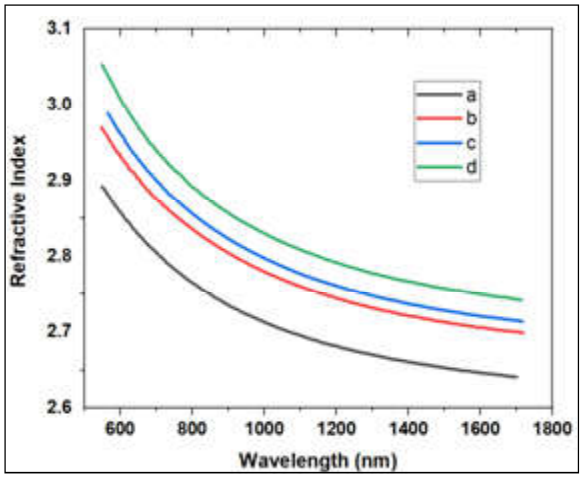

Fig.2 Variation of Refractive index with wavelength for CuAlSe2 films deposited at different duty cycle (a) 50 % (b) 33 % (c) 15 % (d) 9 %

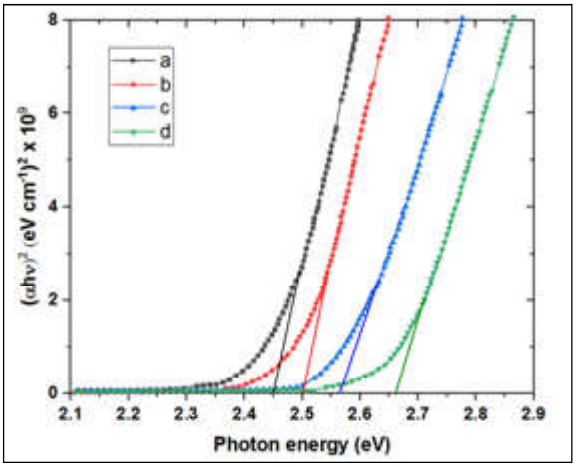

Fig.3 Tauc's plot of CuAlSe2 films deposited at different duty cycle (a) 9 % (b)15 % (c) 33 % (d) 50 %

The increase in band gap at the lower duty cycle is due to the small crystallite size. The band gap values agree well with the earlier report [17].

The absorption coefficient was calculated as extinction coefficient (k) using the following relation. Fig.4 shows the variation of the extinction coefficient with wavelength.

$$k = \alpha\lambda/4\pi \quad \ldots\ldots\ldots \quad (4)$$

where į is the absorption coefficient, and ė is the wavelength. As understood from the figure, the extinction coefficient decreases with the increase in the

wavelength.The amount of light lost owing to scatter and absorbance drops as wavelength increase due to a decrease in extinction coefficient.

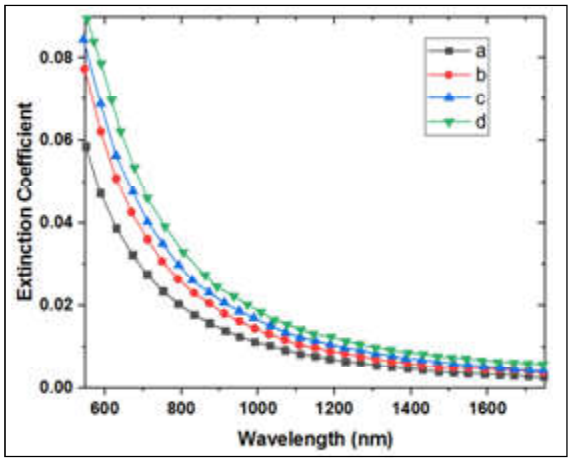

Fig.4 Variation of extinction co-efficient with wavelength of CuAlSe2 films deposited at different duty cycle (a) 9 % (b)15 % (c) 33 % (d) 50 %

Wemple and DiDomenico [18] state that the single-effective oscillator model is established and that the relation can approximate the optical data accurately.

$$n^2 - 1 = (E_d E_0)/ (E_o^2 - E^2) \quad \ldots\ldots\ldots\ldots (5)$$

where E= hν is the photon energy, n is the refractive index, E_0 is the single-effective oscillator energy, and E_d is the dispersion energy, a measure of the average strength of the interband optical transitions. Plotting $(n_2 -1)^{-1}$ against E^2 gives the oscillator parameters by appropriate straight line.

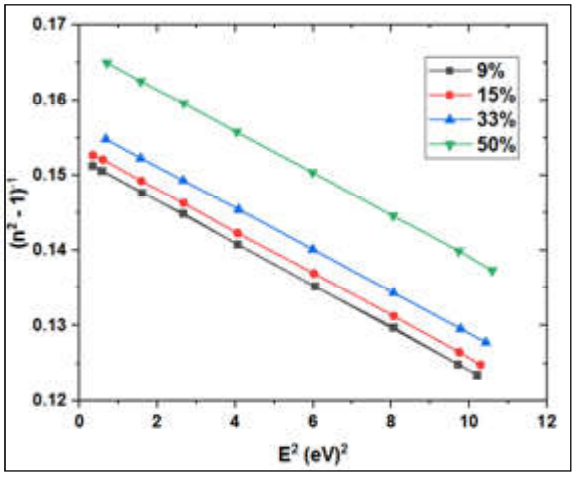

Fig.5 $(n^2 - 1)^{-1}$ vs E^2 plot of $CuAlSe_2$ films deposited at different duty cycle

Figure 5 shows the plot of $(n_2-1)^{-1}$ vs E^2 for the films deposited at different substrate temperatures. The values of E_0 and E_d can then be calculated from the slope $(E_0E_d)^{-1}$ and the intercept on the vertical axis (E_0/E_d). By extrapolating the Wemple–DiDomenico dispersion equation (5) to $E \rightarrow 0$, the values of the static refractive index (n_0) can be calculated. The calculated values of n0 are 2.66, 2.72, 2.80 and 2.82 for the films deposited at a different duty cycle. The calculated values of n_0, E_0 and E_d are listed in table 1. As the duty cycle increases, the value of the static refractive index decreases and the value of E_0 and E_d increases with an increase in the duty cycle. Also, the optical band gap (E_g) values obtained from Tauc's plot and the Wemple-DiDomenico dispersion parameter E_0 using the relation $E_g=E_0/1.4$ agree.

The moments of the optical dispersion spectra M_{-1} and M_{-3} can be evaluated using the relationships [19]

$$E_o^2 = M_{-1}/M_{-3} \quad \text{---------- (6)}$$
$$E_d^2 = M_{-1}^3/ M_{-3} \quad \text{---------- (7)}$$

The growth of the thin film microstructure to a more ordered phase is usually connected to the significant increase in oscillator strength, E_d (more than two times) [20]. Our observation is that the oscillator energies $E_0 \approx 1.4Eg$.

Earlier, it was reported that $E_0 \approx 2E_g$ [20,21].

In a transparent region, the relation between the optical dielectric constant, ε_1, the wavelength,λ, and the refractive index,n, is given by the following equation [22]:

$$\varepsilon_1 = n^2 = \varepsilon_L - D\lambda^2 \quad \ldots\ldots\ldots\ldots (8)$$

where ε1 is the fundamental part of the dielectric constant, εL is the lattice dielectric constant or (the high-frequency dielectric constant), and D is a constant depending on the ratio of carrier concentration to the effective mass;

$$D = (e^2 N)/ (4\pi^2\varepsilon_0 m^*c^2) \quad \ldots\ldots\ldots\ldots (9)$$

where e is the electron's charge, N is the free charge carrier concentration, εo is the permittivity of free space, m* is the effective mass of the electron, and c is the velocity of light [23].

Figure 6 shows the relation between n2 and ė2 for the CASe thin films deposited at different duty cycles. It is observed that the dependence å1 (= n2) on ė2 is linear at longer wavelengths. The value of åL can be obtained by extrapolating the linear portion of this dependence to zero wavelength. The constant D can be determined by calculating the slope of this linear portionfrom which the value (N/m*) for the thin films can be obtained (Table-1).

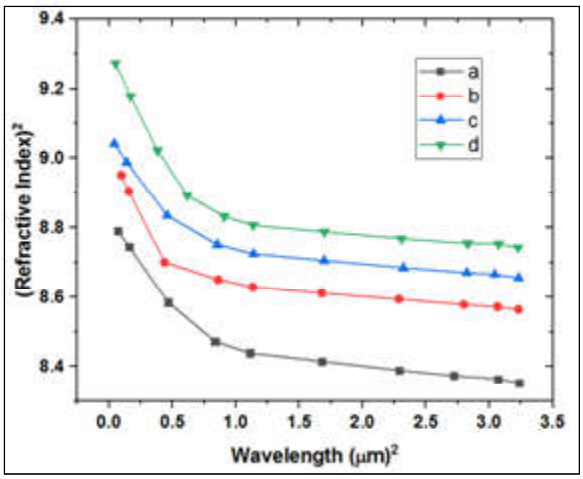

Fig.6 Variation of square of refractive index with square of wavelength of CASe films deposited at different duty cycles (a) 50 % (b) 33 % (c) 15 % (d) 9 %

4. CONCLUSION

The pulse plating technique has deposited CASe2 films at different duty cycles. This method is easily reproducible, economically viable, and can be scaled up for the deposition of large-area films. Optical absorption measurements indicate a band in the 2.45 eV – 2.66 eV range from a plot of (įhķ)2 vs hķ for the films deposited at different duty cycles. The films exhibited photoconductive responses. The films can also be used in photoconductive applications and photocatalytic applications.

Table 1 Dispersion energy values of CuAlSe2 films deposited at different duty cycle

Duty cycle (%)	n_0	E_0	E_d	E_g (eV)	M_1	M_3	N/m* x10^{48} ($cm^{-3}gm^{-1}$)
50	2.66	3.72	24.50	2.66	6.59	0.48	2.10
33	2.72	3.60	23.52	2.57	6.53	0.50	1.95
15	2.80	3.50	22.44	2.50	6.41	0.52	1.85
9	2.82	3.43	20.66	2.45	6.02	0.51	1.75

REFERENCES

[1] K.-C. Huang, C.-L. Liu, P.-K. Hung, M.-P. Houng, Appl. Surf. Sci., Vol.273, 2013, pp.723.

[2] R.S.Kumar, A.Sekar, N.V.Jaya, S.Natarajan and S.Chichibu, J. AlloysCompd., Vol.312, 2000, pp.4.

[3] L. Barkat, M. Morsli, C. Amory, S. Marsillac, A. Khelil, J.C. Bernčde and C.El.Moctar, Vol.99, 2003, pp.431-432.

[4] Y.B.K. Reddy and V.S. Raja, Mater. Chem. Phys., Vol.100, 2006, pp.152.

[5] N. Kuroishi, K. Mochizuki, K. Kimoto, Mater. Lett., Vol.57, 2003, pp.1949

[6] S. Chichibu, A. Iwai, S. Matsumoto and H. Higuchi, J. Cryst. Growth, Vol.126, 1993, pp.635.

[7] J. López-Garcķa, C. Guillén, J. Mater. Sci., Vol.46, 2011, pp.7603.

[8] K. Kimoto, K. Mochizuki, K. Masumoto, Jpn. J. Appl.Phys., Vol.32, 1993, pp.147.

[9] M. Thirumoorthy, K. Ramesh and K.R. Murali, "Characteristics of Pulse Electrodeposited CuAlSe2 films", J Mater Sci: Mater Electron, https://doi.org/10.1007/s10854-015-2883-9, Vol.26, 2015, pp.3657-3663.

[10] T. Borkar and S.P. Harimkar, Surf. Coat. Technol. Vol.205, 2011, pp.4124.

[11] M.S. Chandrasekar and M. Pushpavanam, Electrochim. Acta, Vol.53, 2008, pp.3313.

[12] F. Su, C. Liu and P. Huang, J. Alloys Compd., Vol.557, 2013, pp.228.

[13] T. Frade, V. Bouzon and A. Gomes, Surf. Coat. Technol. Vol.204, 2010, pp.3592.

[14] C. Kollia, Z. Loizos, N. Spyrellis, Surf. Coat. Technol., Vol.45, 1991, pp.155.

[15] D. Thiemig, R. Lange and A. Bund, Electrochim. Acta., Vol.52, 2007, pp.7362.

[16] H. Karaagac, M. Kaleli and M. Parlak, J. Phys. DAppl. Phys. Vol.42, 2009, pp.165413.

[17] S H Wemple and M DiDomenico,Phys. Rev., Vol.B3, 1971, pp.1338.

[18] J.N. Zeng, J.K. Low, Z.M. Ren, T. Liaw and Y.F. Lu, Appl. Surf. Sci., Vol.362, 2002, pp.197-198.

[19] N.K. Sahoo, S. Thakur and R.B.T. Okas, Applied Surface Science, 2006.

[20] A. F. Quasrawi and M. M. Shukri Ahmad, Cryst. Res. Technol., Vol.41, 2006, pp.364.

[21] J.M.Gonzalez-Leal, A.Ledesma, A.M.Bernal-Oliva, R.Prieto-Alcon,E.Marquez, J.A.Angel and J.Carabe, Materials Letters, Vol.39, 1999, pp.232.

[22] P.O.Edward, "Hand Book of Optical Constants of Solids", Academic Press,New York,.1985, pp.265.

Indian Journal of Engineering, Science, and Technology (IJEST)

(ISSN: 0973-6255)
(A half-yearly refereed research journal)

Information for Authors

1. All papers should be addressed to The Editor-in-Chief, Indian Journal of Engineering, Science, and Technology (IJEST), Bannari Amman Institute of Technology, Sathyamangalam - 638 401, Erode District, Tamil Nadu, India.
2. Two copies of manuscript along with soft copy are to be sent.
3. A CD-ROM containing the text, figures and tables should separately be sent along with the hard copies.
4. Submission of a manuscript implies that : (i) The work described has not been published before; (ii) It is not under consideration for publication elsewhere.
5. Manuscript will be reviewed by experts in the corresponding research area, and their recommendations will be communicated to the authors.

Guidelines for submission

Manuscript Formats

The manuscript should be about 8 pages in length, typed in double space with Times New Roman font, size 12, Double column on A4 size paper with one inch margin on all sides and should include 75-200 words abstract, 5-10 relevant key words, and a short (50-100 words) biography statement. The pages should be consecutively numbered, starting with the title page and through the text, references, tables, figure and legends. The title should be brief, specific and amenable to indexing. The article should include an abstract, introduction, body of paper containing headings, sub-headings, illustrations and conclusions.

References

A numbered list of references must be provided at the end of the paper. The list should be arranged in the order of citation in text, not in alphabetical order. List only one reference per reference number. Each reference number should be enclosed by square brackets.

In text, citations of references may be given simply as "[1]". Similarly, it is not necessary to mention the authors of a reference unless the mention is relevant to the text.

Example

[1] M.Demic, "Optimization of Characteristics of the Elasto-Damping Elements of Cars from the Aspect of Comfort and Handling", International Journal of Vehicle Design, Vol.13, No.1, 1992, pp. 29-46.

[2] S.A.Austin, "The Vibration Damping Effect of an Electro-Rheological Fluid", ASME Journal of Vibration and Acoustics, Vol.115, No.1, 1993, pp. 136-140.

SUBSCRIPTION

The annual subscription for IJEST is Rs.600/- which includes postal charges. To subscribe for IJEST a Demand Draft may be sent in favour of IJEST, payable at Sathyamangalam and addressed to IJEST. Subscription order form can be downloaded from the following link http:// www.bitsathy.ac.in./ ijest.html.

For subscription / further details please contact:

IJEST
Bannari Amman Institute of Technology
Sathyamangalam - 638 401, Erode District, Tamil Nadu Ph: 04295 - 226340 - 44
Fax: 04295 - 226666 E-mail: ijest@bitsathy.ac.in Web:www.bitsathy.ac.in

Indian Journal of Engineering, Science, and Technology

Volume 16, Number 1&2, January - December 2022

CONTENTS